

University of Dundee

DOCTOR OF PHILOSOPHY

Characterization of Parkinson's Disease-associated LRRK2 Kinase

Katsemonova, Kristina

Award date:
2016

[Link to publication](#)

General rights

Copyright and moral rights for the publications made accessible in the public portal are retained by the authors and/or other copyright owners and it is a condition of accessing publications that users recognise and abide by the legal requirements associated with these rights.

- Users may download and print one copy of any publication from the public portal for the purpose of private study or research.
- You may not further distribute the material or use it for any profit-making activity or commercial gain
- You may freely distribute the URL identifying the publication in the public portal

Take down policy

If you believe that this document breaches copyright please contact us providing details, and we will remove access to the work immediately and investigate your claim.



Characterization of Parkinson's Disease-associated LRRK2 Kinase

Kristina Katsemonova

A thesis submitted for the degree of Doctor of Philosophy

University of Dundee

August 2016

ACKNOWLEDGEMENTS

I would like to take this opportunity to express my gratefulness to the people who provided me with technical and moral support throughout my PhD. First and foremost to my supervisor Professor Dario Alessi for providing me with continuous guidance, constant inspiration, great support and thorough advice. I would also like to acknowledge Dr. Paul Davies for introducing me to the laboratory and providing excellent advice and support. A special thanks to my thesis committee members, Professor Philip Cohen and Professor Stephen Keyse, for their stimulating scientific discussions. I would like to thank my collaborators: Dr. Francesco Marchesi from the University Of Glasgow Veterinary School Of Medicine, Dr. Nicolas Dzamko from Neuroscience Research Australia (NeuRA), Dr. Thomas McWilliams from the University of Dundee MRC PPU, Dr. Matthias Trost from the University of Dundee MRC PPU, and Dr. Piotr Szyniarowski from the University of Dundee MRC PPU. I want to thank Dr. Sonal Das for engaging me into the world of science communication and being a great motivator.

This thesis would not be possible without a huge support from the Division of Signal Transduction Therapy. In particular I want to thank Tom McCartney and Melanie Wightman for cloning, Fiona Brown for raising antibodies, Natalia Shpiro for synthesising phos-tag reagents and LRRK2 kinase inhibitors and everyone at DSTT. A huge thanks to Elaine Forsyth and Gail Gilmour for helping me to take care of my mice. I would very much like to thank Dr. David Campbell and Bob Gourlay for their enormous help and advice in using mass spectrometry. I want to thank Dr. Rosie Clarke for helping me with FACS machine and single cell cloning. Also, I would like to thank Kirsten McLeod, Janis Stark and Laura Fin for their support in the TC. Big thanks to MRC PPU support staff Judith Hare, Alison Hart, Allison Bridges and Rachel Naismith.

I would like to thank all the past and present members of Dario's lab: Chandana and Agne for introducing me to the lab and their encouraging scientific and philosophical discussions, Eeva for being a great PhD buddy and constant inspiration, Sourav for making us laugh and bringing a lot of chocolate to the lab! George for his positive attitude and optimism, Gerrit for words of wisdom, Ruzica and Esther for their encouragement. I want to thank our lab LRRK2 team: Francesca for being a prime

example of hard work and dedication, Genta for sharing his scientific knowledge with me and interesting scientific discussions, Jinwei for our fun moments in the lab, Pawel and Federico for bringing new life to the LRRK2 project! Particularly, I want to thank my bay mates: Chiara for her calm and positive attitude. Annika for bringing so much enthusiasm and happiness to our bay – thank you for being a great friend! Hannah for her fun moments and excitement in the lab! A special thanks to Nazma, my dear PhD friend – thank you for your inspirational scientific talks and the great moments we shared together! I cannot emphasize how important your support was throughout all the ups and downs.

In spite of the fact that Dundee was not the city I particularly enjoyed, I am very grateful for some amazing friends who I met here and will cherish for life. Thank you Polly for being my dear friend, for all the amazing times we spent together in and outside the lab, including singing the “shake it off” song and for your constant support. I was happy to come back to Dundee after holidays knowing you were here! I want to thank Kristin, Yosua, Mark, Riccardo and Fabio for being great humans and all their support. Finally, I want to thank all MRC PhD students for being fun and supportive to each other.

I would very much like to thank my mother for her love, patience and encouragement.

This thesis is dedicated to my husband Alexander, who has been an incredible source of inspiration and whom I deeply love. Thank you for motivating me, for all your affection and support.

DECLARATIONS

I hereby declare that the following thesis is based on the results of investigations conducted by myself, and that this thesis is of my own composition. Work other than my own is clearly indicated in the text by reference to the researchers or their publications. This thesis has not in whole or in part been previously presented for a higher degree.

Kristina Katsemonova

I certify that Kristina Katsemonova has spent the equivalent of at least nine terms in research work in the School of Life Sciences, University of Dundee and that she has fulfilled the conditions of the Ordinance General No. 14 of the University of Dundee and is qualified to submit the accompanying thesis in application for the degree of Doctor of Philosophy.

Prof. Dario R. Alessi, FRS, FRSE

LIST OF PUBLICATIONS

The work presented in this thesis has resulted in the following publication:

Ito G, **Katsemonova K**, Tonelli F, Lis P, Baptista M, Shpiro N, Duddy G, Wilson S, Ho WL, Ho SL, Reith AD, Alessi DR. Phos-tag analysis of Rab10 phosphorylation by LRRK2: a powerful assay for assessing kinase function and inhibitors. *Biochem J*. 2016 Jul 29.

ABBREVIATIONS

ACN	acetonitrile
ATP	adenosine 5'-triphosphate
BSA	bovine serum albumin
cAMP	cyclic adenosine mono-phosphate
CaMK	calcium/calmodulin dependent kinase
Cas9	Cas9 CRISPR associated protein 9
CTNNA1	catenin alpha 1
cpm	counts per minute
CRISPR	clustered regularly interspaced short palindromic repeat
C-terminal	carboxy terminus
Da	Dalton
DAPI	4',6-diamidino-2-phenylindole
DMEM	Dulbecco's modified Eagle's medium
DMSO	dimethyl sulphoxide
DNA	deoxyribonucleic acid
DSTT	Division of Signal Transduction Therapy
DTT	dithiothreitol
ECL	enhanced chemiluminescence
E. coli	Escherichia coli
EDTA	sodium ethylenediaminetetraacetic acid
EGTA	sodium ethylene glycol tetra acetic acid
FBS	foetal bovine serum
FLAG	DYKDDDDKG peptide
FRT	Flp recombination target
GFP	green fluorescent protein
GAPDH	glyceraldehyde 3-phosphate dehydrogenase
GAP	GTPase Activating Protein
GDI	GDP-dissociation inhibitors
GEF	guanine nucleotide exchange factor
gRNA	guide ribonucleic acid
GST	glutathione S-transferase

h	hour
HA	hemagglutinin
HEK 293	human embryonic kidney 293 cells
HEPES	4-(2-Hydroxyethyl)piperazine-1-ethanesulfonic acid
HPLC	high performance liquid chromatography
HRP	horseradish peroxidase
IB	immunoblot
IgG	immunoglobulin G
IP	immunoprecipitation/immunoprecipitate
IPTG	Isopropyl β -D-1-thiogalactopyranoside
kDa	kilo Dalton
KD	kinase dead
KO	knockout
L	litre
LB	Luria-Bertani medium
LDS	lithium dodecyl sulphate
LRRK2	leucine rich repeat kinase 2
M	molar
μ	micro
MALDI-TOF MS	matrix-assisted laser-desorption ionization time-of-flight mass spectrometry
MAPK	mitogen activated protein kinase
MEF	mouse embryonic fibroblasts
Mg-ATP	magnesium adenosine 5'-triphosphate complex
Min	minute
MAP kinase kinase	MAP kinase kinase
mol	mole
M-RIP	myosin phosphatase Rho-interacting protein
MRC-PPU Unit	Medical Research Council Protein Phosphorylation and Ubiquitylation Unit
MYPT	myosin phosphatase targeting subunit
n	nano
NaCl	sodium chloride
N-terminal	amino terminal
NUAK	NUAK family SNF1-like kinase

NRAS	Neuroblastoma RAS viral oncogene homolog
p	phospho
PAGE	polyacrylamide gel electrophoresis
PALM	paralemmin
PBS	phosphate-buffered saline
PCR	polymerase chain reaction
PD	Parkinson's disease
PKD1	3-phosphoinositide-dependent protein kinase 1
PEI	polyethylenimine
PINK1	PTEN-induced putative kinase 1
PKA	protein kinase A
PKG	protein kinase G
PKC	protein kinase C
PMSF	phenylmethansulphonyl fluoride
Rab8A	Ras-related protein 8A
Rab10	Ras-related protein 10
Rab12	Ras-related protein 12
RNA	ribonucleic acid
rpm	rotations per minute
RT	room temperature
s	second
SDS	sodium dodecyl sulphate
shRNA	small interfering ribonucleic acid
SNAP23	synaptosome associated protein 23
TBS	tris-buffered saline
TBS-T	tris-buffered saline with Tween 20
TCEP	tris(2-carboxyethyl)phosphine
TEMED	tetramethylethylenediamine
TOM/TIM2	Translocase of Outer Membrane/ Translocase of Inner Membrane
VDAC	Voltage dependent anion channel

AMINO ACID CODE

Amino acid or residue	Three letter code	One letter code
alanine	Ala	A
arginine	Arg	R
asparagine	Asn	N
aspartate	Asp	D
cysteine	Cys	C
glutamate	Glu	E
glutamine	Gln	Q
glycine	Gly	G
histidine	His	H
isoleucine	Ile	I
leucine	Leu	L
lysine	Lys	K
methionine	Met	M
phenylalanine	Phe	F
proline	Pro	P
serine	Ser	S
threonine	Thr	T
tryptophan	Trp	W
tyrosine	Tyr	Y
valine	Val	V
any amino acid	Xaa	X
hydrophobic residue	Hyd	Ψ

SUMMARY

Parkinson's disease (PD) is a progressive neurodegenerative disorder, which primarily results from the selective loss of dopaminergic neurons in the substantia nigra. Mutations in leucine-rich repeat kinase 2 (LRRK2) have been linked to autosomal familial and sporadic PD. It is now estimated that approximately 1% of Parkinson's disease (PD) results from mutations in LRRK2. Previous studies have established that the most common mutation, which replaces G2019, located within the magnesium binding DFG motif in the kinase domain, with a serine residue enhances protein kinase activity between 2 to 4 folds. Recently our lab in collaboration with Matthias Mann's lab discovered that LRRK2 phosphorylates a subset of Rab GTPases including Rab8A and Rab10. Moreover, it was shown that LRRK2 PD-associated mutations including G2019S, Y1669C and R1441C/G exhibit an enhanced phosphorylation of Rab10 and Rab8A in cells. Based on this data it was suggested that overactivation of LRRK2, which leads to an increased phosphorylation of indicated Rab GTPases, may lie behind the mechanism by which LRRK2 causes disease. To date, a number of compounds such as LRRK2-IN-1, GSK2578215A and MLI-2 have been described as fairly selective LRRK2 inhibitors. It was reported that treatment of cells and mice with these inhibitors completely blocks Rab10 and Rab8A phosphorylation in cells. These results indicated that inhibition of the LRRK2 kinase activity could be a possible treatment for PD. In a previous work, our laboratory found that treatment of cells or mice with structurally diverse LRRK2 inhibitors results in rapid dephosphorylation of LRRK2 at two residues: S910 and S935. Our results suggest that these sites do not comprise LRRK2 autophosphorylation sites but are instead regulated by a distinct signalling mechanism that is controlled by LRRK2.

In the first part of my thesis I investigate the physiological function of LRRK2 S910 and S935 residues in cell using LRRK2 [S910A+S935A] knock-in mouse model. I found that *in vivo*, LRRK2 S910A+S935A mutation evidently reduced Rab10 and Rab8A phosphorylation in MEFs suggesting that this mutation is important for LRRK2 kinase activity. Moreover, I found that LRRK2 [S910A+S935A] mutation leads to decreased total levels of full length LRRK2 in kidneys, indicating that LRRK2 could be regulated differently in these tissues. In this chapter I also report the histopathological data for brains, kidneys and lungs that shows that the LRRK2

[S910A+S935A] mutation does not cause any major pathology in these tissues. This data indicates that the previously reported kidney and lung phenotype observed in LRRK2 KO and KD mice is not likely to be due to S910 and S935 dephosphorylation. However, behaviour phenotyping of LRRK2 [S910A+S935A] knock in mice revealed that they performed significantly worse in the rotarod test compared with their littermate wild type mice. In future, it would be interesting to perform additional behaviour tests with these mice to confirm these results.

In the second chapter, the initial aim was to address whether or not MYPT1 comprised a physiological substrate of LRRK2, and if so to investigate whether it was involved in the negative feedback regulation of LRRK2 on S910/S935. For this purpose, I used transcription activator-like effector nucleases (TALENs) as well as CRISPR/Cas9 gene editing techniques to attempt to knock out MYPT1 from HEK293 cells but I was unable to obtain homozygous knockout cell lines, which might be result of inviability of MYPT1 deficiency. In parallel experiments, in an attempt to confirm the interaction of MYPT1 and LRRK2, I immunoprecipitated endogenous LRRK2 and MYPT1 from wild type and homozygous LRRK2 knockout mouse embryonic fibroblasts (MEFs). This revealed that MYPT1 did not co-immunoprecipitate with endogenous LRRK2, casting doubt over the previously reported data suggesting these proteins interact. Finally, I used orbitrap-based phospho-site mass spectrometry to analyse changes in overexpressed and endogenous MYPT1 phosphorylation, and was unable to demonstrate that treatment of cells with LRRK2 inhibitors induced dephosphorylation of MYPT1 on residues that had been identified to be phosphorylated *in vitro* by LRRK2. In conclusion, results presented in this study cast doubt that MYPT1 is a direct LRRK2 substrate.

In the third part of the thesis, my aim was to widen to identify novel LRRK2 substrates or regulators. For this purpose I performed a comparative mass spectrometry analysis to analyse LRRK2 interactors that co-immunoprecipitate with endogenous LRRK2 immunoprecipitated from LRRK2 wild type, LRRK2 [S910A+S935A] knock-in and LRRK2 KO MEFs. I present the table comprising identified potential LRRK2 interactors and attempt to validate some of the proteins from the list. Unfortunately, my data showed that tested proteins including PALM protein do not seem to bind LRRK2. In this chapter, I also performed LRRK2 substrate specificity analysis, which suggested that LRRK2 could phosphorylate serines as well as threonines *in vitro*. Particularly, LRRK2 G2019S seems to

phosphorylate serine residues much more efficiently than threonine. This data is supported by previous studies, for instance, LRRK2 G2019S was reported to have an enhanced autophosphorylation at S1292. Moreover, Rab12 is another LRRK2 substrate being validated at the moment and it was shown that it is phosphorylated by LRRK2 at S106. In future, it would be interesting to investigate how LRRK2 G2019S mutation affect phosphorylation at this site.

TABLE OF CONTENTS

Chapter 1: <i>Introduction</i>	18
1.1 Signalling transduction	19
1.2 Protein phosphorylation	21
1.2.1 The significance of protein phosphorylation in signal transduction	21
1.2.2 Protein kinases - the human kinome.....	23
1.2.3 General characteristics of protein kinase.....	26
1.2.4 Phosphorylation and human disease	29
1.3 Overview of Parkinson’s disease	31
1.3.1 Introduction to Parkinson’s disease	31
1.3.2 Epidemiology, risk factors and clinical s of Parkinson’s disease	32
1.3.3 Genetics of Parkinson’s disease	33
1.3.4 Autosomal Dominant Parkinson’s disease.....	35
1.4 LRRK2	41
1.4.1 Discovery of LRRK2 and LRRK2 mutations associated with PD	41
1.4.2 Domain architecture of LRRK2	43
1.5 Cell signal transduction by LRRK2	47
1.5.1 Discovery of a subset of Rab GTPases as LRRK2 physiological substrates	47
1.5.2 Evidence supporting link between Rab GTPases and PD.....	52
1.5.3 Identification of S910 and S935 as major LRRK2 phosphorylation sites	54
1.6 Genetic and pharmacological studies of LRRK2 using a mouse model	55
1.6.1 Phenotype of LRRK2 knock-out and knock-in genetic mice models	55
1.6.2 Phenotype of pharmacological inhibition of the LRRK2 kinase activity	59
CHAPTER 2: <i>Materials & Methods</i>	61
2.1 Materials	62
2.1.1 Commercial reagents	62
2.1.2 In-house reagents	64
2.1.3 Antibodies	64
2.1.3.1 In-house antibodies.....	64
2.3.1.2. Commercial/gifted antibodies.....	65
2.1.4 Plasmids.....	66
2.1.5 Inhibitors.....	68
2.1.6 Buffers.....	69
2.1.6 Cell lines.....	71
2.1.7 Animals.....	71
2.1.8 Instruments	71
2.2 Methods	73
2.2.1 MOLECULAR BIOLOGY METHODS	73
2.2.1.1 Transformation and plasmid purification from <i>E.coli</i>	73
2.2.1.2 Purification of plasmid DNA from <i>E.coli</i>	73
2.2.1.3 Measurement of DNA concentration.....	73
2.2.1.4 Restriction enzyme digests of plasmid DNA	74
2.2.1.5 DNA mutagenesis	74
2.2.1.6 Genome editing-TALENs: (Knocking out MYPT1 from HEK293 cells using TALENs). 74	
2.2.1.7 Genome editing-CRISPR/Cas9: (Knocking out MYPT1 from HEK293 cells stably over-expressing GFP MYPT1 protein using CRISPR/Cas9).	75
2.2.1.8 Agarose gel electrophoresis	77
2.2.1.9 DNA sequencing	77

2.2.2 MAMMALIAN CELL CULTURE	77
2.2.2.1 Cell culture	77
2.2.2.2 Freezing/thawing of cell lines	77
2.2.2.3 Transfection of cells using polyethylenimine (PEI)	78
2.2.2.4 Treatment of cells with inhibitors and other agents	78
2.2.2.5 Generation of stable cell lines	78
2.2.2.6 Cell/tissue lysis.....	79
2.2.3 PROTEIN BIOCHEMISTRY	79
2.2.3.1 Purification of GST recombinant proteins from HEK293 cells	79
2.2.3.2 Estimation of protein concentration.....	79
2.2.3.3 Covalent coupling of antibodies	80
2.2.3.4. Immunoprecipitation.....	81
2.2.3.5 Resolution of protein samples via SDS-PAGE	81
2.2.3.6 Resolution of protein samples via Phos-tag gel and immunoblot analysis.....	82
2.2.3.7 Coomassie staining of polyacrylamide gel.....	83
2.2.3.8 Desiccation of polyacrylamide gels and autoradiography.....	84
2.2.3.9 Transfer of proteins onto nitrocellulose membranes.....	84
2.2.3.10 Immunoblotting.....	84
2.2.4 IN-VITRO ASSAYS	85
2.2.4.1 Kinase assay.....	85
2.2.5 MASS SPECTROMETRY ANALYSIS	86
2.2.5.1 Processing protein bands for analysis by mass spectrometry.....	86
2.2.5.2 Processing protein bands for analysis by mass spectrometry.....	86
2.2.5.3 <i>In vitro</i> ³² P-labelling of proteins and phospho-sites mapping using HPLC and Edman degradation	87
2.2.5.4 <i>In vivo</i> Phospho-site mapping of LRRK2 substrate	88
2.2.6 MOUSE MODEL	89
2.2.6.1 Generation of LRRK2 knock-in mouse model of the corresponding S910A+S935A mutations.....	89
2.2.6.2 Genotyping of mice via PCR	90
2.2.6.3 Mouse motor phenotyping: rotarod test	91
2.2.6.4 Lysis of mouse tissues	92
2.2.6.5 Generation of LRRK2 [S910A+S935A] mouse embryonic fibroblasts (MEFs).....	92
2.2.6.6 Statistics.....	92
Chapter 3: <i>Characterization of LRRK2 [S910A+S935A] Mouse Model</i>	94
3.1 Introduction	95
3.2 Results	98
3.2.1 Generation of mouse embryonic fibroblasts	98
3.2.2 Assessment of endogenous LRRK2 WT and LRRK2 [S910A+S935A] kinase activity in vitro	100
3.2.3 Assessment of endogenous LRRK2 WT and LRRK2 [S910A+S935A] kinase activity in vivo	101
3.2.4 Assessment of total endogenous LRRK2 expression levels in 4 months old LRRK2 [S910A+S935A] and LRRK2 WT mice tissues	105
3.2.5 Histopathological evaluation of LRRK2 WT and LRRK2 [S910A+S935A] mouse kidneys.	111
3.2.6 Histopathological evaluation of LRRK2 WT and LRRK2 [S910A+S935A] mouse lungs.	116
3.2.6.7 Behavioural phenotyping of LRRK2 [S910A+S935A] knock-in mouse model.....	119
3.2.7 Histopathological evaluation of LRRK2 WT and LRRK2 [S910A+S935A] mouse brain.	125
3.3 Summary.....	133

Chapter 4: <i>Investigating MYPT1 as a Potential LRRK2 Substrate</i>	136
4.1 Introduction	137
4.2 Results	140
4.2.1 MYPT1 is phosphorylated by LRRK2 in vitro at T500, T524, T529, T671, T761 and T891	140
4.2.2 Mutation of T500, T524, T529, T671, T761 and T891 to alanine only reduces but does not abolish MYPT1 phosphorylation by LRRK2 <i>in vitro</i>	144
4.2.3 In over-expressed system there are no significant changes in MYPT1 phosphorylation because of LRRK2 kinase inhibitor treatment.....	145
4.2.4 In MEFs, inhibition of endogenous LRRK2 with ML-I inhibitor, results in a trend of T500 and T671 phosphorylation reduction.....	152
4.2.5 Validation of MYPT1 phospho-T500 antibody	158
4.2.6 Evidence that endogenous LRRK2 does not interact with MYPT1 in MEF cells.....	160
4.2.7 Generation of MYPT1 KO cells.....	162
4.2.7.1 Attempt to generate MYPT1 KO cells using TALENs.....	162
4.2.7.2 Attempt to generate MYPT1 KO cells using Crispr/Cas9 technology.....	167
4.3 Summary	171
Chapter 5: <i>Validation of Mass Spectrometry Hits</i>	173
5.1 Introduction	174
5.2 Results	175
5.2.1 Studies undertaken to attempt to validate RPS15 protein as LRRK2 substrate.....	175
5.2.2 Proteomic fingerprint analysis of endogenous LRRK2 immunoprecipitated from MEF WT, MEF [S910A+S935A] and MEF KO cells.....	186
5.2.3 Validation of proteomic hits in over-expressed cells.....	192
5.2.3.1 Attempt to validate PALM as an interactor of LRRK2.....	192
5.2.3.2 Validation of other proteomic hits by <i>in vitro</i> phosphorylation.....	205
5.2.4. LRRK2 might not be a threonine specific kinase	206
5.2.5 MAP4 kinases phosphorylate LRRK2 Ser910 and Ser935 in vitro but not in vivo	212
5.3 Summary	215
BIBLIOGRAPHY	218

LIST OF FIGURES

Figure 1.1: Schematic representation of the fight-or-flight response	20
Figure.1.2: Summary of protein phosphorylation and its function.....	21
Figure 1.3: The Human Kinome.....	25
Figure 1.4: Schematic ribbon representation of the subdomain structure of a kinase domain of Abl tyrosine kinase inhibited by imatinib	29
Figure 1.5: Schematic diagram of Parkin protein.....	38
Figure 1.7: Schematic diagram of PINK/Parkin mechanistic interplay	40
Figure 1.8: Schematic representation of the LRRK2	44
Figure 1.9: LRRK2 phosphorylates Rab10 at T73 located within switch II domain	50
Figure 1.10: Evidence points to LRRK2 inhibiting Rab isoforms by preventing association with GDIs and GEF	51
Figure 1.11: Overview of PINK1 and LRRK2 converge on regulating Rab GTPase biology	53
Figure 3.1: Schematic representation of LRRK2 protein highlighting S910 and S935 location	95
Figure 3.2: Schematic representation of LRRK2 S910 and S935 regulation within the cell under normal and inhibitor-treated conditions	97
Figure 3.3: Targeting strategy for generation of LRRK2 [S910A+S935A] knock-in mice by Taconic Artemis, PCR and sequencing data	98
Figure 3.4: Generation of LRRK2 [S910A+S935A] knock-in MEFs.....	99
Figure 3.5: Assessment of immunoprecipitated endogenous LRRK2 kinase activity from LRRK2 [S910A+S935A] and LRRK2 WT MEFs.....	101
Figure 3.6: Use of the Phos-tag approach to assess the impact of LRRK2 S910A/S935A mutations on its substrate Rab10	103
Figure 3.7: Use of the Phos-tag approach to assess the impact of LRRK2 S910A/S935A mutations on its substrate Rab8A.....	104
Figure 3.8: Schematic representation of the LRRK2 protein domain structure	106
Figure 3.9: Assessment of total LRRK2 expression levels in LRRK2 WT and LRRK2 [S910A+S935A] knock-in brain.....	108
Figure 3.10: Assessment of total LRRK2 expression levels in LRRK2 WT and LRRK2 [S910A+S935A] knock-in kidneys.....	109
Figure 3.11: Assessment of total LRRK2 expression levels in LRRK2 WT and LRRK2 [S910A+S935A] lungs.....	111
Figure 3.12: Overview of LRRK2 [S910A+S935A] phenotype	113
Figure 3.13: A representative image showing that there is no kidney pathology in LRRK2 [S910A+S935A] mice	114
Figure 3.14: Histological evaluation of mouse lungs	118
Figure 3.15: Assessment of body weight in relation to its gender and genotype	120
Figure 3.16: The overview of Rotarod.....	121
Figure 3.17: Behavioural phenotyping of LRRK2 [S910A+S935A], WT and KO mice. (A) Rotarod accelerating speed	123
Figure 3.18: Behavioural phenotyping of LRRK2 [Ser910Ala+Ser935Ala], WT and KO mice.....	124
Figure 3.19: Dopamine system and pathological changes in the SN	128
Figure 3.20: Changes of dopamine synthesis in axon terminals in the dorsolateral striatum	130
Figure 3.21: Assessment of total VMAT2 and LRRK2 levels in young and aged LRRK2 WT and LRRK2 [S910A+S935A] mice	132
Figure 4.1: Comparative phosphoproteomic analysis of LRRK2 WT vs LRRK2 [A2016T] MEF cells (two sample t-test, FDR=2%) Data generated by Martin Steger from Matthias Mann's lab	138
Figure 4.2: Proposed model of LRRK2 regulation	140
Figure 4.3: MYPT1 phosphorylation by LRRK2 in vitro	142
Figure 4.4: LRRK2 phosphorylates MYPT1 at T500, T524, T529, T671, T761 and T892	143
Figure 4.5: Mutation of T500+T524+T529+T671+T761+T892 to alanine reduces LRRK2 phosphorylation in vitro	145
Figure 4.6: Assessment of MYPT1 phosphorylation in HEK23 cells o/e LRRK2 G2019S	147
Figure 4.7: Assessment of MYPT1 phosphorylation in HEK23 cells o/e LRRK2 G2019S	149
Figure 4.8: Assessment of MYPT1 phosphorylation in HEK23 cells o/e LRRK2 G2019S	151
Figure 4.9: Assessment of MYPT1 phosphorylation in MEF cells	154
Figure 4.10: Assessment of MYPT1 phosphorylation in MEF cells	157
Figure 4.11: Validation of MYPT1 pT500 antibody	159
Figure 4.12: Validation of MYPT1 pT500 antibody	160

Figure 4.13: Co-immunoprecipitation of LRRK2 with MYPT1	161
Figure 4.14: A schematic representation of TALENs.....	164
Figure 4.15: Example of MYPT1 knockout screening.....	166
Figure 4.16: Generation of MYPT1 null cell lines using Crispr/Cas9 technology	170
Figure 5.1: RPS15 is phosphorylated by LRRK2 in vitro	176
Figure 5.2: Mapping of RPS15 phosphorylation site	179
Figure 5.4: Assessment of pT136 and total RPS15 antibody on purified RPS15 protein phosphorylated by LRRK2 in vitro	182
Figure 5.5: Assessment of total RPS15 antibody in over-expressed cells	184
Figure 5.6: Assessment of pT136 RPS15 antibody in over-expressed cells	185
Figure 5.7: Conserved organization of paralemmin isoform genes	193
Figure 5.8: Validation of mass spectrometry hits in over-expressed cells	195
Figure 5.9: PALM interaction with LRRK2 is not affected by LRRK2 kinase activity	197
Figure 5.10: Co-immunoprecipitation of HA-PALM with Flag-LRRK2 fragments	198
Figure 5.11: PALM co-expression with different proteins in Hek293 cells.....	200
Figure 5.12: HA-tagged PALM co-localization with GFP-tagged LRRK2 proteins in Hek293 cells..	201
Figure 5.13: Assessment of PALM isoforms phosphorylation by LRRK2 in vitro	202
Figure 5.14: Assessment of PALM phosphorylation by LRRK2 in vitro	204
Figure 5.15: In vitro phosphorylation screen by LRRK2	206
Figure 5.16: Determination of the preferred T/S phosphorylation site for LRRK2	211
Figure 5.17: MAP4K3 phosphorylates LRRK2 in vitro at S910 and S935	213
Figure 5.18: LRRK2 S935 phosphorylation is not affected by deletion of MAP4K1-9 isoforms	214

LIST OF TABLES

Table 1.1: Kinases mutated in human diseases	29
Table 1.2: Genes linked to Parkinson’s disease	34
Table 1.3: The criteria for validating LRRK2 substrate	49
Table 2.1: List of in-house antibodies	65
Table 2.2: List of commercial antibodies used in this thesis	66
Table 2.3: Mammalian expression constructs.....	66
Table 2.4: Bacterial expression constructs	67
Table 2.5: Kinase and phosphatase inhibitors	69
Table 2.6: Buffers and compositions.....	70
Table 2.7: TALENs construction details	74
Table 2.8: CRISPR/Cas9 construction details	75
Table 3.1: Histological evaluation of mouse kidneys	115
Table 3.2: Histological evaluation of mouse lungs.....	117
Table 3.3: Mean and standard error for the estimated percentages relative to WT of subcortical and hippocampal cells in the different genotypes covarying for gender	126
Table 3.4: Calculated numbers of TH-positive dopamine neurons in SNC	127
Table 4.1: Comparative mass-spectrometry analysis of LRRK2 immunoprecipitates from LRRK2 WT, LRRK2 [Ser910Ala+Ser935Ala] and LRRK2 KO MEFs	162
Table 4.2: CRISPR/Cas9 construction details	168
Table 5.1.A: Identity of proteins found in immunoprecipitates derived from LRRK2 WT but not LRRK2 KO MEFs.....	187
Table 5.1.B: Identity of proteins found in immunoprecipitates derived from LRRK2 WT but not LRRK2 [S910A+S935A] or LRRK2 KO MEFs	188
Table 5.1.C: Identity of proteins found in immunoprecipitates derived from LRRK2 [S910A+S935A] but not LRRK2 KO MEFs	190
Table 5.1.D: Identity of proteins found in immunoprecipitates derived from LRRK2 [S910A+S935A] but not LRRK2 WT or LRRK2 KO MEFs.	191

Chapter 1:

Introduction

1.1 Signal transduction

All living organisms are made of cells. The cell is the basic unit of life and in order to survive, cells must respond to changes in the surrounding environment that would allow them to navigate towards nutrients, to communicate with other cells and to divide. Often, a single cell is subjected to numerous signals at the same time, and it then assimilates the information it encounters into a mechanism of action called cell signal transduction. Usually, cell signal transduction begins with the external signal molecule (for instance, a growth factor, hormone or amino acid) binding to a receptor situated in the cell membrane. Following stimulation of the receptor, activation of different cellular enzymes leads to a cell's response.

To transmit and amplify signals, cells employ specific intracellular molecules like enzymes and small molecules called secondary messengers (for instance, Ca^{2+} or cAMP). Activated enzymes propagate the signal by catalysing a huge number of distinct enzymatic reactions such as a covalent attachment or a proteolytic cleavage. On the other hand, secondary messengers diffuse in large quantities, bind and trigger signalling proteins. As a result, enzymes and secondary messengers activate a chemical transmission to their downstream effectors.

One interesting example of cell signaling transduction is the fight-or-flight response, which takes place when a harmful event or threat for survival is encountered. In a situation of stress, adrenaline is released. The binding of adrenaline to an adrenergic receptor, situated in the liver cell's plasma membrane, starts a cascade of reactions inside the cell. Adenylyl cyclase, a membrane-bound enzyme, becomes activated by G-protein molecules associated with the adrenergic receptor. Activated adenylyl cyclase catalyses the formation of multiple cAMP molecules, which diffuse within the

cytoplasm, bind and activate protein kinase A (PKA). In the liver, PKA phosphorylates another enzyme, glycogen phosphorylase, which converts glycogen into glucose-6-P (Figure 1.1).

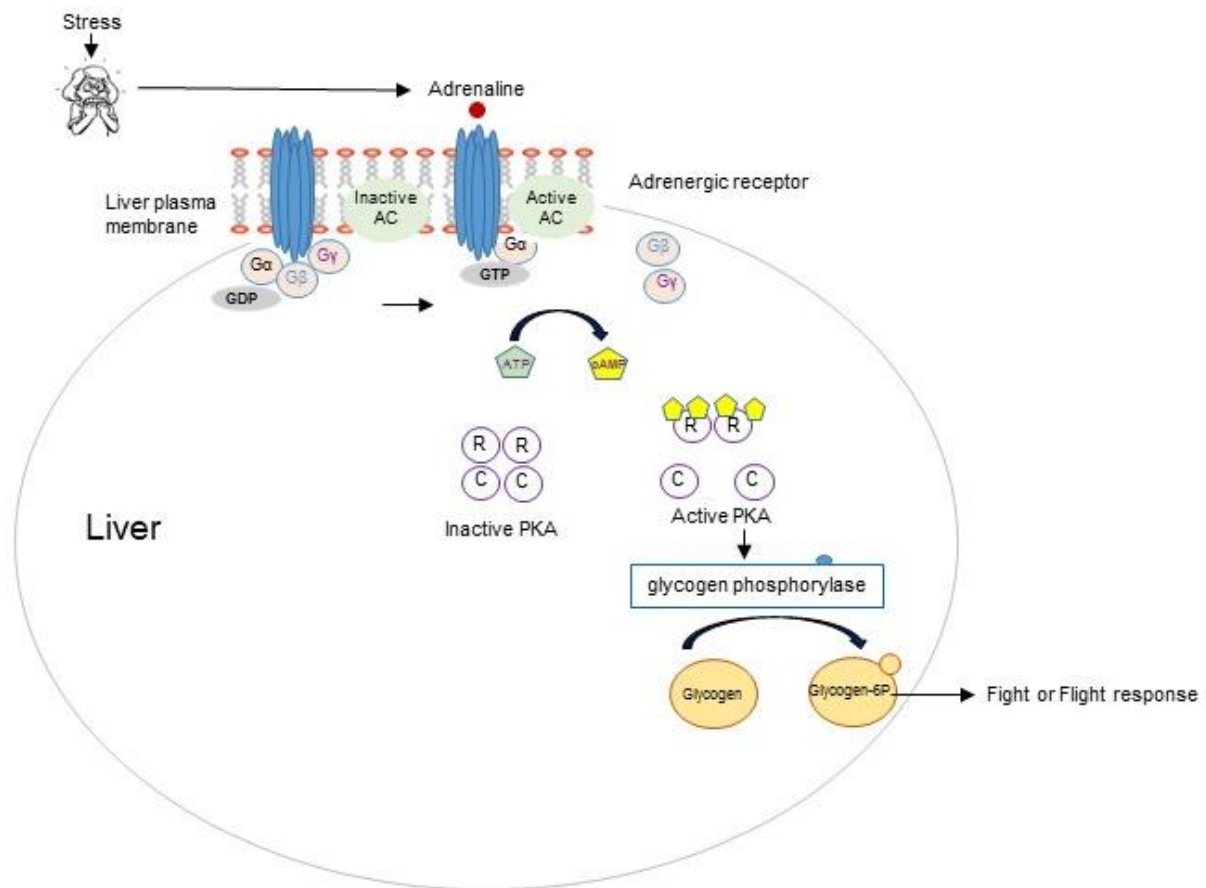


Figure 1.1: Schematic representation of the fight-or-flight response. During stress, adrenaline is released from adrenal glands. The binding of adrenaline to an adrenergic receptor, situated in the liver cell's plasma membrane activates adenylyl cyclase, which then catalyses the formation of cAMP that diffuse through the cytoplasm and trigger the activity of a PKA. Activated PKA phosphorylates glycogen phosphorylase that converts glycogen into glycogen-6P. Glucose is then secreted into the blood and used for fight-or-flight response.

Through this cell signalling cascade adrenaline provokes the liver to secrete glucose into the blood during the fight-or-flight response. Increased concentration of glucose in blood supplies body with extra energy resulting into a visible increase in strength and performance (Lehninger Principles of Biochemistry, 2008).

1.2 Protein phosphorylation

1.2.1 The significance of protein phosphorylation in signal transduction

Phosphorylation is performed by enzymes called protein kinases, which catalyse the transfer of the γ -phosphate from ATP to specific amino acid residues of the substrate protein. It was shown that in eukaryotes these are typically Ser, Thr and Tyr amino acids (Ubersax & Ferrell, 2007). Protein kinases are encoded by one of the largest families of genes in eukaryotes as they contribute almost to 2% of the genome (Rubin et al., 2000). As a matter of fact, protein kinases phosphorylate approximately 30% of human proteins (Manning, 2005). Not surprisingly, protein phosphorylation is a very important type of post-translational modification observed in signal transduction as it affects every cellular aspect, including metabolism, growth, division, differentiation, motility, organelle trafficking, membrane transport, muscle contraction, immunity, learning and memory. Phosphorylation is a reversible process and it is controlled by protein phosphatases. Phosphorylation and dephosphorylation can alter the function of a protein in almost every possible manner (Figure 1.2).

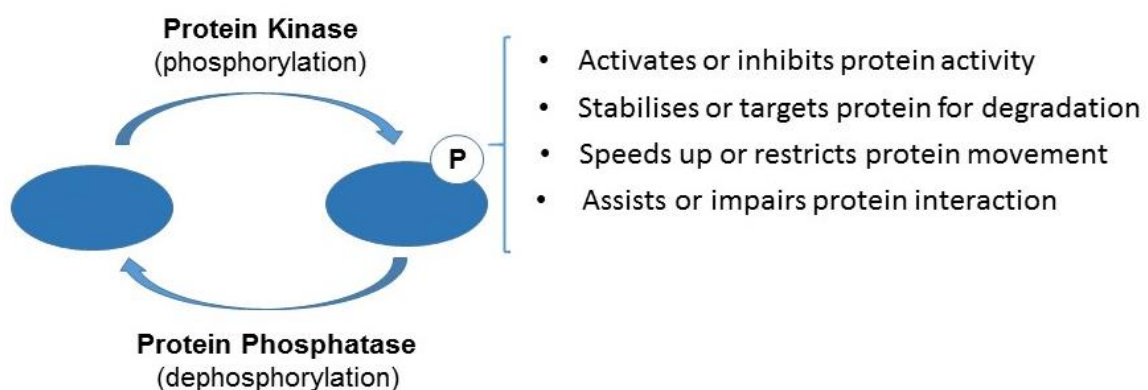


Figure.1.2: Summary of protein phosphorylation and its function. Protein phosphorylation is catalysed by protein kinases whereas protein dephosphorylation is catalysed by protein phosphatases. Phosphorylation can alter a targeted protein in different ways, including protein activity, stability, localization and its interaction.

This is because the phosphate group is negatively charged and its addition or removal results in a local charge change. As a consequence, this can lead to an increased or decreased biological activity of the enzyme, stabilise it or target it for destruction. Furthermore, phosphorylation may speed up or restrict the movement of the enzyme between subcellular organelles, assist or inhibit protein–protein interactions. The simplicity, and reversibility of phosphorylation together with the availability of ATP, as a phosphoryl donor, justifies its selection as the most universal regulatory mechanism acquired by eukaryotic cells (Cohen, 2000).

Kinase activity was first mentioned in 1954 when Gene Kennedy described a liver enzyme, which catalysed the phosphorylation of casein (Burnett & Kennedy, 1954). Soon after its discovery, Fischer and Krebs revealed that the interconversion of phosphorylase *b* to phosphorylase *a* was associated with a phosphorylation/dephosphorylation process (Fischer & Krebs, 1955). In particular, they demonstrated that the *b* form could be transformed to the *a* form in the presence of Mg^{2+}/ATP and an enzyme they termed phosphorylase kinase (Krebs & Fischer, 1956). Phosphorylase kinase was consequently shown by other groups to catalyse the transfer of the γ -phosphoryl group of ATP to a specific serine residue on phosphorylase *b* (Fischer, Graves, Crittenden, & Krebs, 1959). Furthermore, in 1950, Earl Sutherland demonstrated that glycogenolysis could be triggered if liver slices were incubated with adrenalin (Robison & Sutherland, 1971). Then he established that the activity of phosphorylase *a* was augmented under these conditions, revealing that a hormone could influence the activity of a protein kinase. Recent research in the field of phosphorylation pushed forward the development of specific protein kinase inhibitors for treating different human diseases such as cancer. The

remarkable importance of protein kinases phosphorylation explains a huge scientific interest in this area.

1.2.2 Protein kinases - the human kinome

The discovery of the first protein kinase in the late fifties led to subsequent findings of other protein kinases. It turned out that kinases share a similar conserved catalytic region (kinase domain) of approximately 250-300 residues, which is responsible for the transfer of a γ -phosphate from ATP to its substrate, but considerably differentiate outside the kinase region. Interestingly, these distinct regions of the kinase often comprise other auxiliary domains that provide it with additional function including specific localization, protein-protein interaction or even another catalytic activity. In 2001, the Human Genome Project allowed for the sequencing of the entire human genome. This permitted to identify all 518 human protein kinases (Manning, Whyte, Martinez, Hunter, & Sudarsanam, 2002). The identified kinases were arranged in a phylogenetic tree based on their evolutionary deviations of the kinase domain residues, creating the so called kinome (Figure 1.3). Based on sequence similarity the human kinome is divided into seven major groups: AGC (PKA, PKC and PKG family), CAMK (Ca^{2+} /Calmodulin-dependent kinases family), CK1 (Caesin kinase 1 family), CMGC (CDK, MAPK, GSK3 and CLK family), STE (homologues of the yeast Sterile kinase family), TK (Tyrosine kinases family) and TKL (Tyrosine-kinase like family) (Manning et al., 2002). Members of the same group are normally activated and regulated in a similar fashion as well as have similar substrate preference.

In addition, there is also another group of kinases called atypical kinases, which does not share the sequence similarity with the rest of the kinome but folds in the same three-dimensional structure and possesses the same kinase activity. Remarkably, about 10% of members of the human kinome are so-called

pseudokinases that have preserved the kinase fold but that have lost important catalytic residues (Manning et al., 2002). The role of pseudokinases remains unclear, however it was hypothesized that these proteins might serve as a scaffold for other proteins or allosterically control another functional kinase (Boudeau, Miranda-Saavedra, Barton, & Alessi, 2006).

Legend:
 Protein in PDB database
 Protein used in Karaman et al. 2008
 Protein in both Karaman and the PDB database

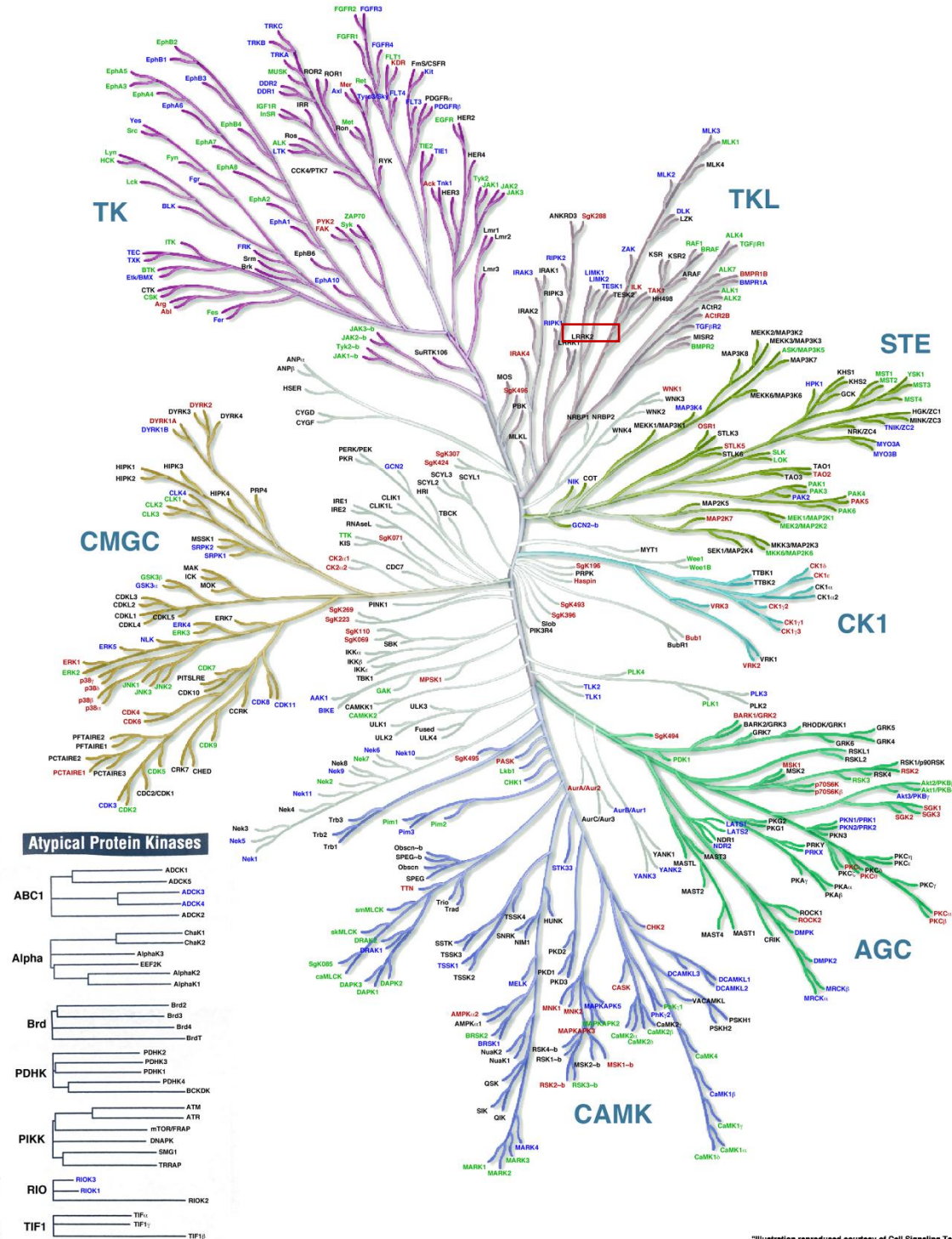


Figure 1.3: The Human Kinome. Phylogenetic tree of human protein kinases adopted from (Chartier, Chenard, Barker, & Najmanovich, 2013). LRRK2 is highlighted in red.

1.2.3 General characteristics of protein kinase

For the first time, the crystal structure of a catalytic domain of cyclic adenosine monophosphate (cAMP)-dependent protein kinase (PKA) was solved by Knighton in 1991 (Knighton et al., 1991). Further studies by distinct groups have revealed that the kinase domain is very well conserved (Hanks & Hunter, 1995). In fact, a kinase fold usually possesses roughly 250-300 amino acids, which form 12 subdomains arranged into two lobes (Figure 1.4). The role of the smaller N-terminal lobe (N-lobe) is to bind and coordinate ATP whereas the larger C-terminal lobe (C-lobe) is responsible for substrate binding and for providing the residues that are crucial for catalysis. The N-lobe (subdomains I-IV) is composed of five-stranded β -sheets and one α -helix called the C-helix while the C-lobe (subdomains VI-XII) is composed of six α -helices. In addition, the two lobes are interconnected by a hinge region, which forms a part of the active site and allow them to be flexible to acquire active or inactive conformations.

In the N-lobe, the subdomain I contains a flexible glycine rich loop with a GxGxxG motif (where "x" stands for any amino acid) and the subdomain II comprises a conserved lysine in the VAIK motif, which binds to and coordinates the α and β phosphates of ATP by main-chain amide interactions. This interaction is maintained by subdomain III. The C-lobe comprises an essential HRDxxxN motif of subdomain V positioned in the catalytic loop. It contains an aspartate, which acts as a base of phosphotransfer and of an asparagine residue that sustains the catalytic loop and chelates the secondary Mg^{2+} ion. Another highly conserved DFG motif of subdomain VII includes an important aspartate residue that chelates the primary Mg^{2+} and secures correct positioning of the γ phosphate of ATP. Subdomain VIII possesses the substrate binding motif APE, which contains a glutamic acid that makes a salt

bridge with the conserved arginine in subdomain XI in order to promote stability of the C-lobe. The region between the DFG and APE motifs is called the activation loop (or T-loop) that contains the crucial Ser/Thr residue (Hanks & Hunter, 1995).

Kinases are normally activated by phosphorylation within the T-loop, which is responsible for the rearrangement of the C-helix and the stabilization of the N- and C-lobes in the active conformation allowing the correct positioning of the substrate. For instance, the maximal activation of PKA-C α subunit takes place upon phosphorylation of Thr197 in the activation loop (Cheng, Ma, Moore, Hemmings, & Taylor, 1998). Moreover, kinases are reported to be capable of phosphorylating themselves, a process called autophosphorylation (cis-phosphorylation) as well as to phosphorylate adjacent kinases with a dimer or a higher order multimer (Hanks & Hunter, 1995). Autophosphorylation is reported to be critical for protein kinase activity and/or stability. Sometimes, a stimulus is needed to prime a substrate so that kinase can phosphorylate it. For instance, GSK3 can only phosphorylate numerous substrates after these are phosphorylated three residues away by a priming kinase such as casein kinase 2 (CK2) (Hagen & Vidal-Puig, 2002). The other example is the ribosomal protein S6 kinase 1 (S6K1), which phosphorylates S6K1 on the hydrophobic motif at the conserved threonine residue Thr 389. This phosphorylation causes a docking site for phosphoinositide-dependent kinase-1 (PDK1), which subsequently phosphorylates S6K1 on the T loop at the conserved threonine residue Thr 229 promoting full activity of S6K (Frodin et al., 2002).

The majority of the kinases phosphorylate their specific substrates at a specific site. In fact, by analysing different substrates of a particular kinase a possible consensus motif sequence could be deduced. The consensus sequence stands for the amino acid preference for this particular kinase around the Ser/Thr or Tyr phosphorylation

site. For example, a consensus sequence for phosphorylation site of CDK is [S/T*]PX[K/R], where S/T* stands for the phosphorylated serine or threonine, P for proline, K for lysine, R for arginine and X could be any amino acid (Holt et al., 2009).

As overactivation of multiple protein kinases have been shown to be implicated in several human diseases, over the last decades pharmaceutical companies focused on the development of highly specific structurally based ATP competitive kinase inhibitors in a hope to cure diseases. For example, the drug Imatinib (marketed by Novartis as Glivec) was approved for clinical use in 2001 for the treatment of some types of leukaemia, blood disorders and cancers. It works by specifically inhibiting tyrosine kinases such as Abl kinases. (Figure 1.4)

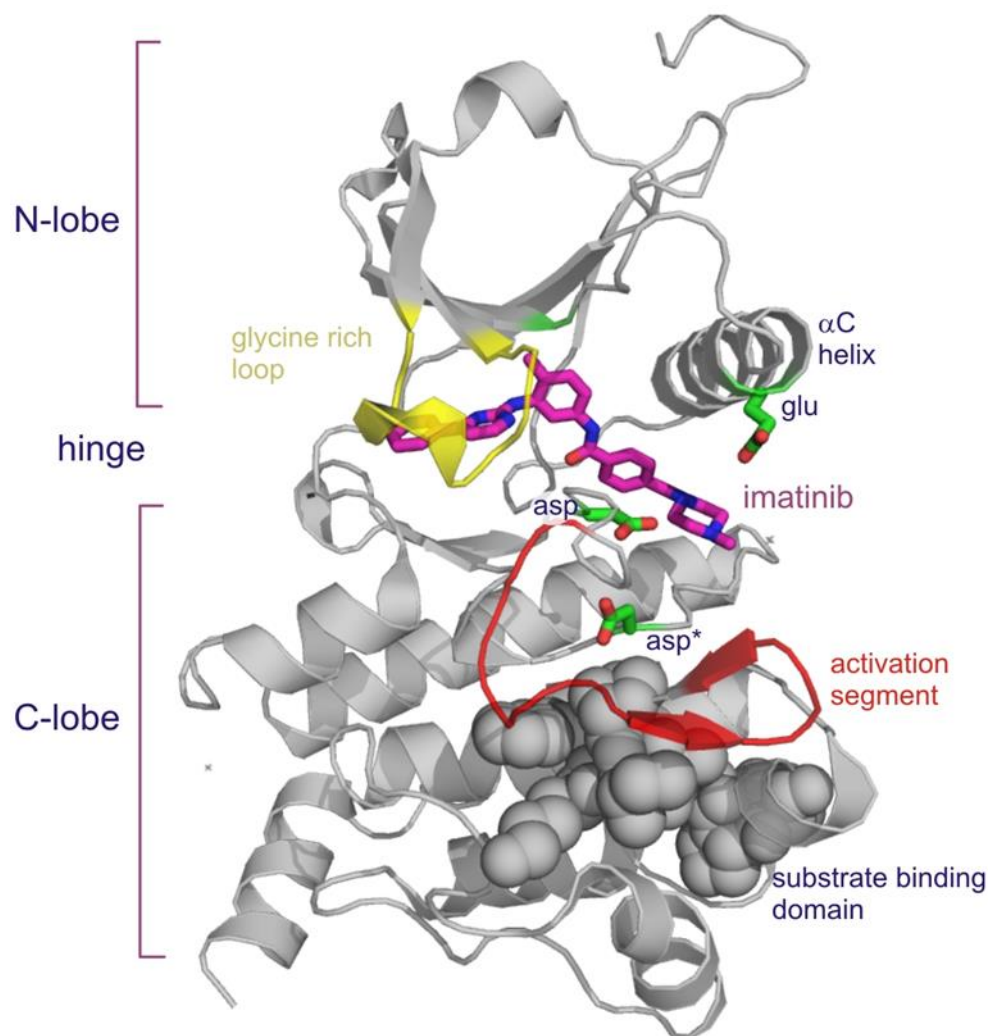


Figure 1.4: Schematic ribbon representation of the subdomain structure of a kinase domain of Abl tyrosine kinase inhibited by imatinib (adopted from Cell Biology Promotion). Imatinib binds the ATP binding pocket of the kinase inhibiting the kinase. The activation segment is not phosphorylated and hides the substrate binding site. Glu and Asp are no longer coordinating ATP binding.

1.2.4 Phosphorylation and human disease

As mentioned previously, protein phosphorylation is important in cell signal transduction and is likely to influence every possible cellular process. In spite of the fact that kinases experience a selective pressure to prevent genetic mutations, they still take place. This could lead to inactivation of a kinase, an abnormal increase in its activity, mislocalization or aggregations, subsequently resulting in serious human diseases. Table 1.1 summarized some of protein kinases identified to be mutated in inherited human diseases (Lahiry et al, 2010).

Table 1.1: Kinases mutated in human diseases.

Protein Kinase	Human disease
ABL	Chronic myeloid leukemia
ALK1	Hereditary haemorrhagic telangiectasia type 2
AMRH2	Persistent Muellerian dust syndrome
AMPK	Wolff-Parkinson-White Syndrome
ATM	Ataxia telangiectasia
ATR	Seckel syndrome type 1
BMPR1A	Juvenile polyposis syndrome primary pulmonary hypertension
BMPR2	Primary pulmonary hypertension
B-Raf	Cardiofaciocutaneous syndrome (CFC), melanoma, sporadic cancers
BTK	X-linked agammaglobulinemia
CASK	X-linked mental retardation
CDK4	Melanoma, sporadic cancers
CDKDL5	X-linked infantile spasm syndrome
CHK2	Li-Fraumeni syndrome, sporadic cancers
CHK1δ	Familial advanced sleep phase syndrome
DMPK	Myotonic dystrophy
EGFR	Non-small cell lung cancers
EIF2AK3	Wolcott-Rallison syndrome
ERBB2	Hereditary familial diffuse gastric cancer, glioma
FGFR1	Kallmann syndrome, Pfeiffer syndrome

FGFR2	Apert syndrome, Antley-Bixler syndrome, Beare-Stevenson cutis gyrate syndrome, Crouzon syndrome, Familial scaphocephaly syndrome, Jackson-Weiss syndrome, Pfeiffer syndrome
FGFR3	Achondroplasia, Crouzon syndrome, Muenke syndrome, Thanatophoric dysplasia
FLT3	Acute myeloid leukemia
FLT4	Milroy disease, Juvenile hemangioma
GRK1	Oguchi disease
GRK4	Hypertension
GUCY2D	Leber congenital amaurosis type 1, Cone-rod dystrophy
INSR	Insulin resistance, leprechaunism
IRAK4	Hyporesponsiveness to bacterial infection
JAK2	Polycythaemia
JAK3	Severe combined immunodeficiency
KIT	Gastrointestinal stromal tumours
LCK	Leukaemia
LIMK1	Williams-Beuren syndrome
LRRK2	Hereditary Parkinson's disease
LTK	Systemic lupus erythematosus
MAP2K3	Colon cancer
MAST3	Inflammatory bowel disease
MASTL	Thrombocytopenia
MERTK	Retinitis pigmentosa
MET	Hereditary papillary renal carcinoma
MYLK2	Cardiomyopathy
NTRK1	Congenital insensitivity to pain, thyroid papillary carcinoma
PAK3	X-linked mental retardation
PDGFR β	Chronic myelogenous leukemia
PHK γ 2	Autosomal liver glycogenosis
PI3K	Sporadic cancers
PINK	Hereditary early-onset Parkinson's disease
PKC γ	Spinocerebellar ataxia type 14
PRKX/Y	XX male syndrome and Swyer's syndrome (XY females)
RET	Hirschsprung disease, sporadic cancers
ROR2	Robinow disease
RSK2	Coffin-Lowry syndrome
STK11	Peutz-Jeghers syndrome, sporadic cancers
TEK	Venous malformations
TTBK2	Spinocerebellar ataxia type 11
TGFBR2	Various cancers
WINK1/4	Pseudohypoaldosteronism type II
ZAP70	Severe combined immunodeficiency

1.3 Overview of Parkinson's disease

1.3.1 Introduction to Parkinson's disease

The first clear medical description of Parkinson's disease (PD) as a neurological syndrome was written nearly two hundred years ago, in 1817 by a British physician named James Parkinson in his monograph "An essay on the Shaking Palsy" (Parkinson, 1817). He documented the clinical features as follows (Parkinson, 1817):

Involuntary tremulous motion, with lessened muscular power, in parts not in action and even when supported; with a propensity to bend the trunk forward, and to pass from a walking to a running pace: the senses and intellects being uninjured.

Fifty years later, the French neurologist Jean-Martin Charcot categorized bradykinesia, a slowness of movement, as a separate cardinal symptom of the illness (Parkinson, 2002) and subsequently named it as Parkinson's disease in honour of James Parkinson. Further clinical descriptions and studies presented more clinical and morphological information about Parkinson's disease however it was not until the early twentieth century that the substantia nigra in the midbrain was reported as the most significant pathological hallmark of PD (Greenfield & Bosanquet, 1953). In fact, PD was shown to be characterized by the selective loss of pigmented dopaminergic neurons in the substantia nigra, particularly affecting the ventral component of the pars compacta (Zecca et al., 2001). By the time of death, this region of the brain has lost 50-70% of its neurons compared with the same region in unaffected individuals (Riederer & Wuketich, 1976). Moreover, neurons that survive typically comprise of proteinaceous cytoplasmic inclusions called 'Lewy

bodies', first observed in 1912 by Frederick Lewy in a post-mortem PD brain (Lewy, 1992).

1.3.2 Epidemiology, risk factors and clinical s of Parkinson's disease

Parkinson's disease is one of the most common progressive neurodegenerative disorders that develops over many years, leading to motor symptoms including tremor, rigidity, reduced motor activity and postural instability as well as non-motor symptoms such as cognitive impairment, mood disorders, sleep difficulties, loss of sense of smell, speech and swallowing problems (Dauer & Przedborski). PD is incurable and characterised pathologically by the progressive loss of dopaminergic neurons from the substantia nigra. The substantia nigra cells generate dopamine, a chemical messenger responsible for transmitting signals within the brain that allow for coordination of movement. Loss of dopamine leads to neuronal death without normal control, leaving patients less able to control their movement (Goldenberg, 2008). Parkinson's primarily affects people aged ≥ 50 , however younger people can get it too. It is estimated that one in every 500 has PD, which is about 127,000 people in the UK (Parkinson's UK data). Moreover, the majority of studies report men to be slightly more often affected than females (Gillies, Pienaar, Vohra, & Qamhawi, 2014). Furthermore, some studies suggest that the incidence of PD varies according to the race or the ethnicity, and it is the highest among Hispanics, followed by non-Hispanic Whites, Asians and Blacks (Gillies et al., 2014). With the world aging population, the management of PD is likely to prove to be a very vital and challenging task of medical practice and general physicians. However, in spite of huge efforts in research, to date there is no treatment to arrest the progression of PD. Available pharmaceutical and surgical methods can only alleviate some of the symptoms and are associated with serious side effects but do not slow the

progression of the disorder. Furthermore, identification of environmental factors that predispose to the development of PD has proven difficult. It was suggested by several studies that living in a rural environment appears to increase the risk of PD (Berry, La Vecchia, & Nicotera, 2010). This was justified by the fact that some epidemiological studies have shown a correlation between exposure to pesticide use and wood preservatives. Interestingly, the only consistent environmental factor is a strong negative correlation between cigarette smoking, caffeine intake and the development of the disease (Checkoway et al., 2002) and the most reliable risk factor for developing PD is a positive family history. The mechanism by which smoking might protect PD is unclear.

1.3.3 Genetics of Parkinson's disease

The cause of PD remains unknown and it is usually described as a sporadic disease. However, our understanding of the pathogenesis of the disease has been boosted in the last decade with the identification of several gene mutations, which might give some insights on the mechanism of pathogenesis in sporadic PD (Klein & Westenberger, 2012). Investigation of these genes and proteins that they encode for provide significant understanding into the mechanism of the disease. Once we comprehend the mechanism it will be possible to develop better treatments for PD by identifying and therapeutically exploiting key molecules involved in the pathogenic process. The most evident genes linked to PD are summarised in Table 1.2.

Table 1.2: Genes linked to Parkinson's disease (LRRK2 is highlighted in red).

LOCUS	MODE	TYPE	GENE	FUNCTION	REFERENCES
PARK 1/4	Autosomal-dominant	Early/Late onset PD	α -synuclein	Unknown	(Polymeropoulos et al., 1997)
PARK 2	Autosomal-recessive	Early onset PD	Parkin	Ubiquitin ligase	(Lucking et al., 2000)
PARK 3	Autosomal-dominant	Late onset PD	Unknown		(Gasser et al., 1998)
PARK 5	Autosomal-dominant	Late onset PD	UCH-L1	DUB	(Y. Liu, Fallon, Lashuel, Liu, & Lansbury, 2002)
PARK 6	Autosomal-recessive	Early onset PD	PINK1	Kinase	(Valente et al., 2004)
PARK 7	Autosomal-recessive	Early onset PD	DJ-1	Oxidative Chaperone	(Bonifati et al., 2003)
PARK 8	Autosomal-dominant	Late onset PD	LRRK2	Kinase	(Paisan-Ruiz et al., 2004; Zimprich et al., 2004)
PARK 9	Autosomal-recessive	Early onset PD	ATP13A2	ATPase	(Ramirez et al., 2006)
PARK 10	Complex	Late onset PD	Unknown		(Farrer et al., 2006)
PARK 11	Complex	Late onset PD	GIGYF2		(Lautier et al., 2008)
PARK 12	X-linked	Late onset PD	Unknown		
PARK 13	Autosomal-dominant	Late onset PD	HtrA2/Omi	Serine protease	(Strauss et al., 2005)
PARK 14	Autosomal-recessive	Early onset PD	PLA2G6	Phospholipase A2	(Yoshino et al., 2010)
PARK 15	Autosomal-recessive	Early onset PD	FBXO7	F Box protein	(Di Fonzo et al., 2009)
PARK 16	Complex	Late onset PD	Rab7L1 and 4 other genes		(Satake et al., 2009)
PARK 17	Complex	Late onset PD	GAK	Kinase	(Y. P. Chen et al., 2013)
PARK 18	Complex	Late onset PD	HLA	Immune recognition	(Hamza et al., 2010)
PARK 19	Autosomal-dominant	Late onset PD	VPS35	Vesicle trafficking	(Vilarino-Guell et al., 2011)
PARK 20	Autosomal-dominant	Late onset PD	EIF461	m-RNA translation initiation	(Quadri et al., 2013)
PARK 21	X-linked	Early onset PD	RAB39B	Vesicle trafficking	(Lochte et al., 2016)
PARK22	Autosomal-dominant	Late onset PD	CHCHD2	Transcription factor	(Funayama et al., 2015)
PARK23	Autosomal-recessive	Early onset PD	VPS13C	Vesicle trafficking	(Lesage et al., 2016)

1.3.4 Autosomal Dominant Parkinson's disease

It has been reported by several studies that mutations in the α -synuclein gene (SNCA) and leucine-rich repeat kinase 2 (LRRK2) are the most common mutations that lead to familial autosomal dominant PD.

A lot of attention was focused on α -synuclein protein as it was found as a main component of Lewy body aggregates identified in post-mortem brain of sporadic and inherited (Spillantini et al., 1997). In 1997, mutations in SNCA were for the first time shown to be linked to PD in an Italian kindred and three unrelated families of Greek origin with autosomal-dominant inheritance for the PD phenotype (Polymeropoulos et al., 1997). Mutations are responsible of autosomal dominant early-onset PD (<40 years) (Conway, Harper, & Lansbury, 1998). To date five missense mutations including A53T, A30P, E46K, G51D and H50Q as well as gene duplications and triplications have been described in different families of Greek, Korean, Swedish, German and Spanish origin (Klein & Westenberger, 2012). Penetrance of mutations tends to be high and brain pathology is characterized by abundant α -synuclein-positive neuronal inclusions. In spite of a lot of effort being made there is not much information regarding SNCA function and it remains unknown. SNCA is described as a presynaptic protein thought to be implicated in neuronal plasticity (Stefanis, 2012). In addition, SNCA is known to be natively unfolded and be able to form toxic protofibrils (Conway et al., 2000). Several missense mutations have been reported to accelerate the formation of these and lead to formation of toxic β -sheets (Wise-Scira, Aloglu, Dunn, Sakallioglu, & Coskuner, 2013). The occurrence of gene duplications or triplications leads to an early onset of clinical symptoms with a more severe phenotype and faster progression with increased gene dosage (Ross et al., 2008).

In 2004, the human leucine-rich repeat kinase 2 (LRRK2) gene was identified as the most common causative gene of autosomal-dominant inherited and sporadic PD (Paisan-Ruiz et al., 2004; Zimprich et al., 2004). It accounts for 1-2% of all Parkinson's cases (Pankratz & Foroud, 2007). The frequency in familial cases is 5-15% while in sporadic cases it is around 1%, and it is clinically indistinguishable from typical, idiopathic and late-onset PD (Klein & Westenberger, 2012). Thus, the LRRK2 protein has emerged as a promising therapeutic target for the treatment of PD. LRRK2 G2019S is a particularly common mutation, occurring in up to 2-7% of Caucasian cases of familial Parkinson's disease and 1% in sporadic cases (J. Q. Li, Tan, & Yu, 2014). In total, over 50 variants have been identified in LRRK2 thus far, but only some of them were consistently proven to be pathogenic. Amongst them is the G2019S mutation that is the most common one with a frequency of 2% in the North American clinical populations and the British Parkinson's Disease Brain Bank specimens, and it is particularly frequent in Ashkenazy Jewish, Portuguese and North African Arabian PD patients even in the absence of a clear family history (Hardy, Cai, Cookson, Gwinn-Hardy, & Singleton, 2006). In general, the clinical characteristics of patients with the LRRK2 gene mutations, in particular those with the common G2019S mutation, are very similar to those of idiopathic PD (Williams-Gray et al., 2006). Nigrostriatal cell loss and gliosis are common observations in patients with LRRK2 mutations, and the majority also have Lewy bodies. The structure of LRRK2 has not been solved yet. Yet it is known that LRRK2 possesses kinase and GTPase activities both *in vitro* and *in vivo*. The protein domain structure of LRRK2 is discussed in detail later (Section 1.4.2).

1.3.5. Autosomal Recessive Parkinson's disease

Mutations in PARKIN (PARK2), PINK1 (PARK6) and DJ1 (PARK7) are the most common cause of autosomal recessive forms of PD described to date. In this thesis section I will describe two proteins that our laboratory currently is working on: PINK (a kinase) and PARKIN (an E3 ligase).

Mutations in the Parkin protein are shown to be the main cause of an early onset of autosomal recessive PD (between 30-40 years old). In addition, there are reports of Juvenile PD (less than 21 years old), which were also linked to Parkin (Hedrich et al., 2004). Parkin is a 465 amino acid protein, which comprises of a regulatory Ubl domain (residues 1-76); a RING0 domain (residues 145-215); a RING1 domain (residues 236-293) that binds to an E2; an IBR domain (residues 327- 380); and a RING2 domain that mediates the enzyme's catalytic activity (413- 450) (Zhang et al., 2000) (Figure 1.5). Parkin contains a highly conserved catalytic cysteine C431 that acts as an ubiquitin acceptor that forms an intermediate thioester bond prior to ubiquitylation of its substrate (Wenzel, Lissounov, Brzovic, & Klevit, 2011). Studies revealed that the C431F mutation completely blocks Parkin's catalytic activity (Trempe et al., 2013). It was reported that Parkin exhibits auto-ubiquitylation, mono and multi-mono ubiquitylation functions but it lacks of preference for a single ubiquitin type topology (Hampe, Ardila-Osorio, Fournier, Brice, & Corti, 2006; Kazlauskaite et al., 2014). PD missense mutations can occur in any domain throughout the protein and rearrangements such as deletions or duplications of exons also occur. The exact role of Parkin within cell is unclear. It was reported that it has a neuroprotection role against mitochondrial dependent apoptosis (Moore, 2006) but it was also shown that Parkin KO possesses an increased vulnerability to stress-induced cell death (Exner, Lutz, Haass, & Winklhofer, 2012). Interestingly,

Parkin, a cytoplasmic protein, was shown to translocate to mitochondria upon mitochondria stress (Zheng & Hunter, 2013).

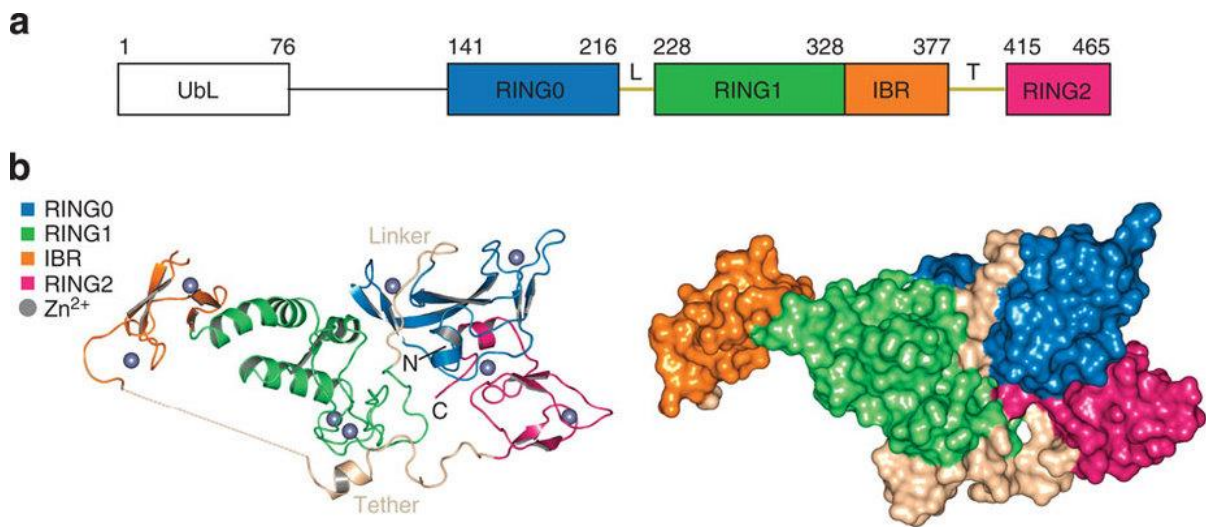


Figure 1.5: Schematic diagram of Parkin protein (a) Linear domain organization and structural domain boundaries. L denotes linker and T, the tether. (b) Overall ribbon diagram of R0RBR (left) and overall surface structure (right). Adopted from (Riley et al., 2013).

Another protein that is most commonly mutated in autosomal recessive PD is PINK. PINK is known as a 581 amino acid Ser/Thr kinase. It is a unique kinase as it comprises mitochondrial targeting sequence (MTS) and a transmembrane domain. Moreover, the catalytic kinase domain comprises three insertions that are not common in other kinases (Cardona, Sanchez-Mut, Dopazo, & Perez-Tur, 2011). Because of MTS, PINK gets imported to mitochondria, where it translocates first to the outer membrane through translocase of the outer membrane TOM and then to the inner membrane through TIM23 and TIM40 complexes (Lazarou, Jin, Kane, & Youle, 2012). Upon mitochondrial translocation PINK experiences sequential cleavage by different mitochondrial proteases (Greene et al., 2012). The remaining C-terminal fragment of PINK is then released to the cytoplasm where it gets degraded by the N-terminal pathway. As a result, typically cells have very low levels

of PINK. Quite recently, it was established that mitochondrial membrane potential controls PINK's stability (Lin & Kang, 2008). In fact, mitochondrial depolarization inhibits PINK cleavage and degradation, leading to its accumulation on the outer mitochondrial membrane where it gets exposed to cytosol and to its potential substrates and interactors. PD mutations in PINK1 are found to be distributed throughout the length of the protein and most of these mutations lead to loss-of-function of PINK kinase activity.

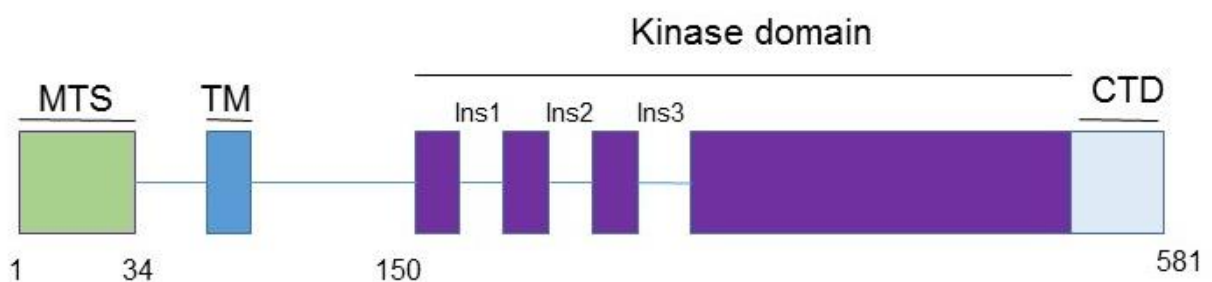


Figure 1.6: Schematic diagram of Pink protein. MTS- mitochondrial targeting sequence, TM –transmembrane helix, Ins1, Ins2, Ins3 – insertions 1,2 and 3 respectively, CTD – C-terminal domain.

It is now established that PINK1 and Parkin share a mechanistic pathway in the pathogenesis of PD. First of all it was discovered that upon mitochondrial depolarization PINK gets accumulated in the outer mitochondrial membrane where it phosphorylates Parkin at S65, located within its Ubl domain (Kondapalli et al., 2012). This phosphorylation results in Parkin conformational change, release of Ubl domain and Parkin activation (Kazlauskaitė et al., 2014). Secondly, it was found that PINK also phosphorylates ubiquitin at S65 (Kazlauskaitė et al., 2015). Phosphorylated ubiquitin is then capable of binding to non-phosphorylated Parkin making it more accessible to PINK-dependent phosphorylation (Kazlauskaitė et al., 2015). The discovery of phospho-ubiquitin mediated Parkin activation (Figure 1.7) provides a platform for the development of small molecule activators of Parkin that mimic

phospho-ubiquitin as potential therapeutic compounds (Kazlauskaite & Muqit, 2015). However, at the moment the development of activators has proven very difficult in contrast to inhibitors in drug discovery.

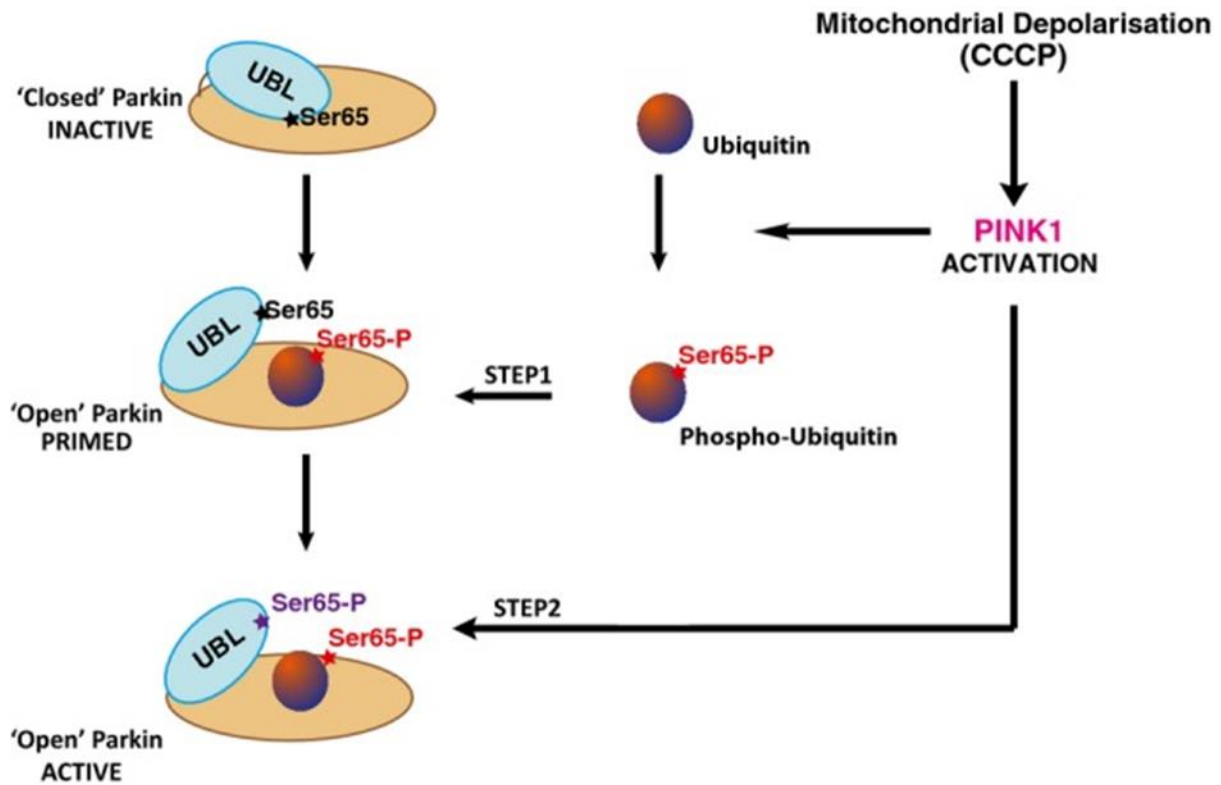


Figure 1.7: Schematic diagram of PINK/Parkin mechanistic interplay. Upon activation of PINK1 by mitochondrial depolarisation, PINK1 can phosphorylate ubiquitin to generate phospho-ubiquitin^{Phospho-Ser65}. Binding of ubiquitin^{Phospho-Ser65} to non-phosphorylated Parkin can disrupt intramolecular interaction of Ubiquitin-like (Ubl) domain to Parkin C-terminus. The Ser65 residue on Ubl becomes more accessible for PINK1-dependent phosphorylation leading to an open and active conformation of Parkin. Adopted from (Kazlauskaite et al., 2015)

1.4 LRRK2

1.4.1 Discovery of LRRK2 and LRRK2 mutations associated with PD

The LRRK2 gene is the greatest genetic contributor to Parkinson's disease discovered to date and it is found in 1-2% of all Parkinson's cases. It was discovered in 2004, following the previous identification of a new locus for Parkinson's disease called PARK8, which maps to chromosome locus 12p11.2-q13.1 and corresponds to approximately 116 genes (Funayama et al., 2002). Two independent research laboratories led by Thomas Gasser and Nic Woods identified a novel gene to comprise missense mutations segregating with PARK8-linked PD. In Wood's laboratory, this gene was named a dardarin (derived from the Basque word "dardara" meaning tremor) that was identified to comprise two missense mutations segregated with the disease in four Basque families R1396G and a fifth British family Y1654C (Paisan-Ruiz et al., 2004). In Gasser's laboratory, LRRK2 (dardarin) was reported to possess missense mutations in the same amino acid residues of the LRRK2 gene in two large pedigrees of German-Canadian origin. In the former case, the identified mutation results in an identical missense mutation Y1699C, with the different numbering due to the addition of an extra 45 amino acids corresponding to exon 6), while in the latter case a different mutation leads to a substitution of the same arginine residue with a cysteine R1441C (Zimprich et al., 2004). Moreover, the analysis of an additional 32 families led to the identification of R1441C mutation in an unrelated family as well as two more missense mutations (I2020T and I1122V) and a putative splice site mutation in three other families (Zimprich et al., 2004). Importantly, in both studies mutations were segregated with the disease and appeared highly penetrant (Shen, 2004). Further studies by a Japanese group identified the LRRK2 I2020T mutation in the Sagamihara family, which is identical to

the one reported by Zimprich (Funayama et al., 2005). It was also reported that the R1441H (Spanaki, Latsoudis, & Plaitakis, 2006) and N1437H (Puschmann et al., 2012) mutations are linked to PD. However, the most common and prevalent mutation reported by multiple studies, including the study by Kachergus, is the LRRK2 G2019S mutation that accounts for PD in several families within Europe and North America (Kachergus et al., 2005). G2019S is the most commonly reported LRRK2 mutation. In fact, in some populations the frequency of the G2019S mutation is extremely high, accounting for up to 20% in Ashkenazi Jews and 40% in North African Arabs (Ozelius et al., 2006). Moreover, the penetrance of the G2019S mutation is 28% in people that are 59 years old, 51% in 69 years old people and 74% in those that are 79 years (Kalinderi, Bostantjopoulou, & Fidani, 2016). Interestingly, the phenotype of the LRRK2 mutations in observed families were remarkably similar. It was noted that the mean age at onset was 65 years, with the majority of patients in these families displaying unilateral hand or leg tremor and an absence of cognitive impairment as well as an excellent response to L-Dopa treatment. Although numerous mutations have been reported since the discovery of LRRK2, the seven mutations described in the present thesis are the ones best established and studied. Intriguingly, PD-associated mutations affect nearly every catalytic and protein-protein interaction domain of LRRK2 indicating that LRRK2 might function as upstream central integrator of multiple signalling pathways that are crucial for the proper functioning of neurons (Mata, Wedemeyer, Farrer, Taylor, & Gallo, 2006). A molecular understanding of how LRRK2 interacts with its neuronal signalling partners and how it transduces cellular signals is likely to reveal novel therapeutic targets, in addition to LRRK2 itself, for the treatment of PD.

1.4.2 Domain architecture of LRRK2

The LRRK2 gene contains 51 exons and its encoded protein is 2527 amino acids long (286 kDa) (Figure 1.8). LRRK2 is mainly a cytoplasmic protein with several functional domains. Sequence analysis indicates several domain, including armadillo repeat folds (35-660 residues), ankyrin repeats (702-822 residues), a leucine-rich repeats (LRRs) (983-1319 residues), a GTPase (1335-1845 residues), a kinase (1859-2138 residues) and a WD40-repeat domain (2142-2498 residues) (Mata et al., 2006) (Figure 1.8). The presence of multiple protein interaction domains (armadillo, ankyrin, LRR and WD40) suggests that LRRK2, in addition to its predicted protein kinase and GTPase activities, might serve as a scaffold for the assembly of a multiprotein signalling complex (Mata et al., 2006). However, because these domains can bind distinct proteins, the physiological LRRK2 binding partners cannot be predicted *a priori* and require extensive experimental identification. Interestingly, four major phosphorylation sites including S910, S935, S955 and S973 were discovered to be located between ankyrin and LRR domains (Doggett, Zhao, Mork, Hu, & Nichols, 2012; Dzamko et al., 2010). It was shown that treatment of cells with distinct LRRK2 kinase inhibitors results in dephosphorylation of these sites. In addition, it was reported that these sites are not LRRK2 autophosphorylation sites and are regulated indirectly by LRRK2-dependent protein kinase or protein phosphatase (Doggett et al., 2012; Dzamko et al., 2010). This data suggests functional importance of these domains. (S910 and S935 sites will be discussed in details in Chapter 3).

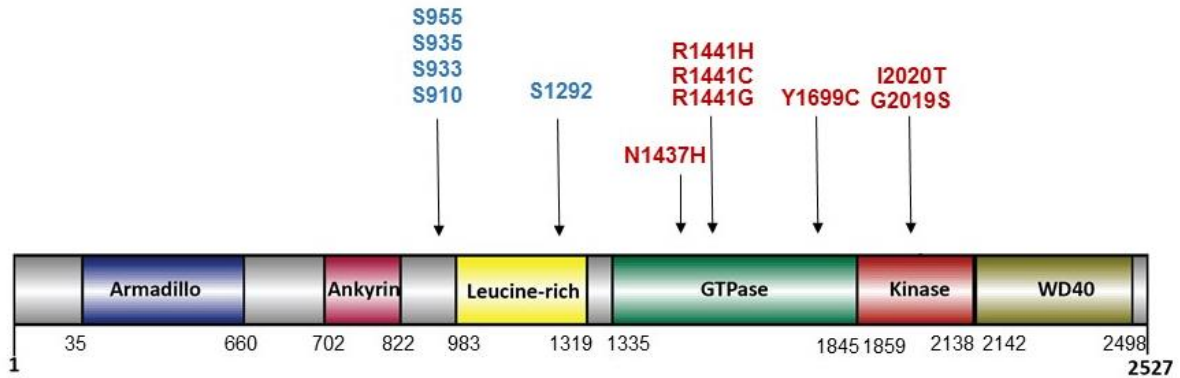


Figure 1.8: Schematic representation of the LRRK2 protein with the seven proven pathogenic mutations (in red) above the protein organization (Corti et al., 2011). LRRK2 has 2,527 amino acids and comprises several conserved domains: ARM (Armadillo), ANK (ankyrin repeat), LRR (leucine-rich repeat), GTPase, kinase and WD40 domain.

LRRK2 (and related LRRK1 protein, which possess a similar domain structure) is an exceptional protein because it encodes two enzymatic activities, a protein kinase and a putative GTPase within a single polypeptide chain. Biochemical studies revealed that LRRK2 is capable of undergoing autophosphorylation (Greggio et al., 2008) and phosphorylation (Jaleel et al., 2007) as well as GTP hydrolysis (L. Guo et al., 2007) both *in vitro* and *in vivo*.

In terms of the LRRK2 kinase domain, LRRK2 belongs to the Tyrosine Kinase-Like (TKL) subfamily of human protein kinases, whose members show sequence similarity to both Ser/Thr and Tyr kinases, though these kinases only phosphorylate Ser/Thr residues and not Tyr. LRRK2 substrate specificity analysis employing a positional scanning peptide approach revealed that LRRK2 tolerates a wider range of amino acids in its substrate compared with other protein kinase but importantly, it has a strong preference for phosphorylating threonine *in vitro* (Nichols et al., 2009b). The TKL subgroup includes several MAPKKs, including the Raf proteins and mixed-lineage kinases (MLKs), which primarily trigger the ERK and JNK pathways, respectively. (Mata et al., 2006). Raf proteins and MLK3 can be activated by the

monomeric GTPases Ras and Cdc42/Rac, respectively (Mata et al., 2006). Furthermore, activation of Raf requires Ras-induced membrane targeting and multiple phosphorylation events, including activation-loop phosphorylation and possibly dimerization ((Mata et al., 2006). Likewise, Cdc42 promotes dimerization, activation-loop phosphorylation and membrane targeting of MLK3 ((Mata et al., 2006)). The similarity of LRRK2 to these kinases indicates that they may share some aspects of regulation. This is also supported by the fact that immunoprecipitated LRRK2 appears to display low specific activity suggesting that it is in an inhibited, less active state, and might be activated by some unknown activator. It could be that an important cofactor or stimulus is absent in the preparation. It could also be that the large LRRK2 protein depends on chaperones for proper folding and activity and it is possible that only a fraction of the immunoprecipitated LRRK2 is functional. Recently, our laboratory made a significant breakthrough in identifying a subset of Rab GTPases, including Rab10 and Rab8A as LRRK2 physiological substrates (Steger et al., 2016). It was demonstrated that LRRK2 directly regulates Rab isoforms by phosphorylating conserved threonine residue in the Rab Switch-II domain, which is important for interacting with Rab's effectors such as Rabin-8 and GDI that activate them (Steger et al., 2016). This data indicated that LRRK2 phosphorylation is likely to be inhibitory on Rab biology (details will be discussed later in Section 1.5.1.1). There are two PD-associated LRRK2 mutations that are located within the kinase domain: G2019S and I2020T, and lie at the N-terminal boundary of the activation segment, with position 2019 corresponding to the glycine residue of the conserved DFG sequence. It was reported that *in vitro and vivo*, these mutations result in an increase of Rab10 phosphorylation and therefore enhanced LRRK2 kinase activity (Steger et al., 2016).

The GTPase domain of LRRK2 is classified to a family of the small G-protein superfamily of Ras-like GTPases called the ROC family (Taymans, 2012). In contrast with most of members of the Ras-GTPase superfamily that exist as single-domain proteins, the GTPase sequence of the ROC family proteins is embedded in large multidomain proteins. Although LRRK2 encodes both a GTPase and a kinase domain, several of its homologues, including MFHAS1 or plant and prokaryotic ROCO proteins, do not contain a kinase sequence and only encode the ROC-GTPase catalytic domain (Taymans, 2012). This suggests that the GTPase function could be primarily a function of ROCOs. On the basis of homology with its ROC domain, the closest homologous GTPase to LRRK2 is LRRK1 with a 48% amino acid similarity and 27% amino acid identity. Several studies have now confirmed the biochemical activity of the LRRK2 GTPase domain using radioactivity-labelled guanine nucleotides. Further testing of GTP binding of multiple disease GTPase domain mutants demonstrated that the GTPase activities of R1441C/G/H and Y1699C mutants are inhibited to levels comparable with the functional mutants K1347A or T1348N (Tsika & Moore, 2013). By contrast, the GTPase activity of kinase domain mutants (G2019S and I2020T) are unchanged compared with the wild-type. Interestingly, GTPase domain mutations did not appear to affect the LRRK2 kinase activity *in vitro*. However, *in vivo*, all disease-associated mutants located within GTPase domain, including R1441H, R1441C, R1441G, N1437H and Y1699C appeared to evidently enhance Rab10 phosphorylation in MEF cells, indicating that these mutants enhance LRRK2 kinase activity (G. Ito et al., 2016; Steger et al., 2016).

As kinases are common effectors of the Ras family proteins, one hypothesis that has been investigated is that the LRRK2 kinase function is the downstream effector of

the LRRK2 GTPase. However, there is no evidence to date to support this hypothesis as it was also suggested that autophosphorylation of LRRK2 controls GTPase activity (Z. Liu, Mobley, DeLucas, Kahn, & West, 2016). In fact, a major LRRK2 S1292 phosphorylation sites has been identified and recently pS1292 antibody was generated (Sheng et al., 2012). This would allow in future to monitor LRRK2 autophosphorylation *in vivo*. However, to date the exact mechanism of interplay between these two domains remains unclear.

At the moment, it seems that overactivation of LRRK2 leading to inhibition of Rab GTPases may lie behind the mechanism by which LRRK2 causes disease. Due to this, many drug companies as well as our laboratory have generated a number of structurally diverse and highly selective LRRK2 inhibitors, these include compounds such as LRRK2-IN-1 (Deng et al., 2011), GSK2578215A (Reith et al., 2012) or the recently developed MLI-2 compound (Fell et al., 2015).

1.5 Cell signal transduction by LRRK2

1.5.1 Discovery of a subset of Rab GTPases as LRRK2 physiological substrates

It was not until 2016, following a great multi-national effort by groups sponsored by the Michael J Fox Foundation, that a subset of Rab GTPases, including Rab10 and Rab8A were established to be direct physiological LRRK2 substrates (Steger et al., 2016). For this purpose, a dual phosphoproteomic screening approach was implemented in parallel with genetic, biochemical and pharmaceutical approaches. Primary mouse embryonic fibroblasts (MEFs) derived from LRRK2 [G2019S] and WT littermate mice were treated with two structurally different LRRK2 inhibitors (GSK257821A and HG-10-102-01) and DMSO as a control to observe the changes in phosphosites in response to LRRK2 inhibition. In addition, primary LRRK2

[A2016T], a drug resistant mutant, and WT littermate, were treated with the recently developed powerful inhibitor MLI-2 to observe the changed in phosphosites in LRRK2 WT but not [A2016T] mutant (Steger et al., 2016). A state-of-the-art workflow for phosphopeptide enrichment, label-free LC-MS/MS and the MaxQuant environment for stringent statistical data evaluation performed by Steger identified 900 high-confidence phosphopeptides in each of replicate in both screens. By overlapping the results of two orthogonal screens surprisingly only two phosphopeptides passed stringent filtering criteria: pS935 LRRK2 and T73 Rab10 (Steger et al., 2016). This small number of identified phosphosites suggests that LRRK2 is a very low activity kinase or that it is in inhibited state.

To verify that Rab10 is a physiological LRRK2 substrate, a number of experiments took place. Table 1.3 shows the criteria for validating LRRK2 substrates that have been met for Rab10 and Rab8A proteins. These includes *in vitro* validation of LRRK2 phosphorylation to prove that Rabs are direct LRRK2 substrates, *in vivo* pharmaceutical evidence that inhibition of LRRK2 kinase activity by distinct LRRK2 kinase inhibitors results in suppression of Rabs phosphorylation at the mapped site as well as genetic confirmation, for instance known LRRK2 disease-associated mutants enhance phosphorylation of the Rabs compared with the wild type but this phosphorylation is significantly suppressed in LRRK2 KO cells. Together these results strongly indicate that Rab10 and Rab8A are indeed direct LRRK2 physiological substrates.

Table 1.3: The criteria for validating LRRK2 substrate

Criteria For Validating LRRK2 Potential Substrates have been met for Rabs
1. Phosphorylation of endogenous substrate in wild type or LRRK2[G2019S] mice/cells is suppressed by at least two structurally diverse LRRK2 inhibitors
2. Phosphorylation of substrate is suppressed by low doses of MLI2 in wild type but not inhibitor resistant LRRK2[A2016T] cells/mice
3. Phosphorylation of substrate enhanced in LRRK2[G2019S] versus wild type MEFs and mouse brain
4. LRRK2 efficiently phosphorylates substrate in vitro at site that is influenced by LRRK2 in vivo
5. Overexpression of pathogenic LRRK2 mutations including those outside kinase domain increase the phosphorylation of substrate to a greater extent than wild type
6. Results are reproduced by at least two independent laboratories

Rab10 and Rab8a are members of Rab GTPases that comprise of 70 family members in humans, and they are critical players in all forms of intracellular vesicular trafficking events. They cycle between the cytosol, in which they are GDP bound and inactive, and specific membrane compartments, where they are activated by GDP/GTP exchange. Equivalent site of Rab10 T73 and Rab8A T72 was shown to be highly conserved in approximately 50 human Rab-family, indicating that this site could have an important functional role. Typical Rab GTPase exhibits a similar core structure comprising a conserved P loop, switch I and switch II domains. T73 Rab10 residue is located in the switch II domain (Stenmark & Olkkonen, 2001) (Figure 1.9).

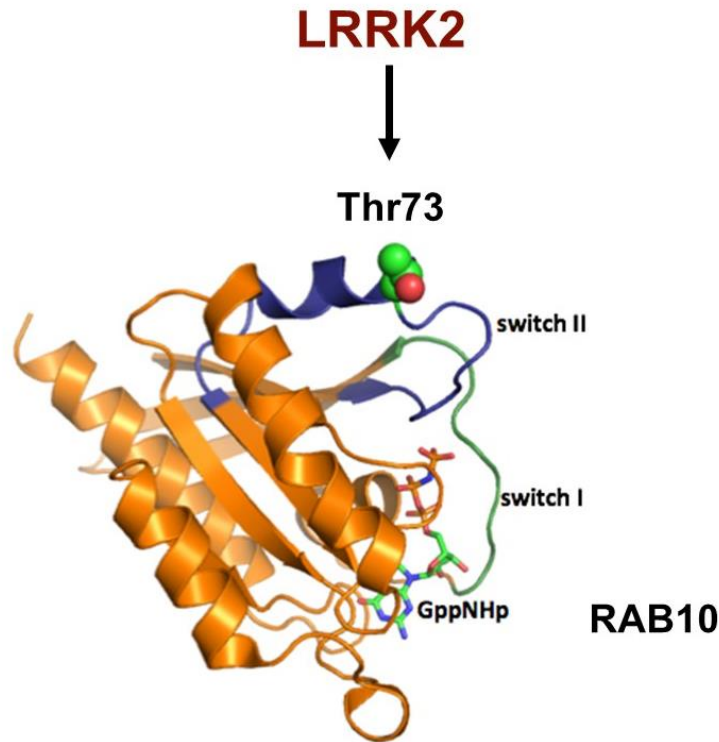


Figure 1.9: LRRK2 phosphorylates Rab10 at T73 located within switch II domain.

Switch II was established to change the conformation upon nucleotide binding and regulate the interaction of Rabs with multiple regulatory proteins such as guanosine nucleotide dissociation inhibitors (GDIs) and guanine exchange factors (GEFs). Typically, prenylated Rab GTPases are localized in the cytosol in their GDP-bound (inactive) conformations bound to a cytosolic protein GDIs (Hutagalung & Novick, 2011). Cytosolic Rab-GDI complexes represent a pool of recycling proteins that can deliver Rabs to specific membrane compartments. Rab delivery to cellular membrane compartments requires release of GDIs and the membrane-associated Rab protein are activated by exchanging its bound GDP for GTP (GEFs facilitates exchange of GDP to GTP) (Hutagalung & Novick, 2011). It was reported that the affinity of GDIs and GEFs for Rabs are evidently diminished in response to increased LRRK2 phosphorylation of Rabs (Steger et al., 2016). This data indicates that

overactive LRRK2, which results in increased Rab phosphorylation, leads to Rab dissociation from GDIs in the cytosol with concomitant membrane insertion. As a result, the relative pool of membrane bound and cytosolic Rab is altered, disturbing intracellular trafficking. Moreover, PD-associated LRRK2 mutations would shift the membrane-cytosol balance of Rabs toward the membrane compartment, thereby causing accumulation of inactive Rabs in the membranes (Steger et al., 2016) (Figure 1.10).

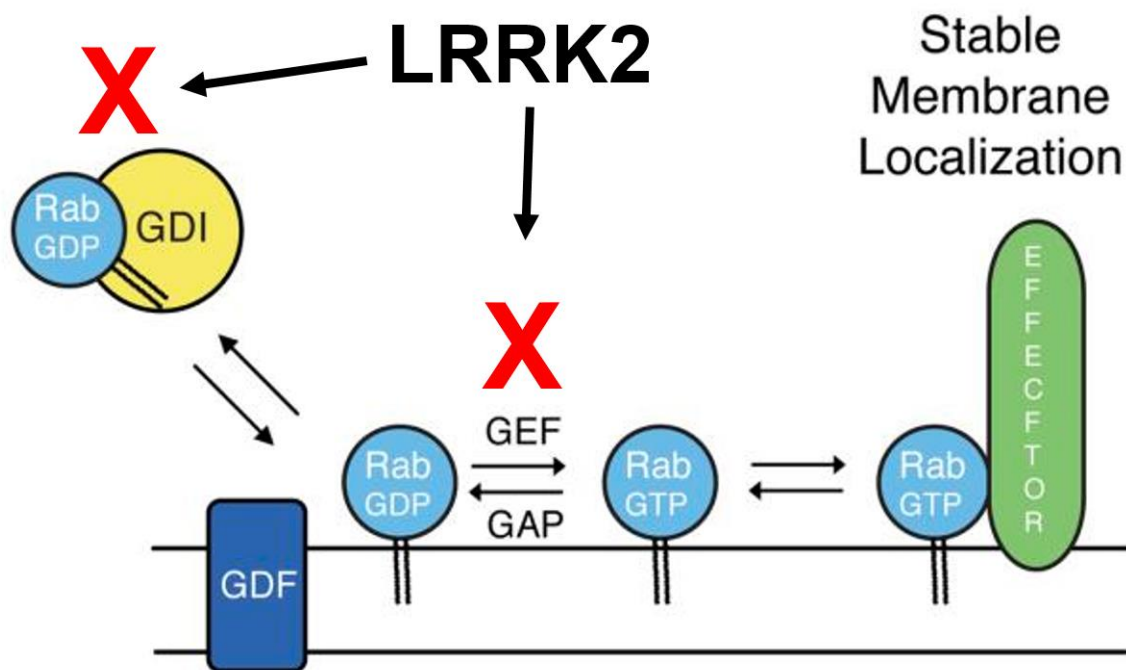


Figure 1.10: Evidence points to LRRK2 inhibiting Rab isoforms by preventing association with GDIs and GEF.

1.5.2 Evidence supporting link between Rab GTPases and PD

Several mutations in a subset of Rab GTPases including Rab39B and Rab7L1 were reported to be linked to PD.

Mutations in Rab39B were shown to be associated with the X-linked early onset PD (Lochte et al., 2016). To date, there are four X-linked *Rab* genes and three of them, including Rab39B, are specific to the brain (Lesage et al., 2015). Most identified mutations in Rab39B lead to a complete loss of function, for instance, a ~45-kb deletion resulting in the complete loss of *RAB39B* in an Australian kindred and a missense mutation in a large Wisconsin kindred (Lesage et al., 2015). This indicates that Rab39b loss of function may lie behind mechanism of PD.

Another Rab protein widely reported to be mutated in PD is Rab7L1 (Satake et al., 2009). Rab7L1 (also known as Rab29), is one of 5 genes that is mutated in Parkinson's patients that have the PARK16 mutation. It was reported by some that mutation in Rab7L1, the rs1572931 single-nucleotide polymorphism (SNP) of the putative promoter of the member RAS oncogene family-like 1 (*RAB7L1*) gene, is associated with reduced risk for Parkinson's disease (PD) in the Ashkenazi Jewish population but not in Chinese population (X. Y. Guo et al., 2014). Whereas other lab demonstrate that *RAB7L1* (p.K157R) and *SLC41A1* (p.A350V) variants are causing PD (Tucci et al., 2010). Overall studies suggest that mutation in Rab7L1 cause a complex late onset PD. Moreover, it was shown that *RAB7L1* interacts with *LRRK2* (Beilina et al., 2014) and together they regulate axonal morphology and lysosome integrity in diverse cellular contexts (Kuwahara et al., 2016). Depletion of Rab7L1 reportedly induced loss of dopaminergic neurons, similar to that observed with *LRRK2*-G2019S expression (MacLeod et al., 2013). These findings suggest that interplay between *LRRK2* and Rab7L1 could be linked to PD.

Moreover, overexpression of Rab8a, Rab1 and Rab3a protein attenuated α -synuclein-induced cytotoxicity in cellular and animal models of PD (G. Ito et al., 2016).

As mentioned previously LRRK2 phosphorylates Rab10 and Rab8A at T73 and T72 respectively. Interestingly, it was also reported that PINK regulates phosphorylation of Rab8A at S111 and that this phosphorylation at S111 significantly impairs Rab8A activation by its cognate guanine nucleotide exchange factor (GEF) (Lai et al., 2015). This data suggests that PINK1 and LRRK2 converge on regulating Rab GTPase biology. This findings are of great interest as they suggest a link between the PINK and LRRK2 pathways in controlling PD biology (Figure 1.11).

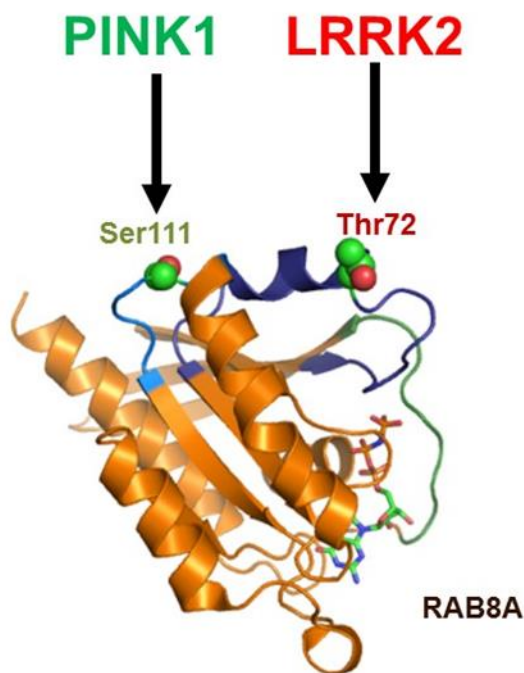


Figure 1.11: Overview of PINK1 and LRRK2 converge on regulating Rab GTPase biology.

1.5.3 Identification of S910 and S935 as major LRRK2 phosphorylation sites

In a previous study, our laboratory identified a useful biomarker for LRRK2 activity. We revealed that treatment of cells or mice with every structurally distinct LRRK2 kinase inhibitor, tested in our lab, causes dephosphorylation of LRRK2 at two residues: Ser910 and Ser935 (Dzamko et al., 2010). Moreover, the data indicated that these sites do not comprise LRRK2 autophosphorylation sites but are instead regulated by a distinct signalling mechanism that is controlled by LRRK2. One of the reported evince is that in macrophages, S910 and S935 were shown to be phosphorylated by the IkappaB kinase family and that pharmacological inhibition of LRRK2 kinase activity did not cause dephosphorylation of these sites, suggesting that these sites are not LRRK2 autophosphorylation sites (Dzamko et al., 2012). Furthermore, it was reported that LRRK2 binds to 14-3-3 isoforms via the phosphorylation of S910 and S935 (Dzamko et al., 2010; Nichols et al., 2010). 14-3-3s comprise an abundant family of proteins that primarily targets phosphorylated S and T residues (MacKintosh, 2004). They acts as dimers allowing phosphorylated peptides to dock directly into each side of the inner groove of the 14-3-3 dimer (MacKintosh, 2004). The ability of 14-3-3s to simultaneously bind phosphosites has an important functional impact. For example, they can induce a dramatic conformational change in the target protein or cause its dissociation resulting in a change of protein subcellular localization. It was shown that dephosphorylation of S910 and S935 residues results in disruption of 14-3-3s binding and LRRK2 accumulation within inclusion bodies *in vitro* (Dzamko et al., 2010). In addition, dephosphorylation of S910 and S935 are used in our laboratory as biomarkers to assess the LRRK2 kinase activity *in vivo*.

1.6 Genetic and pharmacological studies of LRRK2 using a mouse model

1.6.1 Phenotype of LRRK2 knock-out and knock-in genetic mice models

LRRK2 knock-out (LRRK2 KO) mouse model

To study the normal function of LRRK2 *in vivo*, LRRK2 KO mice were generated and examined throughout their life span by different laboratories. It was reported that LRRK2 KO mice appear normal and display no obvious phenotype (Tong et al., 2012). Moreover, deletion of LRRK2 did not appear to influence the number of dopaminergic neurons and the levels of striatal dopamine in mice (Tong et al., 2012). Besides, in LRRK2 KO mice there was no evidence of abnormal accumulation and aggregation of α -synuclein and ubiquitin, which is normally observed in PD patients, in aged LRRK2 KO brains (Tong et al., 2012). Unexpectedly, it was reported that LRRK2 KO mice develop age-dependent abnormalities in the kidneys. It was shown that by approximately 20 months of age, LRRK2 KO kidneys appeared significantly smaller in size (30% less in weight), much darker in color and displayed a rough and granular surface (Tong et al., 2012). Biochemical analysis of aged LRRK2 KO kidneys showed an evident increase in the levels of α -synuclein, ubiquitinated proteins and abnormal accumulation of lipofuscin granules (Tong et al., 2012). It was then hypothesized that the autophagy-lysosomal pathway, which has been implicated in neurodegenerative disorders such as PD, was impaired in LRRK2 KO kidneys. Furthermore, additional research showed that deletion of LRRK2 causes alterations in proximal tubule secondary lysosomes and lung type II pneumocyte lamellar bodies (Herzig et al., 2011), suggesting LRRK2's role in homeostasis of lamellar bodies in lung type II pneumocytes. It was reported that there is no compensatory upregulation of LRRK1 in the absence of LRRK2 (Reyniers et al., 2014) as well as no evidence to suggest that mutations in the LRRK1 gene are

linked to PD (Schulte et al., 2014), indicating that the observed phenotype is linked to the removal of the LRRK2 protein. Studies of LRRK2-deficient rats confirmed kidney and some lung morphological and histological alterations observed in LRRK2 KO mice suggesting that LRRK2's involvement with kidney and lung homeostasis is not only observed in mice and may be conserved across various species (Baptista et al., 2013). These observations are of potential concern for a drug that would be used for the chronic treatment of PD, as they suggest that LRRK2 inhibition can lead to a severe phenotype in the peripheral organs.

LRRK2 kinase dead (LRRK2 KD) mouse model

In order to determine how kinase function contributes to the roles of LRRK2 *in vivo*, mutant mice were generated by distinct laboratories carrying kinase-inactivating point mutations, including D1994S. It was reported that no brain phenotype was observed in LRRK2 KD as well as LRRK2 KO mice (Herzig et al., 2011). However, the LRRK2 KD mice were reported to develop a dark kidney phenotype at an age of 26 months similar to that observed in LRRK2 KO mice (Herzig et al., 2011). These studies strongly indicated that LRRK2 kinase activity might be responsible for kidney phenotype. However, there was no evidence to suggest that the lung phenotype observed in LRRK2 KO mice was due to the inactivation of the LRRK2 kinase activity, and thus indicating that other functions of LRRK2 such as scaffold or GTPase activity could be implicated in this phenomenon (Herzig et al., 2011). Interestingly, it was reported that the loss of the LRRK2 kinase function in the kidneys results in a significant reduction in full-length LRRK2 protein levels, and this might be responsible for triggered changes in the kidneys (Herzig et al., 2011). As it was previously described, LRRK2 inhibition results in dephosphorylation of LRRK2 at S910 and S935, suggesting that these sites are indirectly regulated by LRRK2

activity. Interestingly, it was observed that in the LRRK2 [D2017A] KD knock-in S910 and S935 are still phosphorylated despite loss of LRRK2 activity (Genta Ito, Fujimoto, Kamikawaji, Kuwahara, & Iwatsubo, 2014). This could be explained by a compensation mechanism, which took place in LRRK2 [D2017A] KD mice and in which the upstream kinase that phosphorylates these sites becomes uncoupled from LRRK2.

LRRK2 gain of function mutation: [G2019S] and [R1441G] mouse model

G2019S is the most commonly reported LRRK2 mutation, which accounts for the vast majority of LRRK2-associated PD cases. As it was previously described, it is located within the subdomain VII DFG of the kinase domain and was shown to increase LRRK2 kinase activity two to three folds both *in vitro* and *in vivo*. It was shown that G2019S mutant mice do not display a dark kidney phenotype as observed in LRRK2 KO and KD mice (Herzig et al., 2011). It was also observed that no lung phenotype was associated with the G2019S mutant as well as KD. Interestingly, the G2019S mutation that enhances kinase activity did not show any destabilization effects on the protein in the kidney of mutant mice. It also was noted that the G2019S mutation did not result in an enhanced phosphorylation at the S910 and S935 sites suggesting that stimulated LRRK2 kinase activity does not increase phosphorylation of these residues further. (Herzig et al., 2011). Furthermore, it appears that this mutation does not cause any major brain phenotype (Herzig et al., 2011). However, a recent report suggests altered development of the synapse structure and function in striatum in mice caused by the G2019S mutation (Matikainen-Ankney et al., 2016). Therefore, these observations provide a novel insight into the early functional and structural aberrations in striatal connectivity that

may predispose striatal circuitry to both motor and nonmotor dysfunction later on in life (Matikainen-Ankney et al., 2016).

R1441G is another well-characterized LRRK2 PD-associated mutation (Y. Li et al., 2009). It is known to be located within the GTPase domain and it was not shown *in vitro* to alter the LRRK2 kinase activity. However, after the discovery of the Rab10 protein as a physiological LRRK2 substrate, it was possible to assess the impact of LRRK2 R1441G mutation *in vivo* (G. Ito et al., 2016). Remarkably, in this mouse model LRRK2 phosphorylates Rab8A and Rab10 more than 4 fold compared with the wild type. These observations strongly suggest that overactivation of LRRK2 kinase activity is implicated in the disease. A R1441G transgenic mouse displayed the most evident PD-associated phenotype (Y. Li et al., 2009). It was reported that it had an age-dependent and progressive motor-activity deficits, beginning with reduced mobility that was reminiscent of hypokinesia in PD (Y. Li et al., 2009). Moreover, levodopa and a direct-acting dopamine agonist, apomorphine, both reversed these deficits. Furthermore, a pathological analysis of the brain revealed no general abnormalities in brain structure but substantia nigra pars compacta (SNpc) abnormalities such a decrease of the average cell body size, a marked diminution in the number of tyrosine hydroxylase–positive dendrites as well as impaired dopamine release. These findings suggest that R1441G transgenic mice are to date the best PD models that successfully recapitulate the motor behaviour, neurochemical and histopathological features of controlled human disease (Y. Li et al., 2009). In fact, these mice could serve as a powerful tool for *in vivo* mechanistic studies and therapeutic development. Interestingly enough, it is reported that both *in vitro* and *in vivo*, R1441G mutation results in dephosphorylation of S910 and S935 sites (Muda et al., 2014), and since it was previously published that dephosphorylation of these

sites results in loss of 14-3-3 binding *in vitro* and mislocalization, it was hypothesized that phosphorylation of S910 and S935 sites could be associated with PD. This is the reason why our laboratory aimed to understand the biological significance of these sites.

1.6.2 Phenotype of pharmacological inhibition of the LRRK2 kinase activity

Inhibition of the LRRK2 kinase activity is under investigation as a possible treatment for PD. However, the safety implications of targeting the LRRK2 activity are not fully understood. It was reported that treatment of non-human monkeys (NHPs) with distinct LRRK2 kinase inhibitors resulted in the abnormal accumulation of lamellar bodies in type II pneumocytes (Fuji et al., 2015). Furthermore, it was suggested that lung toxicity may be the primary clinical safety liability of LRRK2 kinase inhibitors in patients (Fuji et al., 2015). Due to the fact that the same lung toxicity was observed in LRRK2 KO mice but not in LRRK2 KD mice, it could be that employed inhibitors altered another aspect of the LRRK2 function or the observed phenotype could be due to an off-target effect. In future, it would be important to test the effect of different, more specific inhibitors such as ML-2 in NHPs to completely rule out the possibility of off-target effect. It is interesting to note that no lung phenotype in mice or rats treated with the same inhibitors was observed, which highlights the importance of species selection when evaluating clinical safety of LRRK2 kinase inhibitors. In fact, rodents might not be adequate model to recapitulate the effect of LRRK2 kinase inhibitors. Interestingly, pharmacological inhibition of LRRK2 kinase activity in NHPs resulted in a trend towards a decrease in the total LRRK2 in kidneys and PBMCs. This is consistent with LRRK2 KD results and suggests that the LRRK2 kinase activity could be implicated in the kidney phenotype. As it is known that LRRK2 kinase activity results in dephosphorylation of S910 and S935, it would be

important to assess whether dephosphorylation of these sites is implicated in the kidney pathology or LRRK2 stability.

CHAPTER 2:

Materials & Methods

2.1 Materials

2.1.1 Commercial reagents

Adenosine 5'-triphosphate sodium salt (ATP), anti-HA-agarose, anti-FLAG-agarose, ammonium persulphate (APS), ampicillin, benzimidazole, bovine serum albumin (BSA), bromophenol blue (BPB), dimethyl pimelimidate (DMP), dimethyl sulphoxide (DMSO), ethidium bromide, hydrogen peroxide, iodoacetamide, puromycin, N-ethylmaleimide (NEM), sodium dodecyl sulphate (SDS), sodium tetraborate, thymidine, N, N, N', N'-Tetramethylethylenediamine (TEMED), Triton-X-100 and Tween-20 were from Sigma-Aldrich (Poole, UK). Protein A-agarose, Protein G-sepharose, Glutathione-sepharose, Enhanced chemiluminescence (ECL) kit and Hyperfilm MP were from Merck. Dulbecco's modified eagle medium (DMEM), Opti-MEM reduced serum media, Foetal bovine serum (FBS), tissue culture grade Dulbecco's phosphate buffered serum (PBS), Trypsin/EDTA solution, L-glutamine, non-essential amino acids, vitamins, sodium pyruvate and antibiotic/antimycotic were from GIBCO (Paisley, UK). [γ 32P]-labelled ATP was purchased from Perkin Elmer. Acetic acid, acetone, ammonium bicarbonate, ethanol, glycerol, glycine, 4-(2-Hydroxyethyl)piperazine-1-ethanesulfonic acid (Hepes), isopropanol, magnesium chloride, manganese chloride, methanol, 2-mercaptoethanol, orthophosphoric acid, potassium chloride, sodium chloride, sodium ethylenediaminetetraacetic acid (EDTA), sodium ethylene glycol tetraacetic acid (EGTA), sodium fluoride, sodium β -glycerophosphate, sodium orthovanadate, sucrose and Tris(hydroxymethyl)methylamine (Tris) were from BDH (Butterworth, UK) or Sigma-Aldrich (Poole, UK). Microcystin-LR was from Enzo Life Sciences (NY, USA). 6, 24 and 96 well tissue culture plates, cell culture dishes, cryovials and Spin-X columns were from Corning Incorporated (NY, USA). Cellophane films and All Blue Precision

Plus pre-stained protein markers were from Bio-Rad (Herts, UK). Cell scrapers were from Costar (Cambridge, USA). 40% (w/v) 29:1 Acrylamide: Bis-Acrylamide solution was from Flowgen Bioscience. Pre-cast NuPAGE Novex SDS polyacrylamide 4-12% Bis-Tris gels, NuPAGE MES and MOPS running buffer (20X), 10X NuPAGE sample reducing agent, 4X NuPAGE LDS sample buffer, Colloidal blue staining kit, Alexa Fluor donkey secondary antibodies were from Invitrogen (Paisley, UK). Instant-Blue stain was from Expedeon, UK. Photographic developer (LX24) and liquid fixer (FX40) were from Kodak (Liverpool, UK). X-ray films were from Konica Corporation (Japan). Agarose, phenylmethanesulphonylfluoride (PMSF), Geneticin (G418) and Isopropyl- β -D-thiogalactopyranoside (IPTG) were from Melford Laboratories (Chelsworth, UK). Restriction enzymes, DNA ligase and DNA ladder were from New England Biolabs (Hertfordshire, UK). Coomassie protein assay reagent (Bradford reagent) was from Pierce (Chester, UK). Hygromycin, blasticidin and polyethylenimine (PEI) were from Polysciences (Warrington, PA). Skimmed milk (Marvel) was from Premier Beverages (Stafford, UK). Taq DNA polymerase in storage buffer A, sequencing grade trypsin and nucleotide mix (dNTP) were from Promega (UK). Sequencing grade Asp-N was from Roche. P81 paper and 3 mm chromatography paper were from Whatman InterInternational Ltd (Maidstone, UK). Plasmid Maxi kits were from Qiagen Ltd (Crawley, UK). Acetonitrile (HPLC grade), trichloroacetic acid (TCA) and trifluoroacetic acid (TFA) were from Rathburn Chemicals (Walkerburn, UK). Protran BA nitrocellulose membrane was purchased from Schleicher and Schuell (Anderman and Co. Ltd., Surrey, UK). HRP-conjugated secondary antibodies and Super Signal West Dura extended duration substrate were from Thermo-scientific (Essex, UK). Mouse Rota-Rod was purchased from Ugo Basile Monvalle VA, Italy.

2.1.2 In-house reagents

Oligonucleotide primers were custom synthesised by the University of Dundee oligonucleotide synthesis service. Bacterial culture medium Luria Bertani broth (LB) and LB agar plates were provided by the College of Life Sciences media kitchen service.

2.1.3 Antibodies

2.1.3.1 In-house antibodies

In-house sheep polyclonal antibodies (Table 2.1) were generated by the Division of Signal Transduction Therapy (DSTT, University of Dundee). For this purpose, antisera were raised in sheep by Diagnostics Scotland (Carluke - Lanarkshire, UK). Then, all in-house antibodies were affinity purified on CH-Sepharose covalently coupled to the corresponding antigen.

In-house phospho-specific antibodies were produced by Division of Signal Transduction Therapy (DSTT, University of Dundee). For this purpose, the phospho-peptide immunogen was conjugated to BSA and also separately to keyhole limpet haemocyanin (KLH). Then, these BSA and KLH conjugates were injected into sheep along with Freund's Adjuvant. Treated sheep was left to recover for three weeks and then were injected again with a booster and the first bleed was collected a week later. This was repeated to produce a total of 3-5 bleeds. Each bleed was allowed to clot overnight at 4°C, centrifuged at 1500xg for 60 min at 4°C and filtered through glass wool prior to storage at -20°C. To purify the antibodies, serum was heated for 20 min at 56°C and filtered through a 0.4 micron filter. The anti-serum was diluted with an equal volume of 50 mM Tris-HCL pH 7.5 containing 2% Triton-X 100 and passed through a column of phospho-peptide immunogen couple to Sepharose. Antibodies were then eluted with 50 mM Glycine (pH 2.5) and dialyzed overnight

against PBS. Solubility of respective non-phospho peptide was determined and dissolved in a buffer of appropriate pH range. In my experiments antibodies were used at a concentration of 1 µg/ml in 5% skimmed milk in TBST (0.1% Tween20). Phospho-specific antibodies were used at a concentration of 1 µg/ml in 5% BSA in TBST supplemented with non-phospho peptide (10 µg/ml) to increase specificity.

Table 2.1: List of in-house antibodies

Antibody	Antigen	Species	Bleed
anti-LRRK2	Human LRRK2 (100 - 500)	Monoclonal Rabbit 10-12	1
anti-pS935 LRRK2	NLQRHSNS*LGPIFDH [residues 928 - 942 of human]	Monoclonal Rabbit 10-12	1
anti-pS910 LRRK2	VKKKSNS*ISVGEFY [residues 904 - 917 of human]	Monoclonal Mouse 1D8	1
anti-MYPT1	Human MYPT1 (714-1005)	Polyclonal S662B	1
anti-pThr500 MYPT1	GTRLAYVTPT*IPRRLASTSSS [residues 491 - 509 of mouse]	Polyclonal S980D	1-5
anti-RPS15	Human RPS15	Polyclonal S775D	1-3
anti-pT136 RPS15	HGRPGIGAT*HSSRFIPLK [residues 128-145 of human]	Polyclonal S780D	1-3

2.3.1.2. Commercial/gifted antibodies

Table 2.2 presents antibodies obtained from the indicated commercial sources and used at the concentration recommended by the manufacturer/collaborator.

Table 2.2: List of commercial antibodies used in this thesis

Antibody	Company	Catalogue Number	Host
HA-HRP	Roche	12013819001	-
FLAG-HRP	Sigma	A8592	-
14-3-3	Santa Cruz	Sc-629	Rabbit
GAPDH	Cell Signalling	2118	Rabbit
Rab10	Cell Signalling	8127	Rabbit
Rab8A	Cell Signalling	D22D8	Rabbit
MYPT1	Celli Signalling	2634	Rabbit
PALM	Sigma-Aldrich	356-370	Rabbit
MAP4K4	Cell Signalling	5146	Rabbit
GFP	Chromotek	3H9	Rat

2.1.4 Plasmids

Dr. M. Wightman, Dr. M. Peggie, and Mr. T. McCartney performed the cloning, subcloning and mutagenesis of the constructs reported in my thesis. Table 2.3 summarises all the mammalian constructs used in this work while Table 2.4 lists the constructs used to purify recombinant proteins from E.coli BL21 DE3 cells (2.2.4).

Table 2.3: Mammalian expression constructs

Expressed Proteins	Plasmid	Clone ID
FLAG-LRRK2 [1-1326](WT)	pcDNA5-FRT/TO-FLAG LRRK2 N-Term(1-1326)	DU13369
FLAG-LRRK2 [1326-end](WT)	pcDNA5-FRT/TO-FLAG LRRK2C-Term(1326-end)	DU13588
FLAG-LRRK2 [full length](WT)	pcDNA5-FRT/TO-FLAG LRRK2	DU13952
GST-LRRK2[1326-end](G2019S)	pEBG LRRK2 1326-end G2019S	DU44733
FLAG-MYPT1 [A498T+T500A]	pcDNA5D frtTO FLAG MYPT1 A498T	DU48541
FLAG-RPS15(WT)	pcDNA5D frtTO FLAG MYPT1 A498T T500A	DU48540
FLAG-RPS15 T136A	pCMV5D FLAG RPS15	DU25491
FLAG-EMPTY	pCMV5D FLAG RPS15 T136A	DU48728
FLAG-KCC3A T1039E	pcDNA5 FRT/TO	DU41457
FLAG-SGK2	pCMV5 FLAG KCC3A T1039E	DU44587

FLAG-SGK3	pcDNA frtTO FLAG SGK3	DU42867
FLAG MYPT1 WT	pcDNA frtTO FLAG MYPT1 WT	DU30035
GFP-EMPTY	pcDNA frtTO GFP	DU52527
GFP-LRRK2 WT	pcDNA frtTO GFP LRRK2 full WT	DU13363
GFP-LRRK2 [S910A+S935A]	pcDNA frtTO GFP LRRK2 S910A+S935A	DU30902
GFP-MYPT1 WT	pcDNA5D frtTO GFP MYPT1 rescue	DU52526
GFP-MYPT1 [T500A]	pcDNA5D frtTO GFP MYPT1 (guide protected)	DU52526
GFP-MYPT1 [T500A+T524A+T529A+T671A+T76 1A+T892A]	pcDNA5D FRT/TO GFP MYPT1 guide protected + T500A	DU50641
HA-EMPTY	pcDNA5 FRT/TO HA empty	DU50659
HA-14-3-3	pCMV-HA 14-3-3 zeta	DU6742
HA-PALM	pcDNA5D frtTO HA PALM	DU48752
HA-GNAI2	pCMV5-HA2 GNAI2	DU16892
HA-MRIP	pCMV5-HA M-RIP	DU11147
HA-NRAS	pCMV5D HA NRAS	DU48137
HA-SNAP23	pCMV5D HA SNAP23	DU25495
HA-THBS1	pCMV5D HA THBS1	DU25544

Table 2.4: Bacterial expression constructs

Expressed Proteins	Plasmid	Clone ID
GST-MYPT1	pGEX-6-MYPT1 (human) protein phosphatase 1, regulatory (inhibitor) subunit 12A	DU17840
GST-MYPT1 [T500A+T524A+T529A+T671A+T761A+T 892A]	pGEX-6-MYPT1 [T500A+T524A+T529A+T671A+T761A+ T892A]	DU48124
GST-RPS15	pGEX RPS15 WT	DU48445
GST-RPS15 T136A	pGEX RPS15 T136A	DU48444
GST-PALM	pGEX PALM	DU25823
GST-PALM2	pGEX PALM2	DU48735
GST-PALM3	pGEX6P1 PALM3	DU48825
GST-PALMD	pGEX6P3 PALMD	DU48940
GST-NRAS	pGEX6P1 NRAS	DU48916

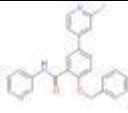
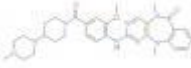

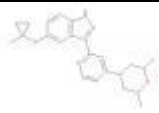
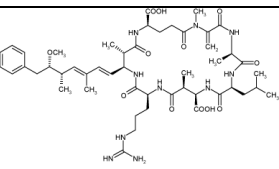
GST-SNAP23	pGEX6P1 SNAP23	DU48915
GST-CTNNA1	pGEX6P1 CTNNA1	DU25458
GST-M-RIP	pGEX6P-1 M-Rip	DU46333
GST-MME(1-29)	pGEX6P1 MME	DU25496
GST-MME(52-end)	pGEX6P1 MME Y52-end	DU25562
GST-CAPZB	pGEX6P-1-CAPZB	DU3292
GST-GNAI2	pGEX6P1 GNAI2	DU46316

In addition to described plasmids I used TALE monomer template plasmids (Addgene): pNI_v2, pNG_v2, pNN_v2, pHD_v2; TALE transcriptional activator (TALE-TF) plasmids (Addgene): pTALE-TF_v2 (NI), pTALE-TF_v2 (NG), pTALE-TF_v2 (NN), pTALE-TF_v2 (HD); TALE nuclease (TALEN) backbone plasmids (Addgene): pTALEN_v2 (NI), pTALEN_v2 (NG), pTALEN_v2 (NN), pTALEN_v2 (HD) were obtained as a single kit from the Zhang Lab plasmid collection at Addgene.

2.1.5 Inhibitors

Table 2.5 summarises the various small molecule inhibitors used in this thesis. All LRRK2 kinase inhibitors were synthesized in house by Dr Natalia Shpiro (DSTT, University of Dundee).

Table 2.5: Kinase and phosphatase inhibitors

Compound	Target	Structure	MW (g/mol)	Publication
GSK2578215A	LRRK2		399.42	Reith A. (2012) Bioorg. Med. Chem. Lett.
LRRK2-IN1	LRRK2		570.69	Deng X. (2011) Nat. Chem. Biol. 7 203
CZC-25146	LRRK2		488.54	Ramsden N. (2011) ASC Chemical Biology
MLi-2	LRRK2			Matthew J. Fell (2015) Journal of Pharmacology and Experimental Therapeutics 355(3) 397-409
Microcystin-LR			995.189	(MacKintosh, Beattie, Klumpp, Cohen, & Codd, 1990)

2.1.6 Buffers

Table 2.6 summarises buffers used in this work. Lysis buffers comprise a cocktail of different phosphatase inhibitors. For instance, sodium fluoride, sodium pyrophosphate, sodium β -glycerophosphate inhibit serine/threonine protein phosphatases whereas sodium orthovanadate (Na_3VO_4) inhibits protein tyrosine phosphatases. Sodium orthovanadate was prepared by several rounds of boiling, cooling to room temperature on ice and then adjusted to pH 10. This was repeated until the pH was stable at pH 10 and the solution remained colourless. This ensures that the majority of sodium orthovanadate is in the monomeric state enabling inhibition of tyrosine phosphatases. EDTA and EGTA are chelating agents. EDTA chelates divalent cations including Mg^{2+} and thus inhibits metal dependent enzymes such as kinases and many phosphatases. EGTA is a chelator with higher affinity

towards Ca²⁺. Benzamidine and PMSF are added to inhibit serine proteases and metallo, aspartyl, cysteinyl, and seryl proteinases.

Table 2.6: Buffers and compositions

Buffer	Composition
1% Triton Lysis Buffer	50 mM Tris/HCl pH 7.5, 1 mM EGTA, 1 mM EDTA, 1% (v/v) Triton X-100, 1 mM sodium orthovanadate, 50 mM sodium fluoride, 5 mM sodium pyrophosphate, 0.27 M sucrose, 0.1% β-mercaptoethanol, 1 mM benzamidine and 0.1 mM phenylmethanesulphonylfluoride (PMSF) and one mini Complete™ protease inhibitor cocktail tablet per 10ml of lysis buffer.
1% Triton Phosphatase lysis Buffer	50 mM Tris/HCl pH 7.5, 1 mM EGTA, 1 mM EDTA, 1% (v/v) Triton X-100, 0.27 M sucrose, 0.1% β-mercaptoethanol, 1 mM benzamidine and 0.1mM phenylmethane-sulphonylfluoride (PMSF) and one mini Complete™ protease inhibitor cocktail tablet per 10ml of lysis buffer.
Phosphate buffered saline (PBS)	137mM NaCl, 2.7mM KCl, 8.1mM di-sodium hydrogen phosphate, 1.5mM potassium dihydrogen phosphate pH 7.4.
GST bacterial lysis buffer	50 mM Tris/HCl pH 7.5, 270 mM sucrose, 150 mM NaCl, 0.1 mM EGTA, 1 mM benzamidine 0.2 mM PMSF and 0.1% β-mercaptoethanol.
GST bacterial elution buffer	50 mM Tris/HCl pH 7.5, 270 mM sucrose, 150 mM NaCl, 0.1 mM EGTA, 50 mM glutathione, 1 mM benzamidine 0.2 mM PMSF and 0.1% β-mercaptoethanol. Adjust pH to 7.5.
8 M Urea Lysis Buffer	Add 8 M urea to the 1% Triton lysis buffer described previously.
Buffer A	50mM Tris-HCl pH 7.5, 0.1mM EGTA, and 0.1% β-mercaptoethanol.
TBST	50 mM Tris-HCl pH 7.5, 0.15 M NaCl and 0.1% (v/v) Tween-20
5X SDS-PAGE Sample Buffer	5% SDS, 5% (v/v) β-mercaptoethanol, 250mM Tris-HCl pH 6.8, 32.5% (v/v) glycerol, Bromophenol Blue for blue colour intensity.
SDS-PAGE Running Buffer	25mM Tris-HCl pH 8.3, 192mM Glycine, 0.1% (w/v) SDS.
4x Laemmli's Sample Buffer	250 mM Tris-HCl pH 6.8, 8% (w/v) SDS, 40% (v/v) glycerol, 0.02% (w/v) Bromophenol Blue. Add MnCl ₂ at a final concentration of 10 mM to all samples.
Phos-tag lysis buffer	50 mM Tris-HCl pH 7.5 , 1%(v/v) Triton X-100, 1 mM EGTA, 1 mM sodium orthovanadate, 50 mM NaF,0.1%(v/v) β-mercaptoethanol,10 mM β-glycerophosphate, 5 mM sodium pyrophosphate, 1µg/ml mycrocystin-LR, 0.27 M sucrose and one mini Complete™ protease inhibitor cocktail

	tablet per 10ml of lysis buffer.
Phos-tag washing buffers	Wash 1-2: transfer buffer containing 10 mM EDTA and 0.05% SDS. Wash 3: transfer buffer containing 10 mM EDTA (no SDS).
Western Blotting Transfer Buffer	48mM Tris-HCl, 39mM Glycine, 20% (v/v) Methanol.
ECL Solution 1	0.1M Tris-HCl pH 8.5, 2.5 mM Luminol, 0.4mM p-Coumaric acid.
ECL Solution 2	0.1M Tris-HCl pH 8.5, 5.6mM Hydrogen peroxide.
TAE buffer	40mM Tris-acetate pH 8, 1mM EDTA.
Kinase assay reaction buffer	50mM Tris-HCl (pH 7.5), 0.1 mM EGTA, 10 mM MgCl ₂ , 2 mM DTT and 0.1 mM [γ - ³² P] ATP (approx. 500 cpm/pmol).

2.1.6 Cell lines

I generated LRRK2 WT, LRRK2 [S910A+S935A] knock-in and LRRK2 KO mouse embryonic fibroblasts (MEFs) by prolonged passaging of MEF cells derived from LRRK2 WT, LRRK2 [S910A+S935A] knock-in or LRRK2 KO mouse.

HEK293 [MAP4K4 (1-9) KO] cells were kindly provided by Professor Kun-Liang Guan's laboratory from University of San Diego.

2.1.7 Animals

LRRK2 [S910A+S935A] mice were purchased from Taconic-Artemis GmbH, Germany. Animals were maintained under specific pathogen-free conditions and routine animal tail and ear notching was carried out by staff in the College of Life Sciences Transgenic Unit (University of Dundee). All procedures were carried out in accordance with the regulations set by the University of Dundee and the United Kingdom Home Office.

2.1.8 Instruments

X-Cell SureLock Mini-cell electrophoresis systems and X-Cell II Blot modules were from Invitrogen (Paisley, UK). AE6450 Atto Vertical Dual Mini Slab Kits were from Genetic Research Instrumentation. Trans-Blot Cells, automatic western blot

processors and gel dryer apparatus were from BioRad (Herts, UK). X-omat autoradiography cassettes with intensifying screens were from Kodak. Automatic film processor was from Konica Corporation. The Procise 494C Sequenator was from Applied Biosystems (Foster City, USA). HPLC system components were obtained from Dionex (Camberley, UK). The Vydac 218TP54 C18 reverse phase HPLC column was from Separations group. The LTQ-orbitrap mass spectrometer and Nanodrop was from Thermo Scientific. The PCR thermocycler (PTC-200) was from MJ Research. The 96-well Versamax plate reader was from Molecular Devices (Wokingham, UK) Thermomixer IP shakers were purchased from Eppendorf (Cambridge, UK). Centrifuge tubes, rotors and centrifuges were from Beckmann. Biofuge pico microcentrifuge was from Heraeus Instruments (Osterode, Germany). pH meters and electrodes were from Horiba (Kyoto, Japan). Scintillation counter (Tri-Carb 2800 TR) was from Perkin-Elmer. Vibrax-VR platform shaker was from IKA. Balances were from Ohaus. Sonicators were from Sonics and Materials. Speed-vacs were from CHRIST. Gel Electrophoresis System (Horison 11-14) was from Life Technologies. Tissue culture class II safety cabinets were from Medical Air Technology (Oldham, UK). CO₂ incubators were from Mackay and Lynn (Dundee, UK). The LiCOR odyssey infrared imaging system was from Li-COR biosciences (Cambridge, UK).

2.2 Methods

2.2.1 MOLECULAR BIOLOGY METHODS

2.2.1.1 Transformation and plasmid purification from *E.coli*

Calcium competent *E.coli* DH5 α cells were kindly provided by Dr Mark Peggie using a previously described method (Inoue et al, 1990). For each transformation, approximately 5-20 ng DNA was added to 35 μ l of competent cells and incubated on ice for 5 min. Cells were then subjected to heat shock at 42°C for 90 s in a water bath to induce the uptake of DNA and briefly placed back on ice. Bacteria were then spread onto LB agar plates containing 100 μ g/ml ampicillin and incubated at 37°C overnight. DNA for mammalian cell transfection was amplified in *E.coli* DH5 α strain.

2.2.1.2 Purification of plasmid DNA from *E.coli*

Transformed *DH5 α E.coli* were cultured in 150 ml LB containing 200 mg/L ampicillin at 37°C overnight and cells were pelleted by centrifugation at 6000 g for 15 min. Plasmid DNA was purified using a Qiagen plasmid Maxi kit according to the manufacturer's instructions. This yields an approximate of 0.5-1 mg plasmid DNA.

2.2.1.3 Measurement of DNA concentration

DNA concentration was measured using NanoDrop according to manufacturer's instructions. DNA absorb at 260nm. Absorbance was also measured at 280nm because calculation of 260/280 ratio permits the calculation of purity. Ratios of greater than 1.8 are considered as pure. Lower ratios suggest the presence of contaminants such as proteins or phenol.

2.2.1.4 Restriction enzyme digests of plasmid DNA

Restriction digests were carried out using 1 µg DNA in the presence of 2 µl 10X stock of the appropriate digestion buffer and 1U of corresponding restriction enzyme in a final volume of 20 µl. Reactions were incubated at 37°C for 3 hrs and analyzed via agarose gel electrophoresis.

2.2.1.5 DNA mutagenesis

All mutagenesis reactions were performed using the QuikChange site directed mutagenesis method (Stratagene) with KOD polymerase (Novagen) as per manufacturing instructions. DNA constructs were verified by DNA sequencing.

2.2.1.6 Genome editing-TALENs: (Knocking out MYPT1 from HEK293 cells using TALENs).

Transcription activator-like nucleases (TALENs) were synthesized and assembled by Golden Gate digestion-ligation, using a standard protocol (Sanjana et al., 2012) with the help of Dr Piotr Szyniarowski. MYPT1 TALENs were designed to target MYPT1 1st exon as shown in a Table 2.7. Spacer strand sequence between two TALENs was chosen so that it comprises PVUII restriction site.

Table 2.7: TALENs construction details

Targeted DNA sequence (Exon1)	TALEN1 repeat-variable di-residue' (RVD)	TALEN2 repeat-variable di-residue' (RVD)	Spacer Strand Sequence	Restriction Enzyme Site in Spacer
TGAAGATGGCGG ACGCGAAGCAGA AGCGGAACGAGC AGCTGAAACGCT GGATCGGCTCCGAGA	NN NI NI NN NI NG NN NN HD NN NN NI HD NN HD NN NI NI NN	HD NG HD NN NN NI NN HD HD NN NI NG HD HD NI NN HD NN	AGAAGCGGAA CGAGCAGCTGA	PVUII (CAGCTG)

Lipofectamine (Invitrogen) was used to transiently transfect HEK293 cells with 4 µg of each TALEN1 and TALEN2 construct. After 24 hours of transfection cells were

single cell cloned manually as well as by FACS machine (Dr Rosie Clarke). Single cell clones were then selected and tested by PCR, and PvuII restriction enzyme digestion. The DNA of clones cleaved by TALENs was then extracted; PCR products were inserted into TOPO vector and sequenced. Then, these clones were re-single cell cloned again and tested by PCR or Western blotting.

2.2.1.7 Genome editing-CRISPR/Cas9: (Knocking out MYPT1 from HEK293 cells stably over-expressing GFP MYPT1 protein using CRISPR/Cas9).

Materials

Table 2.8: CRISPR/Cas9 construction details (All constructs generated by Thomas McCartney, DSTT, University of Dundee)

<i>Materials</i>	<i>Function</i>	<i>Sequence</i>
Guide RNA/Cas9 D10A complex	1) Each guide RNA contains a 20 nucleotide guide sequence, which directs Cas9 D10A nickase to a 20 nucleotide DNA target via Watson-Crick base pairing. 2) Cas9 creates a double-nick induced DSB that can be repaired by either NHEJ or HDR	Targeting MYPT1 exon3: <u>Antisense RNA guide:</u> GTCCTCCTCCGCAATATCTAA cloned into the Cas9 D10A vector pX335 <u>Sense RNA guide:</u> GCAAAATGAAGTTAATCGGCA cloned into pBABED puro U6
Guide protected MYPT1 sequences	Previous studies strongly indicated that MYPT1 KO is lethal. Guide protected MYPT1 sequences allow to rescue this phenotype.	Sequence 1 : pcDNA5D frtTO GFP MYPT1 rescue (guide protected) Sequence 2: pcDNA5D FRT/TO GFP MYPT1 guide protected + T500A Sequence3: pcDNA5 FRT/TO GFP MYPT1 T419/500/524/529/671/761/892A + guide protected

Generation of stable cell lines

Cell lines with the stable inducible overexpression of GFP-MYPT1 wild-type or indicated mutants were generated using Flp-In T-Rex System (Invitrogen) following manufacturer's instructions. This system allows a tetracycline-inducible expression of the protein of interest in HEK293 FLP/IN TREX cells using the pcDNA5/FRT/TO

vector encoding the gene of interest. Critically, over-expressed MYPT1 proteins were designed by Thomas McCartney to be resistant to antisense and sense CRISPR/CAS9 guides created to target endogenous MYPT1 by introducing silent mutations at the targeted region.

Targeting endogenous MYPT1 protein by CRISPR/Cas9

HEK293 cells stably over-expressing GFP MYPT1 WT or mutant protein were harvest in recovery media ((DMEM supplemented with 10% (v/v) foetal bovine serum (FBS), 2 mM L-glutamine, antibiotic/antimycotic, 1X non-essential amino acids, 1mM sodium pyruvate, hygromycin and blasticidin) and transfected with 1 µg of each anti-sense and sense guide RNAs using PEI transfection reagent (see PEI transfection section). 24 hours later media was replaced with selection media comprising 2µg/ml Puromycin. Cells that have been successfully transfected with the puromycin plasmid are likely to have taken up the remaining constructs also. 24 hours later, selection media was replaced again with media containing 2.0 µg/ml Puromycin to continue selection. Then, cells were placed into recovery media and transfected again with guide RNA/Cas9 complex to maximize the chances of transfection. 24 hours after transfection cells were selected again with puromycin containing media. Next day cells were prepared for FAC sorting and sorted into 96 well plates, each contain a single cell. Cells were left to recover in recovering media for couple of weeks and then were screen by western blotting. It is important to note that at all stages, recovery and selecting media was supplemented with hygromycin and blasticidin to ensure the expressing of rescue MYPT1. Experience has proven that in the absence of GFP-MYPT1 over-expression MYPT1 KO cells died.

2.2.1.8 Agarose gel electrophoresis

1.7 g of agarose was boiled in 170 ml of 1X TAE buffer. 10 µl of 10 mg/ml ethidium bromide were added after the boiled agarose solution cooled down to approximately 50-60°C and then poured into the gel casting tray. The gel was allowed to solidify and electrophoresis was carried out at 100 V for 45 min.

2.2.1.9 DNA sequencing

The sequencing was carried out by DNA sequencing service (School of Life Sciences, University of Dundee) using DYEnamic ET terminator chemistry kit (Amersham Biosciences) on Applied Biosystems sequencers.

2.2.2 MAMMALIAN CELL CULTURE

2.2.2.1 Cell culture

HEK293, HEK293T, HEK293 FLP/IN TREX and MEF cells were grown in Dulbecco's modified eagle medium (DMEM) supplemented with 10% (v/v) foetal bovine serum (FBS), 2mM L-glutamine, antibiotic/antimycotic, 1X non-essential amino acids and 1mM sodium pyruvate. Procedures were done under aseptic conditions meeting biological safety category 2 regulations. Cells were grown at 37°C in a 5% CO₂ water-saturated incubator. For the passaging, adherent cells were washed once with PBS and then incubated with Trypsin/EDTA for 3-5 min at room temperature or at 37°C. Fresh media was added and detached cells were resuspended in cell culture medium and split at a 1:2 – 1:20 ratios for continued culture.

2.2.2.2 Freezing/thawing of cell lines

Confluent cells grown in T-75 flasks were trypsinized and collected in culture media by centrifuging at 1500 g for 3 min. Culture media were aspirated and cells

resuspended in 3 ml of freezing media (50% DMEM/ 40%FBS/ 10% DMSO). Aliquots of cells (1 ml) in cryovials were stored in a Nalgene Mr Frosty Freezing Container at -80°C for 2 days, and transferred to liquid nitrogen. To thaw the cells, each vial was placed in 37°C water bath for 3 min and cells were added to a T-25 flask containing 10 ml of culture media. Cells were allowed to attach and given a media change a day later to remove trace amounts of DMSO.

2.2.2.3 Transfection of cells using polyethylenimine (PEI)

Cells were transiently transfected using the polyethylenimine (PEI) method (Durocher et al., 2002). 1 mg/mL PEI stock was prepared in 20 mM Hepes (pH 7). For transfection of cells grown on 10 cm dishes, 5 µg of DNA was mixed with 20 µL 1mg/mL PEI and 1 mL serum-free DMEM and left for 15 min at room temperature before being added to cells. Cells were harvested 36 hrs post transfection.

2.2.2.4 Treatment of cells with inhibitors and other agents

Cells were treated with 1 µM of indicated LRRK2 inhibitor or DMSO control for 1hr (or other time point if otherwise indicated) before whole cell lysis.

2.2.2.5 Generation of stable cell lines

To ensure low-level uniform expression of recombinant proteins, manufacturer's instructions (Invitrogen) were followed to generate stable cell lines that express GFP-tagged forms of proteins (cDNA subcloned into pcDNA5-FRT-TO plasmid) in a tetracycline inducible manner. Flp-In T-REx-293 host cells containing integrated FRT recombination site sequences and Tet repressor, were co-transfected with 9 µg of pOG44 plasmid (which constitutively expresses the Flp recombinase), and 1 µg of pcDNA5/FRT/TO vector containing a hygromycin resistance gene for selection of the gene of interest with GFP tag under the control of a tetracycline-regulated promoter.

Cells were selected for hygromycin and blasticidin resistance three days after transfection by adding new medium containing hygromycin (100 µg/ml) and blasticidin (7.5 µg/ml). After 3 weeks of selection, colonies were trypsinized and expanded. Expression of the recombinant protein was induced with 0.1 µg/ml of tetracycline for 24 hours.

2.2.2.6 Cell/tissue lysis

Cells were lysed using mammalian cell lysis buffer as listed in 2.1.6. Lysates were clarified by centrifugation at 15,000 g for 10 min at 4 °C and the supernatant was collected.

2.2.3 PROTEIN BIOCHEMISTRY

2.2.3.1 Purification of GST recombinant proteins from HEK293 cells

50-60% confluent HEK293 cells were transfected with corresponding GST-tagged LRRK2 constructs by PEI method described previously and harvested following 36-48 hr. Clarified cell lysates were incubated for 1 hour on a rotating platform with glutathione-Sepharose 4B (20 µl beads/5 mg of cell lysate) previously equilibrated in PBS. Afterwards, the beads were washed three times with Lysis Buffer containing 0.5 M NaCl and two times with Buffer A. GST-tagged proteins were eluted from the resin with an equal volume of Buffer A supplemented with 150 mM NaCl, 0.27M sucrose and 40mM glutathione (pH 7.5-8) for 10min at room temperature on a rotating platform. The elution was repeated and all the elutions were pooled together, filtered through a 0.22 µm Spin-X column aliquoted, snap-frozen in liquid nitrogen and stored at -80°C. Concentration of purified recombinant proteins was estimated by Bradford assay and their purity was estimated by SDS-PAGE.

2.2.3.2 Estimation of protein concentration

Protein concentration of purified proteins and cleared cell lysates was evaluated

using the Bradford method in a 96 well plate format (Bradford, 1976). 0.2 ml of Bradford reagent (Pierce) was added to 10 μ l of diluted sample (cell lysates were usually diluted 10-fold in water). 10 μ l of water was used as a blank. For a standard curve 10 μ l of serial dilutions of BSA were used (1, 0.5, 0.25, 0.125 and 0.00063 mg/ml). Absorbance at 595 nm was measured using a 96 well plate reader. All samples were measured in triplicate and a standard curve was generated for each analysis. Bradford method is a colorimetric protein assay, based on an absorbance shift from 465 nm (red) to 595 nm (blue) upon binding to proteins. The Coomassie dye binds to arginines, aromatic amino acids, and histidines. For purified proteins, Coomassie staining of polyacrylamide gel verified sample purity additionally.

2.2.3.3 Covalent coupling of antibodies

Antibodies were covalently coupled to protein G-Sepharose with a dimethyl pimelimidate (DMP) cross-linking procedure. DMP has two functional imine groups, which interact with free amine groups at pH range 7.0-10.0 to form amidine bonds. Antibody-coupled beads (1 μ g antibody per 1 μ l beads) were prepared by incubating antibody with Protein – G Sepharose beads at 4°C for 1hr. The beads were washed 5 times with 10 volumes of 0.1 M sodium borate pH 9 and then resuspended in 10 volumes of 0.1 M sodium borate pH 9 containing freshly added dimethyl pimelimidate (a fresh batch used every time) to a concentration of 20 mM and incubated for 30 min at room temperature with gentle mixing. The beads were pelleted and then reincubated with dimethyl pimelimidate. The beads were washed 4 times with 10 volumes of 50 mM glycine pH 2.5 to remove all the antibodies that were not covalently coupled to the beads. The beads were then washed twice with 0.2 M Tris-HCl pH 8 and incubated in this buffer for a further 2 h at room temp with gentle mixing to ensure that any residual DMP was quenched by reaction with the

amine group of Tris. The antibody-coupled beads were stored in PBS containing 0.02% (w/v) sodium azide at 4°C for up to one month.

2.2.3.4. Immunoprecipitation

1 mg of cell lysate was incubated with 5 µg of antibody coupled to 5 µl of protein G-Sepharose for 2 hrs at 4°C on a rotating wheel. For overexpressed protein immunoprecipitation, depending on the tag of the protein, 5 µl of FLAG-agarose or HA-agarose or GST-sepharose beads was incubated with 200 µg of cell lysate for 2-4 hrs at 4°C on a rotating wheel. The mixture was centrifuged for 1 min at 8,000 g and the supernatant was removed. The immunoprecipitates were washed twice with 0.5 ml of Lysis Buffer containing 0.15 M NaCl and twice with 0.5 ml of Buffer A. Then either they were used for further assays. Alternatively, immunoprecipitates are resuspended in 2xSDS sample buffer (or 2 x NuPAGE LDS sample buffer for mass spectrometry) lacking reducing agent for 10 mins prior to filtering through Spin-X columns to remove antibody-bound bead, then reducing agent was added to the eluted samples and they were heated at 90 °C for 5 mins.

2.2.3.5 Resolution of protein samples via SDS-PAGE

SDS polyacrylamide gel electrophoresis (SDS/PAGE) helps to resolve proteins according to their apparent molecular weight. SDS and LDS are anionic detergents, which coat proteins to give them a net negative charge that is proportional to their molecular weight. This enables the migration of proteins through an acrylamide gel at a rate that is proportional to their size. Samples are also incubated with reducing agents, DTT or βME, to break disulphide linkages and unravel the protein further, to ensure it is linear. Cell extract protein in an LDS buffer (20 µg) was subjected to SDS/PAGE. A stacking gel (pH 6.8) (125 mM Tris HCl pH 6.8, 0.1% SDS, 4% acrylamide, TEMED and ammonium persulphate APS) helps to concentrate the

proteins into a narrow band so that they all enter the resolving gel (pH 8.6) (contained 375 mM Tris-HCl (pH 8.6), 0.1% SDS and 8-10% acrylamide, TEMED and APS) at the same time, enabling proteins of similar molecular weight to migrate in tight bands. Resolving gels were composed of different percentages of acrylamide, which helped to best resolve proteins of a particular molecular weight. The gels were run in Tris-glycine SDS running buffer at a constant 120 V until the dye front had reached the bottom of the gel. The electric field applied to the gel promotes the migration of the negatively charged proteins away from the cathode, at the top of the gel, to the anode. Commercial pre-cast gels (4-12% Bis-Tris, NuPAGE) were used if ubiquitin chains were to be investigated or if proteins were to be subjected to mass spectrometry. Commercial gels were run in MOPS buffer (NuPAGE) if samples were prepared for Mass Spectrometry at a constant 120 V.

2.2.3.6 Resolution of protein samples via Phos-tag gel and immunoblot analysis

Gels for Phos-tag SDS-PAGE consisted of a stacking gel (4%(w/v) acrylamide, 125 mM Tris-HCl pH 6.8, 0.1%(w/v) SDS, 0.2% (v/v) TEMED, 0.08%(w/v) ammonium persulfate (APS)) and a separating gel (12% (w/v) acrylamide, 375 mM Tris-HCl pH 8.8, 0.1% (w/v) SDS, 75 μ M Phos-tag acrylamide, 100 μ M MnCl₂, 0.1%(v/v) TEMED, 0.05% (w/v) APS). Gel mixture was degassed for 10 minutes before adding TEMED and APS.

Cell/tissue were lysed in the absence of EDTA. Lysates were then mixed with 4x SDS-PAGE sample buffer (250 mM Tris-HCl pH 6.8, 8% (w/v) SDS, 40% (v/v) glycerol, 0.02% (w/v) bromophenol blue and 4% (v/v) β -mercaptoethanol), supplemented with 10 mM MnCl₂, heated at 95 °C for 5 minutes and centrifuged at 20,800 g for 1 minute. 10- 20 μ g of samples were loaded onto Phos-tag SDS-PAGE

Bis-Tris 4-12% gels and electrophoresed at 70 V for the stacking part and at 150 V for the separating part with the running buffer (25 mM Tris, 192 mM glycine, 0.1%(w/v) SDS). Gels were then stained with Colloidal Blue Staining Kit (Life Technologies) according to the manufacturer's instructions. For immunoblot analysis, gels were washed for 10 minutes in the transfer buffer (48 mM Tris, 39 mM glycine, 20%(v/v) methanol) containing 10 mM EDTA and 0.05%(w/v) SDS three times, followed by one wash in the transfer buffer containing 0.05% SDS for 10 min. Proteins were electrophoretically transferred to nitrocellulose membranes (Amersham Protran 0.45 µm NC; GE Healthcare) at 100 V for 180 minutes on ice in the transfer buffer without SDS/EDTA. Transferred membranes were blocked with 5% (w/v) non-fat dry milk (NFDM) dissolved in TBS-T (20 mM Tris-HCl pH 7.5, 150 mM NaCl, 0.1%(v/v) Tween-20) at room temperature for 30 minutes. Membranes were then incubated with primary antibodies diluted in 5% Non-fat Dry Milk & Skim Milk Powder in TBS-T overnight at 4 °C. After washing membranes in TBS-T, membranes were incubated with HRP-labelled secondary antibodies diluted in 5% Non-fat Dry Milk & Skim Milk Powder in TBS-T at room temperature for 1 hour. After washing membranes in TBS-T, protein bands were detected by exposing films (Medical Film (Konica Minolta) for normal immunoblot and Amersham Hyperfilm ECL (GE Healthcare) for Phos-tag immunoblot) to the membranes using an ECL solution (Amersham ECL Western Blotting Detection Reagents (GE Healthcare) for normal immunoblot and SuperSignal West Dura Extended Duration (Thermo Fisher Scientific) for Phos-tag immunoblot).

2.2.3.7 Coomassie staining of polyacrylamide gel

Polyacrylamide gels were stained in Instant Blue or Colloidal Coomassie staining solution for 1-2 hrs and destained with MilliQ water.

2.2.3.8 Desiccation of polyacrylamide gels and autoradiography

Before drying, gels were incubated in 5% glycerol for 10 min and sandwiched between two sheets of pre-wet cellophane. The gels were then dried in a GelAir Dryer for approximately 1 hour. Dried gels were then exposed to Hyperfilm MP for 24 hours in an X-Oma autoradiography cassette at -80°C. Films were then developed using Konica auto-developer.

2.2.3.9 Transfer of proteins onto nitrocellulose membranes

Gels were sandwiched between nylon! sponges, Whatman 3 mm filter papers and nitrocellulose membrane all soaked in transfer buffer. The transfer cell was submerged in transfer buffer and transfer carried out at 750 mA for 1 hour.

2.2.3.10 Immunoblotting

After transfer, membranes were stained with Ponceau S and destained in distilled water in order to visualize the transferred proteins. Non-specific binding of antibodies was prevented by incubating the membranes with 5% (w/v) skimmed milk in TBST for 2 hour at room temperature. Membranes were then incubated with primary antibodies diluted according manufacture instructions in either 5% (w/v) skimmed milk or BSA in TBST at 4 °C for 16 hours. Membranes were next washed three times for 10 min with TBST. Horseradish peroxidase (HRP)-conjugated secondary antibodies diluted at 1:2500 in 5% (w/v) skimmed milk in TBST were incubated with the membranes for 1 hour at room temperature and the membranes were washed three more times with TBST. Membranes were then incubated with the enhanced chemiluminescence (ECL) substrate and exposed to X-ray films for various length of time. Films were developed using a Konica automatic developer. Where indicated, signals were visualized using the Odyssey™ Infrared Imaging System instead of ECL. The procedure was the same but the secondary antibodies were labelled with

either IRD800 or Alexa680 dyes and the signal captured and quantified with an Odyssey Infrared Imaging System.

2.2.4 IN-VITRO ASSAYS

2.2.4.1 Kinase assay

Kinase assays employing a protein substrate

Indicated amounts of kinases were incubated with 1 µg of purified protein substrate in the presence of 0.1 mM [γ^{32} P]-ATP and 10 mM Magnesium acetate in Buffer A at 30°C for times indicated in the figure legends. Reactions were terminated with SDS sample buffer.

Kinase assays employing a peptide substrate

In vitro LRRK2 wild-type and mutants' activities were measured using Cerenkov counting of incorporation of radioactive 32 P from [γ^{32} P]-labelled ATP into a corresponding substrate peptide used (Nictide or LRRKtide). A typical 50 µl kinase reaction consisted of 10 mM magnesium acetate, 0.1mM [γ^{32} P] ATP (450-500 cpm/pmol), 0.1% β-mercaptoethanol, 100 or 300 µM of peptide substrate. Control reactions contained either no kinase or IPs with IgG control antibody. Reactions were incubated at 30°C for 30 min and were eventually terminated by pipetting 40 µl onto a 2 square cm of P81 paper (which binds substrates that contain a net basic charge at acidic pH) which was dropped to a beaker containing 50 mM orthophosphoric acid. Papers were washed four times in 50 mM orthophosphoric acid to remove any unbound radioactivity. Papers were then washed in acetone for 3 min and air dried. Papers were folded and transferred to 1.5ml tubes and Cerenkov counting was done on a liquid scintillation counter. Kinase activity was expressed as specific activity (units of activity per mg of protein or lysate used for IP of the protein). One unit of activity was the amount of kinase which was needed to incorporate

1 μ mol of phosphate per 1 μ mol of substrate peptide per minute.

2.2.5 MASS SPECTROMETRY ANALYSIS

2.2.5.1 Processing protein bands for analysis by mass spectrometry

Proteins were reduced with 10 mM DTT at 92°C for 5min and alkylated with 50 mM Iodoacetamide before resolving by SDS-PAGE and stained using Colloidal Coomassie staining solution. Samples for mass spectrometry were prepared in a laminar flow hood. Protein bands were excised from the gel using a sterile scalpel and placed in a 1.5 ml Eppendorf tube. Gel pieces were washed sequentially with 0.5 ml of water, 50% acetonitrile/water, 0.1 M NH_4HCO_3 and 50% acetonitrile/50 mM NH_4HCO_3 . All washes were performed for 10 min on a Vibrax shaking platform. Once colorless, gel pieces were shrunk with 0.3 ml acetonitrile for 15 min. Acetonitrile was aspirated and trace amounts removed by drying sample in a Speed-Vac. Gel pieces were then incubated for 16 h with 5 mg/ml trypsin in 25 mM triethylammonium bicarbonate (TEA) at 30°C on a shaker. An equal volume of acetonitrile (same as trypsin) was added to each sample and further incubated on a shaking platform for 15 min. The supernatants were transferred to clean tubes and dried by Speed-Vac. Another extraction was performed by adding 100 μ l 50 % acetonitrile/2.5 % formic acid for 15 min. This supernatant was combined with the first extract and dried by Speed Vac.

2.2.5.2 Processing protein bands for analysis by mass spectrometry

All mass spectrometric (MS) analysis was performed by Dr. David Campbell, Robert Gourlay and Joby Varghese (College of Life Science, University of Dundee). Analysis of the tryptic peptides by LC-MS were performed on a Thermo LTQ-Orbitrap system. The MS data was analysed through the Mascot search engine (www.matrixscience.com) against the human International Protein Index database.

Tryptic phosphopeptides were identified by LC-MS on an ABI 4000 Q-TRAP system using precursor ion scanning in negative mode to search for release of the (PO₃)-ion (-79 Da) allowing for +/-1 Da (Williamson et al, 2006), followed by MS/MS analysis in positive mode. The resulting data files were searched against the appropriate sequence, using Mascot run on an in-house server, with a peptide mass tolerance of 1.2 Da, a fragment mass tolerance of 0.8 Da, and with variable modifications allowing for phosphorylation of serine/threonine or tyrosine and for methionine oxidation or dioxidation. Mass Finger Printing results from Mascot were viewed using a Scaffold server.

2.2.5.3 *In vitro* ³²P-labelling of proteins and phospho-sites mapping using HPLC and Edman degradation

5 µg of bacterially purified LRRK2 substrate was incubated with HEK293 purified-LRRK2 kinase for 30 min at 30°C in master mix comprising Buffer A, 10 mM magnesium acetate and 0.1 mM [γ -³²P]ATP (11,000-25,000 cpm/pmol) in a total reaction volume of 40 µl. The reaction was then terminated by addition of 4xLDS sample buffer, boiled with 10 mM DTT for 10 mins and resolved on a NuPAGE gel (Invitrogen), which was then stained with Colloidal Coomassie blue. Coomassie-stained bands migrating with the expected molecular mass of corresponding LRRK2 substrate were excised from the gel and digested with trypsin or Asp-N (as described previously). Following digestion with specific protease depending on the protein sequence (Trypsin or Asp-N), > 95% of the ³²P radioactivity incorporated in the gel bands was recovered and samples were then subjected to HPLC on a Vydac C18 column equilibrated in 0.1% (w/v) trifluoroacetic acid (TFA), with a linear acetonitrile gradient at a flow rate of 0.2 ml/minute. Fractions of 0.1 ml were collected and phosphopeptides were analysed by LC-MS/MS. The resultant data files were

searched using Mascot (www.matrixscience.com) run on an in-house system allowing for Phospho (S/T), Phospho (Y), Oxidation (M) and Dioxidation (M) as variable modifications. Individual MS/MS spectra were inspected using Xcalibur 2.2 software. The site of phosphorylation of all the ³²P labelled peptides was determined by solid-phase Edman degradation on an Applied Biosystems 494C sequencer of the peptide coupled to Sequelon-AA membrane (Applied Biosystems) as described previously (Campbell and Morrice, 2002). HPLC, LC-MS and Edman degradation was performed by Mr. Robert Gourlay.

2.2.5.4 *In vivo* Phospho-site mapping of LRRK2 substrate

In over-expressed cell system

Flp-In T-Rex HEK 293 cells stably expressing GFP tagged LRRK2 [G2019S] were co-transfected with the respective HA or FLAG tagged LRRK2 substrates, induced with 0.1 µg/ml of Doxycycline and then treated with DMSO control or 1 µM LRRK2 specific LRRK2 kinase inhibitors for 1 hour (LRRK2-IN1 and GSK2578215A). Approximately 15 mg of lysate was subjected to immunoprecipitation with anti-FLAG-agarose for 2 hours at 4 °C and then eluted in LDS sample buffer. Samples were passed through Spin-X column to remove the bead and boiled with 10 mM DTT to denature proteins. The immunoprecipitated were then resolved on a NuPAGE gel (Invitrogen), which was then stained with Colloidal Coomassie blue. Coomassie-stained bands migrating with the expected molecular mass of corresponding LRRK2 substrate were excised from the gel and digested with trypsin (as described previously) and samples underwent phosphosite analysis with LTQ-Orbitrap Velos. Individual MS/MS spectra containing the phospho-sites of interest were inspected using Xcalibur 2.2 software to determine any obvious changes in phospho-mapped sites in response to LRRK2 inhibition.

In endogenous cell system

MEF LRRK2 wild type or drug resistant LRRK2 [A2016T] mutant cells were treated with 10 nM of MLI-2 inhibitor for 1 hour. Approximately 30 mgs of lysate was subjected to immunoprecipitation with anti-MYPT1 antibody covalently coupled to G-sepharose beads (as described previously) for 2 hours at 4 °C and then eluted in LDS sample buffer. Samples were passed through Spin-X column to remove the bead and boiled with 10mM DTT to denature proteins. The immunoprecipitated were then resolved on a NuPAGE gel (Invitrogen), which was then stained with Colloidal Coomassie blue. Coomassie-stained bands migrating with the expected molecular mass of corresponding LRRK2 substrate were excised from the gel and digested with trypsin (as described previously) and samples underwent phosphosite analysis with LTQ-Orbitrap Velos. Individual MS/MS spectra containing the phospho-sites of interest were inspected using Xcalibur 2.2 software to determine any obvious changes in phospho-mapped sites in response to LRRK2 inhibition.

2.2.6 MOUSE MODEL

2.2.6.1 Generation of LRRK2 knock-in mouse model of the corresponding S910A+S935A mutations

The constitutive LRRK2 [S910A+S935A] knock-in mouse line was produced by implementing a targeting strategy based on NCBI transcript NM_025730.3, to introduce two point mutations S910A and S935A into exon 21 of the LRRK2 gene by homologous recombination in mouse embryonic stem cells (Taconic-Artemis GmbH, Germany).

To start with, the S910A and S935A mutations have been introduced into exon 21 by site-directed mutagenesis with the QuickChangeII site-directed mutagenesis kit (Stratagene) (S910A: TCA to GCC and S935: TCG to GCG of exon 21). The positive

selection marker PuroR has been flanked by FRT sites and inserted into intron 21. 5' & 3' homology arms (approx. 4.1 & 6 kb respectively) flanking exon 21 were generated using Phusion High-Fidelity DNA Polymerase (New England BioLabs) on a C57BL/6J genomic DNA template. The 5' & 3' homology arms comprising mutated exon 21 were subcloned into a parental targeting vector to achieve the positioning of the loxP & FRT sites and PGKneo cassette. For this purpose the targeting vector was generated using BAC clones from the C57BL/6J RPCIB-731 BAC library which then were transfected into the Taconic-Artemis C57BL/6N Tac ES cell line. Homologous recombinant clones were selected using positive (PuroR) and negative (Thymidine kinase - Tk) selection. The constitutive knock-in allele comprising desired mutations was obtained after Flp-mediated removal of the selection marker. The targeting construct was linearized and electroporated into ES cells according to standard methods. Successful gene targeting of ES cells at the 5' and 3' end was confirmed by sequencing of a ~6 kb PCR product. Properly targeted ES cell clones were then subjected to the diploid injection into BALB/c blastocysts and implanted into foster mothers according to standard procedures. Male chimaeras resulting from the S910A+S935A targeted ES cells were bred with C57BL/6J female mice expressing cre recombinase from the ROSA26 locus to facilitate removal of the loxP flanked PGKneo cassette in vivo, and germline transmission was identified by the presence of black, strain C57BL/6, offspring (G1) and PCR.

2.2.6.2 Genotyping of mice via PCR

Genotyping of mice was performed by PCR using genomic DNA isolated from ear biopsies. For LRRK2-S910A+S935A knock-in mouse, primers 5'-GTGCTTGAAGTTTGATCATAATGC-3' and 5'-GCATATAGCATGTAGTGTCATCTCC -3' were used to detect the wild type and

knock-in alleles (WT- 326bp, KI- 401bp; heteroduplex formation). The PCR program consisted of 5 min at 95 °C, then 35 cycles of 30 s at 95 °C, 30 s at 60 °C and 30 s at 72 °C, and then 5 min at 72 °C. DNA sequencing was used to confirm the knock-in mutation and performed by DNA Sequencing & Services (MRC-PPU; <http://www.dnaseq.co.uk/>) using Applied Biosystems Big-Dye version 3.1 chemistry on Applied Biosystems model 3730 automated capillary DNA sequencer. Genotyping was performed by Elaine Forsyth and Gail Gilmour.

2.2.6.3 Mouse motor phenotyping: rotarod test

Accelerating rotarod test

On each testing day, a mouse was placed on each of 5 lanes of a rotarod (Model 47600, Ugo Basile, Italy), with the beam (diameter = 3 cm) rotating at a constant speed of 6 r.p.m. Each mouse occupied the same lane during each testing day, but lane occupancy was counterbalanced between subjects such that each lane was used by approximately the same number of wild type and homozygous mice across the series of runs carried out within each day. Once all lanes were occupied, the beam accelerated at a constant rate from 6 to 50 r.p.m. over a 300-s period. Latency to first lose grip on the beam was recorded. 'Loss of grip' included both falling from the beam and clinging to the rotating beam to avoid falling. If a mouse lost grip because of turning around on the beam, it was immediately placed back on the rotarod facing in the correct direction; these incidents were not counted in the analysis of latency to lose grip. Testing continued for a total of 24 days in 3 sets with 2 weeks breaks after 8 repeats. All trials were recorded and latencies were analysed.

Fixed-speed rotarod test

Fixed-speed rotarod testing was carried out in a single day. Mice were placed on the rotating beam, and latency to lose grip (defined as for the accelerating protocol) was

recorded from the moment the mouse was released. Mice were tested at approximately 1-h intervals using progressively increasing rotational speeds—10, 20, 30 and 40 r.p.m. Mice occupied the same lanes as during accelerating rotarod training. All trials were recorded and latencies were analysed.

2.2.6.4 Lysis of mouse tissues

Mouse tissues were rapidly excised, frozen in liquid nitrogen and stored at -80°C until use. Tissues were weighed and homogenised in a 10-fold excess of ice-cold lysis buffer (usually TRIS-CHAPS buffer unless otherwise stated). Lysates were clarified by centrifugation at 3,000 g for 15 min at 4°C and supernatants then further centrifuged at 18,000 g for 20 min at 4°C. Lysates that were aliquoted, snap frozen and stored at -80°C.

2.2.6.5 Generation of LRRK2 [S910A+S935A] mouse embryonic fibroblasts (MEFs)

Littermate matched wild-type and homozygous LRRK2 [S910A+S935A] mouse embryonic fibroblasts (MEFs) were isolated from mouse embryos at day E12.5 resulting from crosses between heterozygous LRRK2 [S910A+S935A] / WT mice using a previously described protocol [11909979]. Cells were genotyped as described previously. Homozygous LRRK2 [S910A+S935A] knock-in as well as the wild type cells generated from the same littermate were spontaneously immortalised by prolonged passaging in parallel for at least 20 passages before being used for Phos-tag experiments. Genotype of these cells was also confirmed by immunoblot analysis with phospho 910 and 935 antibodies.

2.2.6.6 Statistics

Statistical significance was assessed by one or two-way analysis of variance (ANOVA) using GraphPad Prism 5.0. All the experiments presented in this thesis

were performed at three times with similar results obtained on each occasion. Error bars indicate the standard deviation (SD) or standard error of the mean (SEM), as indicated in figure legends.

Chapter 3:

Characterization of LRRK2

[S910A+S935A] Mouse Model

3.1 Introduction

As discussed in the introduction to this point (Section 1.4), previous studies in our laboratory identified an important biomarker for LRRK2 activity. It was reported that treatment of cells or mice with structurally different LRRK2 kinase inhibitors leads to dephosphorylation of LRRK2 at two residues: S910 and S935 (Dzamko et al., 2010) (Figure 3.1). Moreover, the results strongly indicated that S910 and S935 residues are not LRRK2 autophosphorylation sites (Dzamko et al., 2010; Dzamko et al., 2012).

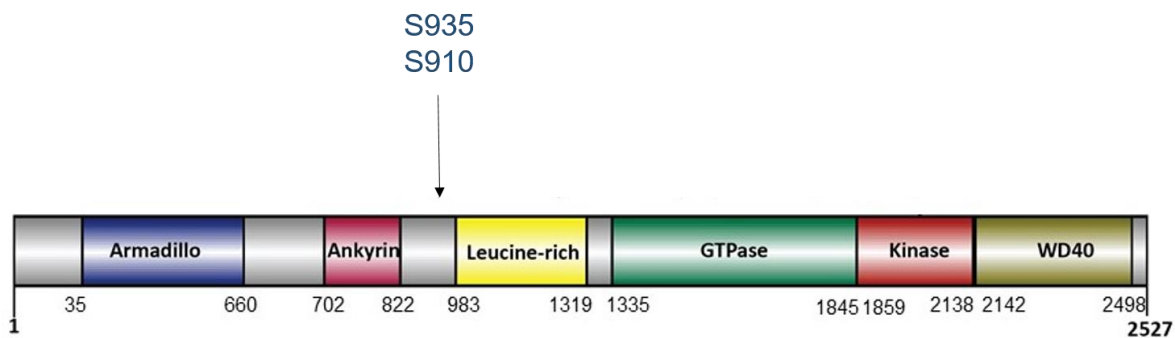


Figure 3.1: Schematic representation of LRRK2 protein highlighting S910 and S935 location.

In our laboratory it was hypothesised that these sites are regulated by a distinct signaling mechanism that is controlled by LRRK2. According to this model, LRRK2 functions as an upstream constituent of a signal transduction pathway that either directly or indirectly stimulates the activity of a protein kinase or inhibits the activity of protein phosphatase that acts on S910 and S935 (Dzamko et al., 2010). In addition, very recent unpublished work by Francesca Tonelli has shown that inhibition of cells with an LRRK2 inhibitor induces dephosphorylation of S935 as well as of S1292 (a known LRRK2 autophosphorylation sites described in Section 1.4.2) and that phosphorylation of S935 but not S1292 is restored following a treatment with

phosphatase inhibitor Calyculin A in the continuous presence of LRRK2 kinase inhibitor. This indicates that LRRK2 can be phosphorylated by an LRRK2 independent kinase.

However, other studies proved that phosphorylation of LRRK2 at these sites could also be uncoupled from LRRK2 kinase activity (Genta Ito et al., 2014). First of all, it was shown that catalytically inactive LRRK2 [D2017A] knock-in mice still have S910 and S935 phosphorylated in cells and that these sites are not dephosphorylated in response to LRRK2 inhibitors, suggesting that phosphorylation of these sites does not require LRRK2 kinase activity (Genta Ito et al., 2014). Secondly, it was also described that the G2019S mutation does not enhance Ser935 phosphorylation, indicating that increased LRRK2 kinase activity does not result in amplified Ser935 phosphorylation (Genta Ito et al., 2014). This result also suggests that monitoring S935 phosphorylation might not be a very useful reporter for intrinsic LRRK2 kinase activity. An alternative model has been put forward suggesting that inhibition of LRRK2 kinase activity with specific LRRK2 kinase inhibitors leads to a conformational change of LRRK2 protein kinase resulting in inhibition of access of a protein kinase or an enhanced access of a protein phosphatase to these sites (Genta Ito et al., 2014). Scientifically for this model to be correct every LRRK2 inhibitor that has been developed thus far would need to have the ability of altering the conformation of LRRK2 and thereby prevent its dephosphorylation at S910 and S935. To sum up, according to the model 1, dephosphorylation of S910 and S935 is dependent on indirect LRRK2 kinase activity (Figure 3.2 A) while model 2 suggests that dephosphorylation of LRRK2 is a result of LRRK2 conformational change induced by LRRK2 inhibitors (Figure 3.2.B).

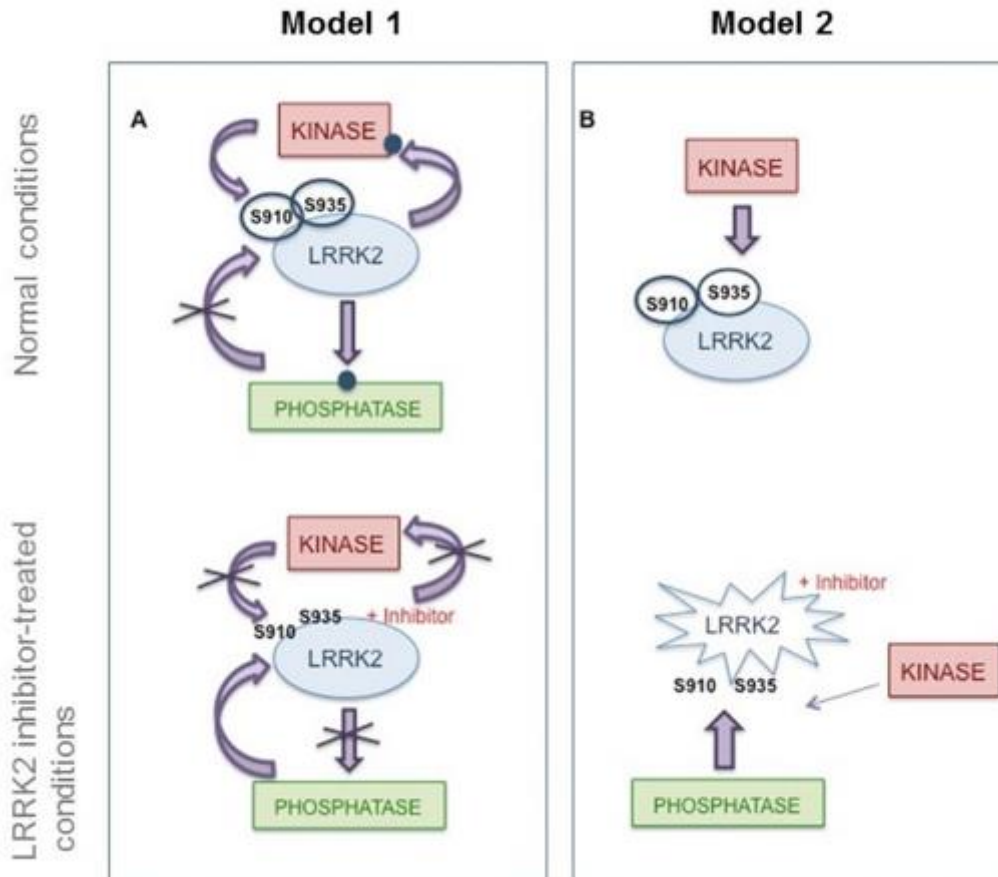


Figure 3.2: Schematic representation of LRRK2 S910 and S935 regulation within the cell under normal and inhibitor-treated conditions. (A) According to the model 1, under normal conditions LRRK2 either activates a protein kinase or blocks the activity of a protein phosphatase that acts on S910 and S935. Upon inhibition of LRRK2 kinase activity occurs dephosphorylation of S910 and S935 through inactivation of a protein kinase activity or recovery of a protein phosphatase activity. **(B)** According to the model 2, under normal condition LRRK2 S910 and S935 residues are constitutively phosphorylated by a protein kinase. Inhibition of LRRK2 kinase activity results in a conformational change, which exposes S910 and S935 sites in such a way that provides an enhanced access of a protein phosphatase to these sites and blocks entree of a protein kinase. As a consequence, these sites are dephosphorylated due to LRRK2 Inhibition.

In this chapter, the work presented addresses whether phosphorylation of S910 and S935 has a biological role *in vivo*. As dephosphorylation of these sites will mimic the effect of long-term LRRK2 inhibitor treatment and could be linked to safety risks associated with LRRK2 inhibition, I also investigate the pathology of aged LRRK2 [S910A+S935A] tissues.

3.2 Results

3.2.1 Generation of mouse embryonic fibroblasts

Taconic Artemis generated heterozygous LRRK2 [S910A+S935A] knock-in mice by introducing S910A and S935A mutations into the exon 21 (2.2.6.1 Materials and Methods section). I then bred heterozygous mice to obtain homozygous LRRK2 [S910A+S935A] knock-in mice with the aim to investigate the importance of S910 and S935 phosphorylation *in vivo*. Homozygous LRRK2 knock-in mice are viable and don't display any obvious overall phenotype compared with the wild type (Figure 3.3). The summary of the targeting strategy for generation of LRRK2 [S910A+S935A] mice, PCR and sequencing data confirming successful mutation of these sites to alanine are shown in the Figure 3.3.

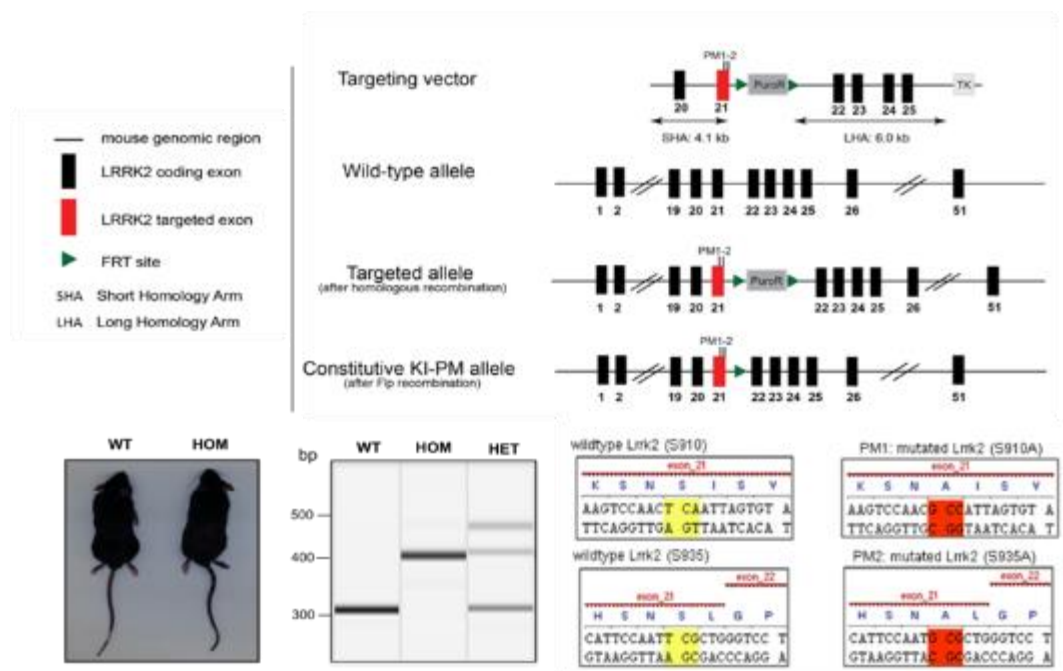


Figure 3.3: Targeting strategy for generation of LRRK2 [S910A+S935A] knock-in mice by Taconic Artemis, PCR and sequencing data.

Mouse embryonic fibroblast (MEF) cells derived from littermate LRRK2 WT, LRRK2 [S910A+S935A] knock-in and LRRK2 KO mice were spontaneously immortalised by prolonged passaging. Cell lysates derived from LRRK2 WT, LRRK2 [S910A+S935A] and LRRK2 KO MEFs were lysed and subjected to immunoblot analysis using total and phospho LRRK2 antibodies (Figure 3.4).

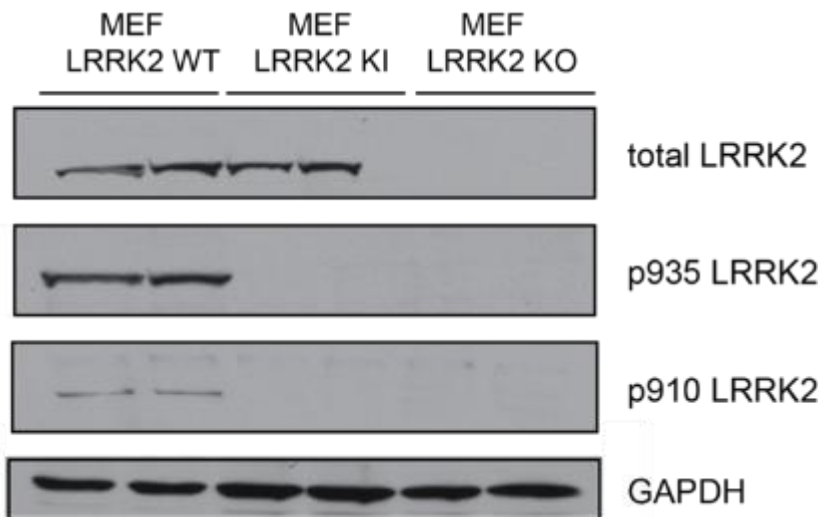


Figure 3.4: Generation of LRRK2 [S910A+S935A] knock-in MEFs. LRRK2 [S910A+S935A], WT and KO MEFs were generated by prolonged passaging. Cell lysates derived from these cells were subjected to immunoblot analysis with indicated monoclonal total and phospho LRRK2 antibodies; GAPDH was used as a loading control.

As expected, no S910 and S935 phosphorylation was detected in LRRK2 knock-in MEFs in contrast to the LRRK2 WT. Moreover, the total levels of endogenous LRRK2 in LRRK2 WT MEFs are similar to the total levels of endogenous LRRK2 in LRRK2 [S910A+S935A] MEFs. These results insinuate that S910A+S935A mutation does not have an effect on LRRK2 stability or expression in MEF cells.

3.2.2 Assessment of endogenous LRRK2 WT and LRRK2 [S910A+S935A] kinase activity *in vitro*

The importance of S910 and S935 is discussed in the Introduction (Section 1.5.2 and 3.1).

Several members of the Rab family, including Rab8a and Rab10 GTPases were recently discovered in our lab to be direct physiological LRRK2 substrates (Steger et al., 2016). In order to examine whether S910A+S935A mutation has an impact on endogenous LRRK2 kinase activity, LRRK2 was immunoprecipitated from MEF LRRK2 WT, MEF LRRK2 [S910A+S935A] knock-in or MEF LRRK2 KO cells. These immunoprecipitates were then incubated with bacterially purified Rab8A protein in the presence or absence of LRRK2 specific kinase inhibitor and Mg^{2+} -[γ - 32 ATP] for 30 mins at 30°C at 1000 rpm. Reactions were stopped with 4xLDS sample buffer and subjected to autoradiography and immunoblot analysis with indicated LRRK2 antibodies (Figure 3.5). My results show that endogenous LRRK2 protein kinase activity is similar to LRRK2 [S910A+S935A] activity *in vitro*, suggesting that S910A+S935A mutation has no effect on LRRK2 kinase activity on its physiological substrate *in vitro*. My data also shows that *in vitro*, inhibition of endogenously immunoprecipitated LRRK2 kinase activity with specific LRRK2 kinase inhibitor does not result in dephosphorylation of S935. This confirms that this site is not LRRK2 autophosphorylation site.

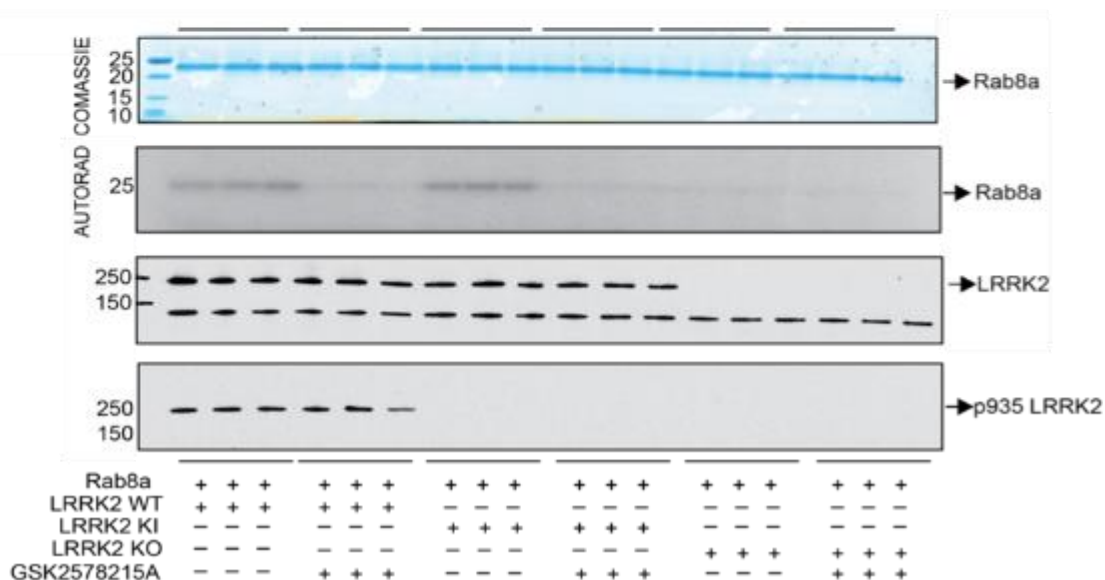
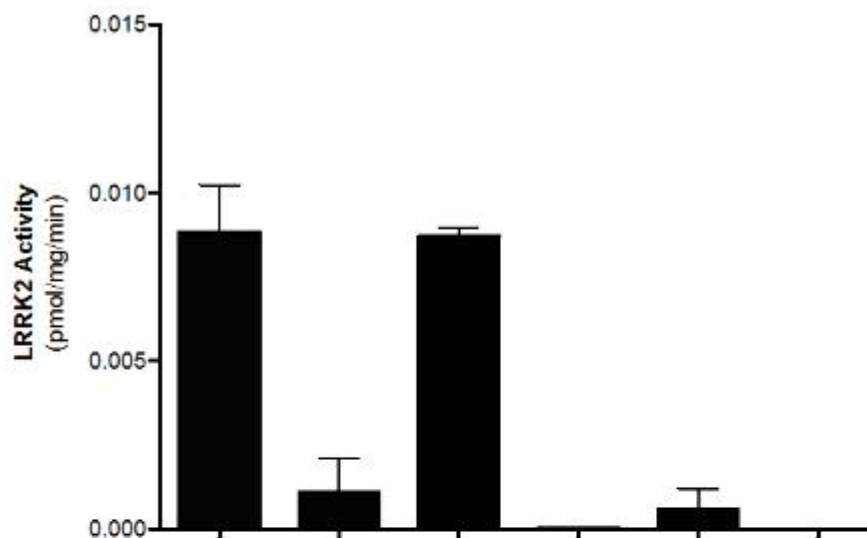


Figure 3.5: Assessment of immunoprecipitated endogenous LRRK2 kinase activity from LRRK2 [S910A+S935A] and LRRK2 WT MEFs. Endogenous LRRK2 proteins were immunoprecipitated with monoclonal total LRRK2 antibody from LRRK2 WT, LRRK2 [S910A+S935A] and LRRK2 KO MEFs. Purified LRRK2 proteins were then incubated with bacterially purified Rab8a and Mg²⁺-[γ -³²ATP] for 30 minutes at 30 °C at 1000 rpm in presence or absence of LRRK2 kinase inhibitor (1 μ M GSK257821A). Immunoprecipitates were then subjected to electrophoresis on a polyacrylamide gel, autoradiography and immunoblot analysis with indicated antibodies.

3.2.3 Assessment of endogenous LRRK2 WT and LRRK2 [S910A+S935A] kinase activity in vivo

To assess whether LRRK2 [S910A+S935A] mutation has an impact on endogenous LRRK2 kinase activity, I used a new technique that has been recently optimised in our lab, the Phos-tag approach (G. Ito et al., 2016), to assess phosphorylation of

endogenous Rab8A and Rab10 in LRRK2 WT and LRRK2 [S910A+S935A] MEFs.

“Phos-tag” or 1,3-bis[bis(pyridin-2-ylmethyl) amino]propan-2-olato dizinc(II) complex, was first described to bind to phosphate ions with much higher affinity ($K_d \sim 25$ nM for phenyl) phosphate than other ions (Kinoshita, Takahashi, Takeda, Shiro, & Koike, 2004). Further studies established that Phos-tag also interacts with high affinity with proteins comprising phosphorylated Ser, Thr or Tyr residues (Kinoshita, Yamada, Takeda, Kinoshita-Kikuta, & Koike, 2005). Based on this finding, a “Phos-tag Acrylamide”, a modified version of Phos-tag, (N-(5-(2-acryloylaminoethylcarbamoyl)pyridin-2-ylmethyl)-N,N',N'-tris(pyridin-2-yl methyl)-1,3-diaminopropan-2-ol) was developed that when polymerised into SDS-polyacrylamide gels retarded electrophoretic mobility of phosphorylated proteins, leading to a substantial mobility shifts (Kinoshita, Kinoshita-Kikuta, Takiyama, & Koike, 2006). This approach has been shown to be particularly useful for analysing phosphorylation of relatively small proteins that are phosphorylated at a single residue such as Rab8A and Rab10.

To assess LRRK2 mediated phosphorylation of endogenous Rab10 (or Rab8A) in MEFs, firstly, LRRK2 WT and LRRK2 [S910A+S935A] knock-in MEFs were treated with DMSO or LRRK2 kinase inhibitor GSK2578215A at 1 μ M concentration for 1 hour. Then treated mouse fibroblasts were lysed in the 1% Triton EDTA free lysis buffer, pre-cleared lysates were then resolved on Phos-tag SDS gel (see Materials and Methods) and subjected into the immunoblot analysis using Rab10 antibody (Figure 3.6).

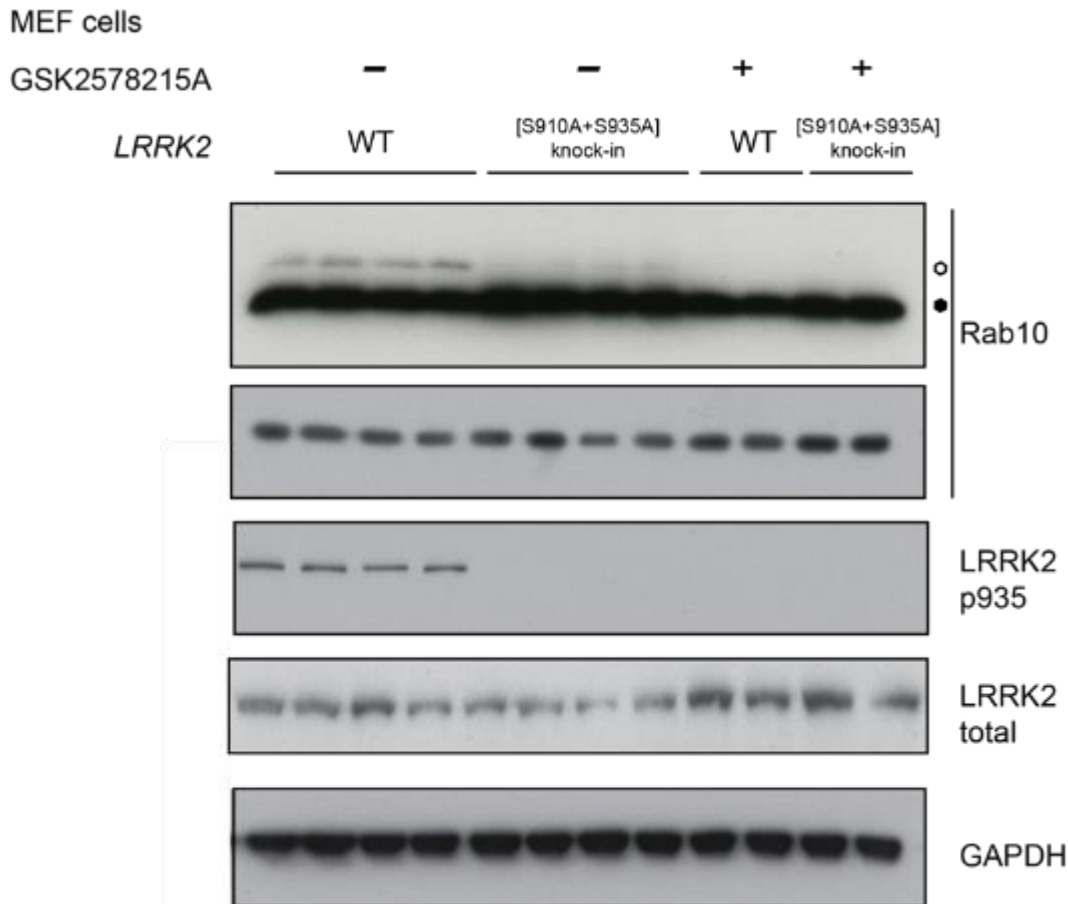


Figure 3.6: Use of the Phos-tag approach to assess the impact of *LRRK2* S910A/S935A mutations on its substrate *Rab10*. Littermate WT and *LRRK2* [S910A+S935A] knock-in MEFs were treated with or without 1 μ M GSK2578215A for 1 hour. Cell lysates were prepared and *Rab10* phosphorylation was analysed by a Phos-tag assay (top panel). Control immunoblots were done on normal gels with the indicated antibodies. Bands corresponding to phosphorylated and non-phosphorylated *Rab10* were marked with open (○) and filled (●) circles, respectively. Similar results were obtained in at least two separate experiments.

According to my results, *Rab10* phosphorylation in *LRRK2* [S910A+S935A] MEFs is remarkably reduced compared to its littermate wild type cells. Importantly, total *LRRK2* levels are not affected by *LRRK2* [S910A+S935A] mutation. This data indicates that *in vivo*, phosphorylation of *LRRK2* at S910 and S935 residues is important for *LRRK2* activity as mutation of these sites to alanine dramatically reduces phosphorylation of its substrate *Rab10*.

My preliminary results also revealed that phosphorylation of Rab8A in LRRK2 [S910A+S935A] knock-in MEFs is also evidently reduced compared with the LRRK2 WT MEFs whereas total LRRK2 levels remained unchanged (Figure 3.7).

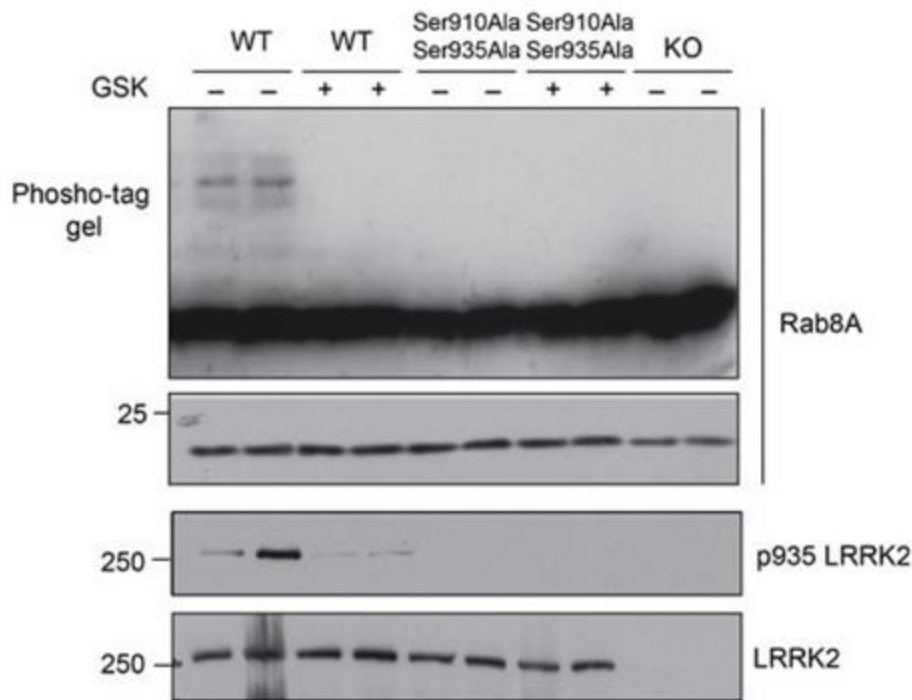


Figure 3.7: Use of the Phos-tag approach to assess the impact of LRRK2 S910A/S935A mutations on its substrate Rab8A. Littermate WT and LRRK2 [S910A+S935A] knock-in as well as LRRK2 KO MEFs were treated with or without 1 μ M GSK2578215A for 1 hour. Cell lysates were prepared and Rab8A phosphorylation was analysed by a Phos-tag assay (top panel). Control immunoblots were done on normal gels with the indicated antibodies.

It was previously reported that in HEK293 cells stably over-expressing GFP-LRRK2 WT or GFP-LRRK2 [S910A+S935A] knock-in proteins, S910A+S935A mutation doesn't have an impact on LRRK2 kinase activity *in vitro* (Nichols et al., 2010), these results are consistent with my *in vitro* kinase data. However, it was also shown that phosphorylation of LRRK2 S910 and S935 residues is important for LRRK2 localization as mutation of these sites to alanine or dephosphorylation of these sites due to LRRK2 inhibition results in loss of 14-3-3 leading to LRRK2 aggregations

within the cytoplasm (Nichols et al., 2010). As according to my phos-tag experiments in MEFs, Rab10 and Rab8A phosphorylation by LRRK2 is significantly reduced in LRRK2 [S910A+S935A] knock-in cells compared to the wild type MEF cells indicating that dephosphorylation of these sites diminishes LRRK2 activity *in vivo*, one explanation could be that in MEF cells, LRRK2 [S910A+S935A] mutation causes aggregations within the cytoplasm making less LRRK2 available for its substrate phosphorylation.

3.2.4 Assessment of total endogenous LRRK2 expression levels in 4 months old LRRK2 [S910A+S935A] and LRRK2 WT mice tissues

As it was described in the Introduction (Section 1.5), kidneys derived from LRRK2 KD D1994A displayed reduced levels of full length LRRK2 (Herzig et al., 2011). Interestingly, it was also shown that inhibition of LRRK2 kinase activity results in reduced LRRK2 levels in kidneys (Fuji et al., 2015). This data suggests that LRRK2 kinase activity could be implicated in its stability. However, in LRRK2 gain-function mouse models such as G2019S or R1441G there is no evidence to support this theory as LRRK2 levels are comparable with the wild type mice (Y. Li et al., 2009; Matikainen-Ankney et al., 2016). I argued whether phosphorylation of S910 and S935 can alter LRRK2 expression levels.

To address whether LRRK2 [S910A+S935A] mutation has an effect on protein stability in brains, lungs or kidneys, three brains, lungs and kidneys were extracted from 4 months old six littermates comprising three LRRK2 WT and three LRRK2 [S910A+S935A] mice. Half of these tissues were lysed in 1% Triton and the other half in 1% Rapigest. 1% Triton buffer was used as it solubilizes all soluble proteins whereas 1% Rapigest buffer solubilizes all protein, including membrane proteins. Although LRRK2 is mainly cytoplasmic protein, Rapigest buffer would allow to detect

LRRK2 even if it localizes at the membrane or forms a non-soluble aggregates. Lysates derived from these samples were then subjected to immunoblot analysis with phospho LRRK2 935 and total (N- and C-terminal) LRRK2 antibodies (Figure 3.8). Resulted blots were then analysed by Li-Cor and quantified by two-way ANOVA test.

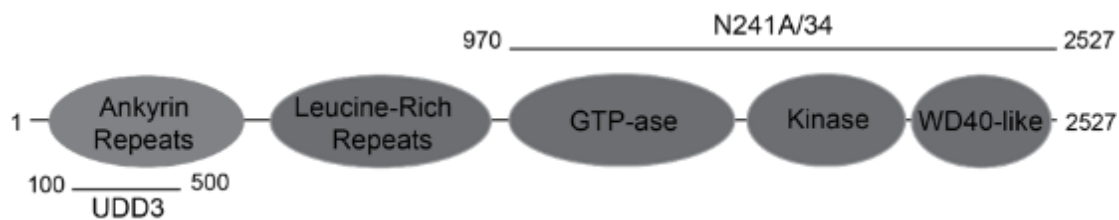
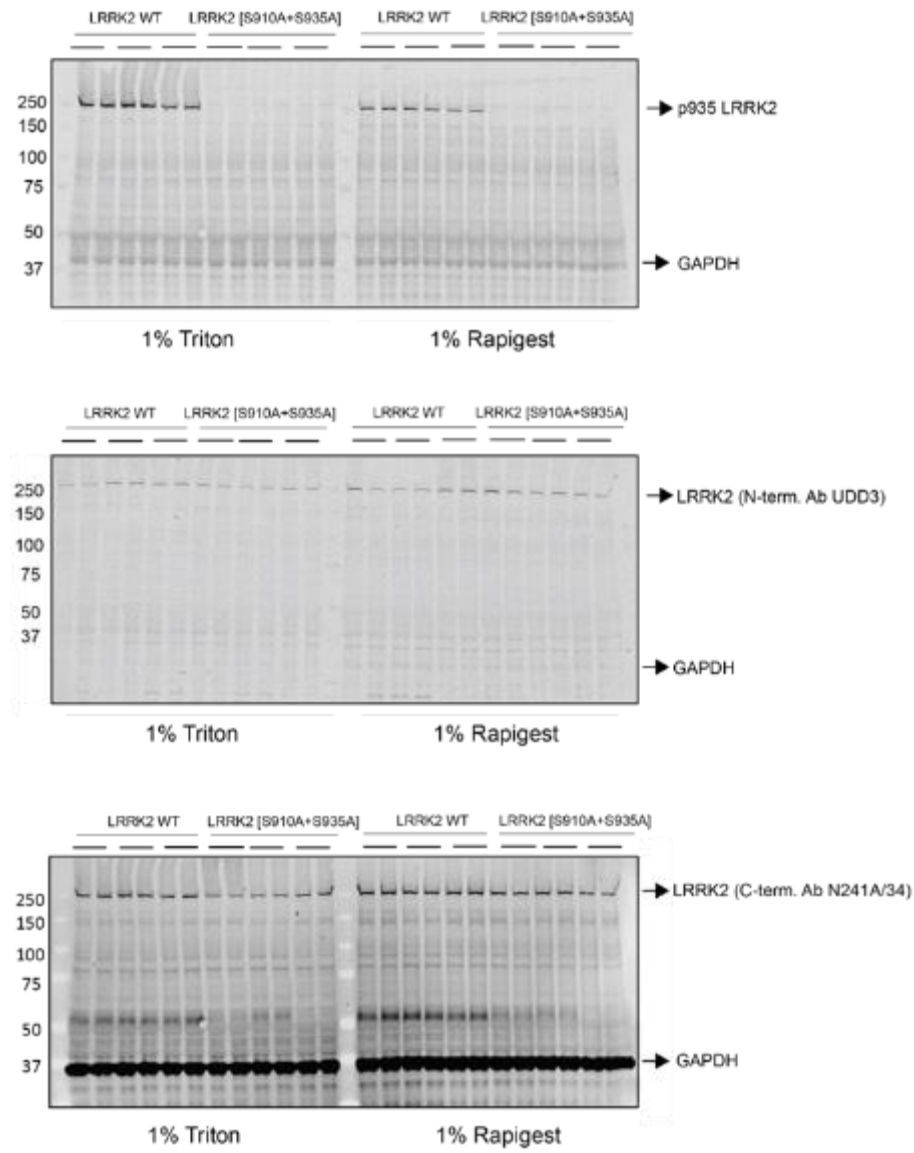


Figure 3.8: Schematic representation of the LRRK2 protein domain structure, indicating the approximate epitope site for two monoclonal antibodies tested: N-terminal LRRK2 antibody (UDD3) and C-terminal LRRK2 antibody (N241A/34).

According to my results, total levels of full length LRRK2 protein in LRRK2 WT brains are the same as in LRRK2 [S910A+S935A] knock-in brains ($n > 0.05$; two-way ANOVA), suggesting that in brain tissues [S910A+S935A] mutation has no influence on LRRK2 stability and expression (Figure 3.9). However, in kidneys, there is a significant decrease in total LRRK2 levels in LRRK2 [S910A+S935A] knock in mice ($n < 0.05$; two-way ANOVA), suggesting that phosphorylation of these sites but not LRRK2 kinase activity affects the stability and expression of LRRK2 protein (Figure 3.10).

A BRAIN



B p935 LRRK2 Total LRRK2 N-term Ab. Total LRRK2 C-term Ab.

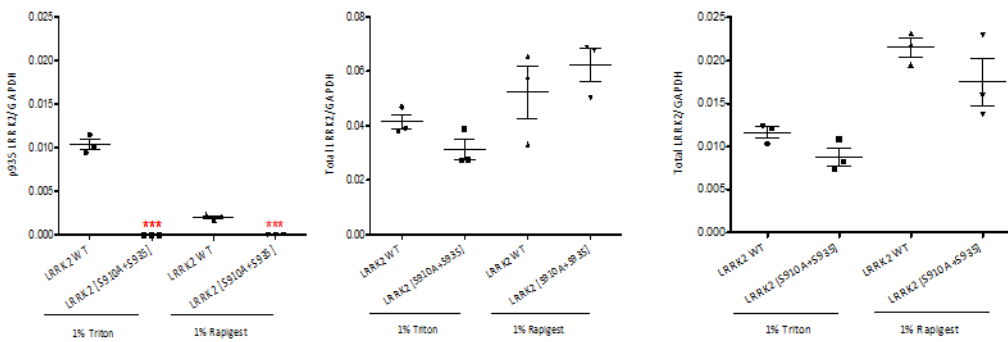
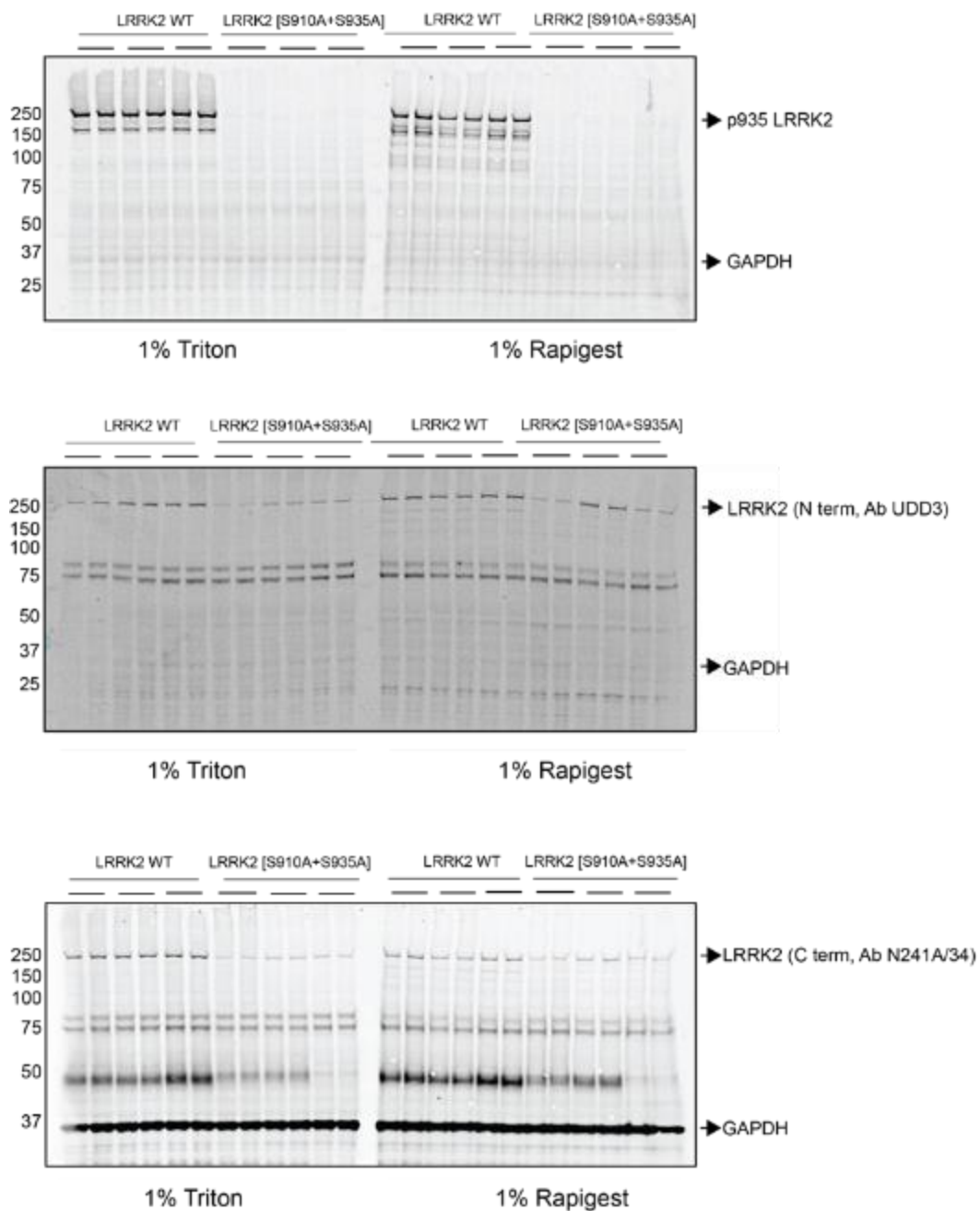


Figure 3.9: Assessment of total LRRK2 expression levels in LRRK2 WT and LRRK2 [S910A+S935A] knock-in brain (A) Brains derived from 3 LRRK2 WT mice and 3 LRRK2 [S910A+S935A] mice were lysed in 1% Triton or 1% Rapigest, prepared lysates were then subjected to immunoblot analysis with indicated phospho and total antibodies. **(B)** Total LRRK2/GAPDH and p935LRRK2/GAPDH ratio was quantified using LI-COR, no differences in total LRRK2 expression levels were detected between LRRK2 WT and LRRK2 [S910A+S935A] brain samples ($n>0.05$; two-way ANOVA).

A KIDNEYS



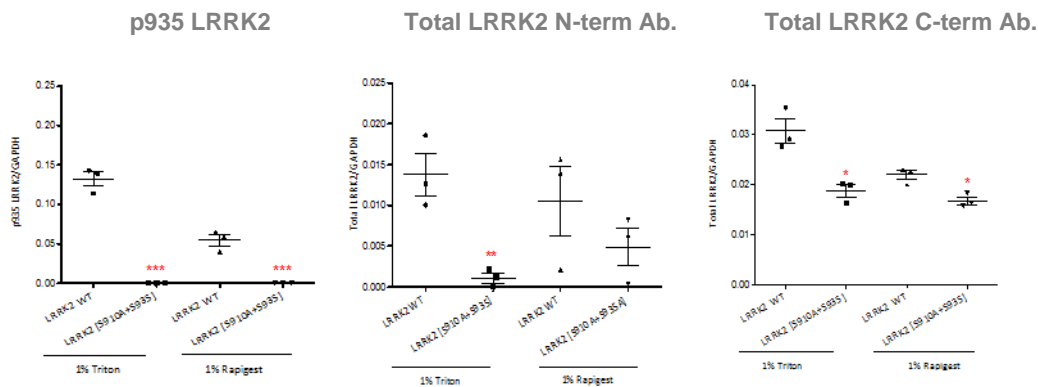
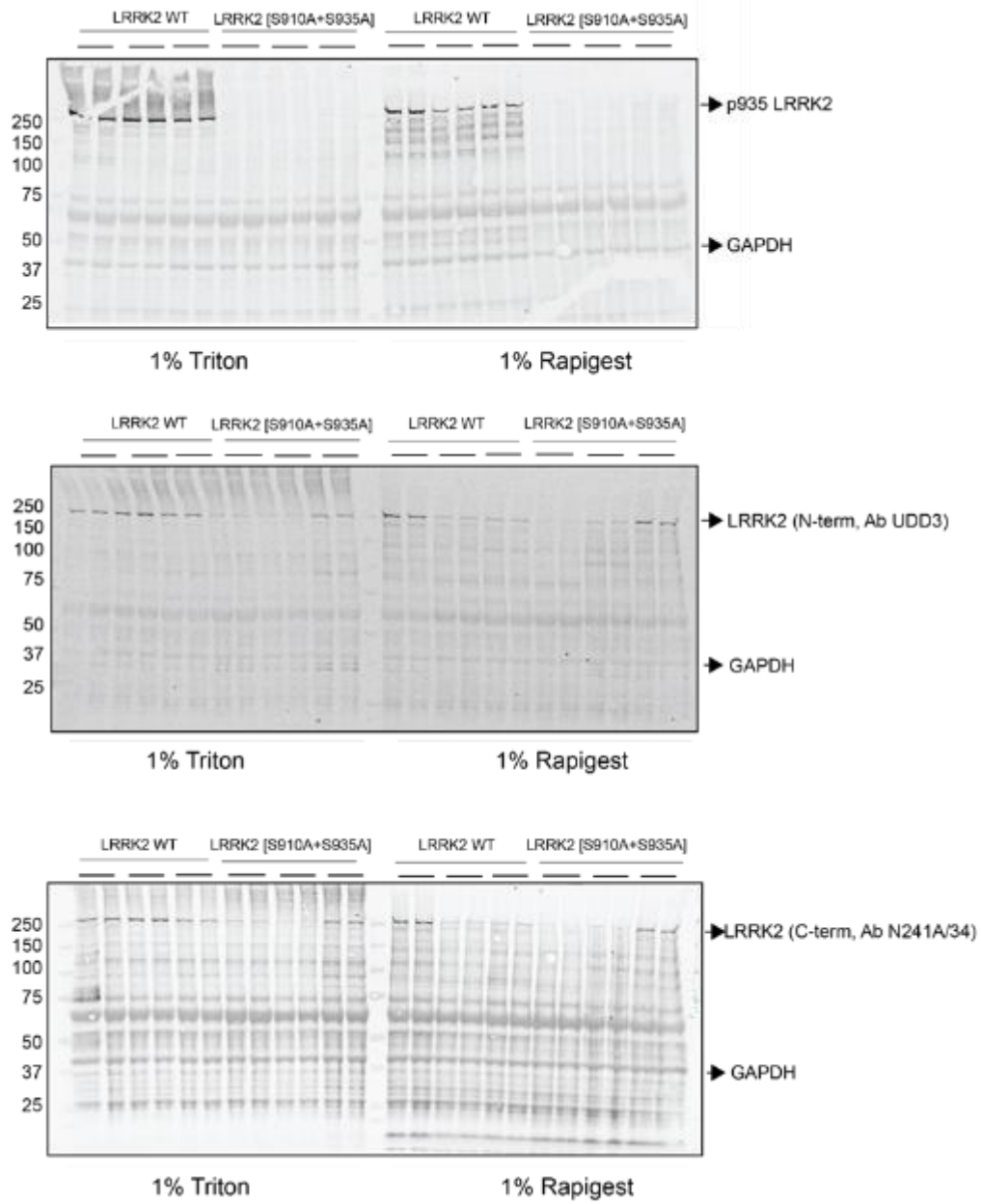
B

Figure 3.10: Assessment of total LRRK2 expression levels in LRRK2 WT and LRRK2 [S910A+S935A] knock-in kidneys (A) Kidneys derived from 3 LRRK2 WT mice and 3 LRRK2 [S910A+S935A] mice were lysed in 1% Triton or 1% Rapigest, prepared lysates were then subjected to immunoblot analysis with indicated phospho and total antibodies. **(B)** Total LRRK2/GAPDH and p935LRRK2/GAPDH ratio was quantified using LI-COR. Total LRRK2/GAPDH and p935LRRK2/GAPDH ratio was quantified using LI-COR, total LRRK2 expression levels of LRRK2 [S910A+S935A] protein were significantly reduced compared to the wild type in kidney samples ($n < 0.05$; two-way ANOVA).

In lungs, the total levels of LRRK2 are very variable but no significant change in total LRRK2 levels were seen between the genotypes ($n > 0.05$; two-way ANOVA) (Figure 3.11). In fact, the variability of LRRK2 expression in lungs from one individual to another has also been observed in previous studies (Fuji et al., 2015).

A LUNGS



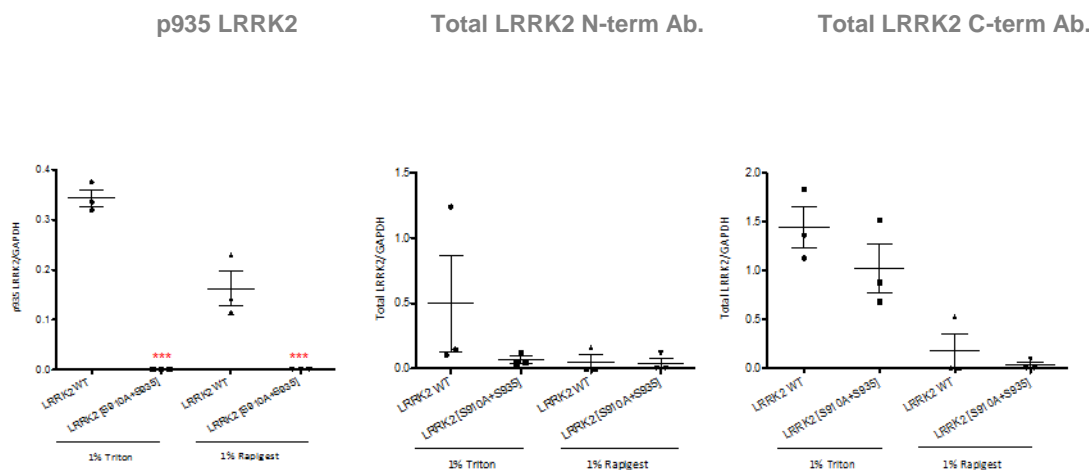
B

Figure 3.11: Assessment of total LRRK2 expression levels in LRRK2 WT and LRRK2 [S910A+S935A] lungs (A) Lungs derived from 3 LRRK2 WT mice and 3 LRRK2 [S910A+S935A] mice were lysed in 1% Triton or 1% Rapigest, prepared lysates were then subjected to immunoblot analysis with indicated phospho and total antibodies. **(B)** Total LRRK2/GAPDH and p935LRRK2/GAPDH ratio was quantified using LI-COR. No differences in total LRRK2 expression levels were detected between LRRK2 WT and LRRK2 [S910A+S935A] brain samples ($n>0.05$; two-way ANOVA).

My results are consistent between N- and C-terminal antibodies as well as 1% Triton and Rapigest lysis buffer treatment. Moreover, my data is supported by previously reported pharmacological and genetic studies, which show that only in kidneys, inhibition of LRRK2 kinase activity results in decrease in total LRRK2 levels. It seems that phosphorylation of S910 and S935 is important for LRRK2 stability. Overall, these results indicate that in kidneys there is a distinct mechanism by which LRRK2 is regulated.

3.2.5 Histopathological evaluation of LRRK2 WT and LRRK2 [S910A+S935A] mouse kidneys.

As previously described in the Introduction (Section 1.6.2) the evidence is clear that LRRK2 KO mice and rats display an abnormal kidney and lung phenotype (Baptista et al., 2013; Herzig et al., 2011). Moreover, it has been shown that catalytically inactive LRRK2 [D1994A] mice exhibit similar kidney pathology (Herzig et al., 2011).

These results point to the fact that inhibition of LRRK2 kinase activity could be associated with kidney and/or lung pathology. However, suppression of LRRK2 kinase activity has been proposed as an effective therapeutic strategy for slowing the progression of PD and reported morphological changes in kidneys and lungs upon LRRK2 deletion might be serious side effects that could prevent pharmaceutical companies from developing LRRK2 inhibitors (Baptista et al., 2013). Therefore, it is important to assess the safety risk of inhibition LRRK2 kinase activity.

I have reasoned that LRRK2 [S910A+S935A] knock-in mice will mimic the long term effect of LRRK2 inhibitor treatment because inhibition of LRRK2 kinase activity results in a rapid dephosphorylation of these sites as it was previously described in our lab (Dzamko et al., 2010). Consequently, I investigated whether the loss of S910 and S935 phosphorylation causes kidney pathology. For this purpose, I set up a collaboration with Dr Francesco Marchesi from Veterinary School of the University of Glasgow.

A total of 24 littermate animals was tested (12 wild-type and 12 homozygous knock-in animals) at a single time point at about 18 months of age. Initial analysis revealed that LRRK2 knock-in kidneys displayed no obvious phenotype compared to the wild type (Figure 3.12). The color, size and weight of 18 months old LRRK2 [S910A+S935A] knock-in kidneys were similar to LRRK2 WT. These results contrast with the reported LRRK2 KO or LRRK2 KD mouse kidney phenotype characterized by abnormal dark kidney staining, rough surfaces and decreased kidney size (Herzig et al., 2011; Tong et al., 2012).

LRRK2 WT KIDNEYS

LRRK2 S910A+S935A KIDNEYS

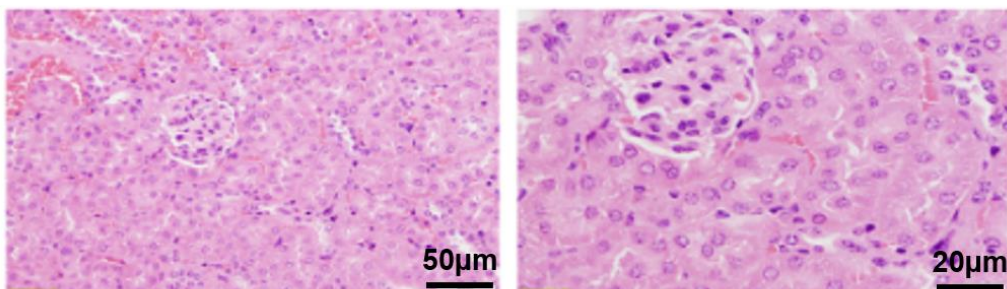


Figure 3.12: Overview of LRRK2 [S910A+S935A] phenotype. Kidneys have been collected from LRRK2 WT and LRRK2 [S910A+S935A) knock-in mice. No obvious kidney phenotype was observed. No difference in pigmentation, size or weight was detected.

To investigate whether there are any microscopic differences between the genotypes I have collected kidneys from mice at the end of perfusion fixation with 4% Paraformaldehyde and transferred to 10% neutral buffered formalin (NBF) (Mice were perfused with the help of Elaine Forsyth and Tom McWilliams). I then sent these tissues for the histopathological evaluation to the School of veterinary medicine at the University of Glasgow. Main histological findings performed by Dr Franchesco Marchesi from the University of Glasgow are summarized in Table 3.1. Blind histopathological analysis of kidneys revealed a spectrum of changes in the kidneys without a clearly distinctive trend across groups and genders. In this analysis Dr Marchesi looked at the cellular protein markers used to describe LRRK2 KO and kinase dead kidneys. His data shows that lymphoplasmacytic inflammatory infiltrates adjacent to the pelvis and with variable interstitial or perivascular distribution are noted in both groups and genders with overall similar severity. Tubular vacuolation, ranging from minimal to marked, was noted only in males from both groups. Additional tubular degenerative changes, including variable extents of dilation, shrinkage/atrophy and loss, with or without intraluminal accumulation of eosinophilic

material, and tubular basophilia, are also observed with overall higher frequency and severity in males. Only one wild type female mouse in shows a distinct phenotype characterised by diffused glomerular changes presented by segmental to extensive accumulation of coarse amorphous pale eosinophilic material causing partial to complete obliteration of the glomerular capillarity loops. The accumulated material is Congo red and Masson's trichrome negative, strongly PAS positive and with a mixed staining pattern. The significance of the prominent glomerular changes noted in this female is unclear given the fact that this mouse is a wild type. Overall, histological evaluation of the kidneys in these cohorts has not identified a clear difference in the spectrum and severity of microscopic changes across the different groups (Figure 3.13).

LRRK2 WT



LRRK2 S910A+S935A

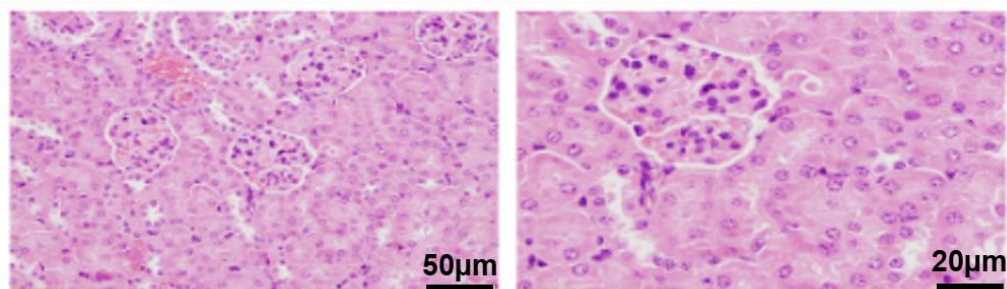


Figure 3.13: A representative image showing that there is no kidney pathology in LRRK2 [S910A+S935A] mice. Kidneys have been collected from LRRK2 WT and LRRK2 [S910A+S935A] mice at the end of perfusion fixation with 4% paraformaldehyde and transferred to 10% neutral buffered formalin (NBF). Tissues have been trimmed and processed to paraffin blocks, microtome sectioned at 4 µm, stained with Haematoxylin and Eosin (HE), and examined by Dr Francesco Marchesi (Glasgow University). Normal glomerulus and proximal convoluted tubules in the cortex detected.

Table 3.1: Histological evaluation of mouse kidneys

Females	Group 1 LRRK2 WT mice				Group 2 LRRK2 [Ser910Ala+Ser935Ala] mice			
Lymphoplasmacytic infiltrates	++	+	+	+	-/+	++	+	++
Glomerular mesangial thickening	-	-/+	+	-/+	-	-/+	-/+	-/+
Increased glomerular cellularity	-	-	+	-	-	-/+	-	-/+
Glomerular eosinophilic deposits	-	-	-	+++	-	-	-	-
Tubular dilation	-/+	-	-	-	-	-	-	-
Tubular vacuolation	-	-	-	-	-	-	-	-
Tubular degeneration/atrophy	-	-	-	+	-	-	-	-
Tubular eosinophilic casts	-	-	-	+	-/+	+	+	+
Tubular basophilia	-/+	-/+	-/+	-/+	-	-/+	-/+	-
Mineralization, collecting ducts	-/+	-	-	-	-	-	-	-
Pigment-laden macrophages	-	-	-	-/+	-	-	-	-/+
Osseous metaplasia	-	-	-	-	-	-	-	-/+
Males	Group 1 LRRK2 WT mice				Group 2 LRRK2 [Ser910Ala+Ser935Ala] mice			
Lymphoplasmacytic infiltrates	+	++	+	-/+	++	++	-	+
Glomerular mesangial thickening	-/+	-/+	-/+	-/+	-/+	-	-/+	-/+
Increased glomerular cellularity	-/+	-	-/+	-	-	-	-/+	-/+
Glomerular eosinophilic deposits	-	-	-	-	-/+	-	-	-
Tubular dilation	-/+	-	-/+	+	++	+	-	-/+
Tubular vacuolation	-/+	+	++	+++	-/+	+	++	+
Tubular degeneration/atrophy	-	-	-/+	+	++	++	-	-/+
Tubular eosinophilic casts	-	-	-	-	+	-	-	-
Tubular basophilia	-/+	+	+	-/+	++	++	+	+
Mineralization, collecting ducts	-/+	-	-	-	-/+	-	-	-

This experiment was carried out by our collaborator Dr Francesco Marchesi (Glasgow University).

Microscopic changes in the kidneys collected from LRRK2 WT and LRRK2 [Ser910Ala+Ser935Ala] have been assessed according to the following basic semiquantitative grading system:

- = change no present; +/- =minimal; + =mild; ++ =moderate; +++ =marked

To sum up, microscopic changes within the examined sections of kidneys in these cohorts of mice are not consistent with those reported in LRRK2 knock-out and kinase dead mutant mice (Herzig et al., 2011; Tong et al., 2012). Histological evaluation of the kidneys in these cohorts has not identified a clear difference in the

spectrum and severity of microscopic changes across the different groups. This data strongly indicates that dephosphorylation of S910 and S935 mice has no major effect on kidney phenotype.

3.2.6 Histopathological evaluation of LRRK2 WT and LRRK2 [S910A+S935A] mouse lungs.

To date, another concern regarding use of LRRK2 inhibitors as potential drugs to cure Parkinson's disease are risks associated with the abnormal accumulation of lamellar bodies in type II pneumocytes in non-human primates reported by Reina N. Fuji (Fuji et al., 2015). The abnormalities in lung tissues caused by LRRK2 kinase inhibitors were reported to be morphologically identical to that detected in LRRK2 knock-out mice but absent in LRRK2 kinase dead mice (Fuji et al., 2015; Herzig et al., 2011). However, treatment of mice with different LRRK2 kinase inhibitors even at high doses resulted in no changes in kidneys or lungs suggesting that mice almost need a complete inhibition of LRRK2 for this effect (Fuji et al., 2015).

To address whether dephosphorylation of S910 and S935 could result in lung pathology in mice I have collected lungs from mice at the end of perfusion fixation with 4% Paraformaldehyde and transferred to 10% neutral buffered formalin (NBF) (mice were perfused with the help of Elaine Forsyth and Tom McWilliams) and then sent the tissues to our collaborator Dr Marchesi for histopathological analysis. Results are summarized in Table 3.2.

Table 3.2: Histological evaluation of mouse lungs

Females	Group 1 LRRK2 WT mice				Group 2 LRRK2 [Ser910Ala+Ser935Ala] mice			
Peribronchial lymphoid infiltrates	+	+	+	++	-/+	+	-	++
Perivascular lymphoid infiltrates	+	+	+	+++	-/+	+++	+	+++
Alveolar macrophage accumulation	-	-	-	+	-/+	+	-	+
Interstitial/alveolar inflammatory infiltrates	-	-	-	-	-	-	-	+
Alveolar haemorrhage	-	-	-	-	-	+	-	-
Males	Group 1 LRRK2 WT mice				Group 2 LRRK2 [Ser910Ala+Ser935Ala] mice			
Peribronchial lymphoid infiltrates	-	+	-	+	+	-	-	-
Perivascular lymphoid infiltrates	-	++	+	-	+++	++	-	+
Alveolar macrophage accumulation	-	-	-	-	-	-	-	-
Interstitial/alveolar inflammatory infiltrates	-/+	-	-	-	-	-	-	-
Type II pneumocyte hyperplasia	-				-	-	-	-/+
Alveolar haemorrhage	-	-	-	-	-	-	-	-

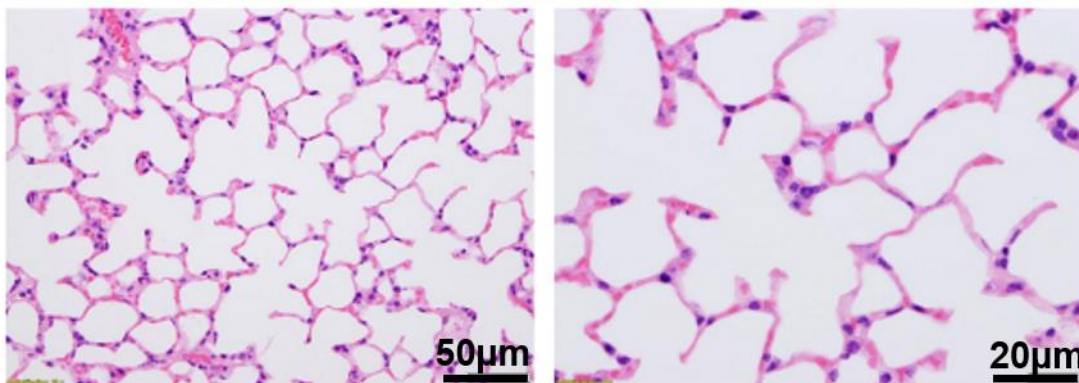
This experiment was carried out by our collaborator Dr Francesco Marchesi (Glasgow University). Microscopic changes in the kidneys collected from LRRK2 WT and LRRK2 [Ser910Ala+Ser935Ala] have been assessed according to the following basic semiquantitative grading system:

- = change no present; -/+ =minimal; + =mild; ++ =moderate; +++ =marked

These findings show that in the lungs perivascular and/or peribronchial infiltrates are observed with overall comparable incidence and severity in females and males from both groups. These infiltrates are composed of large numbers of small to medium sized lymphocytes, in some instances with a proportion of large and apparently immature lymphoid elements, with variable numbers of plasma cells and fewer microphages. Minimal to mild alveolar macrophage accumulation is observed in one female from group 1 (wild type) and three females from group 2 (LRRK2

[S910A+S935A]. In conclusion, histological changes within the examined section of lungs in these cohorts of mice are not consistent with those previously published in LRRK2 knock-out and kinase dead mutant mice. There was no clear difference in the spectrum and severity of microscopic changes across the different groups (Figure 3.14).

LRRK2 WT



LRRK2 S910A+S935A

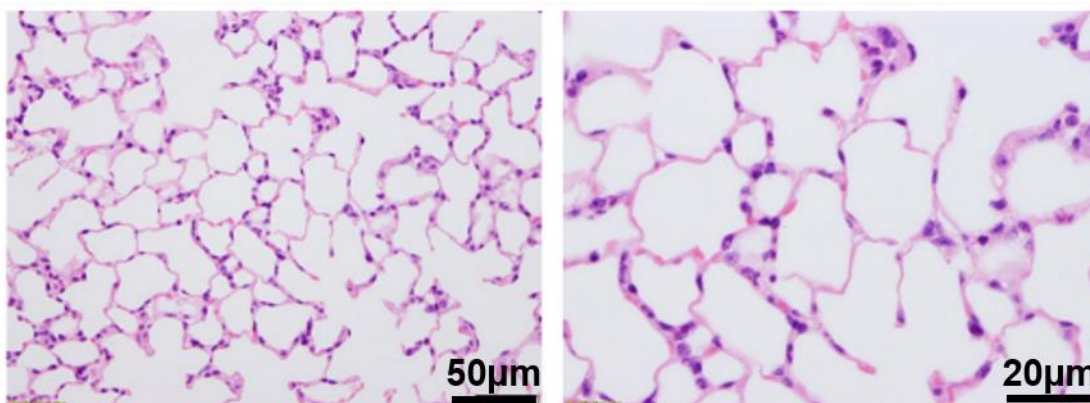


Figure 3.14: Histological evaluation of mouse lungs. Lungs have been collected from LRRK2 WT and LRRK2 [S910A+S935A] mice at the end of perfusion fixation with 4% paraformaldehyde and transferred to 10% neutral buffered formalin (NBF). Tissues have been trimmed and processed to paraffin blocks, microtome sectioned at 4 µm, stained with Haematoxylin and Eosin (HE), and examined by Dr Francesco Marchesi (Glasgow University). Alveoli and alveolar septa appear within normal limits.

This observations represent common background findings in rodents noted with increased incidence and severity in aged animals, suggesting that inhibition of S910 and S935 phosphorylation does not lead to the lung pathology in mice.

3.2.6.7 Behavioural phenotyping of LRRK2 [S910A+S935A] knock-in mouse model

As S910A+S935A mutation mimics the long-term inhibition of LRRK2 kinase I set up an aging experiment using LRRK2 WT and LRRK2 [S910A+S935A] knock-in mice to study how S910A+S935A mutation affects a well-being of a mouse. For my experiment I used 24 littermate animals (12 wild types and 12 homozygous LRRK2 [S910A+S935A] mice). These mice were gender-matched, littermate pairs of heterozygous breedings. I sorted these mice into cages based on their gender and cage capacity (4 to 6 mice per cage) and let them age for 18 months. During this time I was watching these mice and with the help of our animal unit staff noted weekly the individual mouse weight for 55 weeks starting from 4 months of age. LRRK2 [S910A+S935A] mice appeared to be healthily and did not display any obvious behavior phenotype compared to their wild type littermates. However, my results showed that S910A+S935A mutation somehow influences the body weight gain of mice (Figure 3.15). In fact, this mutation has a greater effect in females ($p < 0.01$; two-tailed t-test). Interestingly, among 6 wild type females and their 6 LRRK2 [S910A+S935A] females' littermates, there was a very fat outlier LRRK2 [S910A+S935A] mouse, which reached weight of 70 grams. A picture of this mouse is shown in Figure 3.15. The weight of this mouse was not taken into consideration for my data analysis and this mouse did not participate in any behavioral tests due to its over-weight conditions. Although in males there was not significant difference in body weight between LRRK2 WT and their LRRK2 [S910A+S935A] littermates, it was a clear trend that LRRK2 [S910A+S935A] males are more likely to be heavier than the wild types. Overall, LRRK2 [S910A+S935A] mice are heavier than their wild type littermates ($p < 0.05$) indicating that S910A+S935A is linked to this phenotype.

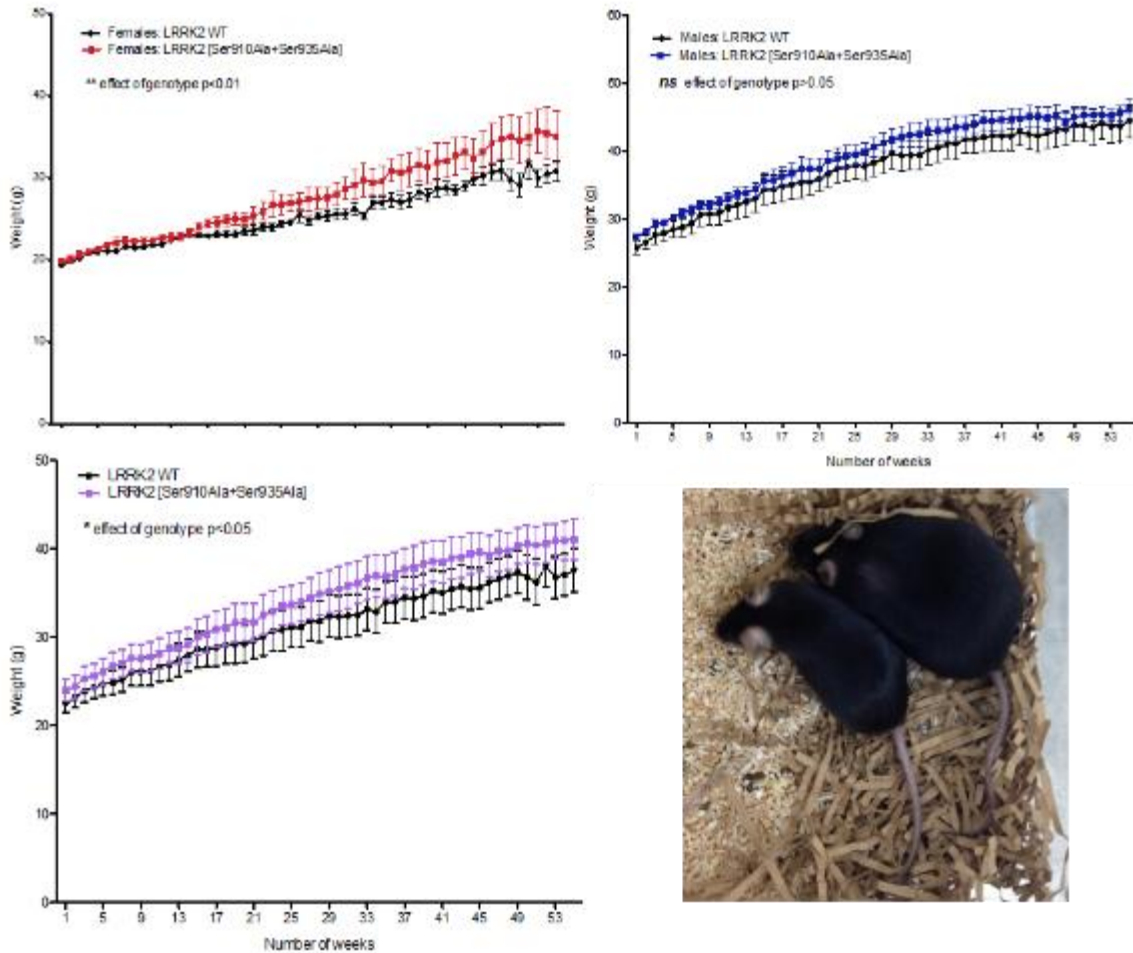


Figure 3.15: Assessment of body weight in relation to its gender and genotype. LRRK2 WT and their LRRK2 [S910A+S935A] littermates' mice were weighted weekly for 55 weeks. These body weight curves represent the body weight difference between these mice in relation to their gender and genotype. LRRK2 [S910A+S935A] females are heavier than LRRK2 WT littermates ($p < 0.01$; two-tailed t-test). There is a trend for LRRK2 [S910A+S935A] males to be heavier than their wild type littermates but this trend is not significant ($p > 0.05$; two-tailed t-test). Overall, LRRK2 [S910A+S935A] mice are heavier than their wild type littermates ($p < 0.05$ two-tailed t-test). This picture shows the over-weighted LRRK2 [S910A+S935A] mouse in comparison to its wild type littermate. No other LRRK2 knock-in females displayed such a dramatic body weight gain, therefore the weight of this mouse was not used in this data set.

It has been previously showed by Heather Melrose's laboratory that LRRK2 KO mice displayed an abnormal exploratory behavior in the open-field test characterized by increased anxiety in these animals (Hinkle et al., 2012). Moreover, motor and coordination test - rotarod, revealed that LRRK2 KO mice performed significantly better than their wild type littermates by staying persistently longer on the rotating

road (Hinkle et al., 2012). Together these results strongly indicated that LRRK2 KO mice possess an abnormal behavior phenotype characterized by the inability of termination of ongoing behavior (Hinkle et al., 2012).

In order to establish whether LRRK2 [S910A+S935A] knock-in mice display a motor function phenotype I also performed a motor coordination and balance rotarod test available in our laboratory. The rotarod test is the most commonly used test of motor function. It consists of a rotating road of 3 cm diameter, on which the mouse is placed and has to maintain its balance, and a trip switch on the floor below, which is set to record the latency until the mouse falls from the rotating rod (Brooks & Dunnett, 2009) (Figure 3.16). Mice are normally tested on separate trials at a series of fixed speeds (fixed speeds rotarod test), or speed increases can be incorporated into a single trial by using an accelerating version of the test (accelerating rotarod test) (Brooks & Dunnett, 2009).

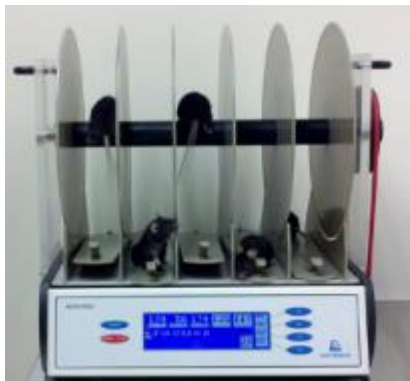


Figure 3.16: The overview of Rotarod.

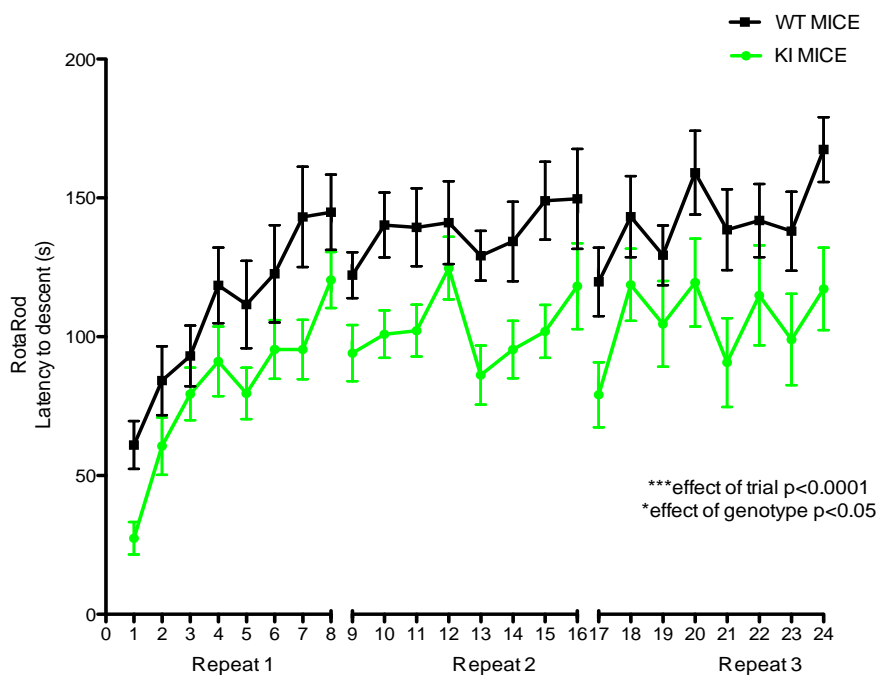
For my experiment I used 24 animals (12 wild types and 11 homozygous LRRK2 [S910A+S935A] knock-in mice) at a single time point at about 18 months of age. These mice were gender-matched, littermate pairs of heterozygous breedings. For a positive control, I employed an additional extra 8 male-littermates, which comprised 4 LRRK2 wild type and 4 LRRK2 KO mice. Dr Leanne Strachan from Ninewells

Hospital and Medical school supervised my experiment and helped me with the data analysis.

I started my trial with accelerating speed rotarod test where the rod accelerates smoothly from 0 to 40 rpm over a 5-minute period. Each trial was repeated 8 times at 3 different time points with the interval of two weeks to ensure reproducibility of this data (Figure 3.17). My results revealed that LRRK2 [S910A+S935A] mice performed significantly worse on the rotarod test than their wild-type littermates ($p < 0.05$, ANOVA) (Figure 3.17.A). This might indicate that phosphorylation of S910 and S935 is implicated in motor coordination of these animals. In my hands, LRRK2 KO mice showed a very inconsistent performance in this test, which overall was not significantly different from their wild type littermates ($p > 0.05$, ANOVA) (Figure 3.17.B).

Overall, my Rotarod results show that LRRK2 [S910A+S935] knock-in mice perform worse on the test compared with their wild type littermates, suggesting that this mutation could affect mice motor behavior.

A



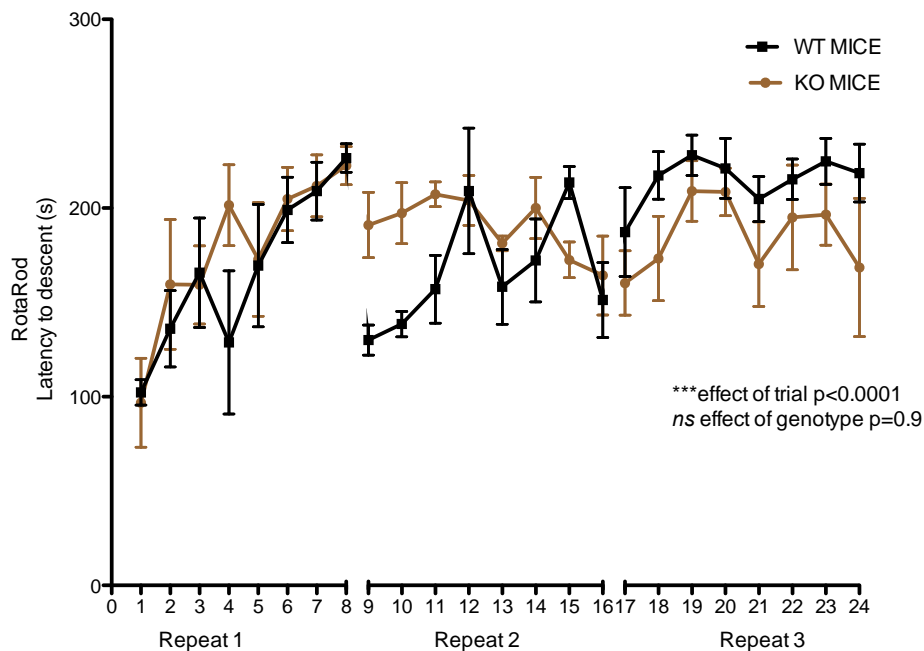
B

Figure 3.17: Behavioural phenotyping of LRRK2 [S910A+S935A], WT and KO mice. (A) Rotarod accelerating speed: Latency to fall in the rotarod test curves of LRRK2 WT versus LRRK2 [S910A+S935A] mice (n=12 per genotype), accelerating speed from 0rpm-40 rpm. Two-way ANOVA for the effect of genotype on latency to fall: $p<0.05$. **(B) Rotarod accelerating speed:** Latency to fall in the rotarod test curves of LRRK2 WT versus LRRK2 KO mice (n=4 per genotype), accelerating speed from 0rpm-40 rpm. Two-way ANOVA for the effect of genotype on latency to fall: $p>0.05$.

In addition, I performed rotarod fixed speeds test at 10 rpm, 20 rpm, 30 rpm and 40 rpm rotation speed to demonstrate that transgenic phenotype is dependent on task difficulty (Figure 3.18). Each trial was repeated 8 times at 3 different time points with the interval of two weeks to ensure reproducibility of the data. My results again showed that LRRK2 [S910A+S935A] mutation might affect motor function in mice as with the increased speed of the rotating rod LRRK2 mutants perform significantly worse than their wild type littermates in this test (Figure 3.18.A). Consistent with the previous studies there is a trend for LRRK2 KO mice to perform slightly better in the fixed speeds rotarod test than their wild type littermates (Figure 3.18.B).

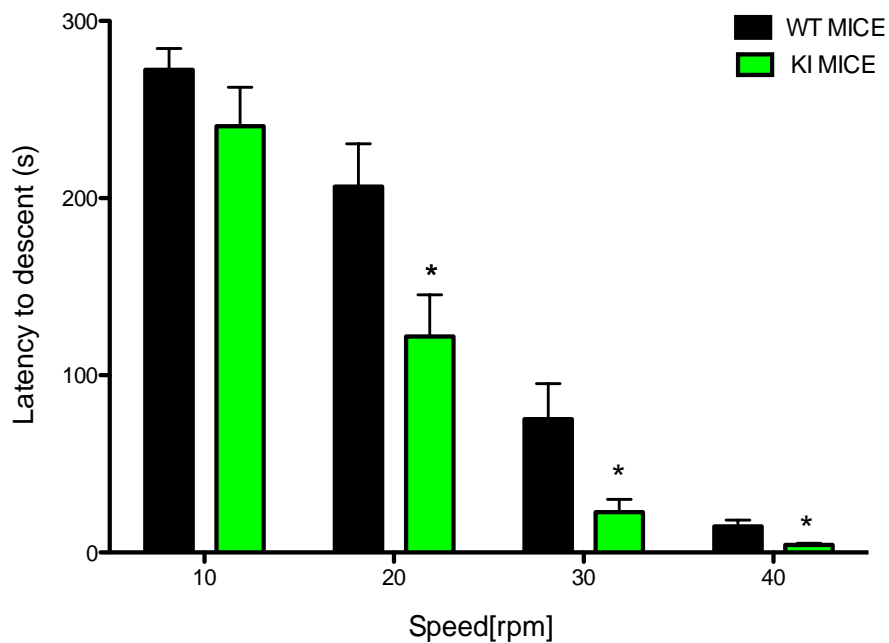
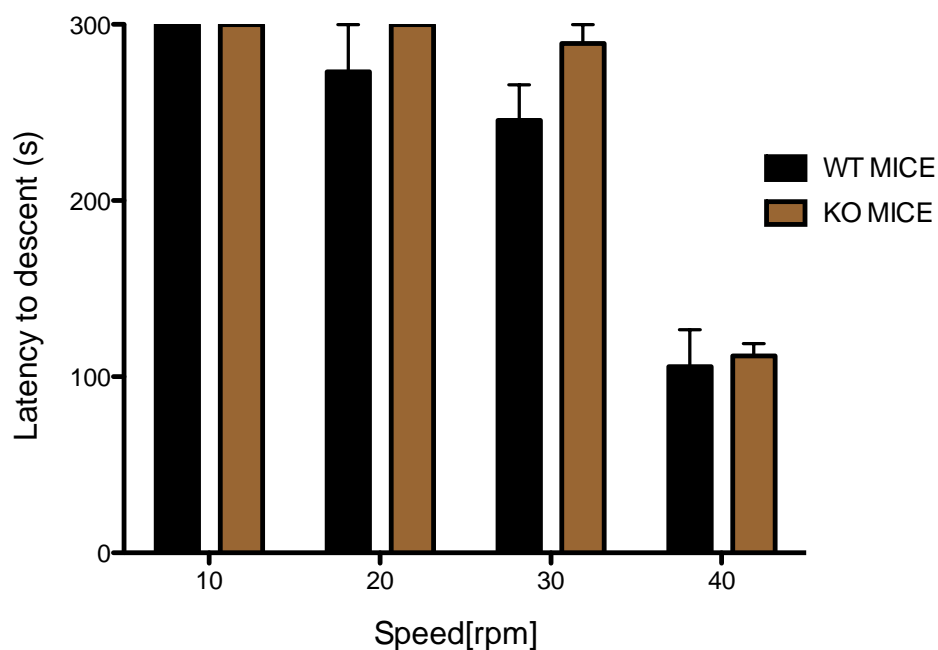
A**B**

Figure 3.18: Behavioural phenotyping of LRRK2 [Ser910Ala+Ser935Ala], WT and KO mice. (A) Rotarod fixed speed: Latency to fall in the rotarod test of LRRK2 WT versus LRRK2 [S910A+S935A] mice (n=12 per genotype) at fixed speed 10 rpm, 20 rpm, 30 rpm and 40 rpm. Two-way ANOVA for the effect of genotype on latency to fall: p<0.05 at 20 rpm, 30 rpm and 40 rpm; p>0.05 at 10 rpm. (B) Rotarod fixed speed: Latency to fall in the rotarod test of LRRK2 WT versus LRRK2 KO mice (n=4 per genotype) at fixed speed 10 rpm, 20

rpm, 30 rpm and 40 rpm. Two-way ANOVA for the effect of genotype on latency to fall: $p > 0.05$ at 10 rpm, 20 rpm, 30 rpm and 40 rpm.

3.2.7 Histopathological evaluation of LRRK2 WT and LRRK2 [S910A+S935A] mouse brain.

In order to investigate whether LRRK2 [S910A+S935A] mutation has an effect on brain pathology I collected 16 brains from gender-matched littermates 8 wild type and 8 homozygous LRRK2 [S910A+S935A] knock-in mice at the end of 4% paraformaldehyde perfusion (mice were perfused with the help of Elaine Forsyth and Tom McWilliams) and sent these samples for further analysis to our collaborators Nic Dzamko and Glenda Halliday in Australia's Neuroscience Research Institute. Ye Zhao and Yuhong Fu performed all experiments associated with histopathological evaluation of LRRK2 WT and LRRK2 [S910A+S935A] knock-in brains, which I report in my thesis.

According to the obtained data regarding estimation of the number of subcortical and hippocampal cells, there are no significant differences in the proportions of total cells, mature neurons, glia, glia/neuron ratios and proliferating cells in the subcortical structures (basal glia, thalamus, hypothalamus and brainstem) between LRRK2 [S910A+S935A] and WT mice (Table 3.3). In the hippocampus of the LRRK2 [S910A+S935A] mice, there was a non-significant trend for a decrease in the percentage of total cells, mature neurons and glia, but glia/neuron ratios and proliferating cells were unchanged (Table 3.4).

Table 3.3: Mean and standard error for the estimated percentages relative to WT of subcortical and hippocampal cells in the different genotypes covarying for gender (data received from Australia's Neuroscience Research Institute)

Regions	LRRK2-WT (%)	LRRK2 [Ser910Ala+Ser935Ala] (%)	P value
Subcortex			
Total cells	100±5.086	102.833±5.086	0.062
Neurons	100±6.196	96.667±6.196	0.163
Glia	100±6.362	104.833±6.362	0.078
Glia/Neuron	2.977±0.268	3.270±0.268	0.696
Proliferating	100±12.073	110.168±12.073	0.674
Hippocampus			
Total cells	100±4.709	83.571±4.709	0.062
Neurons	100±5.736	79.429±5.736	0.163
Glia	100.143±5.890	82.286±5.890	0.078
Glia/Neuron	2.857±0.248	2.946±0.248	0.696
Proliferating	99.996±11.178	100.252±11.178	0.674

To sum up, aged LRRK2 [S910A+S935A] mice did not displayed decreased cell numbers or impaired proliferation in the Subcortex. However, in the hippocampus there was a trend for decreased total cells, mature neurons and glia. This could indicate that S910A+S935A might have an effect on neuro/gliogenesis in the aging hippocampus.

Quantitative assessment of the numbers of TH-positive neurons in the substantia nigra compacta (SNC) did not reveal any significant dopamine neuronal loss in LRRK2 [S910A+S935A] mice (Table 3.4).

Table 3.4: Calculated numbers of TH-positive dopamine neurons in SNC (data received from Australia's Neuroscience Research Institute)

TH-positive dopamine neurons in SNC	Mean	SEM
Female-WT	1698	±78
Male-WT	1752.5	±78
Female-[Ser910Ala+Ser935Ala]	1636	±78
Male- [Ser910Ala+Ser935Ala]	1628.5	±78

Further analysis revealed that aged LRRK2 [S910A+S935A] mice did not display any differences in TH neuron morphology (Figure 3.19.A). Furthermore, all TH-positive SNC neurons colocalised with dopamine active transporter (DAT) and vesicular monoamine transporter 2 (VMAT2). Moreover, there was no significant differences in the staining intensity of dopamine transporters in the LRRK2 [S910A+S935A] mice compared with WT mice (Figure 3.19.B and 3.19.C). There was a trend for an increase in the proportion of T-positive SNC neurons containing α -synuclein. This change was associated with an increase in microglia in the SN of the LRRK2 [S910A+S935A] mice (Figure 3 19. E).

In conclusion, aged LRRK2 mice did not exhibit loss of TH neurons in the SN, there were no differences in TH morphology or the expression of dopamine transporters DAT and VMAT2. This data strongly indicates that LRRK2 [S910A+S935A] mice are unlikely to develop a Parkinson's disease's phenotype under basal conditions. This result is consistent with the previously reported findings describing LRRK2 [R1441C] (Tong et al., 2009) and LRRK2 [R1441G] (Liu HF et al., 2014) knock-in mice, which is also exhibit a loss of S910 and S935 phosphorylation.

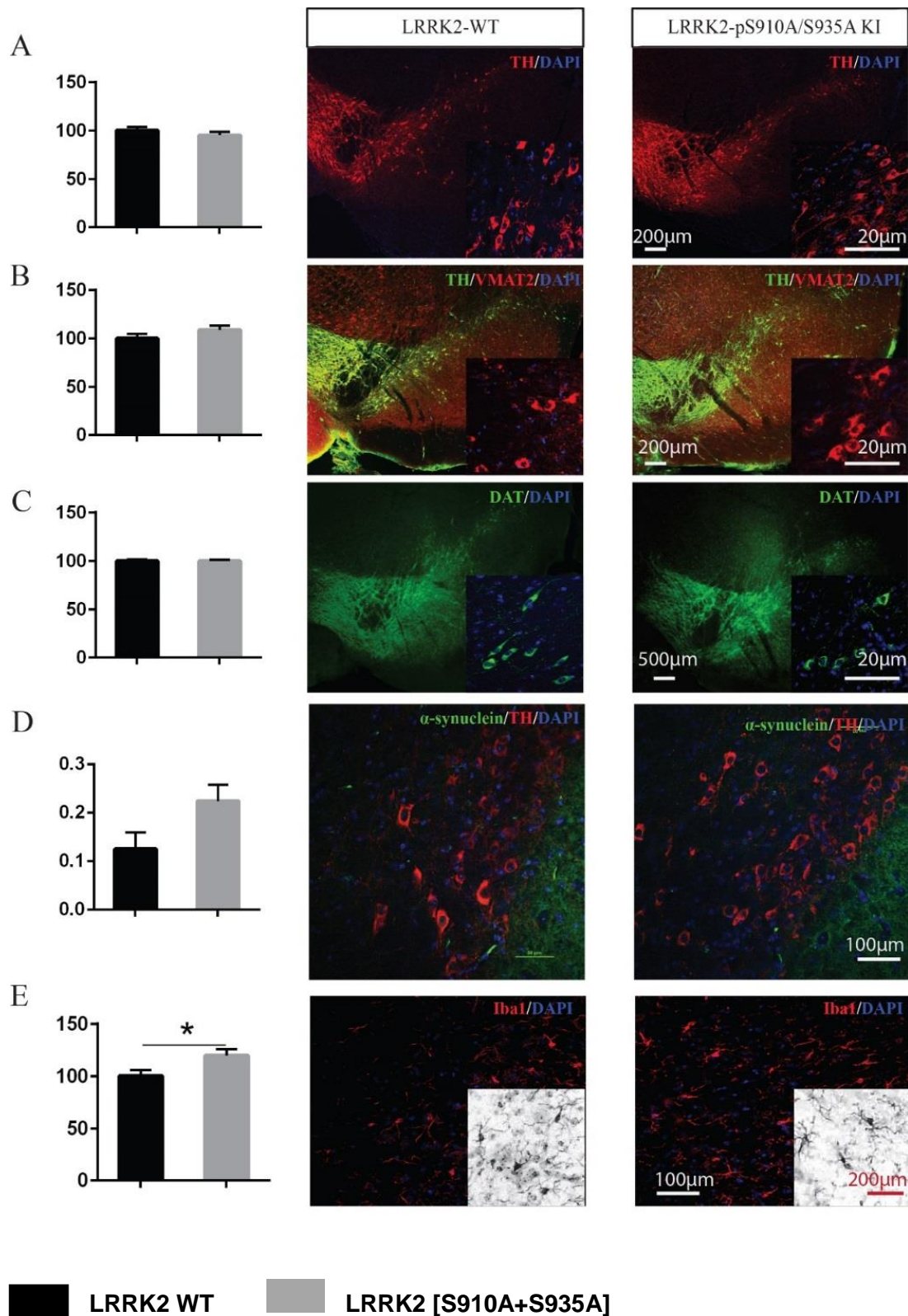


Figure 3.19: Dopamine system and pathological changes in the SN. (A) The numbers of TH-positive dopamine neurons (red) were not significantly changed between WT and KI groups. (B) The labelling intensity of VMAT2 (red) was not significantly different in the KI group. (C) The intensity of dopamine transporters labelled for DAT (green) were unchanged. (D) There was a trend of more α -synuclein colocalization (green) in TH positive dopamine neurons (red) in the SNC of LRRK2 [Ser910Ala+Ser935Ala] mice. (E) Microglia (red) in the entire SN of the LRRK2 [Ser910Ala+Ser935Ala] group outnumbered that of the WT group.

Asterisks denote statistical differences between the indicated groups; * $p < 0.05$. (Data received from Australia's Neuroscience Research Institute).

Further assessment of the integrity of the synapses in the dorsolateral striatum showed that the intensity analysis of synaptophysin and α -synuclein immunoreactivity in the dorsolateral striatum did not differ between LRRK2 [S910A+S935A] and WT mice, indicating no significant changes in these synaptic proteins. However, the intensity of TH-immunopositive dopamine terminals was significantly lower in the LRRK2 [S910A+S935A] compared to WT mice (Figure 3.20.A). This change was shown to be associated with an increase in VMAT2-labelling intensity in the LRRK2 [S910A+S935A] mice compared with the wild type. No morphological abnormalities were identified in the TH or VMAT2 immunoreactive structures at high magnification in LRRK2 [S910A+S935A] mice compared with WT mice (Figure 3.20.B). These changes might suggest reduced dopamine synthesis in intact dopamine neurons with increased synaptic vesicles transporter to maximize the potential for dopamine uptake.

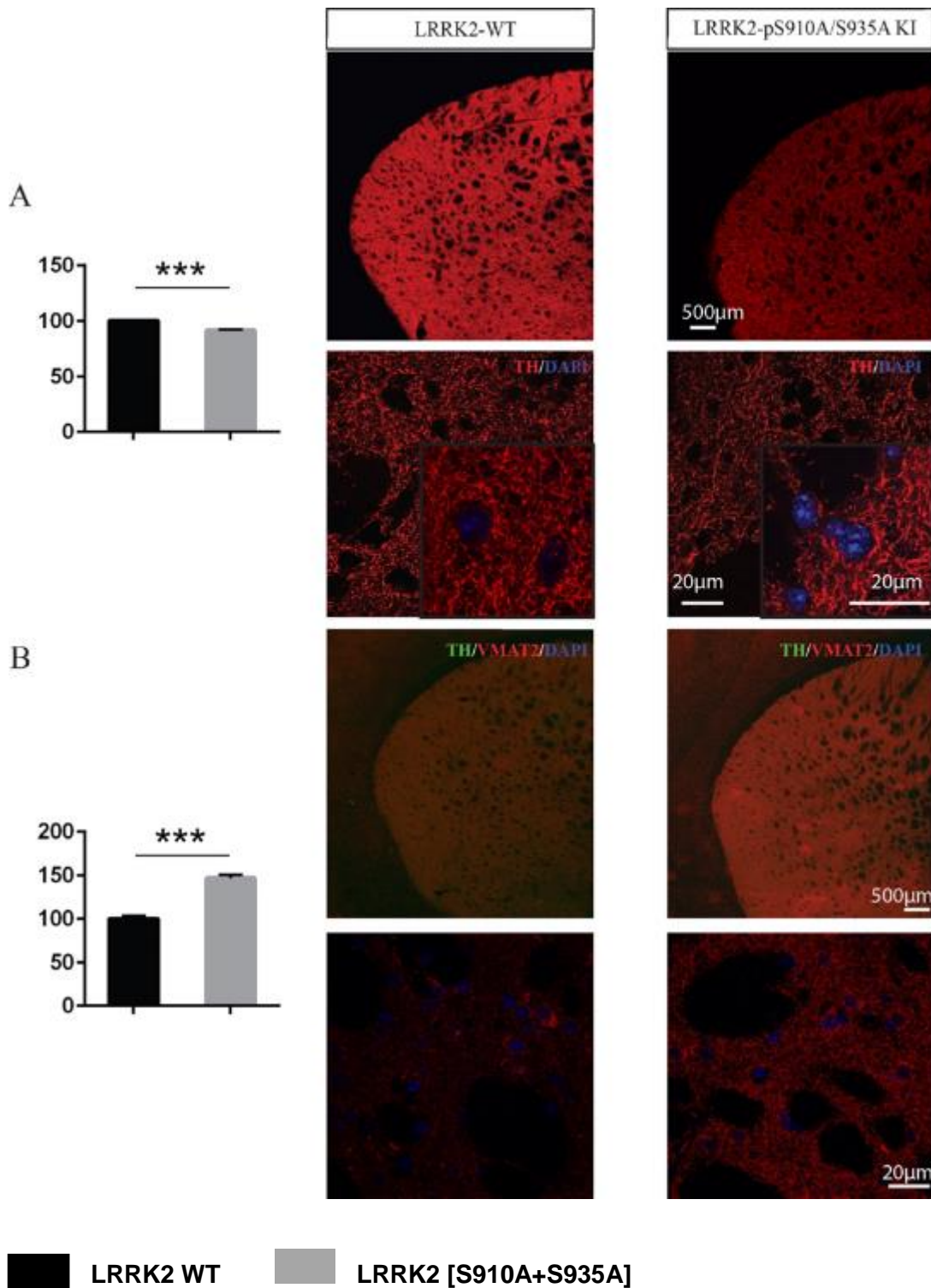
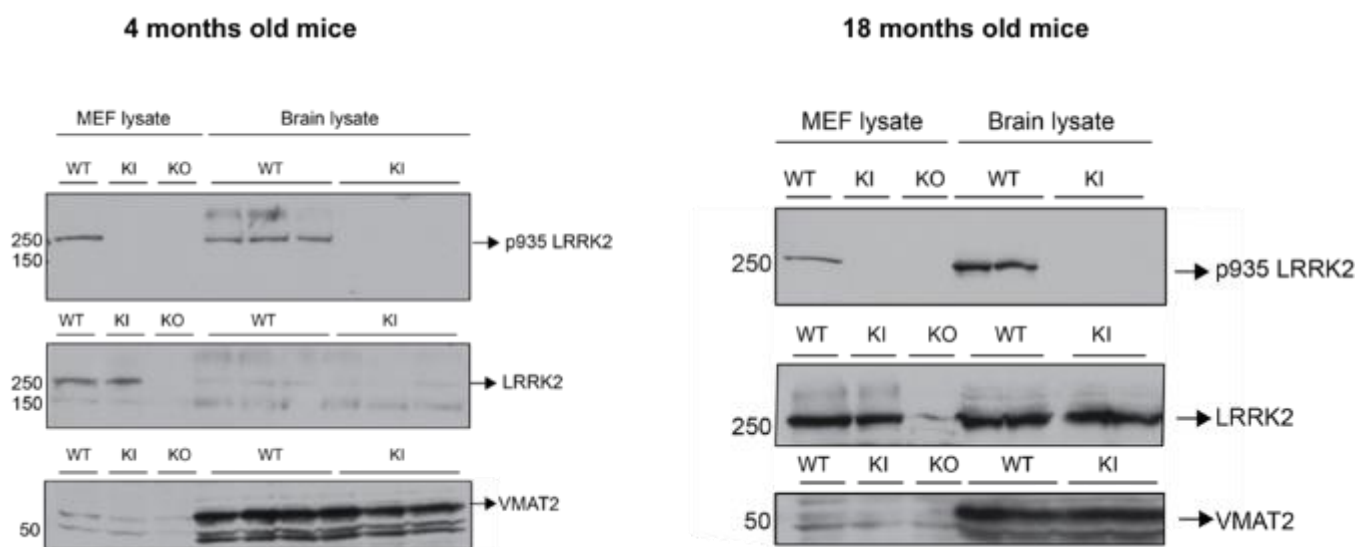


Figure 3.20: Changes of dopamine synthesis in axon terminals in the dorsolateral striatum. (A) The intensity of TH-positive dopamine axon terminals (red) was significantly decreased in KI mice compared with WT mice. High magnification images show similar TH-positive staining patterns (red). (B) The labelling intensity of VMAT2 (red) was significantly elevated in the KI group. Asterisks denote statistical differences between the indicated groups; *** $p < 0.0001$.

Decrease in VMAT2 has been reported in clinical PD due to the loss of synapses, and increasing VMAT2 has been proposed as a therapeutic strategy (M. K. Chen et al., 2008). To test whether the change in VMAT2 is an age-dependent finding I extracted brains from 4 and 18 months old littermate mice comprising LRRK2 [S910A+S935A] and LRRK2 WT animals. Brains were then lysed in 1% Triton and subjected total cell lysates to the immunoblot analysis using VMAT2, LRRK2 total and phospho antibodies (Figure 3.21).

A



B

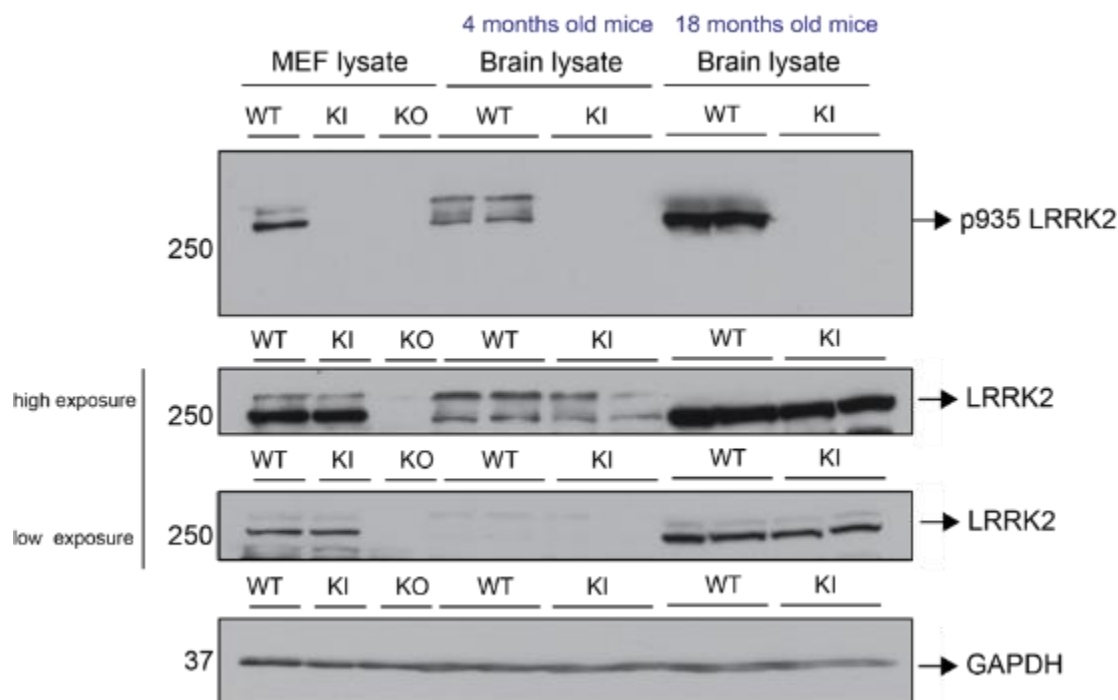


Figure 3.21: Assessment of total VMAT2 and LRRK2 levels in young and aged LRRK2 WT and LRRK2 [S910A+S935A] mice. (A) Six brains were extracted from 4 months old littermates: three LRRK2 WT and three LRRK2 [S910A+S935A] mice. Four brains were extracted from 18 months old littermates: two LRRK2 WT and two LRRK2 [Ser910Ala+Ser935Ala] mice. All brains were lysed in 1% Triton lysis buffer and total brain lysates were then subjected to immunoblot analysis with indicated antibodies. (B) Four brains were extracted from 4 months old littermates: two LRRK2 WT and two LRRK2 [Ser910Ala+Ser935Ala] mice. Four brains were extracted from 18 months old littermates: two LRRK2 WT and two LRRK2 [Ser910Ala+Ser935Ala] mice. All brains were lysed in 1% Triton lysis buffer and total brain lysates were then subjected to immunoblot analysis with indicated antibodies.

According to my findings, there is no difference in VMAT2 levels between LRRK2 WT and LRRK2 [S910A+S935A] mice brain. It could be that the differences observed in histopathological studies are minor and local, and could only be observed in a dorsolateral striatum part of the brain. It would be then interesting to dissect the brain and specifically analyse this specific part. It seems that in 18 months old mice there is a higher LRRK2 expression than in 4 months old mice. 4 brains derived from 4 independent mice were analysed for each genotype. This indicates that with age, LRRK2 expression is increased and it could be that its altered

increased expression could have an impact on LRRK2 kinase activity and be linked to late onset PD.

3.3 Summary

My data suggests that the [S910A+S935A] mutation has no influence in endogenous immunoprecipitated LRRK2 kinase activity *in vitro*, which is consistent with the previously reported over-expressed data. Interestingly, it seems that *in vivo*, LRRK2 [S910A+S935A] mutation markedly reduces Rab10 and Rab8A phosphorylation by LRRK2. It was previously reported that mutation of LRRK2 S910 and S935 to alanine or dephosphorylation of LRRK2 at these sites upon LRRK2 inhibition leads to loss of 14-3-3 binding. It was described that under normal conditions LRRK2 is diffused throughout the cytoplasm but loss of 14-3-3 binding results in its mislocalization and aggregation (Nichols et al., 2010). Therefore, it could be that when a large part of LRRK2 is sequestered into cytoplasmic aggregates, the LRRK2 activity is reduced resulting in diminished Rab10 phosphorylation. Based on this findings, it seems that serines 910 and 935 are important for LRRK2 localization and kinase activity and also for its kinase activity. It would be interesting to study endogenous LRRK2 localization within cell, however, to date there is no good IHC antibody to address this question and needs to be developed. During my PhD, I have tested all available IHC antibodies but did not find one that was specifically recognizing LRRK2 protein in wild type but not LRRK2 KO MEFs.

Furthermore, I showed that the [S910A+S935A] mutation results in decreased LRRK2 expression in kidneys. This is consistent with the previously reported genetic and pharmaceutical data. It could be that LRRK2 protein levels are determined by phosphorylation state of S910 and S935, which alters phosphorylation of LRRK2

substrates Rab10 and Rab8A.

As described before, at the moment there are some safety concerns associated with LRRK2 inhibition as a treatment for PD. As dephosphorylation of serines 910 and 935 resemble the effect of long-term LRRK2 inhibitor treatment and could be linked to safety risks associated with LRRK2 inhibition, in collaboration with Dr Francisco Marchesi, from University of Glasgow School of Veterinary Medicine a histopathological analysis of LRRK2 [S910A+S935A] kidneys and lungs was performed. According to the results reported here, there is no evidence that [S910A+S935A] leads to lungs or kidneys abnormalities, indicating that LRRK2 kinase activity but not the phosphorylation state of S910 and S935 is implicated in kidney phenotype. The findings also suggest that S910 and S935 phosphorylation is not involved in lung phenotype, suggesting that some other LRRK2 function could be linked to it. Based on this data, there are no risks associated with S910 and S935 dephosphorylation in connection to kidneys and lung phenotype. However, safety implications linked to LRRK2 kinase inhibition remain to be addressed.

In addition, I examined whether LRRK2 S910 and S935 phosphorylation has an impact on mice well-being. My data shows that mutant mice are viable and reproduce well. However, I have noticed that S910A+S935A knock in mice seem to be fatter than the wild type littermates. It is an interesting finding consistent with the reported data that shows LRRK2 KO rats are weightier than their wild type littermates (Baptista et al., 2013), indicating that S910 and S935 could play a role in metabolic process abnormality.

I also tested motor coordination of S910A+S935A knock-in mice and its wild type littermates using rotarod and found that knock-in mice performed significantly worse

than the wild type, suggesting that this mutation affects their motor coordination. To study this further, I set up a collaboration with Dr Nic Dzamco at Neuroscience Research Australia to perform a histopathological evaluation of LRRK2 WT and LRRK2 [S910A+S935A] brain. The data reported here shows that LRRK2 knock-in mice did not display decreased cell numbers or impaired proliferation in Subcortex but showed a trend for decrease in total cells in hippocampus, indicating that knock-in mice might have an effect on neuro/gliogenesis. Moreover, no significant dopamine neuronal loss was observed in knock-in mice. No loss of TH neurons in the SN, no differences in TH morphology, suggesting that knock-in mice are unlikely to develop PD under basal conditions. This result is consistent with the previously reported LRRK2 R1441C and R144G knock-in mice that comprise dephosphorylated 910 and 935 sites. Interestingly, it was noted that VMAT2 intensity in knock-in mice was increased in comparison with the wild type. These changes might suggest reduced dopamine synthesis in intact dopamine neurons with elevated synaptic vesicle transporter to maximize the potential for dopamine uptake. Immunoblot analysis of 4 and 18 months old total brain lysates revealed that there is no difference in VMAT2 expression between LRRK2 WT and LRRK2 knock-in mice, indicating that this change is minor and might be present at the localized brain region. My preliminary data suggests that total LRRK2 levels in the aged mice are higher compared with the young mice, indicating that LRRK2 protein levels might be increasing with age and this could be linked to the mechanism, which might lie behind LRRK2 pathology in PD. However, these results need to be studied further as it could be due to the freezing artifacts.

Chapter 4:

Investigating MYPT1 as a Potential LRRK2 Substrate

4.1 Introduction

As described in the introduction, the presence of multiple protein interaction domains suggest that LRRK2, in addition to its kinase and GTPase activities can function as scaffold for the assembly of multiprotein signaling complexes. To elucidate the molecular interaction network of endogenous LRRK2, the Gloeckner's lab in collaboration with Marto's lab performed quantitative immunoprecipitation combined with knockdown (QUICK) experiments (Meixner et al., 2011). This approach assesses interactions between proteins at their endogenous levels and their normal cellular environment by combining stable cell isotope labelling with amino acids in cell culture (SILAC), RNA interference, co-immunoprecipitation and quantitative mass spectrometry. This study linked LRRK2 function to the actin-based cytoskeleton and the list of numerous interactors was published (Meixner et al., 2011). Little validation was undertaken in this study to determine which interactions were genuine. Myosin phosphatase target subunit 1 (MYPT1) was identified as a possible LRRK2 interactor in this screen. At the same time, in our laboratory, Paul Davies also observed that MYPT1 from HEK293 cell extract interacted with recombinant GFP tagged LRRK2 immobilized on a sepharose resin (unpublished data). Furthermore, an *in vitro* kinase assay performed by Dr Paul Davies revealed that recombinant MYPT1 was efficiently phosphorylated by LRRK2. In addition, in 2016, Matthias Mann's lab in collaboration with our laboratory performed a comparative phosphoproteomic analysis of wild type MEF and MEF LRRK2 [A2016T] drug resistant mutant cells treated with MLI-2, a novel potent and specific LRRK2 inhibitor generated by Merck (Fell et al., 2015; Steger et al., 2016). One of the numerous hits that emerged from this screen was MYPT1.

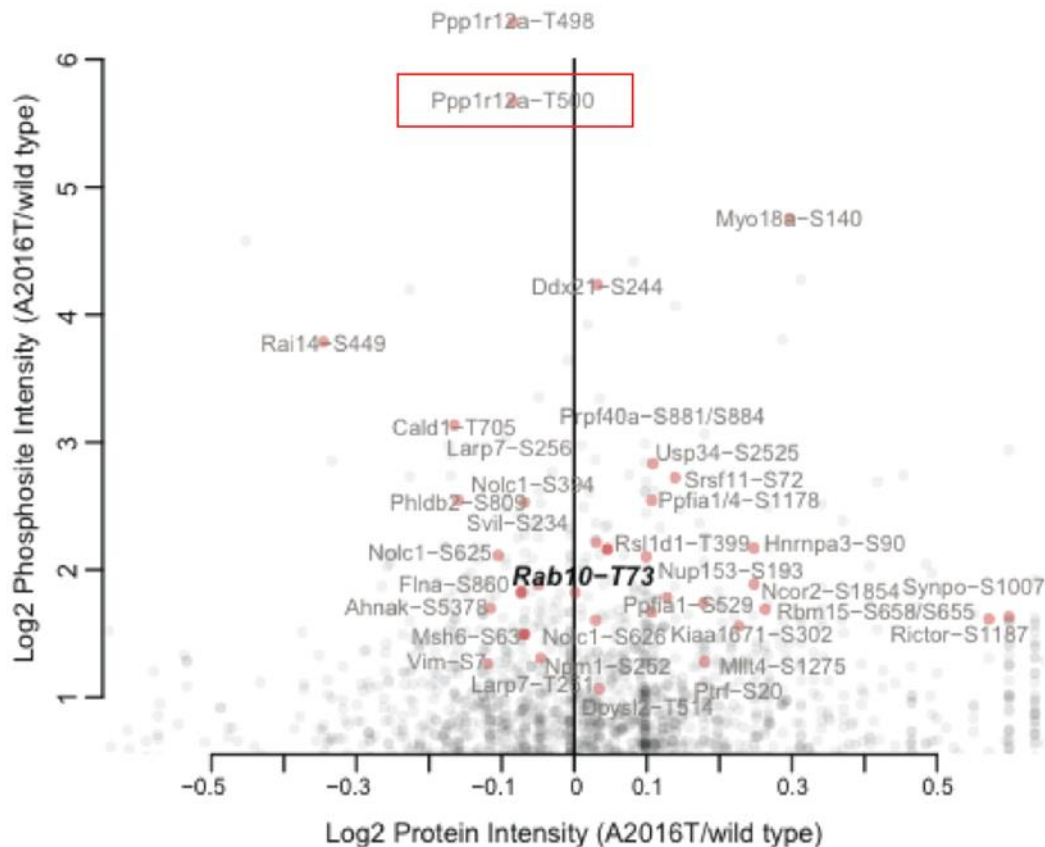


Figure 4.1: Comparative phosphoproteomic analysis of LRRK2 WT vs LRRK2 [A2016T] MEF cells (two sample t-test, FDR=2%) Data generated by Martin Steger from Matthias Mann's lab.

Their data suggested that phosphorylation of MYPT1 at T498 and T500 was inhibited in the wild type MEFs treated with ML-I2 inhibitor but not in LRRK2 [A2016T] (Figure 4.1). MYPT1 peptide phosphorylated at T498 and T500 was one of the top hit in this screen. As MYPT T498 site is not conserved in humans, it was hypothesized that LRRK2 could phosphorylate MYPT1 at T500 in cells. Building on this evidence, we speculated that MYPT might comprise a physiological substrate of LRRK2.

MYPT1 (also termed PPP1R12A, M130/133, M110, MBS) is a targeting subunit of myosin phosphatase. It comprises protein phosphatase1 β (PP1 β) binding motif

(called RVXF) at the N terminal (Figure 4.4.C), which allows MYPT1 to direct PP1 specifically to its substrate. Therefore, it was further hypothesized that phosphorylation of MYPT1 could result in inhibition of myosin phosphatase via disruption of MYPT1:PP1 β complex leading to S910 and S935 phosphorylation. As a result, inhibition of LRRK2 would result in activation of myosin phosphatase and subsequent dephosphorylation of S910 and S935 (Figure 4.2).

Myosin phosphatase consists of myosin phosphatase targeting subunit MYPT1, catalytic subunit PP1 β that belongs to the PP1 family of Ser/Thr phosphatases and M20 subunit of unknown function. Myosin phosphatase holoenzyme was first purified from chicken gizzard by my PhD supervisor Dario Alessi in 1992 as a complex of catalytic subunit (PP1 β), myosin targeting subunit (M130/MYPT1) and a small subunit of unknown function (M20) (Alessi, MacDougall, Sola, Ikebe, & Cohen, 1992; Scotto-Lavino, Garcia-Diaz, Du, & Frohman, 2010; Terrak, Kerff, Langsetmo, Tao, & Dominguez, 2004). The human MYPT family comprises MYPT1, MYPT2, MBS85, MYPT3 and TIMAP (M. Ito, Nakano, Erdodi, & Hartshorne, 2004).

It was described that all family members comprise similar domain structure and importantly, N-terminal ankyrin repeats, which are one of the most common protein-protein interaction domains (Mosavi, Cammett, Desrosiers, & Peng, 2004). MYPT1 is strictly regulated by phosphorylation and interactions with regulatory proteins. Various kinases were already reported to phosphorylate and inhibit MYPT1 including ROCK (Kimura et al., 1996), ILK (Muranyi et al., 2002), DMPK (Muranyi et al., 2001), ZIPK (MacDonald, Eto, Borman, Brautigan, & Haystead, 2001), PAK (Takizawa, Koga, & Ikebe, 2002) and Raf-1 (Broustas et al., 2002). Interestingly, most of these kinases are regulated by small GTPases: ROCK by RhoA, DMPK by Rac, PAK by Rac and/or Cdc42, and Raf-1 by Ras and can phosphorylate myosin regulatory light

chain 2 (MRLC2). MYPT1 plays a key role in regulation of MRLC2 phosphorylation and therefore cell contractile and motile events (Wardle et al., 2006). Also, it was reported to be important in mitotic progression (Matsumura et al., 2011), cytokinesis (Kachaner et al., 2012) and cell detachment (Zagorska et al., 2010).

In this chapter, the aim of my project is to address whether MYPT1 is a physiological substrate of LRRK2 and to investigate whether phosphorylation of MYPT1 by LRRK2 is involved in the regulation of S910 and S935 phosphorylation of LRRK2. The summary of the working hypothesis is summarized in the Figure 4.2.

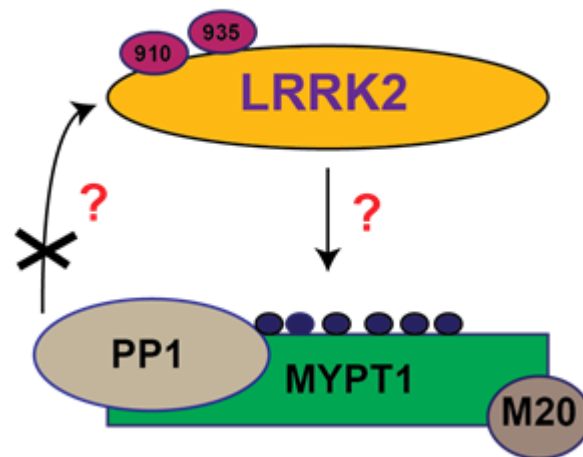


Figure 4.2: Proposed model of LRRK2 regulation. The aim is to investigate whether MYPT1 is a physiological substrate of LRRK2 and if so whether it was implicated in regulating the negative feedback loop on S910 and S935 phosphorylation.

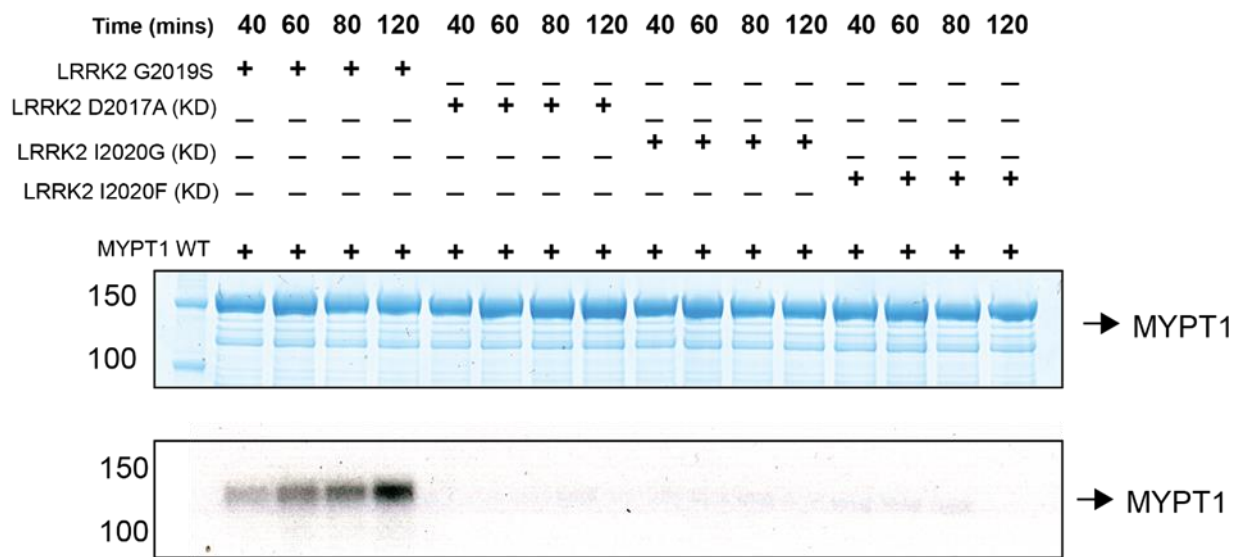
4.2 Results

4.2.1 MYPT1 is phosphorylated by LRRK2 *in vitro* at T500, T524, T529, T671, T761 and T891

To confirm that MYPT1 is indeed phosphorylated by LRRK2 *in vitro*, I phosphorylated bacterially-purified MYPT1 protein in presence of Mg^{2+} - $[\gamma\text{-}^{32}\text{ATP}]$, HEK293 purified GST-tagged LRRK2 [G2019S] in parallel with three different kinase dead LRRK2 proteins mutants generated in the lab: D2017A, I2020G and I2020F for

30 mins at 30°C at 1000 rpm. (Figure 4.3.A). My results indicate that LRRK2 [G2019S], but not catalytically inactive LRRK2 KD, phosphorylates MYPT1 in a time-dependent manner. Gel pieces comprising MYPT1 protein were extracted and MYPT1 phosphorylation was measured by a scintillation counter (4.3.B). This data confirmed that MYPT1 phosphorylation *in vitro* is dependent on LRRK2 kinase activity.

A



B

MYPT1 phosphorylation by LRRK2

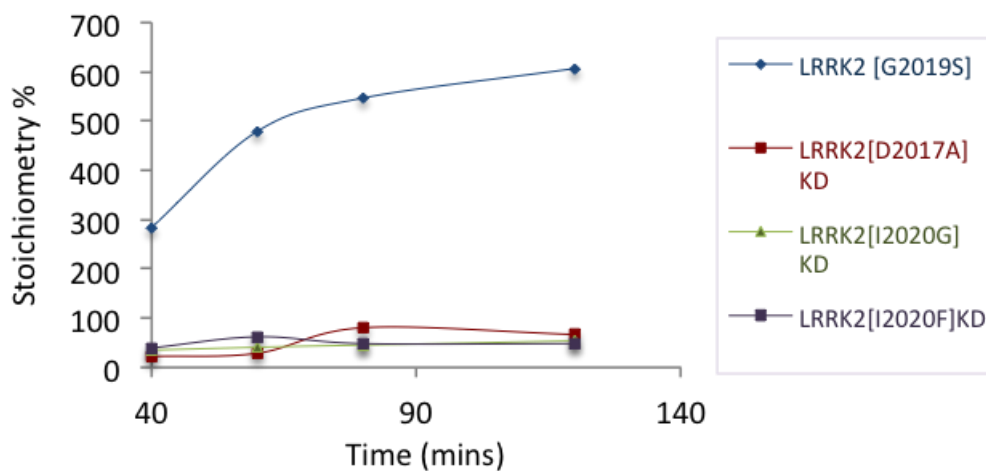
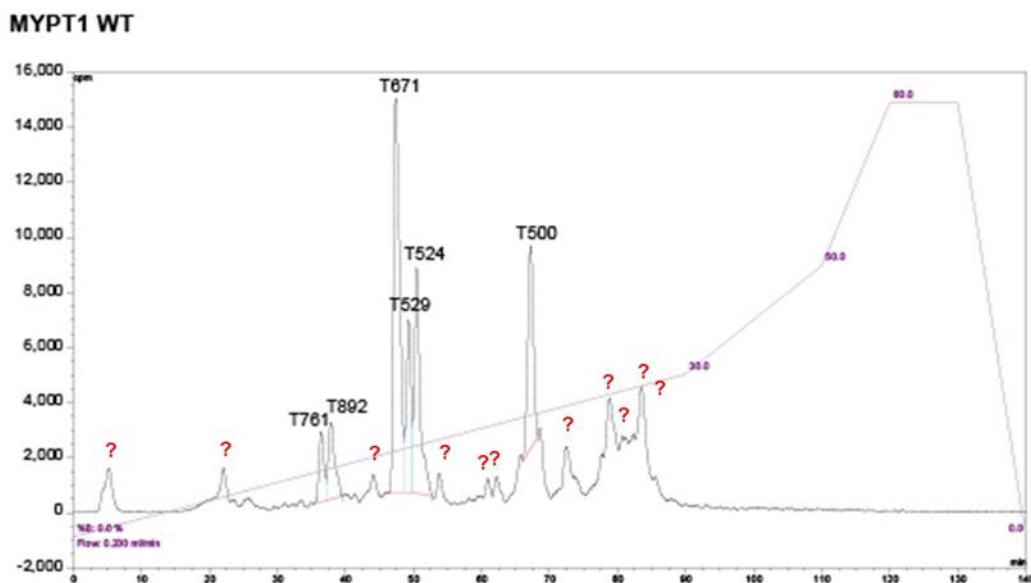


Figure 4.3: MYPT1 phosphorylation by LRRK2 in vitro. (A) GST tagged LRRK2 [G2019S] or GST-tagged kinase-inactive LRRK2 ([D2017A], [I2020G], [I2020F]) proteins were HEK293-purified. Purified LRRK2 proteins were incubated with recombinant GST-tagged MYPT1 and Mg²⁺-[γ-³²P] for the indicated times and subjected to electrophoresis on a polyacrylamide gel and autoradiography. (B) Gel pieces comprising MYPT1 protein were extracted and MYPT1 phosphorylation was measured by a scintillation counter.

In order to map MYPT1 phosphorylation sites, GST-tagged bacterially purified [³²P] MYPT1 WT protein was phosphorylated by HEK293 purified GST-tagged LRRK2 [G2019S] kinase for 120 mins at 30°C at 1000 rpm and digested with the endoproteinase Asp-N. Digests were then analysed by chromatography on a C₁₈ column. Six major ³²-P labelled phospho-peptides were observed in MYPT1 WT comprising sample (Figure 4.4.A). Solid-phase Edman sequencing and mass spectrometry identified phosphorylation sites as T500, T524, T529, T671, T761 and T892. Summary of these sites is shown in the Figure 4.4.B. These sites are located within ankyrin repeats at the C-terminal of MYPT1 protein (Figure 4.4.C). T500 and T671 are the most conserved phosphorylation sites among different species (Figure 4.4.D).

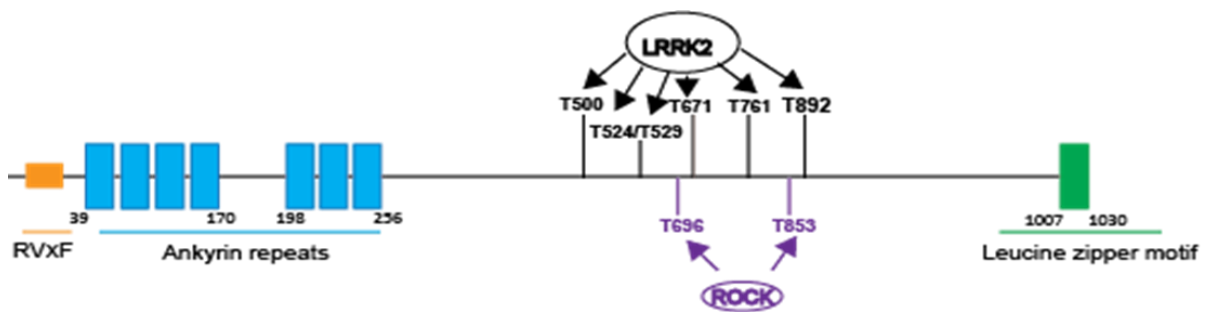
A



B

Phospho-peptides	Phospho site
T.DSISRYE T SSSTSAG.D+P	Thr ⁸⁹²
E.DEYKQKYSR T Y.D+P	Thr ⁷⁶¹
R.ERRRSYL T PVR.D+P	Thr ⁶⁷¹
R.DSSSLR T SSSY T RRKWE.D+P	Thr ⁵²⁴ /Thr ⁵²⁹
K.DSKGTRLAYVAP T IPRRLASTS.D+P	Thr ⁵⁰⁰

C



D

	Thr 419	Thr 500	Thr 524	Thr 529	Thr 671	Thr 761	Thr 892
HUMAN	PTT A TKIS	VAP T IIPR	L R TSSSY T RR	SYL T PVR	S R TYDET	S-- T SAG	
RAT	PT S TTKIS	VAP T IIPR	L R TSSSY T RR	SYL T PVR	S R TYDET	S-- T SSS	
ZEBRAFISH	ST P AGKLS	VAP T IIPR	VR- S GSY T RR	SYL T PVR	RS- F EELK	ST S TSST	
MOUSE	PI S TKIS	V T P T IIPR	L R TSSSY T RR	SYL T PVR	S R TYDET	S-- T SSS	
FROG	PT P PKTS	VAP T IIPR	LR G SSSY T RR	SYL T PVR	AR S TEET	LS S AIST	
CHIMPANZEE	PT T DAKIY	VAP T IIPR	L R TSSSY T RR	SYL T PVR	S R TYDET	S-- T SAG	
CAT	PT S ATKIS	VAP T IIPR	L R TSSSY T RR	SYL T PVR	S R TYDET	S-- T SAS	
DOG	PT S ATKVS	VAP T IIPR	L R TSSSY T RR	SYL T PVR	S R TYDET	S-- T SAG	
TURTLE	PT S TIKVS	VAP T IIPR	IR S GSY T RR	SYL T PVR	S R TLEEP	S I SSSSG	
CHICKEN	PT S TIKVS	VAP T IIPR	IR S GSY A RR	SYL T PVR	S R TVEEP	S L SVSSG	
BOVINE	PA S ATKIS	V T P T IIPR	L R TSSSY T RR	SYL T PVR	S R TYDEA	S-- T SAS	

Figure 4.4: LRRK2 phosphorylates MYPT1 at T500, T524, T529, T671, T761 and T892. (A) Recombinant MYPT1 WT was incubated with LRRK2 [G2019S] in the presence of Mg²⁺-[γ-32P] ATP for 120 min at 30°C at 1000 rpm. Phosphorylated MYPT1 was digested with Asp-N and peptides were separated by reversed-phase high performance liquid chromatography on a C₁₈ column. The peaks containing the ³²P-labeled phospho-peptides are labelled with the identified phosphorylated residue. (B) Summary of the mass spectrometry and solid-phase Edman sequencing data obtained after analysis of the peak fractions. The deduced amino acid sequence of each peptide is shown and the phosphorylated residue is indicated (in red). (C) Domain structure of MYPT1 with the position of residues phosphorylated by LRRK2 (T500, T524, T529, T671, T761 and T892) and previously reported ROCK phosphorylation sites. (D) Sequence alignments of the indicated species of MYPT1 proteins surrounding indicated LRRK2 phosphorylation site.

In summary, my data shows that MYPT1 is efficiently phosphorylated by LRRK2 *in vitro* at least at T500, T524, T529, T671, T761 and T892. This is consistent with the previously reported data showing that LRRK2 preferentially phosphorylates threonines over serines (Nichols et al., 2009b). Interestingly, threonines 500 (Guo A et al., 2011), 529 (Zhou J et al., 2009), 671 (Sharma K et al 2014) and 892 (Mulhern D et al., 2011) were observed to be phosphorylated in cells in global proteomic studies and were reported to be novel MYPT1 phosphorylation sites (<http://www.phosphosite.org/> database), the kinases that phosphorylate these sites are unknown. Therefore, I set out to test whether LRRK2 could potentially phosphorylate these novel sites.

4.2.2 Mutation of T500, T524, T529, T671, T761 and T891 to alanine only reduces but does not abolish MYPT1 phosphorylation by LRRK2 *in vitro*.

My results showed that MYPT1 is phosphorylated by LRRK2 [G2019S] *in vitro* at T500, T524, T529, T671, T761 and T892. However, mutation of all of these residues to alanine although significantly reduces MYPT1 phosphorylation by LRRK2 [G2019S] it does not completely block it (Figure 4.5). This result is expected as HPLC trace revealed numerous minor sites, but the abundance of these sites was too low to identify them, these sites are marked as “?” in the Figure 4.4. However, after several attempts to map these sites (data not shown), I could not find any other major phosphosites but detected several small phosphosites, which were difficult to sequence. I cannot rule out the possibility that mutation of six MYPT1 threonines could lead to conformational change of the protein and create additional artificial phosphosites *in vitro*.

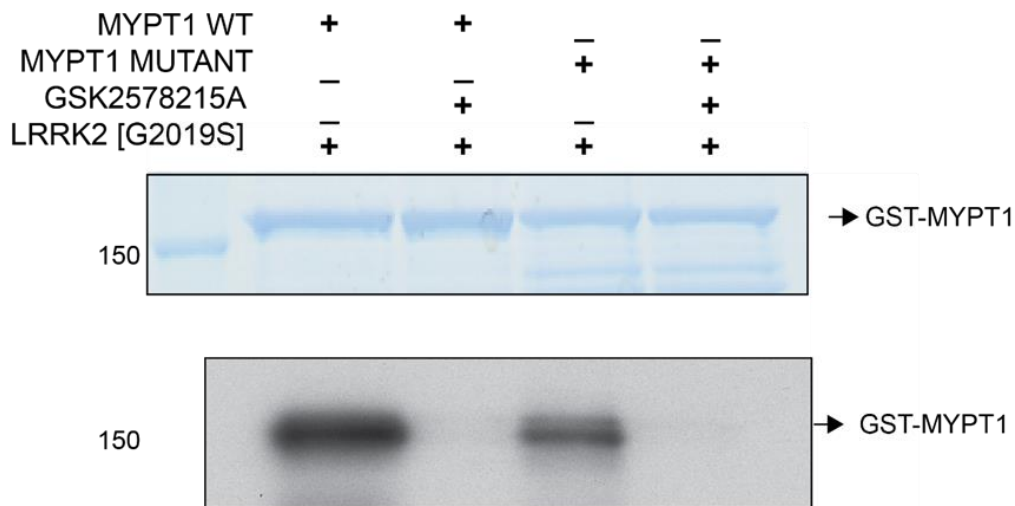


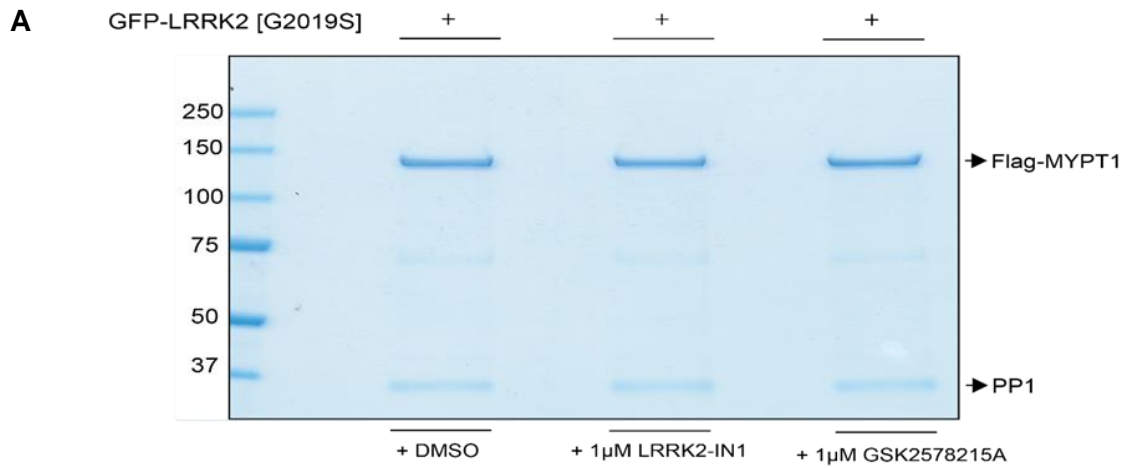
Figure 4.5: Mutation of T500+T524+T529+T671+T761+T892 to alanine reduces LRRK2 phosphorylation in vitro. HEK293-purified LRRK2 [G2019S] was incubated with bacterially purified recombinant MYPT1 WT or mutant [T500A+T524A+T529A+T671A+T761A+T892A] proteins in presence of Mg^{2+} -[γ - ^{32}P ATP] and LRRK2 GSK257821A specific kinase inhibitor as a negative control for 30 mins at 30°C at 1000 rpm. Samples were then subjected to electrophoresis on a polyacrylamide gel and autoradiography.

Building on the fact that I was unable to sequence multiple minor MYPT1 phosphorylation sites, I decided to focus on the six major sites already mapped, and test whether inhibition of LRRK2 kinase activity in cells results in dephosphorylation of these threonines.

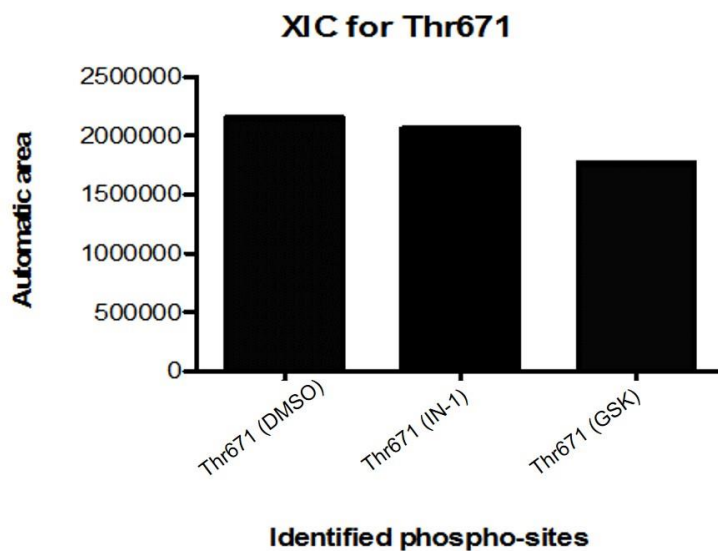
4.2.3 In over-expressed system there are no significant changes in MYPT1 phosphorylation because of LRRK2 kinase inhibitor treatment.

To determine whether inhibition of LRRK2 kinase activity leads to decreased phosphorylation of identified MYPT1 phosphosites (T500, T524, T529, T671, T761 or T892) in cells, HEK293 TReX cells stably overexpressing GFP-tagged LRRK2 [G2019S] were transiently transfected with Flag-tagged MYPT1 and treated with DMSO control or 1 μ M GSK2578215A or LRRK2-IN1 LRRK2 kinase inhibitors. Flag-tagged MYPT1 was immunoprecipitated and resolved on a SDS gel (Figure 4.6.A). The protein bands corresponding to MYPT1 were subjected to in-gel Tryptic

digestion and analyzed by mass spectrometry [Orbitrap-Classic] to determine any obvious changes in MYPT1 phospho-mapped sites. (Figure 4.6.B). To test whether these inhibitors work, cell lysates were subjected to immunoblot analysis with phospho and total LRRK2 antibodies (4.6.C).



B



C

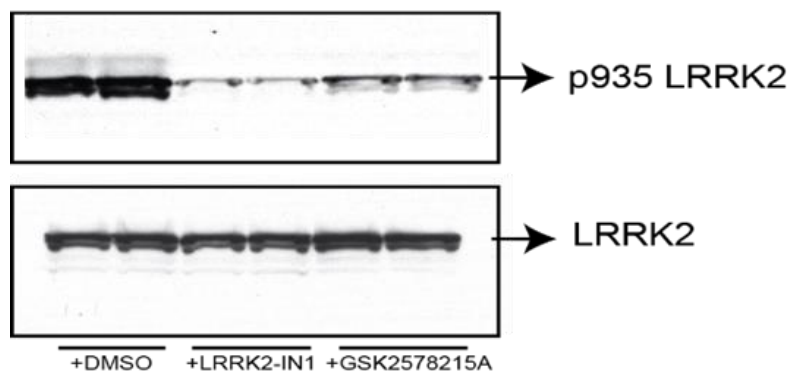


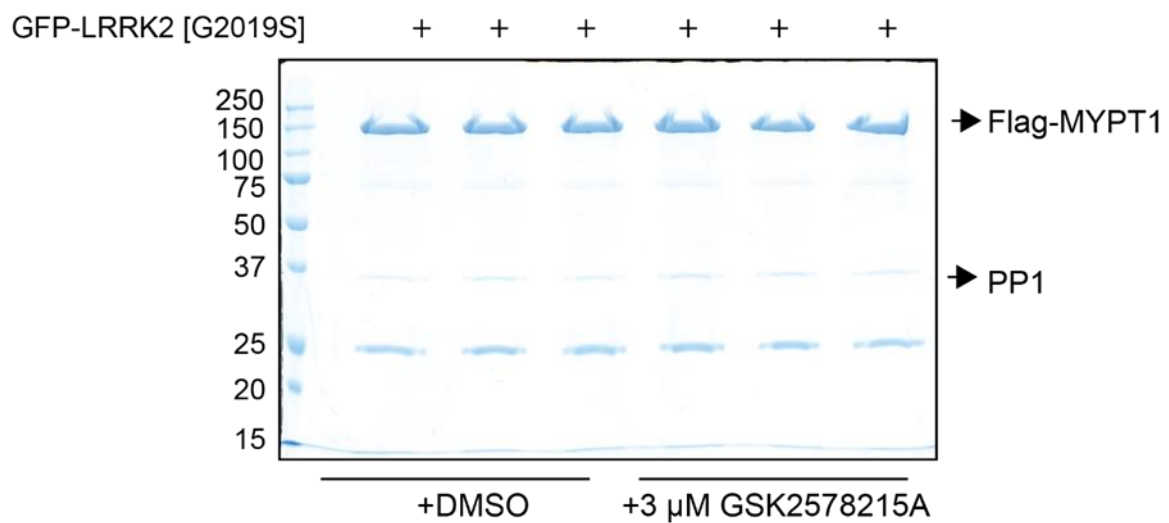
Figure 4.6: Assessment of MYPT1 phosphorylation in HEK293 cells o/e LRRK2 G2019S (A) Transiently over-expressed Flag-tagged MYPT1 was immunoprecipitated from HEK293 T-REx cells stably overexpressing GFP- tagged G2019S LRRK2 treated with DMSO or 1 μ M indicated LRRK2 inhibitors, and resolved on a SDS gel. (B) XIC for Thr671 was generated based on the intensities in a control sample as well as in LRRK2 inhibitor treated samples. No statistical analysis was made. (C) Cell lysates were subjected to immunoblotting analysis with total and phospho LRRK2 antibodies to show that LRRK2 kinase inhibitors worked

Orbitrap analysis gave no evidence that peptides comprising T500, T529, T761 or T892 are phosphorylated in cells. However, peptide R.RRSYLTPVR.D comprising Thr671 was seen to be phosphorylated in a control as well as in LRRK2 inhibitor treated samples. Extracted ion chromatograms (XICs) for these phospho-peptides were made by Dr David Campbell and phosphorylation levels at these sites were compared for the different conditions. This result does not suggest that treatment with LRRK2 inhibitor lead to a significant suppression of phosphorylation of T671 in this experiment.

To determine whether this result is consistent, this experiment was repeated in triplicates but this time with an increased LRRK2 kinase inhibitor concentration. HEK293 T-REx cells stably overexpressing GFP-tagged LRRK2 [G2019S] were transiently transfected with Flag-tagged MYPT1 and treated with DMSO control or 3 μ M GSK2578215A LRRK2 kinase inhibitors. Flag-tagged MYPT1 was

immunoprecipitated and resolved on a SDS gel (Figure 4.7.A). The protein bands corresponding to MYPT1 were subjected to in-gel Tryptic digestion and analyzed by mass spectrometry [Orbitrap-Classic] to determine any obvious changes in MYPT1 phospho-mapped sites. (Figure 4.7.B). To test whether these inhibitors work, cell lysates were subjected to immunoblot analysis with phospho and total LRRK2 antibodies (4.7.C).

A



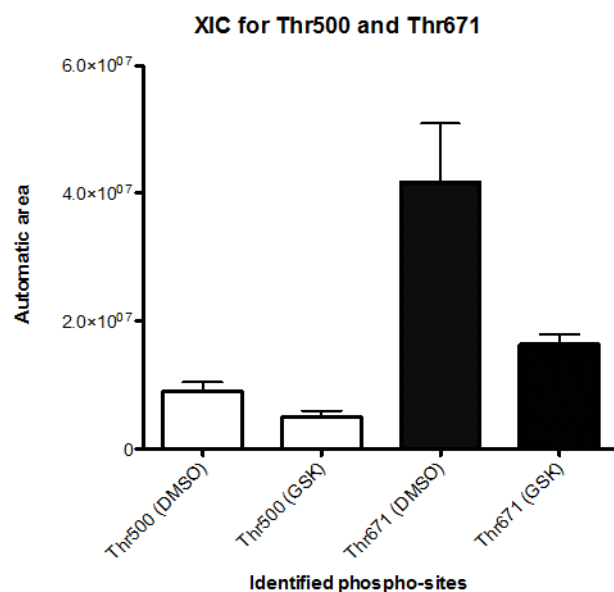
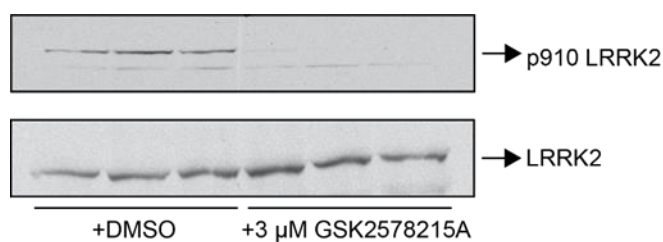
B**C**

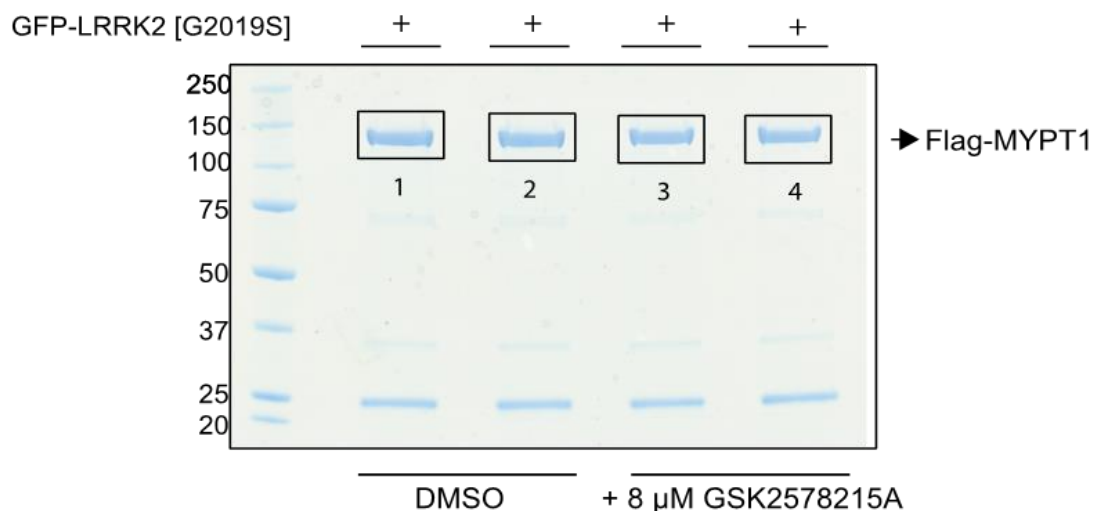
Figure 4.7: Assessment of MYPT1 phosphorylation in HEK23 cells o/e LRRK2 G2019S
(A) Transiently over-expressed Flag-tagged MYPT1 was immunoprecipitated from HEK293 T-REx cells stably overexpressing GFP- tagged G2019S LRRK2 treated with DMSO or 3μM GSK2578215A LRRK2 inhibitors, and resolved on a SDS gel. **(B)** XIC for T671 and T500 was generated based on the intensities in a control sample as well as in LRRK2 inhibitor treated samples. Two sample t-test, showed no significant reduction in phosphorylation of T671 and T500 in the inhibitor treated samples ($p > 0.05$) **(C)** Cell lysates were subjected to immunoblotting analysis with total and phospho LRRK2 antibodies to show that LRRK2 kinase inhibitors worked.

In this experiment, orbitrap analysis gave no evidence that peptides comprising T529, T761 or T892 are phosphorylated in cells. However, peptide comprising T500 and T671 were seen to be phosphorylated in a control as well as in LRRK2 inhibitor treated samples. Extracted ion chromatograms (XICs) for these phospho-peptides were made by Dr David Campbell and phosphorylation levels at these sites were

compared for the different conditions. According to these results, there is a trend for a decrease in phosphorylation at T500 and T671 in response to LRRK2 inhibition.

To test, whether this effect could be enhanced with the increased concentration of LRRK2 kinase inhibitor. This experiment was repeated with 8 μ M of LRRK2 kinase GSK258825A inhibitor. HEK293 TReX cells stably overexpressing GFP-tagged LRRK2 [G2019S] were transiently transfected with Flag-tagged MYPT1 and treated with DMSO control or 8 μ M GSK2578215A LRRK2 kinase inhibitors. Flag-tagged MYPT1 was immunoprecipitated and resolved on a SDS gel (Figure 4.8.A). The protein bands corresponding to MYPT1 were subjected to in-gel Tryptic digestion and analyzed by mass spectrometry [Orbitrap-Classic] to determine any obvious changes in MYPT1 phospho-mapped sites. (Figure 4.8.B). To test whether these inhibitors work, cell lysates were subjected to immunoblot analysis with phospho and total LRRK2 antibodies (4.8.C).

A



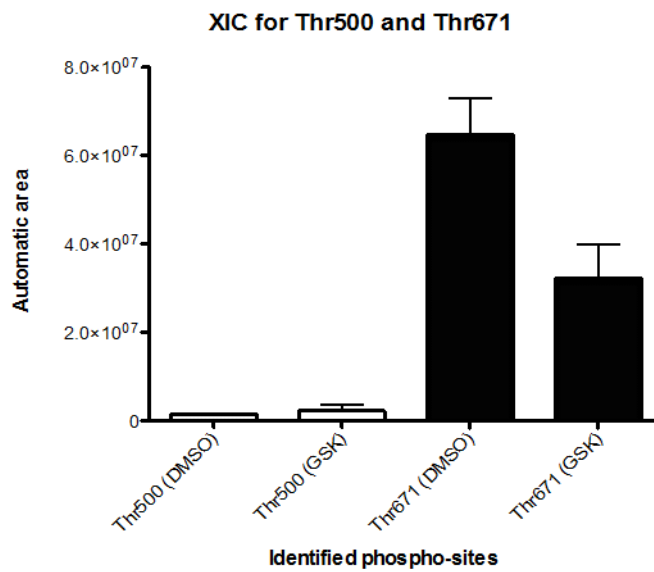
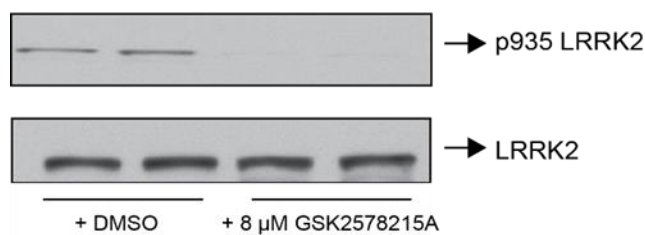
B**C**

Figure 4.8: Assessment of MYPT1 phosphorylation in HEK23 cells o/e LRRK2 G2019S
(A) Transiently over-expressed Flag-tagged MYPT1 was immunoprecipitated from HEK293 T-Rex cells stably overexpressing GFP- tagged G2019S LRRK2 treated with DMSO or 8 μ M indicated LRRK2 inhibitors, and resolved on a SDS gel. **(B)** XIC for Thr671 and Thr500 was generated based on the intensities in a control sample as well as in LRRK2 inhibitor treated samples. Two sample t-test, showed no significant reduction in phosphorylation of Thr671 and Thr500 in the inhibitor treated samples ($p > 0.05$). **(C)** Cell lysates were subjected to immunoblotting analysis with total and phospho LRRK2 antibodies to show that LRRK2 kinase inhibitors worked.

In this experiment, orbitrap analysis again gave no evidence that peptides comprising T529, T761 or T892 are phosphorylated in cells. However, peptide comprising T500 and T671 were observed to be phosphorylated in a control as well as in LRRK2 inhibitor treated samples. Extracted ion chromatograms (XICs) for these phospho-peptides were made by Dr David Campbell and phosphorylation

levels at these sites were compared for the different conditions. According to my results, there is a trend for a decrease in phosphorylation at T671 in response to LRRK2 inhibition but not at T500.

Although this analysis is only semi-quantitative it doesn't suggest that there is a significant suppression of phosphorylation at T500 and T671 in these experiments. In addition, I did not observe a decrease in phosphorylation at these sites in response to increased LRRK2 inhibition. I cannot also rule out an off-target effect resulting from an increased LRRK2 kinase inhibitor concentration affecting my results. Moreover, it could be that usage of over-expressed cells is not ideal as over-expressed MYPT1 may not be folded properly inside the cell and as a result LRRK2 cannot access its phosphorylation sites. To rule out this possibility I performed a similar experiment using endogenous proteins.

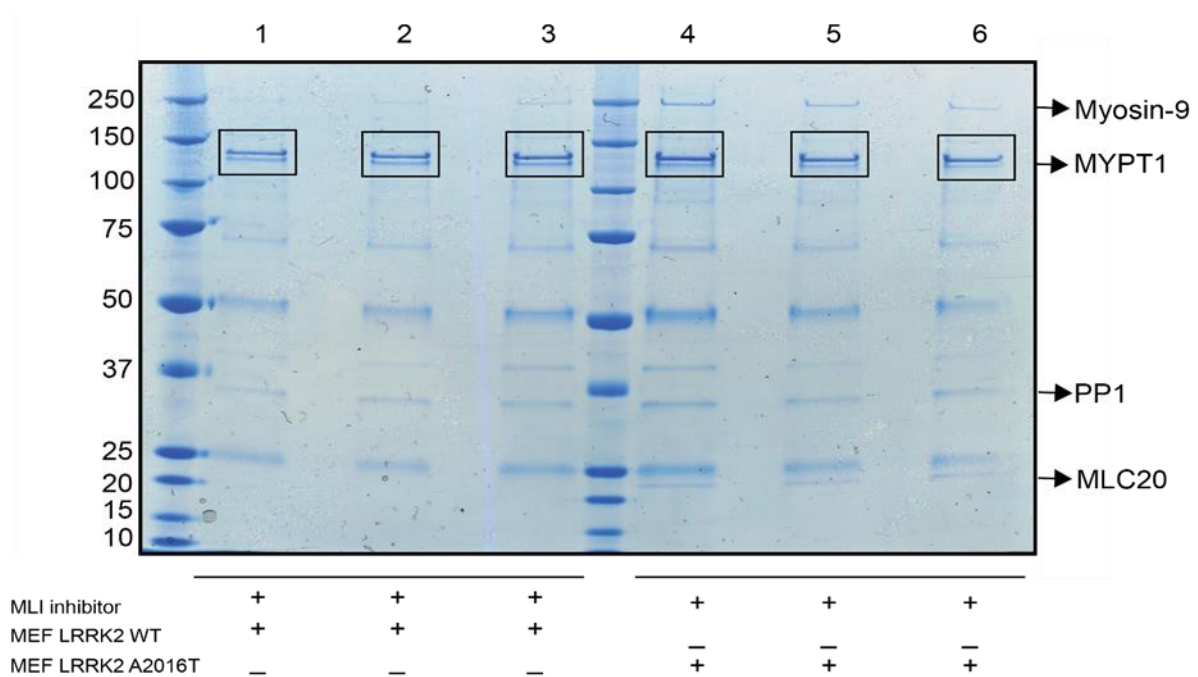
4.2.4 In MEFs, inhibition of endogenous LRRK2 with ML-I inhibitor, results in a trend of T500 and T671 phosphorylation reduction.

My results in over-expressed cells revealed that there are no significant changes in MYPT1 phosphorylation at the mapped residues due to LRRK2 kinase inhibition. This suggests that LRRK2 might not be directly regulating the phosphorylation of MYPT1. However, one limitation of the experiments I have undertaken is that I have focused on studying the phosphorylation of overexpressed MYPT1 that might not be ideal as MYPT1 exists as a complex with the protein phosphatase 1 (PP1) and the overexpressed protein might be mislocalized or not in a physiological conformation that is able to dock with LRRK2. This might explain why I have not been able to establish that it is dephosphorylated after I treat cells with LRRK2 inhibitors.

To investigate how MYPT1 phosphorylation at the mapped sites is affected by LRRK2 inhibition, immunoprecipitated endogenous MYPT1 from MEF LRRK2 WT

and drug resistant MEF LRRK2 [A2016T] treated with DMSO or recently developed highly specific MLI-2 LRRK2 kinase inhibitor was resolved on a SDS gel. Gel bands corresponding to MYPT1 protein were extracted, subjected to Tryptic digestion and analyzed by mass spectrometry [Orbitrap-Classic] to determine any obvious changes in MYPT1 phospho-mapped sites (Figure 4.9A). To test whether these inhibitors work, cell lysates were subjected to immunoblot analysis with phospho and total LRRK2 antibodies. (4.9C).

A



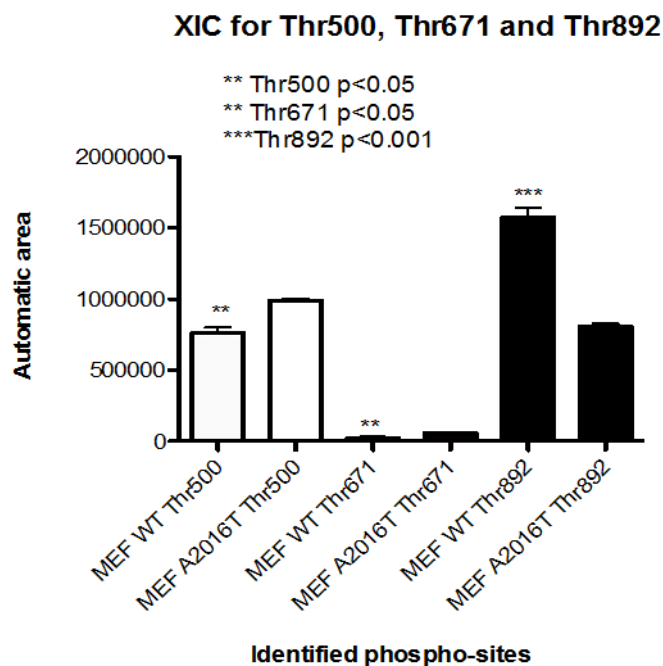
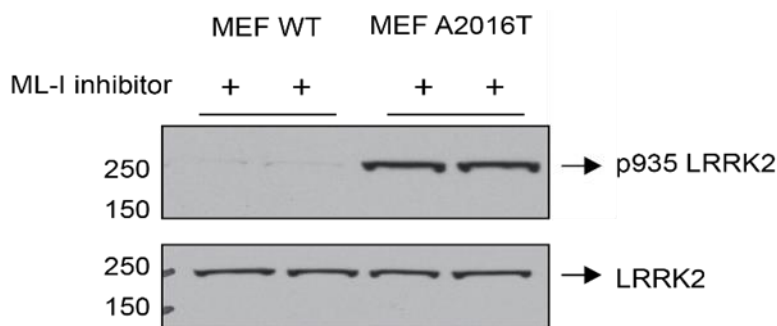
B**C**

Figure 4.9: Assessment of MYPT1 phosphorylation in MEF cells (A) Endogenous MYPT1 was immunoprecipitated from MEF LRRK2 WT and MEF LRRK2 [A2016T] drug resistant cells treated with DMSO or indicated LRRK2 inhibitor, and resolved on a SDS gel. (B) XIC for T500, T671 and T892 was generated based on the intensities in a control sample as well as in LRRK2 inhibitor (MLI-2) treated samples (t-test, T500 downregulated in MEF WT cell, $p < 0.05$; T671 downregulated in MEF WT cell, $p < 0.05$; T892 is unregulated in MEF WT cells ($p < 0.001$). (C) Cell lysates were subjected to immunoblotting analysis with total and phospho LRRK2 antibodies to show that LRRK2 kinase inhibitors worked.

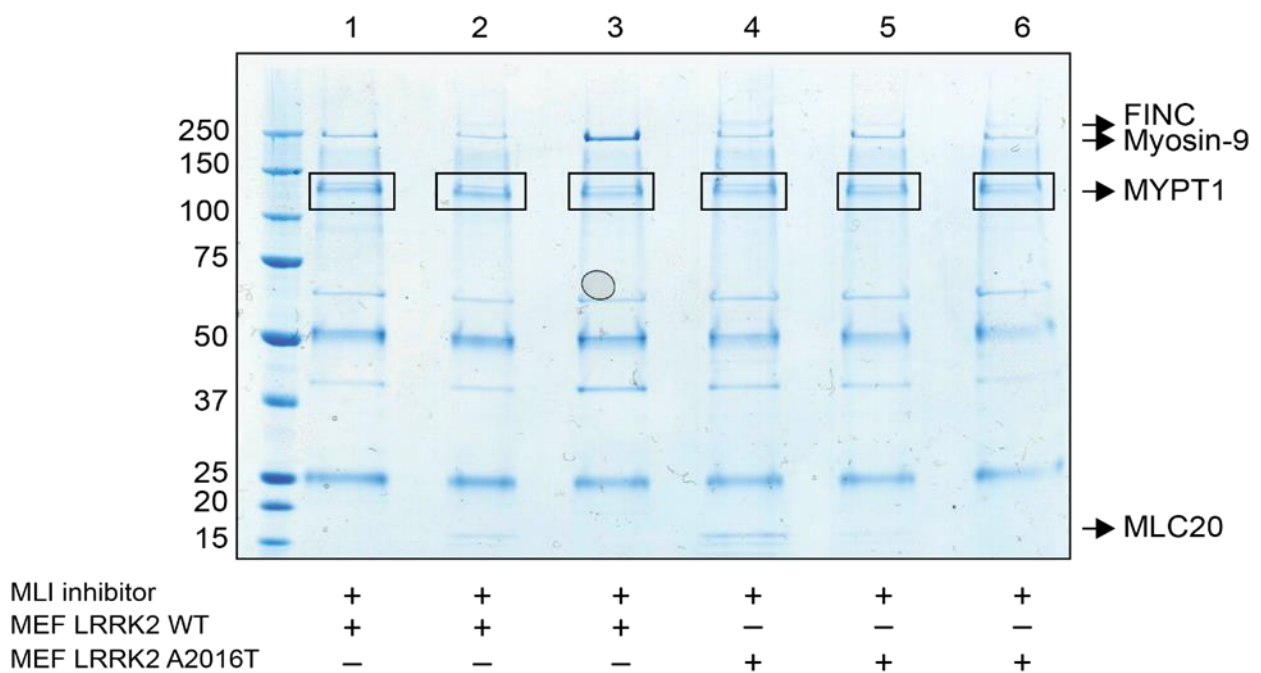
First of all, my results show that MYPT1 seem to be co-immunoprecipitated with PP1 and MLC20 proteins, suggesting that this time it is in its natural conformation. Interestingly, MLC20 was observed to co-immunoprecipitate with MYPT1 in LRRK2 [A2016T] drug resistant MEFs indicating that LRRK2 inhibition could have an effect on myosin phosphatase. Importantly, it can be seen that in MEF LRRK2 WT cells there is a dephosphorylation of S935, which is not present in a drug resistant LRRK2 [A2016T] MEF cells, indicating that the inhibition of endogenous LRRK2 in cells was successful. Finally, I have detected T500, T671 and T892 to be phosphorylated in cells in all samples. However, orbitrap analysis gave no evidence for other sites to be phosphorylated in cells. Moreover, extracted ion chromatograms (XICs) for Thr500 revealed that there is a significant decrease (around 20%) in T500 phosphorylation in MEF LRRK2 WT cells treated with LRRK2 inhibitor but not in a drug resistant MEF LRRK2 [A2016T] cells (t-test. $p < 0.05$). There was also a slight but significant decrease in T671 phosphorylation (t-test. $p < 0.05$) in MEF LRRK2 WT cells. Interestingly, T892 phosphorylation went up in response to LRRK2 inhibition suggesting that this site might be artificial or somehow regulated in a different manner within the cell (Figure 4.9.B).

Overall, my results show that T500 and T761 phosphorylation is reduced in response to LRRK2 inhibition in MEF LRRK2 WT but not in drug resistant cells. This suggests that LRRK2 could phosphorylate MYPT1 at T500 and T671 in cells. However, due to a minor reduction in phosphorylation at these sites, I cannot rule out that LRRK2 is not the only kinase, which phosphorylates these sites in cells so that phosphorylation by LRRK2 under these conditions that I have examined are not rate limiting.

To investigate whether I could enhance phosphorylation of T500 and T671 by adding Microcystin-LR into the lysis buffer I repeated this experiment supplementing my

lysis buffer with Microcystin-LR (Figure 4.10). Microcystins are a family of cyclic peptides that are potent inhibitors of the protein phosphatase families PP1 and PP2A (MacKintosh et al., 1990). We argued whether by adding a Microcystin-LR I could augment the phosphorylation of T500 and T671 by minimizing the activity of PP1 protein phosphatases dephosphorylating MYPT1 during cell lysis and immunoprecipitation. According to my results, addition of Microcystin-LR into the lysis buffer did not result into a dramatic increase in T671 and T500 phosphorylation (Figure 4.10)

A



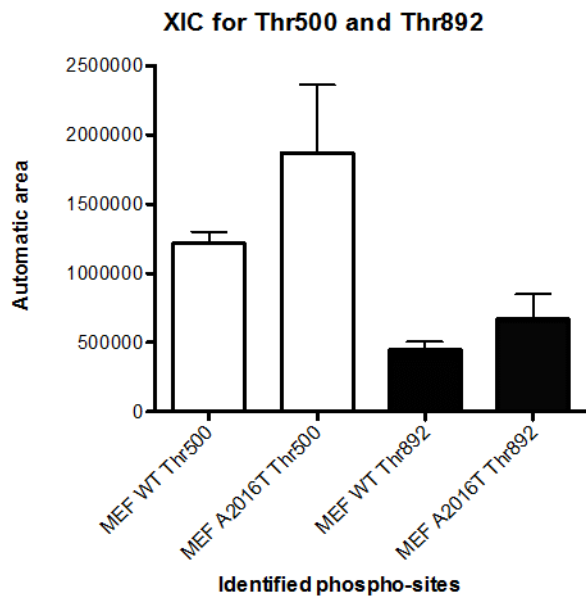
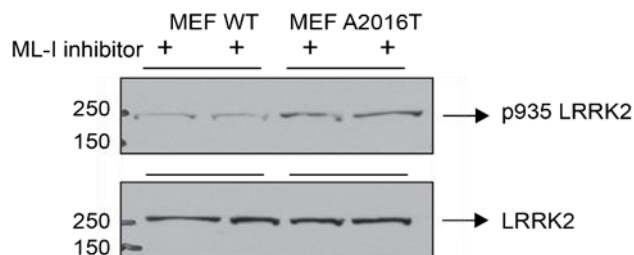
B**C**

Figure 4.10: Assessment of MYPT1 phosphorylation in MEF cells (A) Endogenous MYPT1 was immunoprecipitated from MEF LRRK2 WT and MEF LRRK2 [A2016T] drug resistant cells treated with DMSO or indicated LRRK2 inhibitor, and resolved on a SDS gel. (B) XIC for T500 and T892 was generated based on the intensities in a control sample as well as in LRRK2 inhibitor treated samples (t-test, T500 downregulated in MEF WT cell, $p > 0.05$; T892 is downregulated in MEF WT cells ($p > 0.05$)). (C) Cell lysates were subjected to immunoblotting analysis with total and phospho LRRK2 antibodies to show that LRRK2 kinase inhibitors worked.

In this experiment, Orbitrap analysis gave no evidence that T671, T761, T524 and T529 were phosphorylated in cells. XIC for T500 and T82 were generated based on the intensities and compared among different condition. My results revealed that phosphorylation of T500 in wild type MEFs treated with LRRK2 inhibitor was non-significantly reduced compared with the LRRK2 drug resistant mutant. In addition,

there was a slight reduction in T892 phosphorylation in wild type MEFs. Overall, this data suggests that LRRK2 inhibition did not have an effect on MYPT1 phosphorylation in these conditions. It could be that inhibition of myosin phosphatase by Microcystin-LR could have an effect on these results. It is possible that PP1 inhibition by Microcystin-LR could have resulted in dissociation of PP1: MYPT1: M20 complex leading to its incorrect folding and inability of LRRK2 kinase reach MYPT1 phosphorylation sites. This hypothesis is supported by the fact that according to a SDS gel, MYPT1 was not immunoprecipitated this time as PP1: MYPT1: M20 complex.

To sum up, my results indicate that inhibition of LRRK2 activity in cells results in a slight decrease of MYPT1 phosphorylation at T500 and T671 sites. It could be that LRRK2 is not the only kinase, which phosphorylates these sites in cells, in the conditions described in this thesis.

4.2.5 Validation of MYPT1 phospho-T500 antibody

As mass spectrometry data is only semi-quantitative and did not provide me with the clear evidence that LRRK2 phosphorylates MYPT1 *in vivo*, we generated phospho MYPT1 Thr500 polyclonal antibody (see Materials and Methods) to address this question. Four bleeds of MYPT1 T500 antibody were tested. For this purpose, HEK293 stably overexpressing GFP-tagged LRRK2 G2019S protein were transiently transfected with Flag-tagged MYPT1 WT or Flag-tagged MYPT1 [T500A] constructs, 24 hours after transfection HEK293 cells were induced with the doxycycline to allow LRRK2 protein expression and then 24 hours later were lysed and subjected to immunoprecipitation with indicated MYPT1 pT500 bleeds (Figure 4.11).

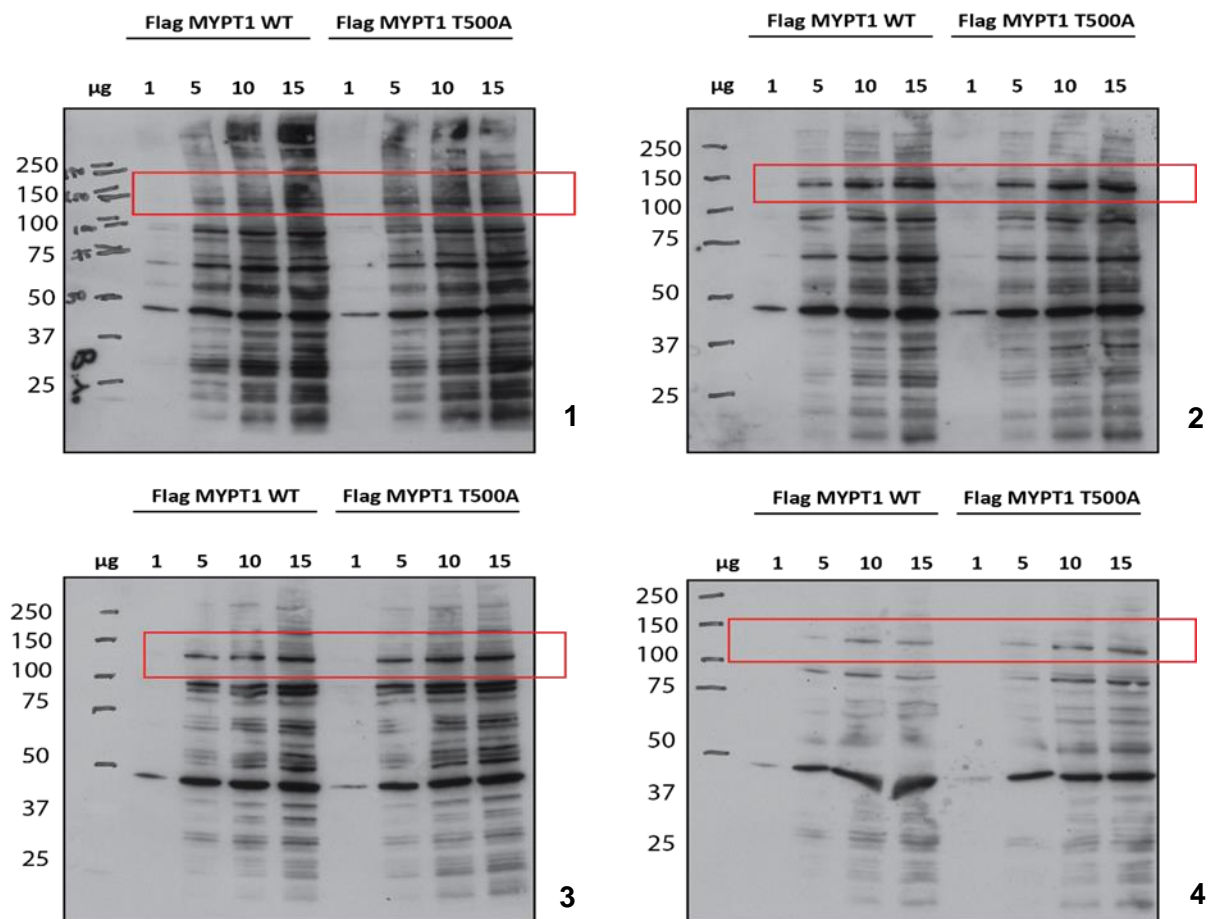


Figure 4.11: Validation of MYPT1 pT500 antibody HEK293 stably overexpressing GFP-tagged LRRK2 G2019S were transiently transfected with Flag-tagged MYPT1 WT or Flag-tagged MYPT1 [T500A] constructs. 48 hours after transfection cells were lysed and subjected to immunoblot analysis with indicated MYPT1 pT500 (1-4) bleeds.

As a result, MYPT1 pT500 antibodies were shown to be unable to specifically recognize MYPT1 pT500 in a total cell lysate. To test whether it is possibly to immunoprecipitate MYPT1 protein phosphorylated at T500 in HEK293 cells stably over-expressing LRRK2 G2019S. HEK293 stably overexpressing GFP-tagged LRRK2 G2019S protein were transiently transfected with Flag-tagged MYPT1 WT or Flag-tagged MYPT1 [T500A] constructs, 24 hours after transfection HEK293 cells were induced with the doxycycline to allow LRRK2 protein expression and then 24 hours later were lysed and subjected to immunoprecipitation with indicated MYPT1 pT500 antibodies (bleeds 1-4). Immunoprecipitates were then subjected to

immunoblot analysis with Flag antibody (Figure 4.12).

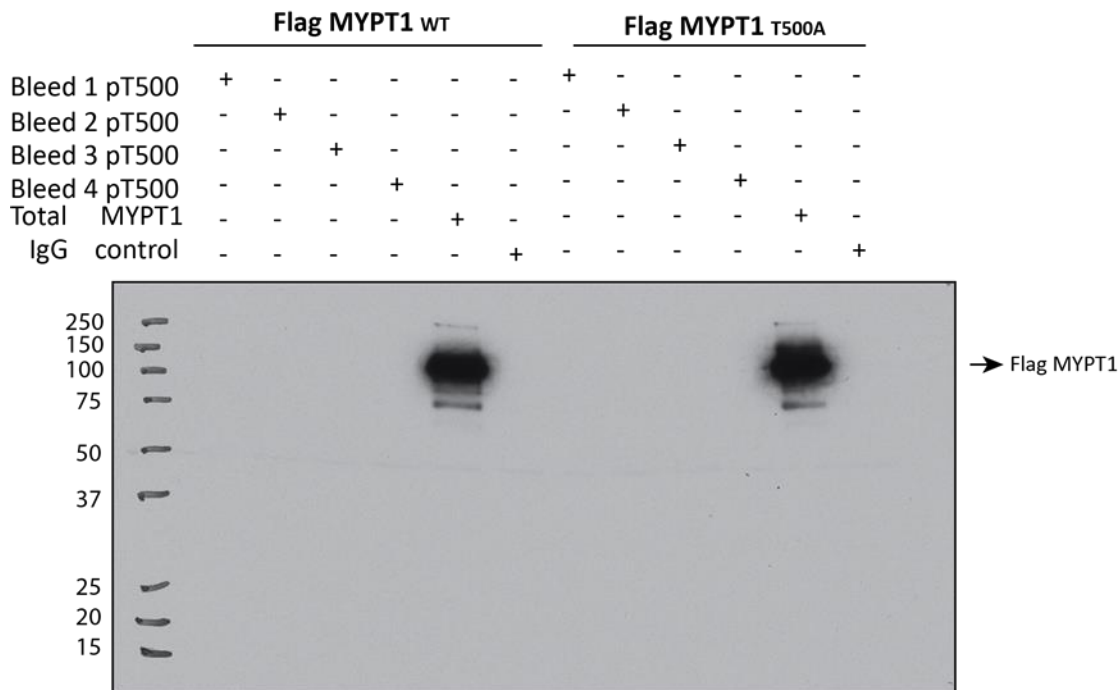


Figure 4.12: Validation of MYPT1 pT500 antibody HEK293 stably overexpressing GFP-tagged LRRK2 G2019S were transiently transfected with Flag-tagged MYPT1 WT or Flag-tagged MYPT1 [T500A] constructs. 48 hours after transfection cells were lysed and subjected to immunoprecipitation with indicated MYPT1 pT500 (1-4) bleeds. Immunoprecipitates were then analysed by immunoblot using Flag antibody.

Unfortunately, tested pT500 MYPT1 antibodies were unable to immunoprecipitated MYPT1 phosphorylated at T500 from HEK293 stably over-expressing LRRK2 G2019S.

As a result, no good polyclonal pT500 MYPT1 were found.

4.2.6 Evidence that endogenous LRRK2 does not interact with MYPT1 in MEF cells.

As described in the introduction, it has been reported that MYPT1 interacts with LRRK2 in mass spectrometry screen. To confirm this finding, endogenous LRRK2 was immunoprecipitated from MEF LRRK2 WT and MEF LRRK2 KO cells using N-

terminal monoclonal LRRK2 antibody. Immunoprecipitates were then subjected to immunoblot analysis by LRRK2 and MYPT1 total antibodies (Figure 4.13).

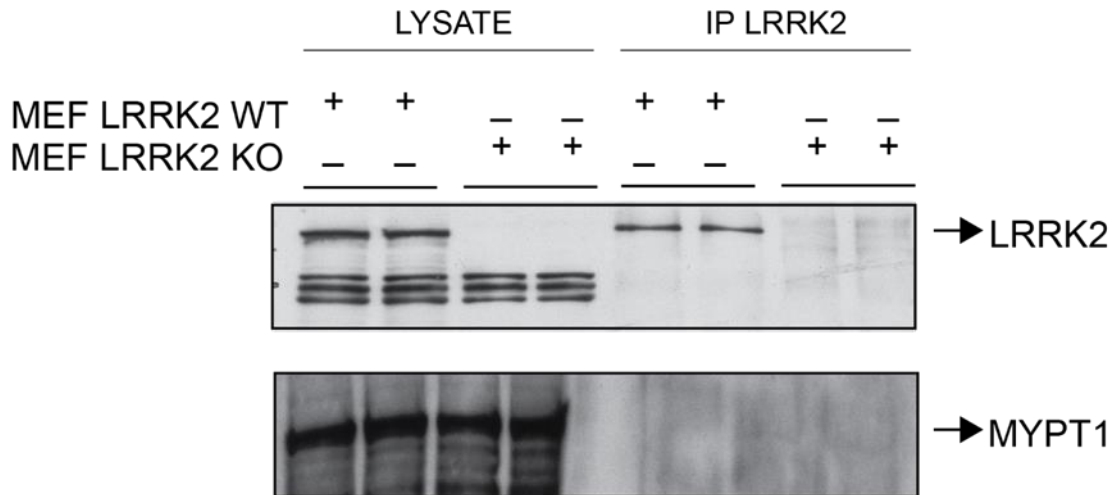


Figure 4.13: Co-immunoprecipitation of LRRK2 with MYPT1. Endogenous LRRK2 was immunoprecipitated with anti-LRRK2 (100-500) (UDD3) antibody from LRRK2 WT as well as from LRRK2 KO MEF cells. Immunoprecipitates were subjected to immunoblotting with anti-LRRK2 and anti-MYPT1 antibodies

According to my results there is no evidence that endogenous MYPT1 interacts with LRRK2 in MEF cells. I have repeated the co-immunoprecipitation several times but observed no binding between these proteins under these immunoprecipitation conditions. Interestingly, in my comparative mass spectrometry analysis I detected a very low amount of endogenous MYPT1 coming down with endogenous LRRK2 WT but not LRRK2 KO immunoprecipitated from MEF cells (Table 4.1).

Table 4.1: Comparative mass-spectrometry analysis of LRRK2 immunoprecipitates from LRRK2 WT, LRRK2 [S910A+S935A] and LRRK2 KO MEFs (Numbers correspond to the number of peptides found in the screen)

Identified Proteins	Abbreviation	kDa	WT	WT	WT	KI	KI	KI	KO	KO	KO
Leucine rich repeat kinase	LRRK2	285	54	51	46	33	31	36	0	0	0
Myosin phosphatase target subunit 1	MYPT1	115	4	2	0	1	0	0	0	0	0

However, mass spectrometry data is not very strong as only 4 and 2 MYPT1 peptides were found interacting with LRRK2 WT protein. Taking into consideration the size of MYPT is about 130 kDa, this data is a very bordering score significant. However, the interaction between the kinase and its substrate can be very transient and therefore it could be very difficult to detect kinase-substrate interaction by co-immunoprecipitation analysis.

4.2.7 Generation of MYPT1 KO cells.

4.2.7.1 Attempt to generate MYPT1 KO cells using TALENs.

To investigate whether MYPT1 plays a role in controlling the S910/S935 regulatory phosphorylation feedback loop I next decided to study how the deletion of MYPT1 protein in cells affects phosphorylation of S910 and S935.

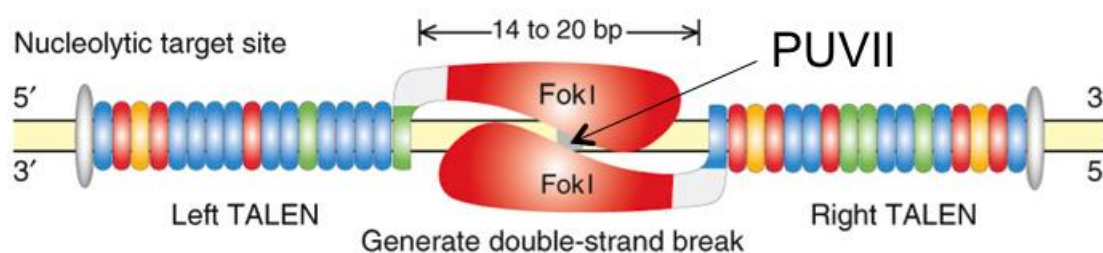
There are no MYPT1 KO cells available at the moment and it has been reported that deletion of MYPT1 in mice results in very early embryonic lethality with no embryos being detected even at embryonic day 7.5 (Okamoto et al., 2005)

I first decided to try and attempt to knockout MYPT1 in HEK293 cells using the transcription activator-like effector nucleases (TALENs). Transcription activator-like effectors (TALEs) are a class of naturally occurring DNA-binding proteins identified in the plant pathogen *Xanthomonas spp.* bacteria (Sanjana et al., 2012). It has been

reported that fusions of transcription activator-like (TAL) effectors of plant pathogenic *Xanthomonas spp.* to the FokI nuclease, TALENs bind and cleave DNA in pairs (Sanjana et al., 2012). In fact, TALENs are peptides made of a DNA binding domain (represented by multiple loop structure) and an endonuclease domain (represented by FokI). Therefore, customized TALENs have been adapted for a wide variety of genome engineering applications, including transcriptional modulation and genome editing. DNA binding domain binds to a specific DNA sequence as each loop is designed in such a way so that it recognizes a specific nucleotide. FokI endonuclease domain produces a double-stranded DNA break when forms a dimer. It was reported that 14-20 base pairs region is an optimum distance between two TALENs so that FokI can be dimerized (Sanjana et al., 2012).

With the help of Dr Piotr Szyniarowski I designed a pair of TALENs to target MYPT1 exon 1 (see Materials and Methods) using a hierarchical ligation procedure described by Sanjana et al., 2012. To facilitate the screening process we designed TALENs in the way that they specifically target MYPT1 exon 1 at the PuvII restriction enzyme site. Our idea was that when FokI produces a double strand break at the targeted exon 1 PuvII site (see Materials and Methods), non-homologous end joining repair (NHEJ) can result in deletion of several nucleotides in this region and this can cause a deletion of this site and also knockout of a desired gene. Digestion with PvuII of such clones will not be possible and they will appear in a gel as a single band. However, if TALENs cleavage did not take place, two bands on the gel will appear, suggesting that TALENs didn't work or NHEJ repaired the target region without causing a frame shift. Three bands on the gel will result if clone is heterozygous or it is a heterogeneous cell population and needs to be re-single cell cloned (Figure 4.2.9.1B).

A



B

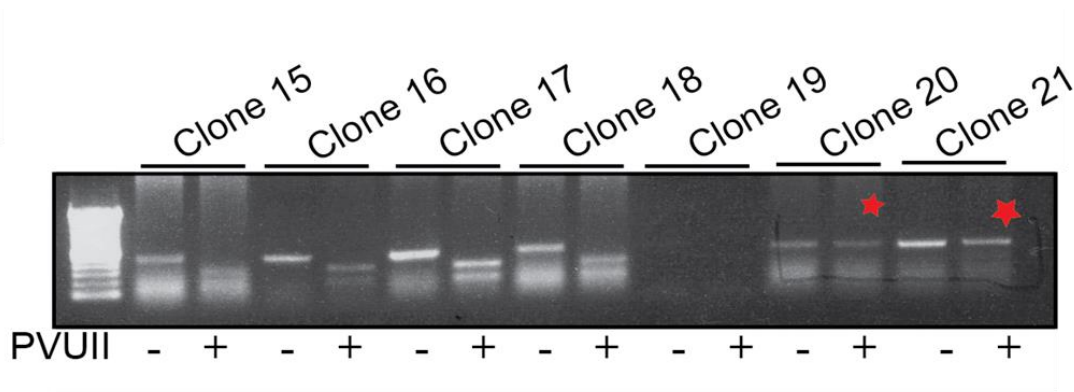
WT		KO		Heterozygous or mixed population	
PvuII		PvuII		PvuII	
+	-	+	-	+	-

Figure 4.14: A schematic representation of TALENs (A) A schematic representation of how TALENs work, a diagram adopted and modified from Sanjana et al., 2012. TALENs can be used to generate site-specific double-strand breaks to facilitate genome editing through non-homologous repair or homology directed repair. Two TALENs target a pair of binding sites flanking a 14-20 bp spacer comprising PvuII restriction site. The left and right TALENs recognize the top and bottom strands of the target sites, respectively. Each TALE DNA-binding domain is fused to the catalytic domain of FokI endonuclease; when FokI dimerizes, it cuts the DNA in the region between the left and right TALEN-binding sites. **(B)** A theoretical digest: a strategy that allows to screen for MYPT1 KO using PvuII restriction site.

Designed TALENs were used to transfect HEK293 cells. The pool of transfected cells was then single cell sorted into 96 well plates via FACS and allowed to grow for 2-3 weeks. Single clones were isolated and their genomic DNA was purified, amplified by PCR, and tested with PvuII restriction enzyme digestion (for more details see material and methods). Example of MYPT1 KO screening at this stage is represented in Figure 30 A. In this experiment, over 800 clones were tested. Clones, which were shown to be resistant to PvuII restriction enzyme cleavage, were

selected. The DNA of these clones was extracted and sequenced (see example Figure 30.B). However, the sequence analysis of the target region of the exon 1 showed that all of these clones possess a cleaved as well as non-cleaved version of this region. This indicated that all of these clones might be heterozygous or, alternatively they could consist of a mixture of clones comprising the wild type MYPT1 comprising cells as well as MYPT1 null cells. To exclude the last option these clones were re-single cell cloned again by FACS and tested by Western blotting analysis (Figure 30 C). After a massive screening analysis of different clones, I was unable to obtain homozygous knockout cell lines that might be because of MYPT1 deletion results in cell lethality. This conclusion is supported by several studies including (Yamashiro et al., 2008), which suggest that depletion of MYPT1 leads to mitotic arrest.

A



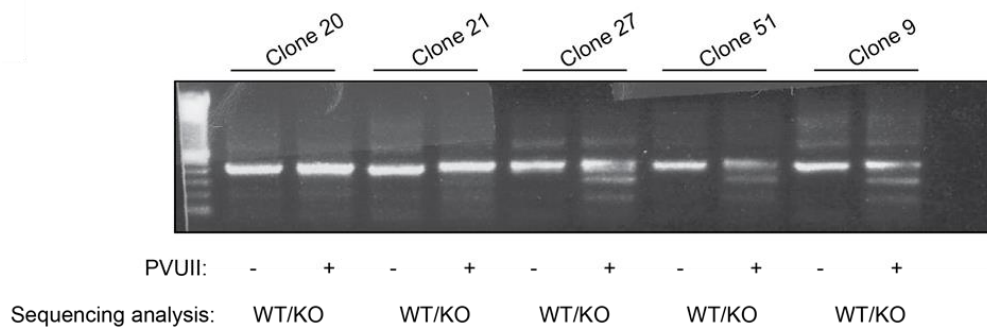
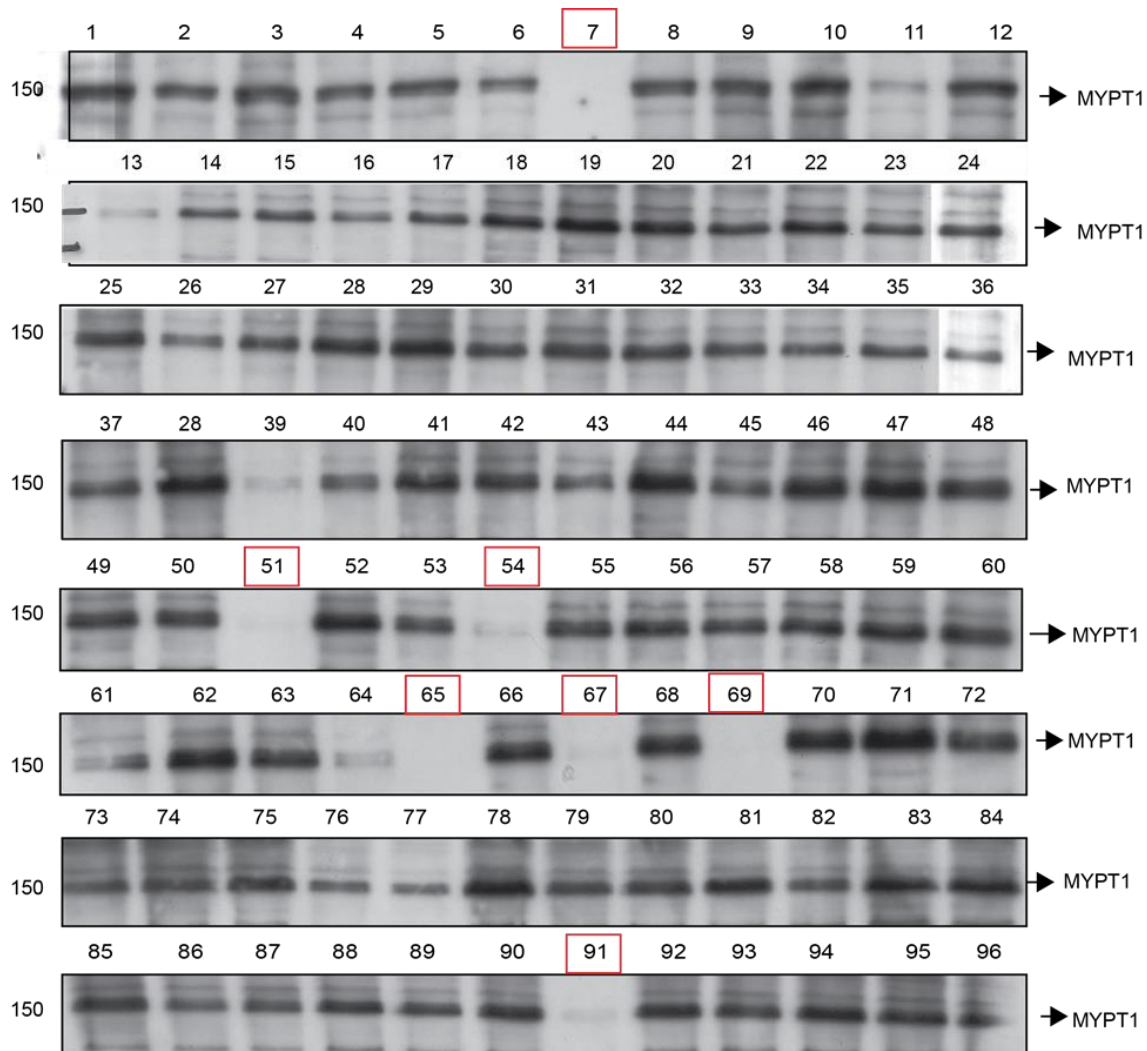
B**C**

Figure 4.15: Example of MYPT1 knockout screening: (A) HEK293 cells were transfected with TALENs and single cell cloned. Single cell clones were then selected and tested by PCR and PVUII digestion. From this screen, Clone 20 and Clone 21 appear to be resistant to PVUII digestion, suggesting that non-homologous end-joining repair of the targeted sequence by TALENs resulted in deletion of PVUII restriction site. (B) Example of some

PVUII cleavage resistant clones: Clones, which were shown to be resistant to PVUII cleavage, were selected. The DNA of these clones was extracted, inserted into TOPO vector and sequenced. However, the sequence analysis of the target region of the exon 1 showed that all of these clones possess a cleaved as well as non-cleaved version of the sequence. This indicated that all of these clones might be heterozygous or, alternatively they could consist of a mixture of clones comprising the wild type MYPT1 comprising cells as well as MYPT1 KO cells. (C) Western blotting analysis of Clone 21. Clone 21 was re-single cell cloned and further analyzed by Western blotting. Although 7, 51, 54, 65, 67, 69 and 91 show no protein, these wells contained no cells and they are highlighted in red.

4.2.7.2 Attempt to generate MYPT1 KO cells using Crispr/Cas9 technology.

After the last few years following my attempt of the TALENs approach to knock-out MYPT1, the RNA-guided CRISPR-Cas nuclease system has been developed and many labs have successfully adopted this technology for gene editing (Rojas-Fernandez et al., 2015). The advantage of this technology is that it is relatively easy to manipulate, highly specific, efficient and fairly fast for genome engineering in distinct cell lines. CRISPR-Cas was initially identified in a microbial adaptive immune system that uses RNA-guided nucleases to cleave foreign genetic material (Marraffini & Sontheimer, 2010). Later, the best characterized type II Crispr system, which consists of the endonuclease Cas9, the crRNA array that encodes the guide RNAs and a supplementary trans-activating crRNA (tracrRNA) that helps the processing of the crRNA array, became widely implemented for customized gene editing. The basic principle behind this technique is that each crRNA contains a 20 nucleotide guide sequence, which directs Cas9 to a 20 nucleotide DNA target via Watson-Crick base pairing (Ran, Hsu et al. 2013). However, further research showed that for more successful binding of Cas9, the genomic target sequence must also contain the correct Protospacer Adjacent Motif (PAM) sequence immediately following the target sequence. The binding of the gRNA/Cas9 complex localizes Cas9 to the genomic target sequence so that the wild-type Cas9 can cut both strands of DNA causing a double strand break (DSB). Cas9 consists of two

functional domains including RuvC and HNH, each cutting a different DNA strand. When both of these domains are active, the Cas9 causes DSBs in the genomic DNA, which can be repaired by either Non-Homologous End Joining (NHEJ) or Homology Directed Repair (HDR) (similar to TALENs). However, the Cas9 enzyme can be modified to possess a single inactive catalytic domain, known as a nickase. The Cas9 nickase is still able to bind DNA based on gRNA specificity (Rojas-Fernandez et al., 2015). The majority of CRISPR plasmids currently used are derived from *S. pyogenes* and the RuvC domain can be inactivated by a D10A mutation while the HNH domain can be inactivated by an H840A mutation (Jinek, Chylinski et al. 2012). Although a single-strand break can be quickly repaired through the HDR pathway, using the intact complementary DNA strand as a template (if one wishes to make a knock-in mutation), two proximal, opposite strand nicks introduced by a Cas9 nickase are treated as a DSB. A double-nick induced DSB can be repaired by either NHEJ or HDR.

For generation of HEK293 MYPT1 KO cells I used the Crispr/Cas9 approach which utilized a Cas9 nickase rather Cas9 wild type and possesses two plasmids: one antisense guide cloned into the Cas9 D10A vector pX335 and a sense guide cloned into pBABED puro U6.

Table 4.2: CRISPR/Cas9 construction details (All constructs generated by Thomas McCartney, DSTT, University of Dundee)

<i>Materials</i>	<i>Function</i>	<i>Sequence</i>
Guide RNA/Cas9 D10A complex	3) Each guide RNA contains a 20 nucleotide guide sequence, which directs Cas9 D10A nickase to a 20 nucleotide DNA target via Watson-Crick base pairing. 4) Cas9 creates a double-nick induced DSB that can be repaired by either NHEJ or HDR	Targeting MYPT1 exon3: <u>Antisense RNA guide:</u> GTCCTCCTCCGCAATATCTAA cloned into the Cas9 D10A vector pX335 <u>Sense RNA guide:</u> GCAAAATGAAGTTAATCGGCA cloned into pBABED puro U6
Guide protected MYPT1 sequences	Previous studies strongly indicated that MYPT1 KO is lethal. Guide protected MYPT1 sequences allow to rescue this phenotype.	Sequence 1 : pcDNA5D FRT/TO GFP MYP1 guide protected Sequence 2:

		pcDNA5D FRT/TO GFP MYP1 T500 guide protected Sequence3: pcDNA5D FRT/TO GFP MYP1 T500/T524/T529/T671/T761/T892A guide protected
--	--	--

As my previous work strongly indicated that deletion of MYPT1 could be lethal for cells. I firstly generated HEK293 cells over-expressing GFP tagged MYPT1 WT and GFP-tagged MYPT1 mutant proteins. We designed these proteins to be resistant to antisense and sense guides created to target endogenous MYPT1 with the aim to delete endogenous MYPT1. This approach would enable to keep cells alive by over-expressing the GFP-tagged protein in case MYPT1 deletion causes cell death.

Following transient transfection of HEK293 cells stably overexpressing GFP-tagged MYPT1 with Crispr/Cas9 D10A antisense and sense guides and selection of cells with puromycin, I have noticed that only cells containing puromycin and doxycycline survived the selection. This suggested that cells lacking MYPT1 are lethal and that MYPT1 is critical for cell survival. Therefore, for further experiments I kept doxycycline in the media to ensure GFP-tagged MYPT1 expression, which is essential for cell survival. The pool of transfected cells selected with puromycin and doxycycline was then single cell sorted into 96 well plates via FACS and allowed to grow for 2-3 weeks. Single cell clones were analyzed by western blotting (Figure 4.16).

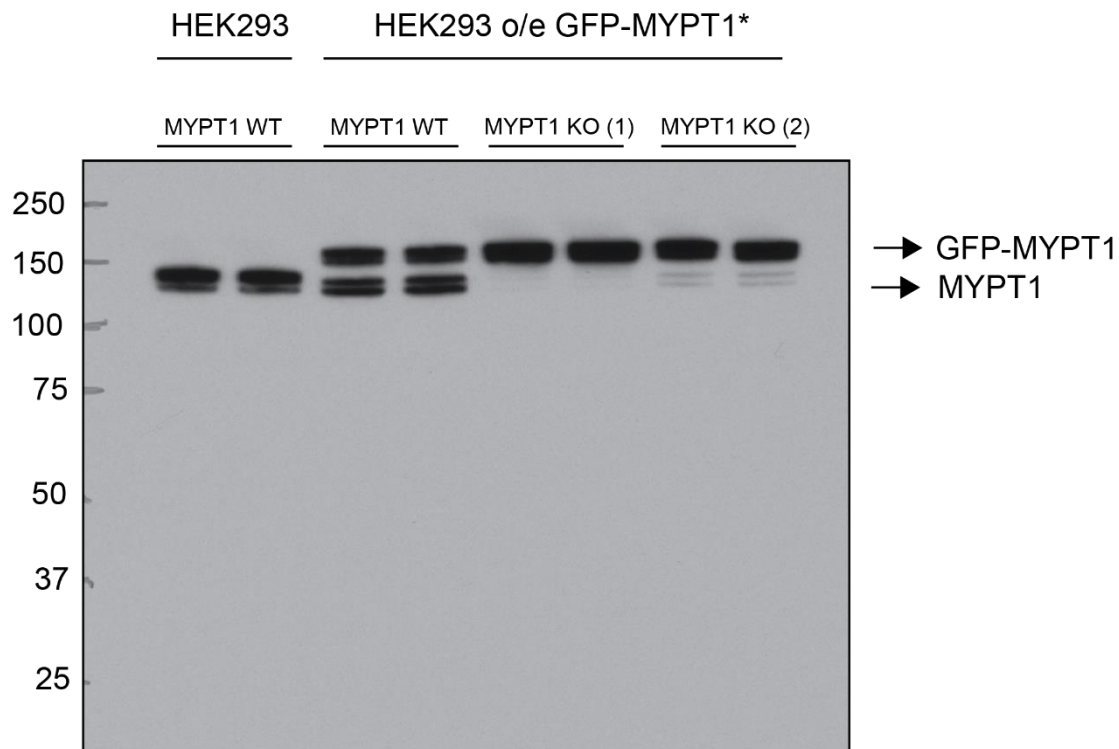


Figure 4.16: Generation of MYPT1 null cell lines using Crispr/Cas9 technology. Following transfection and selection of HEK293 cells, lysates of HEK293 WT cells, HEK293 cells over-expressing MYPT1 and generated clones were subjected to immunoblot analysis with MYPT1 antibody.

I have been able to generate MYPT1 null cells over-expressing GFP-tagged MYPT1 [T500A+T524A+T529A+T671A+T761A+T892A] protein. Unfortunately, MYPT1 null cells did not look very healthily as they didn't attach well to the plate and never recovered after being split into bigger plate. This might be due to the fact that long GFP tag could interfere with MYPT1 being folded properly with PP1 and M20 subunit. In addition, these cells were kept under constant doxycycline, puromycin and blasticidin treatment to ensure constant GFP-MYPT1 expression and these might have added some difficulty for MYPT1 null cells to survive. Unfortunately, I run out of time in my PhD to repeat these experiments.

4.3 Summary

I found that MYPT1 is efficiently phosphorylated by LRRK2 *in vitro* at T500, T524, T529, T671 T761 and T892. There are likely to be more minor LRRK2 phosphorylation sites *in vitro* as mutation of all identified sites to alanine, although greatly suppressed LRRK2 phosphorylation, did not abolish it. After unsuccessful attempts to map additional sites I decided to focus on whether phosphorylation of already identified MYPT1 sites is impaired by inhibition of LRRK2 kinase activity in cells. I observed that in over-expressed cells, T500 and T671 are seen to be phosphorylated and that inhibition of LRRK2 kinase activity results in a slight decrease in phosphorylation at these sites. No other sites were seen phosphorylated in cells. To exclude that in over-expressed system MYPT1 folding is disrupted and this affected my results, I tested phosphorylation of endogenous MYPT1 in MEFs. My data again showed that there is no significant change at T500 or T671 phosphorylation because of LRRK2 inhibition, indicating that LRRK2 might not be a rate-limiting kinase that phosphorylates MYPT1 in cells. Moreover, in cells and immunoprecipitation conditions I used, I found no evidence for MYPT1 to interact with LRRK2. Although my data indicates that MYPT1 is not a physiological LRRK2 substrate. It would be important to assess MYPT1 phosphorylation at identified LRRK2 sites in cell lines other than HEK239 and MEFs and how this is affected by LRRK2 inhibitors.

To address whether myosin phosphatase could act on S910 and S935 LRRK2 sites, I attempted to generate MYPT1 KO cells with the aim to treat them with LRRK2 kinase inhibitor and determine whether this will affect phosphorylation of S910 and S935. In spite of a huge effort I could not generate MYPT1 null cells, indicating that these cells are lethal. However, I managed to create MYPT1 conditional knock-out

cells overexpressing GFP-MYPT1 mutant. Unfortunately, these cells did not live long due to their unhealthy conditions and I could not test the impact of MYPT1 on LRRK2 S910 and S935 phosphorylation.

Chapter 5:

Validation of Mass

Spectrometry Hits

5.1 Introduction

To date only Rab GTPases, including Rab8A, Rab10 and Rab12 were reported and validated by the stringent criteria used within our lab (Figure 1.3) to be direct physiological LRRK2 substrates. However, multiple other proteins such as actin-cytoskeleton-regulated (ERM) proteins (Jaleel et al., 2007; Parisiadou et al., 2009), cellular tumour antigen p53 (Ho et al., 2015), mitogen-activated kinase kinase 3, 4, 6, and 7 (Gloeckner, Schumacher, Boldt, & Ueffing, 2009), microtubule stabilizing tau protein (Bailey et al., 2013), SNARE-associated protein Snapin (Yun et al., 2013), eukaryotic initiation factor 4E-binding protein 1 (4E-BP1) (Imai et al., 2008), Ras-related protein (Rab5b) at non effector site T6 (Yun et al., 2015), 40S ribosomal subunit protein S15 (RPS15) (Martin et al., 2014), Protein kinase B (PKB) (Ohta, Kawakami, Kubo, & Obata, 2011), N-ethylmaleimide-sensitive fusion protein (NSF) (Belluzzi et al., 2016) were reported to be also phosphorylated by LRRK2 in cells. All these reports provided a novel and potential perspective of LRRK2 function within the cell and its potential link to Parkinson's disease. For instance, it was described that LRRK2 phosphorylated NSF protein at threonine 645, a hexameric AAA+ ATPase. Giving that G2019S LRRK2 mutant evidently increased this phosphorylation resulting in an increased ATPase activity and augmented rate of SNARE complex disassembling, it was suggested that mutant LRRK2 might disturb synaptic vesicle dynamics via aberrant phosphorylation of NSF (Belluzzi et al., 2016). Another example of reported LRRK2 substrate is PKB, which was shown to be phosphorylated at S473. Once activated, PKB was suggested to negatively regulate a number of apoptosis-associated molecules such as Bad and caspase 9 as well as induce several signal transduction cascades for cell survival such as GSK-3b and ASK-1 (Ohta et al., 2011). Mutant LRRK2 was reported to significantly decrease

PKB phosphorylation and therefore it is resistance to apoptosis. Based on this, it was suggested that the cell-protective ability of LRRK2 is exerted through phosphorylation and activation of PKB (Ohta et al., 2011).

However, many of these sites have not been properly validated and shown that endogenous protein is indeed phosphorylated by LRRK2, and that phosphorylation of endogenous protein is abolished by treatment with LRRK2 kinase inhibitors. Unless this data is obtained doubts must be cast on the validity of these conclusions.

In this chapter, I am reporting the work I undertook to attempt to validate RPS15 as a LRRK2 physiological substrate. In addition, I report my data from a comparative mass-spectrometry analysis to compare interacting partners derived from LRRK2 immunoprecipitates from LRRK2 WT, LRRK2 [S910A+S935A] and LRRK2 KO mouse embryonic fibroblasts. In particular, I investigate whether Paralemmin (PALM) protein, identified in my analysis, could be a potential LRRK2 substrate or interactor.

5.2 Results

5.2.1 Studies undertaken to attempt to validate RPS15 protein as LRRK2 substrate

Dawson's laboratory reported that ribosomal protein s15 (RPS15) is a crucial pathogenic LRRK2 substrate in *Drosophila* and human neuron PD models (Martin et al., 2014). According to their results, phospho-deficient RPS15 possessing a threonine 136 to alanine substitution rescues dopamine neuron degeneration in G2019S LRRK2 transgenic *Drosophila* and significantly blocks G2019S LRRK2-mediated neurite loss and cell death in human dopamine and cortical neurons (Martin et al., 2014). In addition, it was reported that pathogenic G2019S LRRK2 stimulates mRNA translation and induces a massive increase in protein synthesis in *Drosophila*, which can be prevented by phospho-deficient T136A RPS15 (Martin et

al., 2014). These results suggested a novel mechanism of PD pathogenesis linked to elevated LRRK2 kinase activity and aberrant protein synthesis *in vivo*. Before investigating this hypothesis further I decided first to attempt to confirm the reported results.

To confirm whether RPS15 is phosphorylated by LRRK2 *in vitro*, recombinant GST-tagged LRRK2 [1326-end] (G2019S) was HEK293 purified and incubated in presence of recombinant GST-tagged RPS15 bacterially purified protein and Mg²⁺-[γ -³²ATP] for indicated amount of time at 30°C at 1000 rpm in presence or absence of 1 μ M LRRK2 GSK2578215A kinase inhibitor (Figure 5.1). My results confirmed that RPS15 is efficiently phosphorylated by LRRK2 in a time-dependent manner and that the treatment with LRRK2 kinase inhibitor blocks RPS15 phosphorylation. The stoichiometry of phosphorylation was estimated to be 22% of the protein was phosphorylated.

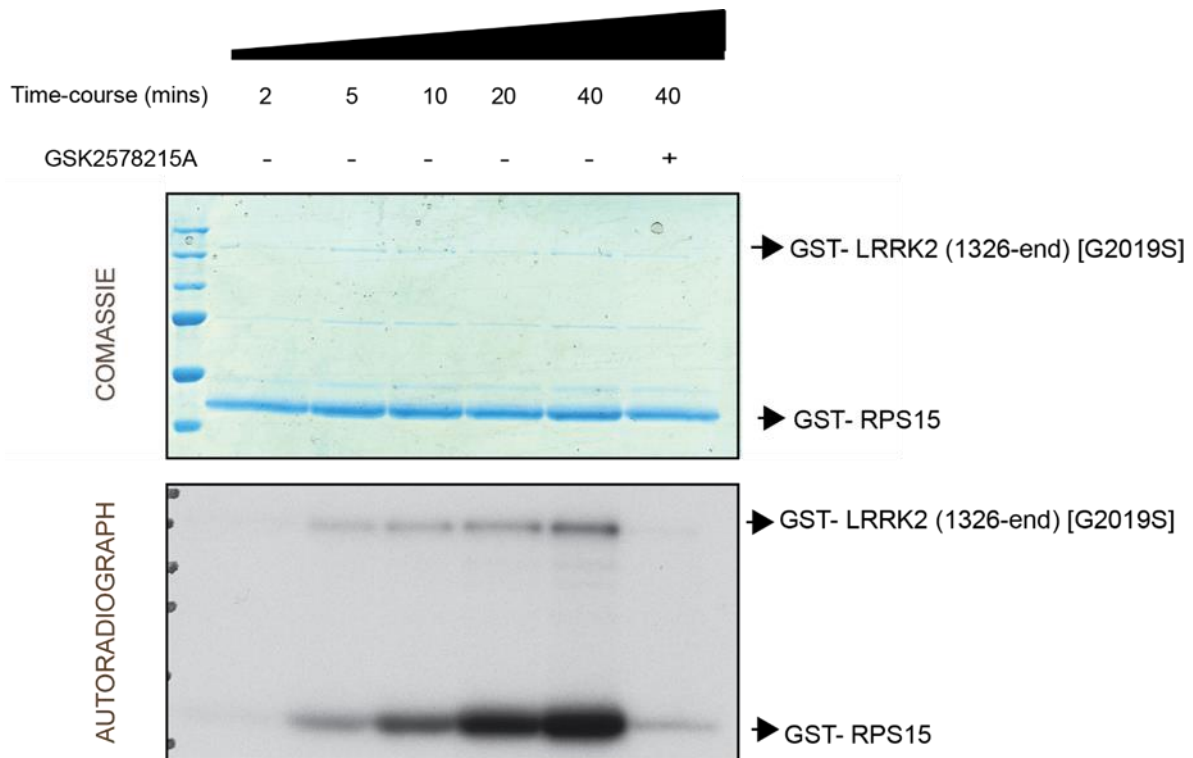
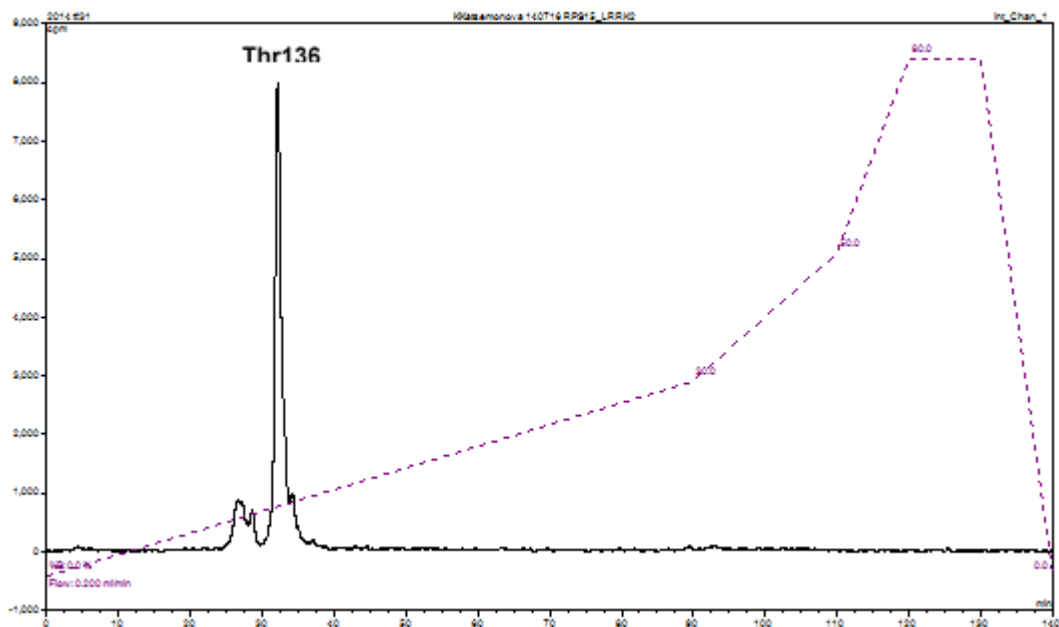


Figure 5.1: RPS15 is phosphorylated by LRRK2 *in vitro*: GST-tagged LRRK2 [1326-end] [G2019S] was HEK293-purified. Purified LRRK2 protein was then incubated with recombinant GST-tagged RPS15 protein and Mg²⁺-[γ -³²ATP] for the indicated times in

presence or absence of 1 μM LRRK2 specific kinase inhibitor (GSK2578215A) at 30°C at 1000 rpm. Samples were then subjected to electrophoresis on a polyacrylamide gel and autoradiography.

To map the phosphorylation site, [^{32}P] RPS15 protein was phosphorylated by Hek293-purified LRRK2 [G2019S] for 40 mins at 30°C at 1000 rpm and digested with the endoproteinase Trypsin. Digests were then analyzed by chromatography on a C18 column. One major ^{32}P labelled phospho-peptide was observed in the HPLC sample (Figure 5.2.A). Solid-phase Edman sequencing and mass spectrometry identified phosphorylation site as T136 (Figure 5.2.B). My results showed that RPS15 is phosphorylated by LRRK2 at T136 in accordance with the previously reported data. Moreover, mutation of T136 to alanine largely blocked LRRK2 phosphorylation (Figure 5.2.C).

A



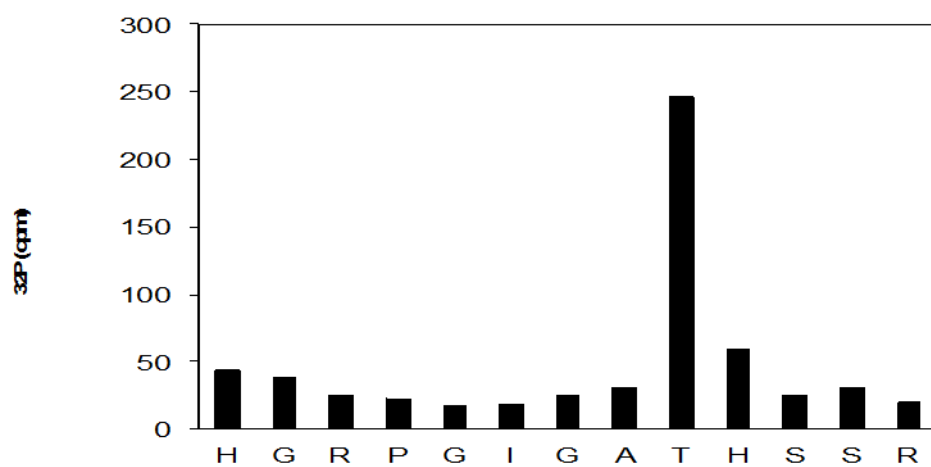
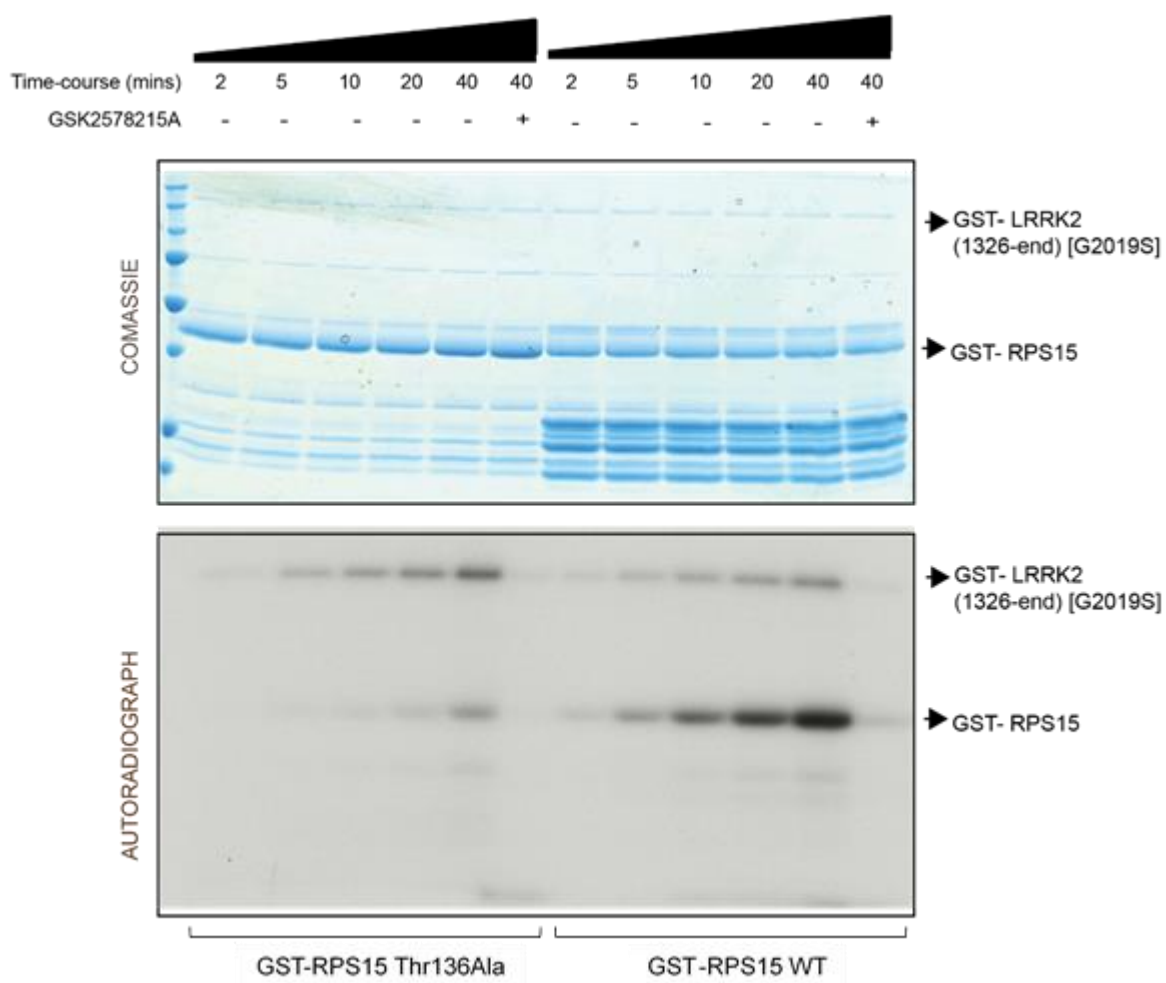
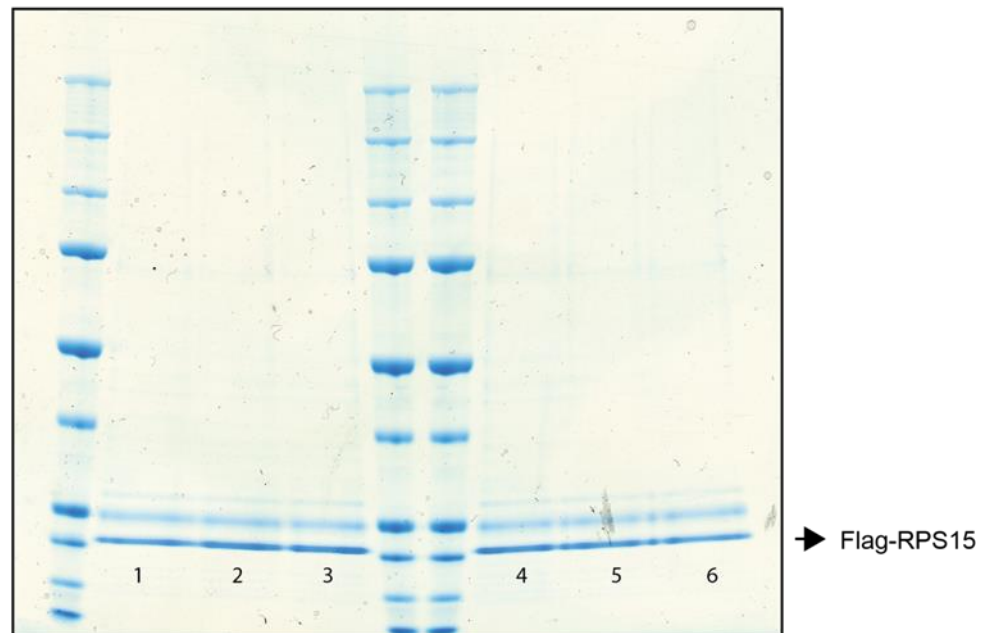
B**C**

Figure 5.2: Mapping of RPS15 phosphorylation site (A) Recombinant GST-RPS15 protein was incubated with LRRK2 (1326-end) [G2019S] in the presence of Mg^{2+} - $[\gamma\text{-}^{32}\text{P}]$ ATP for 40 min at 30°C at 1000 rpm. Phosphorylated RPS15 was digested with Trypsin and peptides were separated by reversed phase high performance liquid chromatography on a C18 column. The peak containing the ^{32}P -labeled phosphopeptide is labelled with the identified phosphorylated residue. **(B)** Summary of the mass spectrometry and solid-phase Edman sequencing data obtained after analysis of the peak fraction. The deduced amino acid sequence of each peptide is shown and the phosphorylated residue is indicated (in bold). **(C)** Purified LRRK2 protein was incubated with recombinant GST-tagged RPS15 WT or GST-tagged RPS15 T136A proteins and Mg^{2+} - $[\gamma\text{-}^{32}\text{P}]$ ATP for the indicated times in presence or absence of 1 μM LRRK2 specific kinase inhibitor (GSK2578215A). Samples were then subjected to electrophoresis on a polyacrylamide gel and autoradiography.

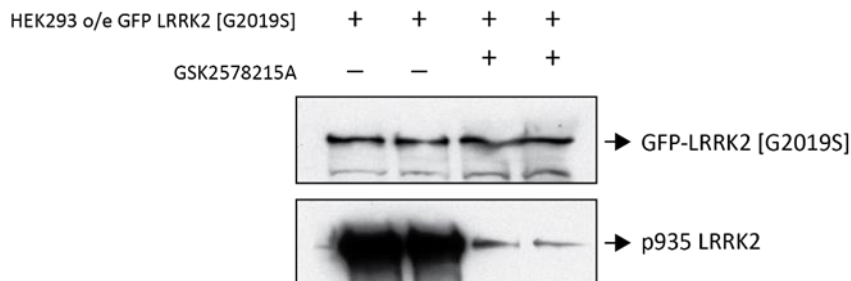
My data, consistent with the previously reported results, indicates that LRRK2 efficiently phosphorylates RPS15 *in vitro* at T136 and mutation of this site to alanine evidently blocks this phosphorylation. To test whether LRRK2 phosphorylates RPS15 in cells, HEK293 cells stably over-expressing GFP-tagged LRRK2 [G2019S] were transfected with Flag-tagged RPS15 and treated with DMSO or 8 μM GSK2578215A LRRK2 kinase inhibitor to determine whether inhibition of LRRK2 kinase activity leads to RPS15 dephosphorylation at T136 (Figure 5.3).

A

GFP-LRRK2 [G2019S]	+	+	+	+	+	+
GSK2578215A (8 μ M)	-	-	-	+	+	+



B



C

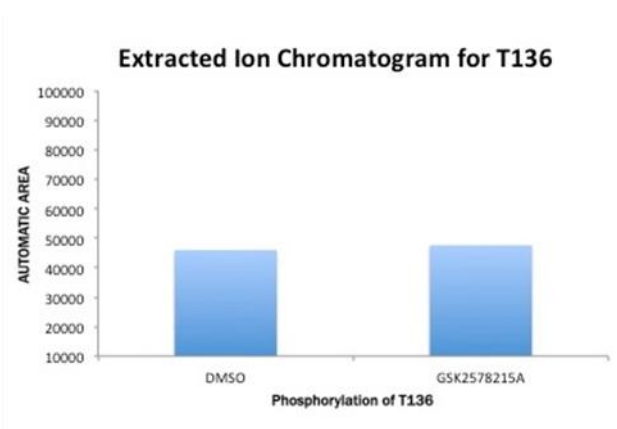
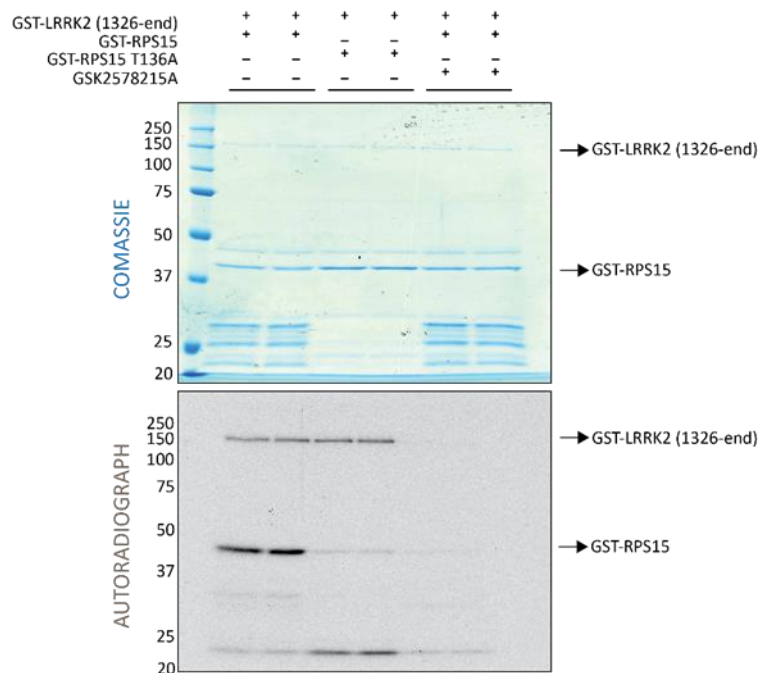


Figure 5.3: RPS15 phosphorylation in cells (A) Transiently over-expressed Flag-tagged RPS15 was immunoprecipitated from HEK293 T-REx cells stably overexpressing GFP-tagged G2019S LRRK2 treated with DMSO or 8 μ M of indicated LRRK2 inhibitor. Immunoprecipitates were then resolved on a SDS gel and stained with coomassie. (B) Cell lysates were subjected to immunoblot analysis with total and phospho LRRK2 antibody to confirm that inhibitor worked. (C) Gel bands corresponding to RPS15 were extracted from the gel and subjected to Orbitrap Velos analysis. XIC for T136 generated based on the intensities in a control sample as well as in LRRK2 inhibitor treated samples.

According to this data, there are no obvious changes in RPS15 phosphorylation due to LRRK2 inhibition in cells. To summarise, LRRK2 phosphorylates robustly RPS15 at T136 *in vitro* but not in over-expressed system in HEK293 cells.

To address whether endogenous LRRK2 phosphorylates RPS15 in cells. I tested DSTT generated (see Materials and Methods) polyclonal phospho T136 RPS15 and total RPS15 antibodies. For this purpose, first of all, HEK293-purified LRRK2 (1326-end) [G2019S] was incubated with the recombinant GST-tagged RPS15 WT or GST-RPS15 T136A proteins in the presence of Mg^{2+} -[γ - ^{32}ATP] and 1 μ M of LRRK2 specific kinase inhibitor as a negative control for 30 mins at 30°C at 1000 rpm. Samples were then subjected to electrophoresis on a polyacrylamide gel and autoradiograph to confirm that the reaction worked (Figure 5.4.A). Subsequently, samples were subjected to immunoblot analysis with different bleeds of RPS15 antibodies to test them (Figure 5.4.B). According to my results, only Bleed 2 of phospho T136 RPS15 antibody specifically recognized phosphorylated T136 residue on bacterially purified GST-tagged RPS15 protein phosphorylated *in vitro* by LRRK2.

A



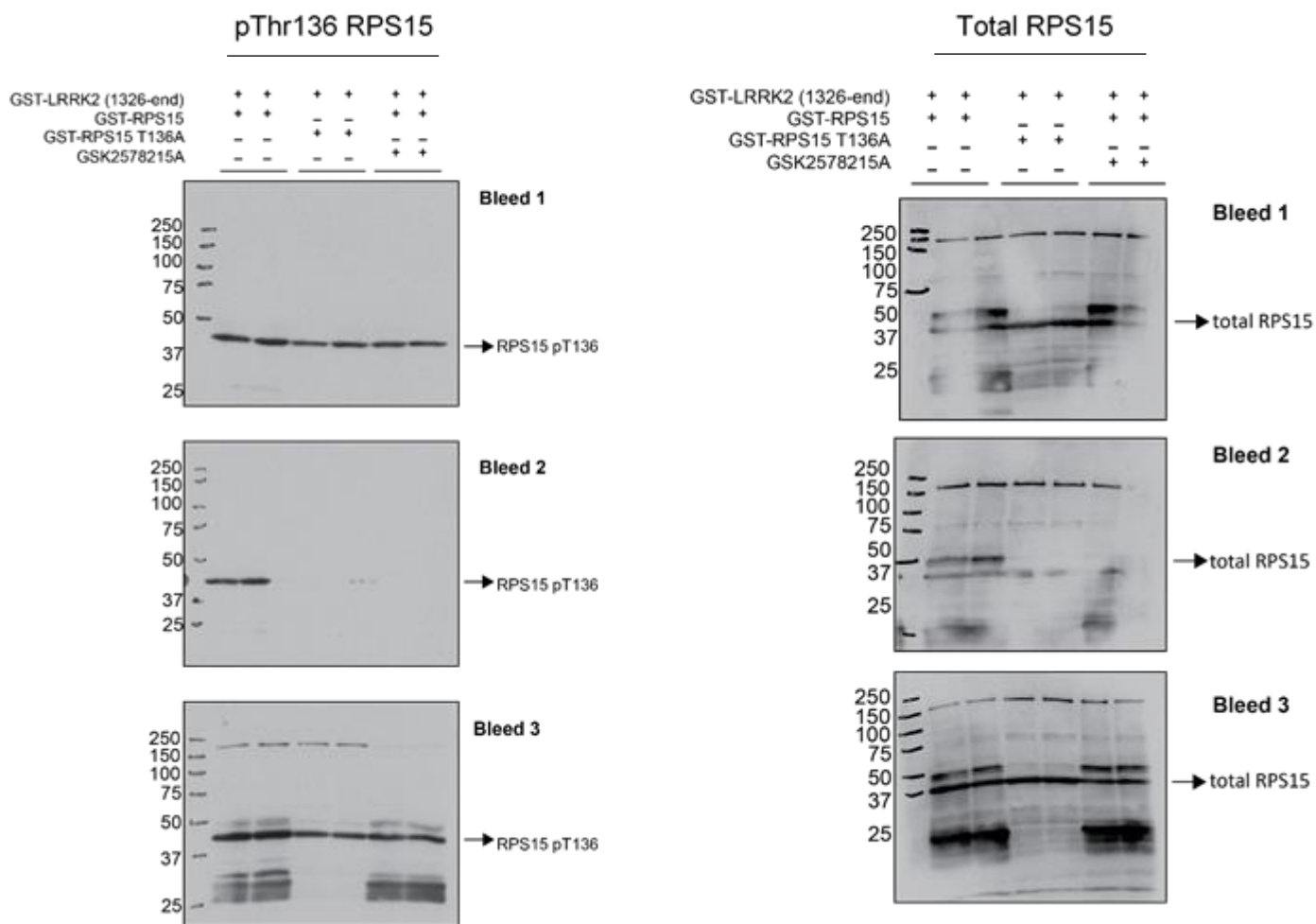
B

Figure 5.4: Assessment of pT136 and total RPS15 antibody on purified RPS15 protein phosphorylated by LRRK2 in vitro. (A) HEK293-purified LRRK2 (1326-end) [G2019S] was incubated with the recombinant GST-tagged RPS15 WT or GST-RPS15 T136A proteins in the presence of Mg^{2+} - $[\gamma\text{-}^{32}\text{ATP}]$ and $1\ \mu\text{M}$ LRRK2 specific kinase inhibitor as a negative control. Samples were then subjected to electrophoresis on a polyacrylamide gel and autoradiograph. (B) Samples were also subjected to immunoblot analysis with different bleeds of indicated pT136 and total RPS15 antibodies.

To test further RPS15 antibody in over-expressed cells, transiently transfected FLAG-tagged RPS15 WT or T136A proteins were immunoprecipitated from HEK293 stably over-expressing GFP-tagged LRRK2 [G2019S] treated with DMSO or $1\ \mu\text{M}$ GSK2578215A LRRK2 kinase inhibitor. The immunoprecipitates as well as cell lysates were resolved on a SDS gel and analysed by distinct bleeds of indicated total RPS15 antibodies (Figure 5.5). My results showed that first of all, the transient transfection of RPS15 protein was successful as Flag antibody detected a good

amount of Flag-tagged RPS15 in the total cell lysate as well as immunoprecipitates. Secondly, I found no total RPS15 antibodies able to specifically recognize RPS15 protein in the total cell lysate. However, all total RPS15 antibody bleeds are capable of specifically recognizing RPS15 protein immunoprecipitated from cells with FLAG antibody. In parallel, pT136 RPS15 antibodies were tested (Figure 5.6). As a result, I found no pT136 RPS15 bleed capable of specifically recognizing phosphorylated RPS15 protein neither in the total cell lysate or immunoprecipitated with FLAG antibody from HEK393 cells stably over-expressing LRRK2 G2019S. Subsequently, I could not test if endogenous RPS15 is phosphorylated by LRRK2 in cells. Matthias Mann's laboratory also detected RPS15 to be phosphorylated in MEF cells at T136 in their mass spectrometry screen, however this phosphorylation was not shown to be affected by LRRK2 kinase inhibitors.

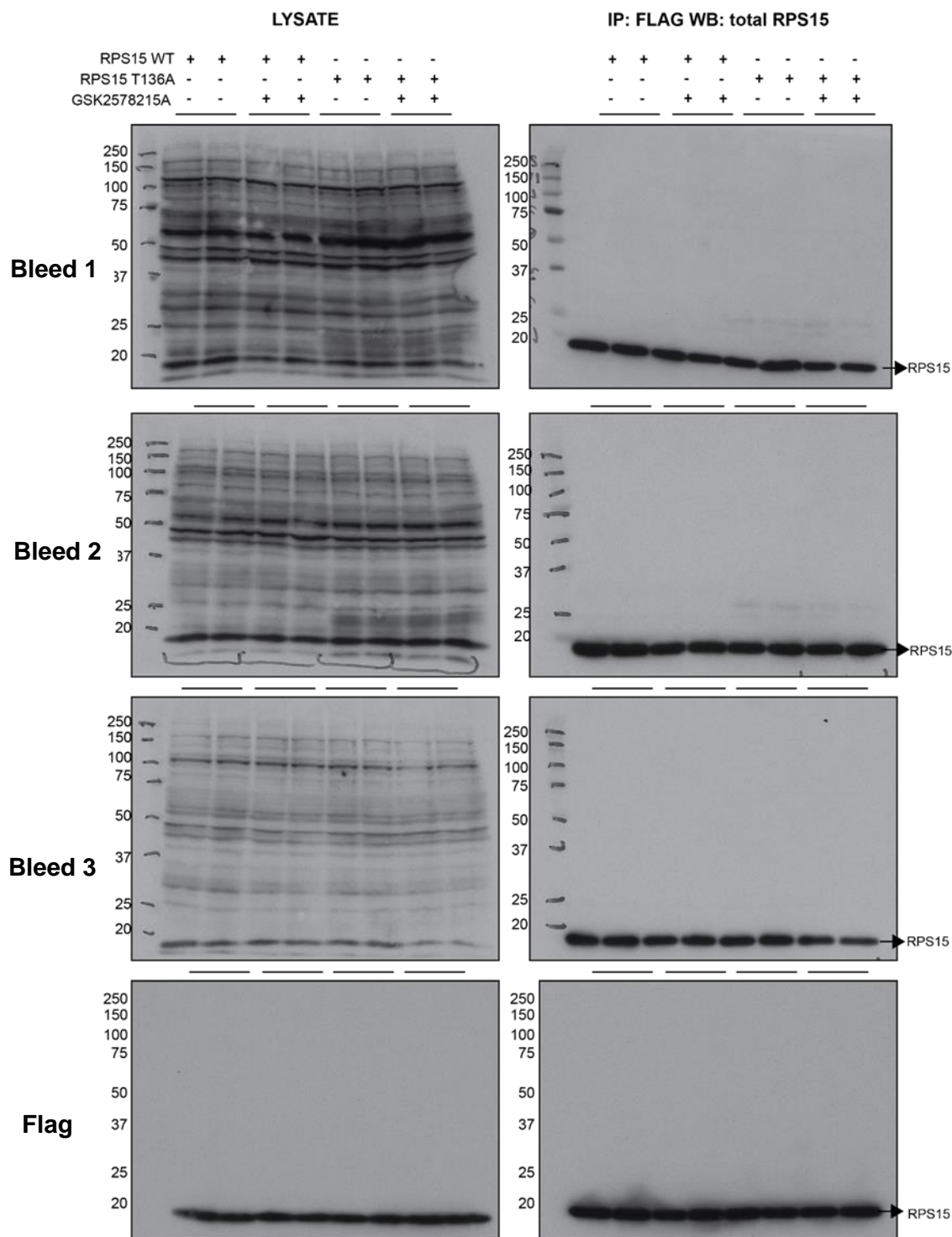


Figure 5.5: Assessment of total RPS15 antibody in over-expressed cells. HEK293 cells stably over-expressing GFP-tagged LRRK2 [G2019S] cells were transiently transfected with FLAG-tagged RPS15 WT or T136A proteins. 24 hours after transfection HEK293 cells were induced with the doxycycline to allow LRRK2 expression and 24 hours later cells were then treated with DMSO or 1 μ M GSK2578215A LRRK2 kinase inhibitor for 1 hour. Cell lysates were then resolved on polyacrylamide gel and subjected to immunoblot analysis with different bleeds of total RPS15 antibody. In addition, FLAG-tagged RPS15 proteins were immunoprecipitated with FLAG antibody and subjected to immunoblot analysis with total RPS15 antibodies.

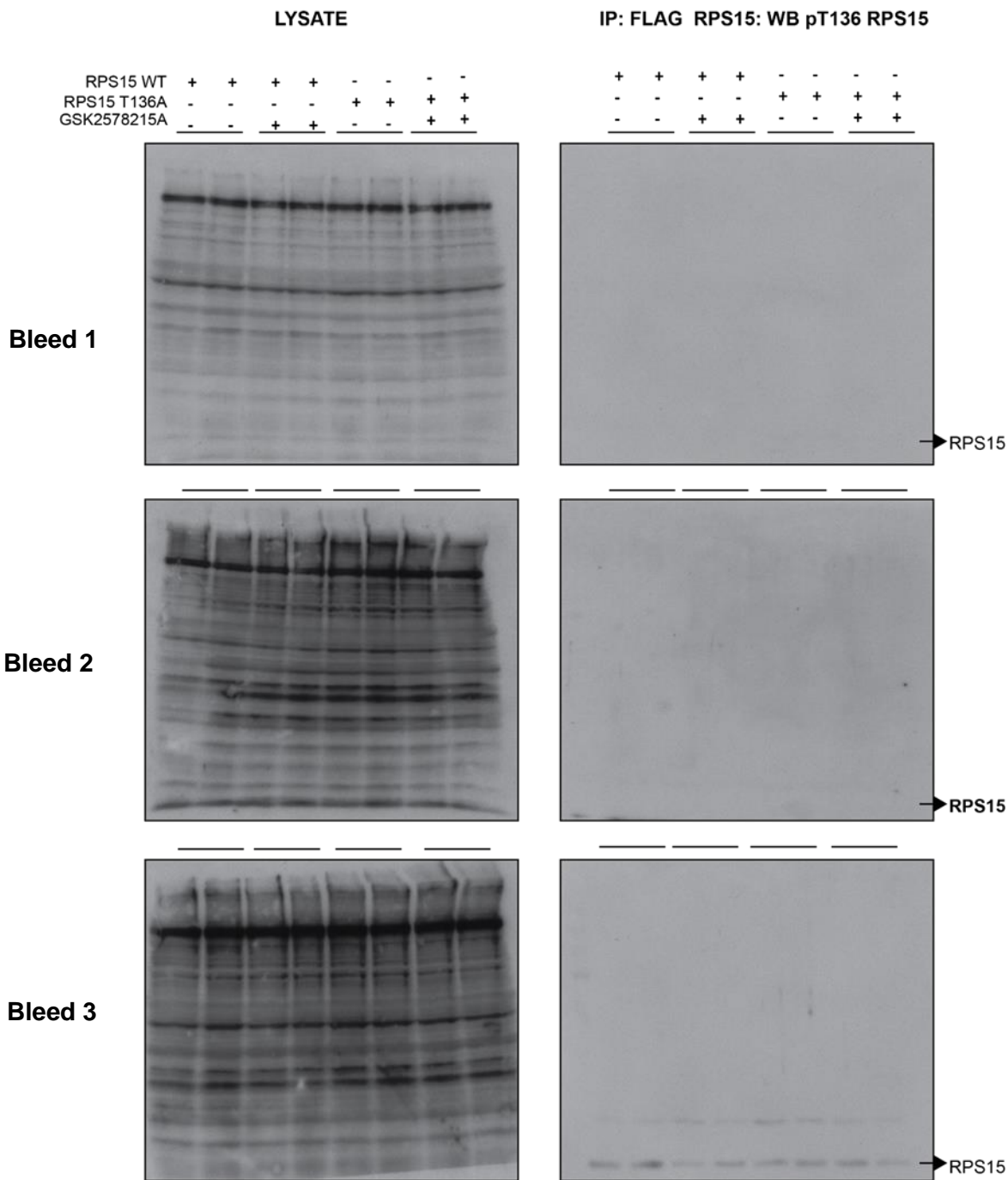


Figure 5.6: Assessment of pT136 RPS15 antibody in over-expressed cells HEK 293 cells stably over-expressing GFP-tagged LRRK2 [G2019S] cells were transiently transfected with FLAG-tagged RPS15 WT or T136A proteins. 24 hours after transfection HEK293 cells were induced with the doxycycline to allow LRRK2 expression and 24 hours later cells were then treated with DMSO or 1 μ M GSK2578215A LRRK2 kinase inhibitor for 1 hour. Cell lysates were then resolved on polyacrylamide gel and subjected to immunoblot analysis with different bleeds of pT136 RPS15 antibody. In addition, FLAG-tagged RPS15 proteins were immunoprecipitated with FLAG antibody and subjected to immunoblot analysis with pT136 RPS15 antibodies.

5.2.2 Proteomic fingerprint analysis of endogenous LRRK2 immunoprecipitated from MEF WT, MEF [S910A+S935A] and MEF KO cells

A comparative proteomic fingerprint analysis was performed with the aim to identify novel LRRK2 interacting partners that possibly could function as LRRK2 kinase potential substrates. For this purpose, a total of three scale biological replicates of endogenous LRRK2 were immunoprecipitated from the wild type, LRRK2 [S910A+S935A] knock-in and knock-out mouse embryonic fibroblast cells using N-terminal (100-500) monoclonal LRRK2 antibody. LRRK2 [S910A+S935A] knock-in MEFs were used in this experiment to investigate whether phosphorylation of serines 910 and 935 can have an effect on LRRK2 binding properties. Resultant immunoprecipitates were then subjected to Tryptic digestion and analysed by mass spectrometry (Orbitrap Velos). Obtained data was analysed using the Proteome Discoverer Software and visualised in Scaffold based on how many peptides of a protein were detected in a particular sample. My results are summarised in the Table 5.1. Endogenous LRRK2 immunoprecipitated from MEF wild type cells brings down a great number of proteins associated with cytoskeleton such as CAPZB, MYO1B, MYO1D, ARC1B, and ARPC4; cell adhesion, for instance, THBS1, VINC, CTNNA1 and MFGM; GTPases, for example, RAB11A, RASN, RRAS2 and RALB; vesicle transport such as SNAP23, PALM and VAPA, and ion transport. In contrast, endogenous LRRK2 derived from [S910A+S935A] MEFs brings down substantially reduced number of interacting partners indicating that this mutation might affect LRRK2 binding properties. For instance, SNAP23, VDAC1, PALM, TSPH1, NRAS and CTNNA1 seem to come down only with endogenous LRRK2 WT but not LRRK2 [S910A+S935A] or LRRK2 KO. In contrast, CYB5, STX12, CARF, MRC2 are detected to interact with LRRK2 [S910A+S935A] only. Also, proteins such as MRIP,

MME, THSB1 and RAB11A proteins appear to be present in both LRRK2 WT and LRRK2 [S910A+S935A] samples. Some of these proteins were shown to be linked to Parkinson's disease such as GNAI2, Rab11, VDAC1 and TSN6. It should be noted that Rab11 is not phosphorylated by LRRK2 in the experiments that have been undertaken thus far in our laboratory by Federico Diaz (unpublished data). Interestingly, 14-3-3 protein was detected in all my samples including LRRK2 KO cells and it was discarded from my analysis by Scaffold as non-specific interactor. It could be that not only LRRK2 but other proteins bind 14-3-3 and bring it with them, making it difficult to study this interaction by immunoprecipitation.

Table 5.1.A: Identity of proteins found in immunoprecipitates derived from LRRK2 WT but not LRRK2 KO MEFs.

	Identified Proteins	Abbreviation	kDa	WT	WT	WT	KO	KO	KO	Number of peptides/100kDa
1	Guanine nucleotide-binding protein G(i) subunit alpha-2	GNAI2	40	20	20	14	0	0	2	45
2	Golgi-associated plant pathogenesis-related protein 1	GAPR1	17	6	4	5	0	0	0	29
3	F-actin-capping protein subunit beta	CAPZB	31	9	9	7	0	0	3	27
4	UPF0444 transmembrane protein C12orf23 homolog	TMEM263	12	3	2	3	0	0	1	22
5	Thrombospondin-1	THBS1	130	28	26	24	0	0	0	20
6	Synaptosomal-associated protein 23	SNP23	23	5	4	4	0	0	0	19
7	Connective tissue growth factor	CTGF	38	7	8	6	0	0	0	18
8	Leucine-rich repeat serine/threonine-protein kinase 2	LRRK2	285	54	51	46	0	0	0	18
9	Voltage-dependent anion-selective channel protein 1	VDAC1	32	5	5	5	0	0	0	16
10	Histone H4	H4	11	4	1	0	0	0	1	15
11	Ras-related protein Ral-B	RALB	23	3	2	5	0	0	0	14
12	Paralemmin-1	PALM	42	7	7	4	0	0	0	14
13	Apoptosis regulator BAX	BAX	21	3	3	3	1	2	0	14
14	Ras-related protein Rab-11A	RB11A	24	3	4	3	0	0	0	14
15	Catenin alpha-1	CTNNA1	100	14	14	13	0	0	0	14
16	Alpha-soluble NSF attachment protein	SNAA	33	7	2	4	1	0	0	13
17	Vesicle-associated membrane protein-associated protein A	VAPA	28	4	3	4	0	0	0	13

18	Ras-related protein R-Ras2	RRAS2	23	4	2	3	0	0	1	13
19	Dolichyl-diphosphooligosaccharide--protein glycosyltransferase 48 kDa	OST48	49	6	7	6	1	0	0	13
20	Caveolin-1	CAV1	21	3	3	2	0	0	0	13
21	GTPase NRas	RASN	21	4	2	2	0	0	0	13
22	Vinculin	VINC	117	20	12	12	0	0	0	13
23	Lactadherin	MFGM	51	8	6	5	0	0	2	12
24	Cluster of Transmembrane emp24 domain-containing protein 9	TMED9	27	3	3	4	0	0	0	12
25	Nepriylsin	NEP	86	13	10	8	0	0	0	12
26	Unconventional myosin-Ib	MYO1B	129	15	13	16	1	0	5	11
27	Tetraspanin-6	TSN6	27	3	3	3	0	0	0	11
28	Cysteine and glycine-rich protein 1	CSRP1	21	1	2	4	0	0	0	11
29	Polymerase I and transcript release factor	PTRF	44	5	5	4	0	1	0	11
30	Actin-related protein 2/3 complex subunit 4	ARPC4	20	3	2	1	0	0	0	10
31	Myosin phosphatase Rho-interacting protein	MPRIP	116	17	10	7	0	0	0	10
32	Actin-related protein 2/3 complex subunit 1B	ARC1B	41	5	4	3	0	0	0	10
33	Adenylyl cyclase-associated protein 1	CAP1	52	9	3	3	0	1	0	10
34	NEDD8-conjugating enzyme Ubc12	UBC12	21	3	3	0	0	1	0	10
35	Inhibitor of nuclear factor kappa-B kinase-interacting protein	IKIP	43	4	5	3	0	0	0	9
36	Golgi reassembly-stacking protein 2	GORS2	47	5	3	5	0	1	0	9
37	Unconventional myosin-IId	MYO1D	116	12	10	10	0	0	0	9
38	Vesicular integral-membrane protein VIP36	LMAN2	40	4	5	2	0	0	0	9
39	Endoplasmic reticulum-Golgi intermediate compartment protein 1	ERGI1	33	3	4	2	0	0	0	9
40	Calponin-1	CNN1	33	4	2	3	0	0	0	9
41	Catenin beta-1	CTNB1	85	8	9	6	0	0	0	9
42	Prostacyclin synthase	PTGIS	57	7	4	4	0	0	0	9

Table 5.1.B: Identity of proteins found in immunoprecipitates derived from LRRK2 WT but not LRRK2 [S910A+S935A] or LRRK2 KO MEFs.

	Identified Proteins	Abbreviation	kDa	WT	WT	WT	KI	KI	KI	KO	KO	KO	Number of peptides/100kDa
1	Golgi-associated plant	GAPR1	17	6	4	5	0	0	0	0	0	0	29

	pathogenesis-related protein 1												
2	Thrombospondin-1	TSP1	130	28	26	24	4	4	5	0	0	0	20
3	Synaptosomal-associated protein 23	SNP23	23	5	4	4	0	0	1	0	0	0	19
4	Connective tissue growth factor	CTGF	38	7	8	6	0	0	0	0	0	0	18
5	Voltage-dependent anion-selective channel protein 1	VDAC1	32	5	5	5	0	0	0	0	0	0	16
6	Ras-related protein Ral-B	RALB	23	3	2	5	0	1	0	0	0	0	14
7	Paralemmin-1	PALM	42	7	7	4	0	0	0	0	0	0	14
8	Cluster of Catenin alpha-1	CTNA1	100	14	14	13	1	0	0	0	0	0	14
9	Cluster of Ras-related protein R-Ras2	RRAS2	23	4	2	3	0	1	0	0	0	1	13
10	Cluster of GTPase NRas	NRAS	21	4	2	2	0	0	0	0	0	0	13
11	Peptidyl-prolyl cis-trans isomerase FKBP1A	FKB1A	12	1	2	1	0	0	1	0	2	1	11
12	Actin-related protein 2/3 complex subunit 1B	ARC1B	41	5	4	3	0	1	1	0	0	0	10
13	Unconventional myosin-IId	MYO1D	116	12	10	10	0	0	1	0	0	0	9
14	Catenin beta-1	CTNB1	85	8	9	6	0	0	0	0	0	0	9
15	Immunoglobulin superfamily containing leucine-rich repeat protein	ISLR	46	5	3	4	0	0	0	0	0	0	9
16	Cluster of Calpain small subunit 1	CPNS1	28	3	2	2	0	0	1	0	1	0	8
17	FERM, RhoGEF and pleckstrin domain-containing protein 1	FARP1	119	10	10	8	0	0	0	0	0	0	8
18	Transforming growth factor beta-1-induced transcript 1 protein	TGFI1	50	4	3	4	0	0	0	0	0	0	7
19	Glypican-4	GPC4	63	4	5	3	1	1	1	0	0	0	6
20	4F2 cell-surface antigen heavy chain	4F2	58	4	3	4	0	0	0	0	0	0	6
21	Catenin delta-1	CTND1	105	8	6	4	0	0	0	0	0	0	6
22	Cadherin-2	CADH2	100	7	4	6	0	0	0	0	0	0	6
23	Flotillin-1	FLOT1	48	2	3	3	0	0	0	0	0	0	6
24	Annexin A6	ANXA6	76	5	3	3	0	0	0	0	0	1	5
25	Cluster of Band 4.1-like protein 2	E41L2	110	7	5	3	1	0	0	0	0	0	5
26	Integrin beta-5	ITB5	88	5	3	3	0	0	0	0	0	0	4
27	Sorbin and SH3 domain-containing protein 2	SRBS2	132	6	4	4	0	0	0	0	0	0	4

28	Neural cell adhesion molecule 1	NCAM1	119	7	2	3	1	0	1	0	0	0	3
29	Cytochrome P450 1B1	CP1B1	61	2	2	2	0	0	0	0	0	0	3
30	Cadherin-11	CAD11	88	4	2	2	0	0	0	0	0	0	3
31	General vesicular transport factor p115	USO1	107	4	2	2	0	0	1	0	0	0	2
32	Extended synaptotagmin-1	ESYT1	122	4	2	2	0	0	0	0	0	0	2

Table 5.1.C: Identity of proteins found in immunoprecipitates derived from LRRK2 [S910A+S935A] but not LRRK2 KO MEFs.

	Identified Proteins	Abbreviation	kDa	KI	KI	KI	KO	KO	KO	Number of peptides/100kDa
1	Atrial natriuretic peptide receptor 3	ANPRC	60	5	8	9	0	0	0	12
2	Leucine-rich repeat serine/threonine-protein kinase 2	LRRK2	285	33	31	36	0	0	0	12
3	Malectin	MLEC	32	4	4	3	0	0	0	11
4	Sulfide:quinone oxidoreductase, mitochondrial	SQRD	50	5	5	3	0	0	0	9
5	Endoplasmic reticulum-Golgi intermediate compartment protein 1	ERG11	33	2	3	3	0	0	0	8
6	Protein ERGIC-53	LMAN1	58	4	4	5	0	0	0	7
7	Prostacyclin synthase	PTGIS	57	5	3	3	0	0	0	6
8	Myosin phosphatase Rho-interacting protein	MPRIP	116	6	5	11	0	0	0	6
9	Vesicular integral-membrane protein VIP36	LMAN2	40	2	2	3	0	0	0	6
10	CDKN2A-interacting protein	CARF	60	4	2	2	0	0	0	4
11	Perilipin-4	PLIN4	139	5	6	4	0	0	0	4
12	Thrombospondin-1	TSP1	130	4	4	5	0	0	0	3
13	Nepriylisin	NEP	86	2	2	3	0	0	0	3
14	Vinculin	VINC	117	3	4	2	0	0	0	3
15	C-type mannose receptor 2	MRC2	167	3	2	2	0	0	0	1

Table 5.1.D: Identity of proteins found in immunoprecipitates derived from LRRK2 [S910A+S935A] but not LRRK2 WT or LRRK2 KO MEFs.

	Identified Proteins	Abbreviation	kDa	WT	WT	WT	KI	KI	KI	KO	KO	KO	Number of peptides/100kDa
1	Cytochrome b5	CYB5	15	0	0	0	2	2	2	0	0	0	13
2	Sulfide:quinone oxidoreductase, mitochondrial	SQRD	50	1	2	1	5	5	3	0	0	0	9
3	Syntaxin-12	STX12	31	0	1	0	3	2	1	0	0	0	6
4	CDKN2A-interacting protein	CARF	60	0	0	0	4	2	2	0	0	0	4
5	C-type mannose receptor 2	MRC2	167	0	0	0	3	2	2	0	0	0	1

One of the limitations of this approach is that the interaction between LRRK2 and any putative substrates needs to be strong enough to resist the handling of the immunoprecipitates that is why some of the potential LRRK2 interactors could be missing from this list. In addition, the interaction could be indirect and we could be detecting proteins that interact with LRRK2 interactors and this will be difficult to validate. Moreover, LRRK2 could share some of its interactors with other proteins that could come down from LRRK2 KO cells, for instance the case with 14-3-3, and in this experiment, it will be hard to identify false negative and positive LRRK2 interactors. The other thing to consider is that some proteins could bind LRRK2 non-specifically and also could bring down with them other non-specific proteins. To reduce this possibility cell lysates were pre-cleared with IgG antibody before cell lysates were incubated with LRRK2 specific antibody. Finally, it is important to note that MEF WT, MEF [S910A+S935A] and MEF KO cells were immortalised simultaneously by prolong passaging and this could result in accumulation of random distinct mutations between these cell lines that could affect the results. Therefore, in order to find a valid physiological LRRK2 binding partner from this list it

is critical to undertake further analysis to confirm that proteins identified also bind to LRRK2.

5.2.3 Validation of proteomic hits in over-expressed cells.

5.2.3.1 Attempt to validate PALM as an interactor of LRRK2.

Paralemmin (PALM), a prenyl-palmitoyl-anchored phosphoprotein abundant in neurons and implicated in plasma membrane dynamics and cell process formation (Kutzleb et al., 1998). Paralemmin is highly expressed in the brain but also less abundantly in many other tissues and cell types. Prenylation and palmitoylation of a COOH-terminal cluster of three cysteine residues confers hydrophobicity and membrane association to paralemmin. Paralemmin is also phosphorylated, and its mRNA is differentially spliced in a tissue-specific and developmentally regulated manner (Kutzleb et al., 1998). It was reported that paralemmin is associated with the cytoplasmic face of the plasma membranes of postsynaptic specializations, axonal and dendritic processes and perikarya, and also appears to be associated with an intracellular vesicle pool. Moreover, it was shown that overexpression in several cell lines shows that paralemmin concentrates at sites of plasma membrane activity such as filopodia and microspikes, and induces cell expansion and process formation. The lipidation motif is essential for this morphogenic activity. It was proposed that function of paralemmin is linked to the control of cell shape, for instance, through an involvement in membrane flow or in membrane–cytoskeleton interaction (Kutzleb et al., 1998). However, little is known about its mode of action, or about the biological functions of the other paralemmin isoforms: paralemmin-2, paralemmin-3 and palmdelphin (PALM D). It was suggested that the four paralemmin isoform genes (PALM1, PALM2, PALM3 and PALMD) arose by quadruplication of an ancestral

gene in the two early vertebrate genome duplications (Hultqvist, Ocampo Daza, Larhammar, & Kilimann, 2012) (Figure 5.7).

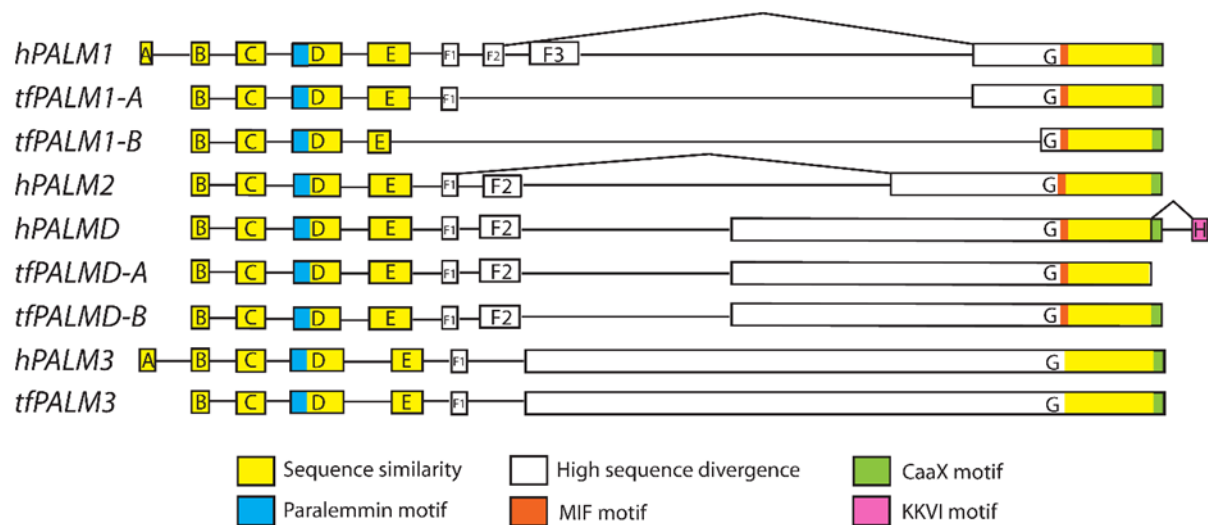


Figure 5.7: Conserved organization of paralemmin isoform genes (Adopted from (Hultqvist et al., 2012))

To validate identified proteomic hits, their interaction with LRRK2 was first of all verified in over-expressed system. For this purpose, HEK293 cells over-expressing Flag-tagged empty or LRRK2 WT proteins were transfected with the corresponding HA-tagged construct from LRRK2 WT vs LRRK2 KO list. HA-tagged empty and 14-3-3 constructs were used as a negative and positive control correspondingly. 14-3-3 was chosen as a positive control because it was found previously to interact with LRRK2 through phosphorylated S910 and S935 residues in over-expressing cells (Nichols et al., 2010). My findings are summarized in Figure 5.9. According to my data, HA-tagged 14-3-3 protein interacts with Flag-tagged LRRK2 but not with empty vector control. This is consistent with the previously reported data and indicates that the experiment worked. Moreover, I found that HA-tagged paralemmin (PALM), also strongly interacts with Flag-tagged LRRK2 in this system. In addition, an evident interaction with LRRK2 was detected between HA-tagged GTPases NRAS and SNAP23. Interestingly, PALM, NRAS and SNAP23 proteins as well as Rab10, a

recently discovered LRRK2 substrate (Steger et al., 2016), were described to be palmitoylated at their C-terminus (Kang et al., 2008). This suggests that palmitoylation could facilitate LRRK2 binding with its interacting partners.

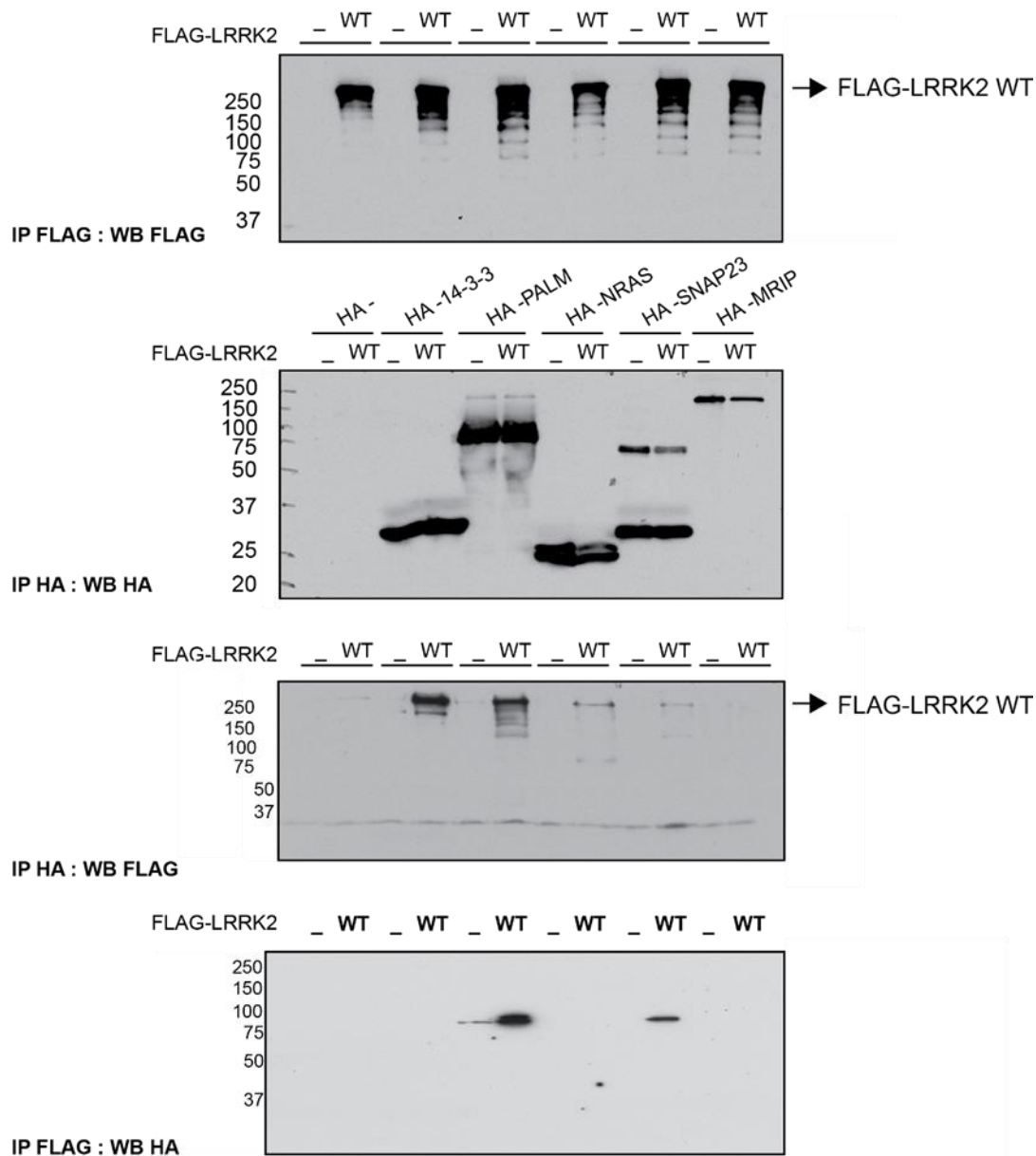


Figure 5.8: Validation of mass spectrometry hits in over-expressed cells. HEK293 cells over-expressing LRRK2 were transfected with indicated HA-tagged proteins, 24 hours later cells were induced with doxycycline. 48 hours after transfection, cell lysates were subjected to immunoprecipitation with FLAG or HA antibodies. Immunoprecipitates were then analyzed by immunoblotting with indicated antibodies.

As my data indicated that PALM interacts with LRRK2 in over-expressed system, this interaction was further investigated by testing whether it is affected by LRRK2 kinase activity and S910+S935 phosphorylation. For this purpose, HEK293 cells stably over-expressing FLAG-tagged empty or LRRK2 WT proteins were transfected with HA-tagged PALM protein in parallel with HA-tagged 14-3-3 protein used as a

positive control and HA-tagged empty used as a negative control. Cells were then induced and subsequently treated with DMSO or 1 μ M of LRRK2 kinase inhibitor GSK2578215A. My results are shown in Figure 5.10. According to this data, 14-3-3 binding with LRRK2 is significantly reduced upon LRRK2 kinase inhibitor treatment, which is consistent with the previously reported data. However, this binding is only detected by immunoprecipitating of HA-tagged protein and blotting for LRRK2 protein using FLAG antibody but not the other way around. PALM interaction with LRRK2 was detected either way but this interaction was not shown to be affected by inhibition of LRRK2 kinase activity. This suggests that PALM interacts with LRRK2 in over-expressed cells but this interaction does not depend on LRRK2 kinase activity.

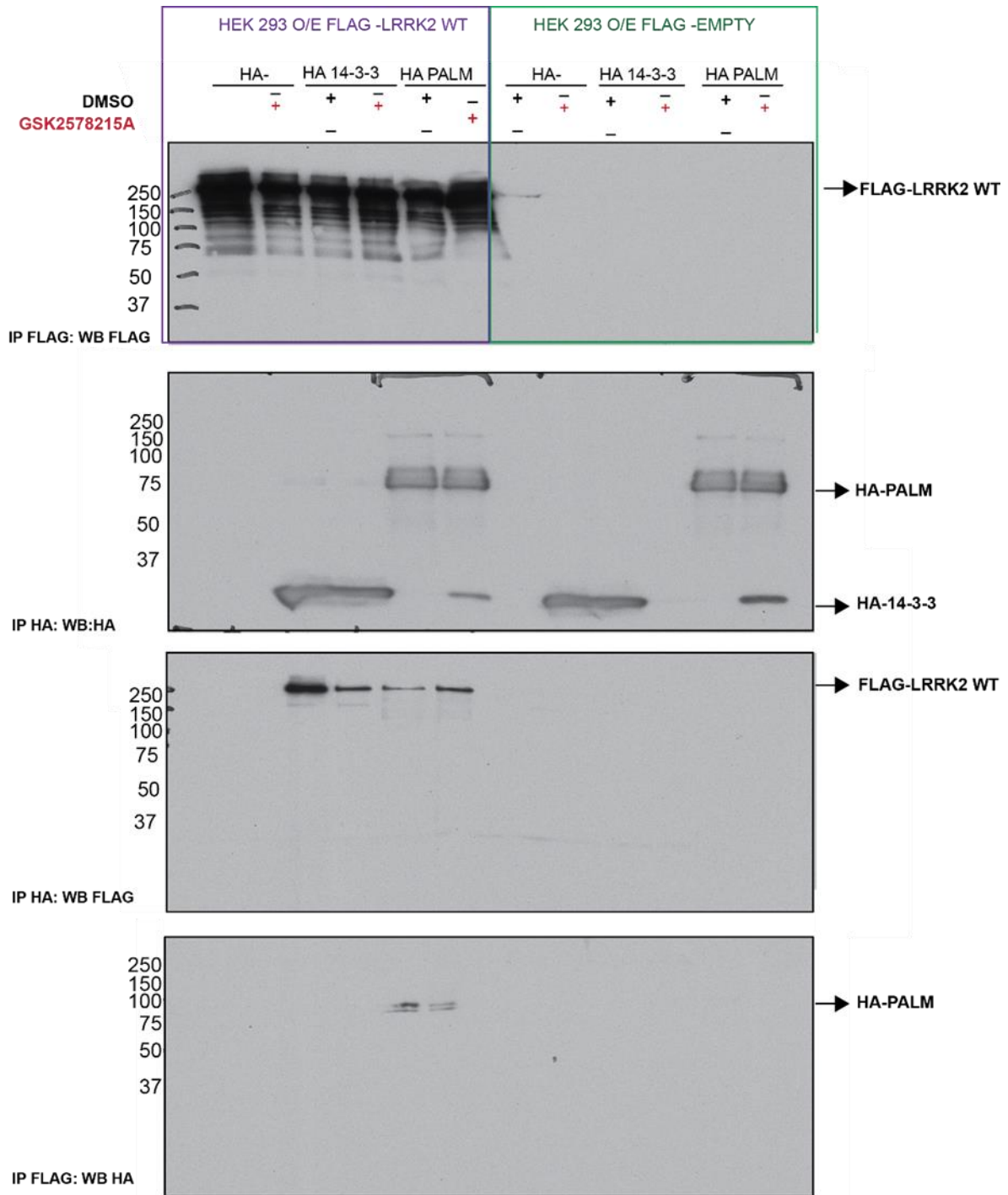
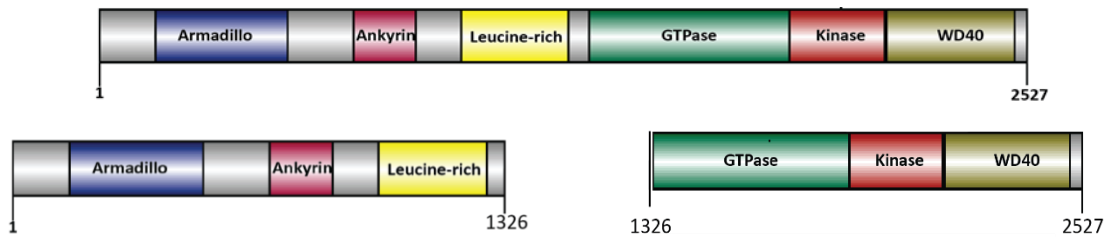


Figure 5.9: PALM interaction with LRRK2 is not affected by LRRK2 kinase activity. HEK293 cells stably over-expressing FLAG-tagged empty or LRRK2 WT were transfected with corresponding HA constructs, 24 hours after transfection cells were induced with doxycycline, 48 hours after transfection cells were treated with DMSO or 1 μ M LRRK2 kinase inhibitor GSK2578215A for 1 hour and lysed. Cell lysates were then subjected to immunoprecipitation with FLAG or HA antibodies. Immunoprecipitates were then analyzed by immunoblot analysis.

In order to identify LRRK2 PALM binding domain, HA-tagged PALM protein was co-expressed with LRRK2 FLAG-tagged N-terminal (1-1326), C-terminal (1326-end) and full length LRRK2 in HEK293 cells (Figure 5.11).

A



B

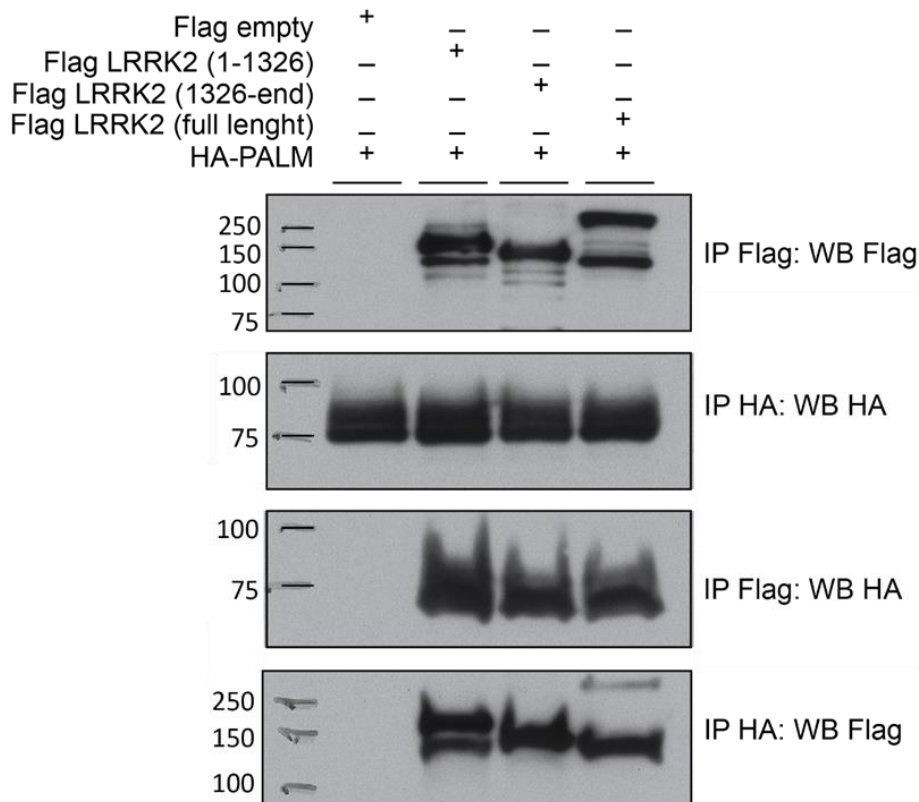


Figure 5.10: Co-immunoprecipitation of HA-PALM with Flag-LRRK2 fragments. HEK293 cells were co-transfected with HA-tagged PALM and indicated Flag-tagged LRRK2 fragments. Cell lysates were then subjected to immunoprecipitation with FLAG or HA antibodies. Immunoprecipitates were then analyzed by western blot.

According to this data PALM is binding to the N-terminal, C-terminal and full length LRRK2. This could be explained by the existence of two LRRK2 PALM binding domains or simply by non-specific interaction.

To verify if this interaction is specific, HA-tagged PALM protein was co-expressed with Flag-tagged LRRK2 WT as well as five other randomly chosen proteins (Figure 5.12). My results revealed that PALM protein is coming down with LRRK2 protein and with other four randomly chosen proteins such as KCC3a, Rab8a, SGK2, and SGK3 but not with MYPT1. This data suggests that PALM interaction with LRRK2 is probably not specific.

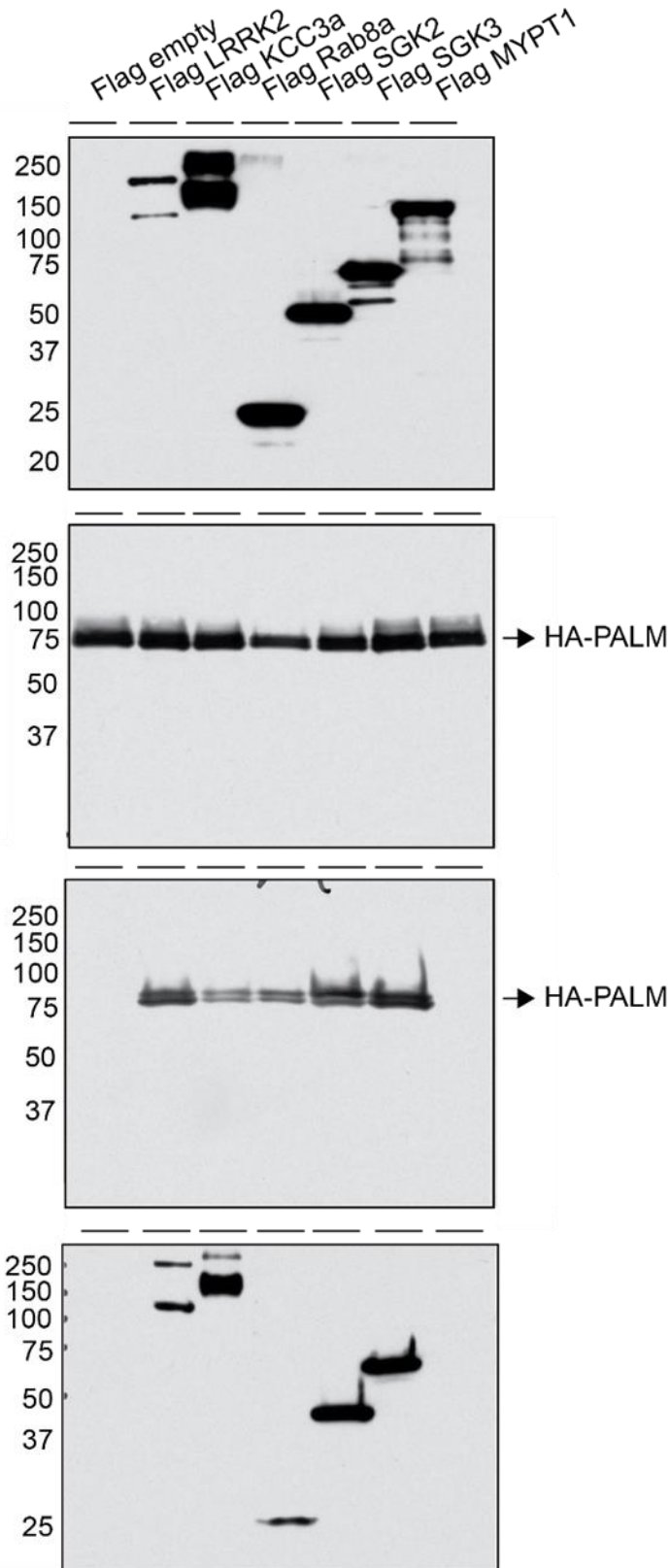


Figure 5.11: PALM co-expression with different proteins in HEK293 cells. HA-tagged PALM was co-expressed with FLAG-tagged indicated proteins. 48 hours after transfection cells were lysed and cell lysates were subjected to immunoprecipitation with indicated antibodies. Immunoprecipitates were then analyzed by western blotting.

To completely rule out the possibility of specific PALM LRRK2 interaction, these proteins were visualized together in over-expressed Hek293 cells with the aim to detect their co-localization. For this purpose, Hek293 cells stably over-expressing GFP-tagged LRRK2 WT or LRRK2 [S910A+S935A] were transiently transfected with HA-tagged PALM. Cells were then, fixed, stained and analyzed by Alan Prescott using Confocal Microscopy (Figure 5.13). According to the obtained data, GFP-tagged LRRK2 is diffused throughout the cytoplasm. Although GFP-tagged LRRK2 [S910A+Ser935A] protein is also diffused throughout the cytoplasm, it accumulates in aggregates. This is consistent with the previously reported data (Nichols et al., 2010) indicating that S910A+S935A mutation causes LRRK2 aggregation in cell. PALM protein is localized at the cell membrane and there is no obvious co-localization observed between these proteins. These results indicate that most probably PALM LRRK2 interaction is not specific.

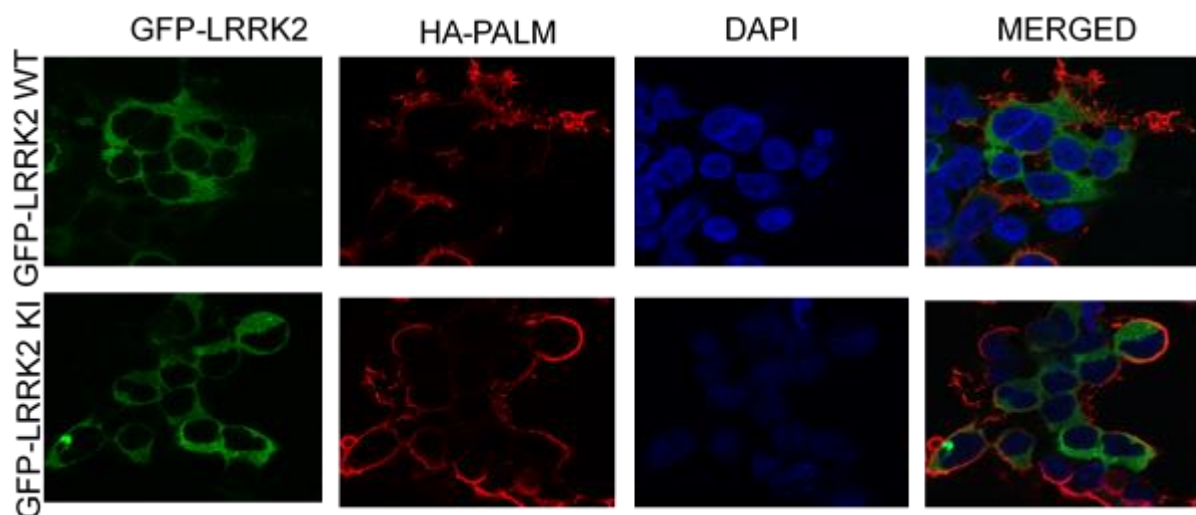


Figure 5.12: HA-tagged PALM co-localization with GFP-tagged LRRK2 proteins in HEK293 cells. HEK293 cells stably over-expressing indicated GFP-tagged LRRK2 protein were transiently transfected with HA-tagged PALM. Cells were fixed to the microscopy slide, stained and analysed by the Confocal Microscopy.

Finally, to test whether PALM is phosphorylated by LRRK2, distinct GST-tagged PALM isoforms were bacterially purified and incubated in presence of HEK293-purified LRRK2 (1326-end) [G2019S] protein, Mg^{2+} and ^{32}P ATP for 30 mins at $30^{\circ}C$ at 1000 rpm. GST-tagged RPS15 protein was used as a positive control (Figure 5.14).

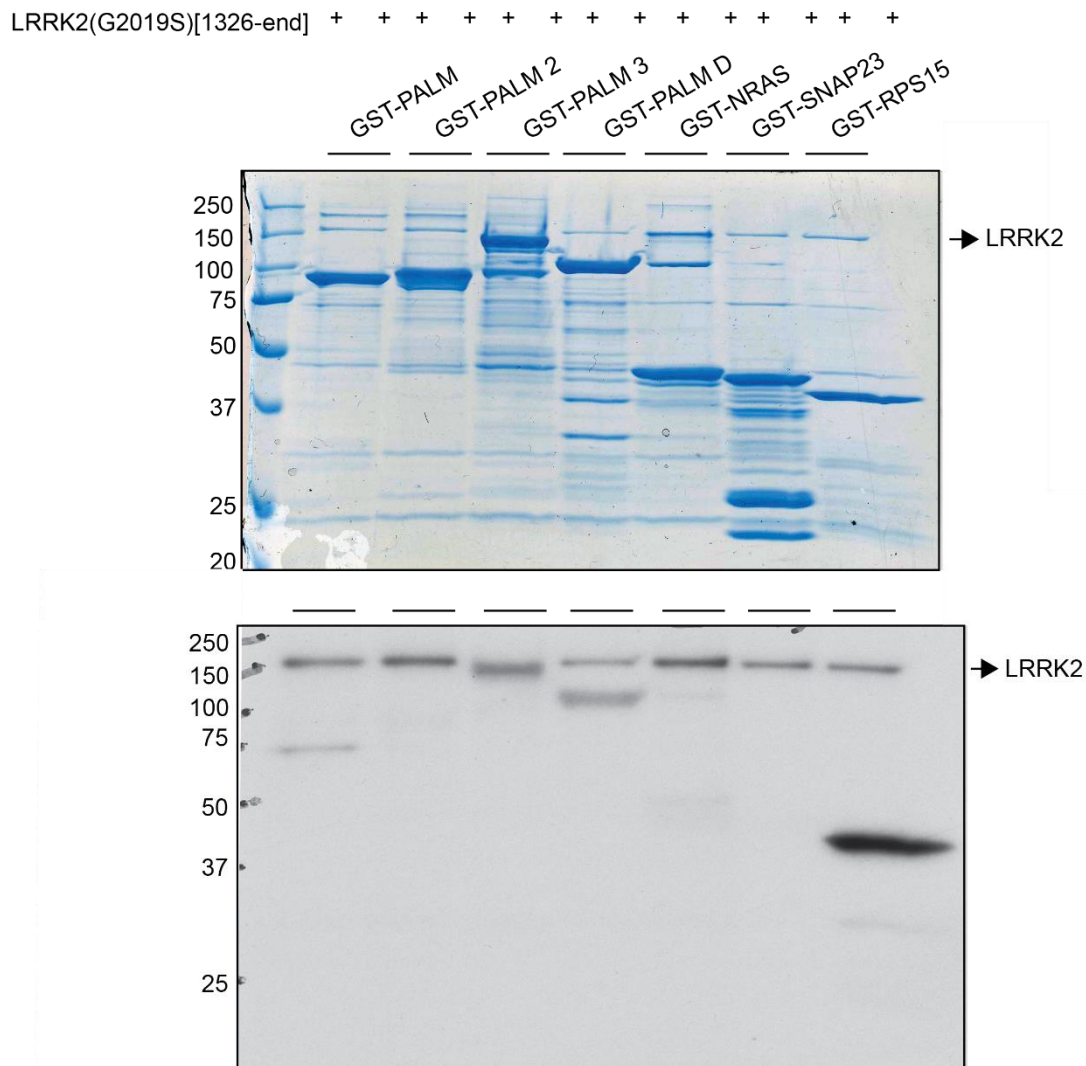


Figure 5.13: Assessment of PALM isoforms phosphorylation by LRRK2 in vitro. GST-tagged LRRK2 [1326-end] [G2019S] was HEK293-purified. Purified LRRK2 protein was then incubated with recombinant GST-tagged RPS15 protein, indicated GST-tagged PALM isoforms and Mg^{2+} -[γ - ^{32}P ATP] for 30 mins at $30^{\circ}C$ at 1000 rpm. Samples were then subjected to electrophoresis on a polyacrylamide gel and autoradiography.

According to my results PALM and PALMD are phosphorylated by LRRK2 *in vitro*. To test whether inhibition of LRRK2 kinase activity blocks PALM phosphorylation. PALM was phosphorylated by LRRK2 in presence of DMSO or 1 μ M GSK257821A and Mg²⁺ and ³²P ATP for 30 mins at 30°C at 1000 rpm (Figure 5.15).

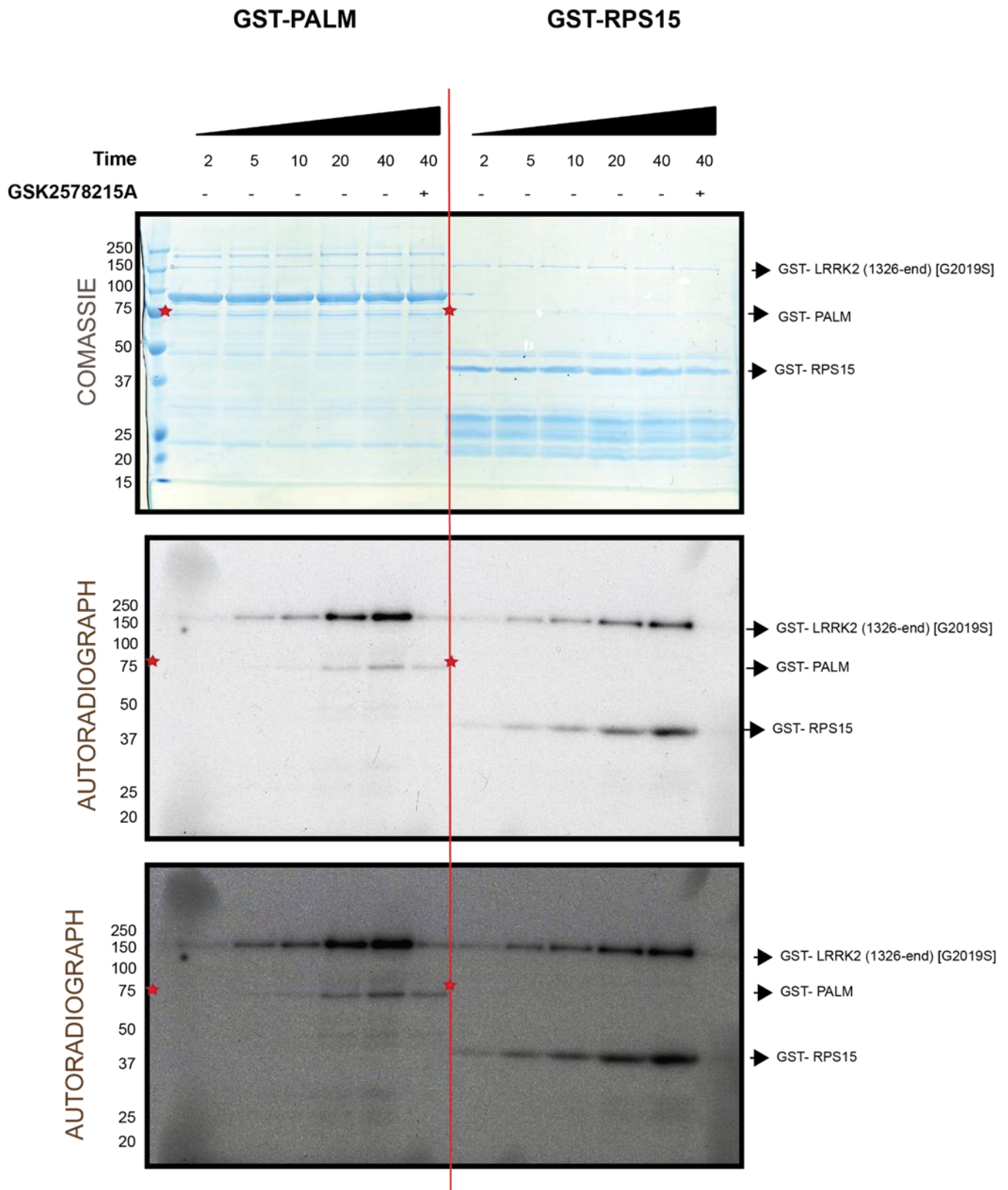


Figure 5.14: Assessment of PALM phosphorylation by LRRK2 in vitro. GST-tagged LRRK2 [1326-end) [G2019S] was HEK293-purified. Purified LRRK2 protein was then incubated with recombinant GST-tagged RPS15 protein, GST-tagged PALM and Mg^{2+} - $[\gamma\text{-}^{32}\text{ATP}]$ for the indicated times in presence or absence of LRRK2 specific kinase inhibitor ($1\mu\text{M}$ GSK2578215A). Samples were then subjected to electrophoresis on a polyacrylamide gel and autoradiography.

My data revealed that inhibition of LRRK2 kinase activity does not block PALM phosphorylation indicating that it is probably non-specific. It might be that another protein kinase could have immunoprecipitated with GST-LRRK2, which has been isolated from HEK293 cells used in this protein, and phosphorylated PALM.

5.2.3.2 Validation of other proteomic hits by *in vitro* phosphorylation

To test whether proteins which came down with LRRK2 such as CTNNA1, M-RIP, MME, CAPZB and GNAI2 could be potential LRRK2 substrates I have subjected bacterially purified GST-tagged proteins *in vitro* phosphorylation by HEK293-purified 1236-end LRRK2 [G2019S in presence of Mg^{2+} and ^{32}P ATP in presence and absence of LRRK2 kinase inhibitor. I used RPS15 as a positive control. My results are summarised in the Figure 5.16.

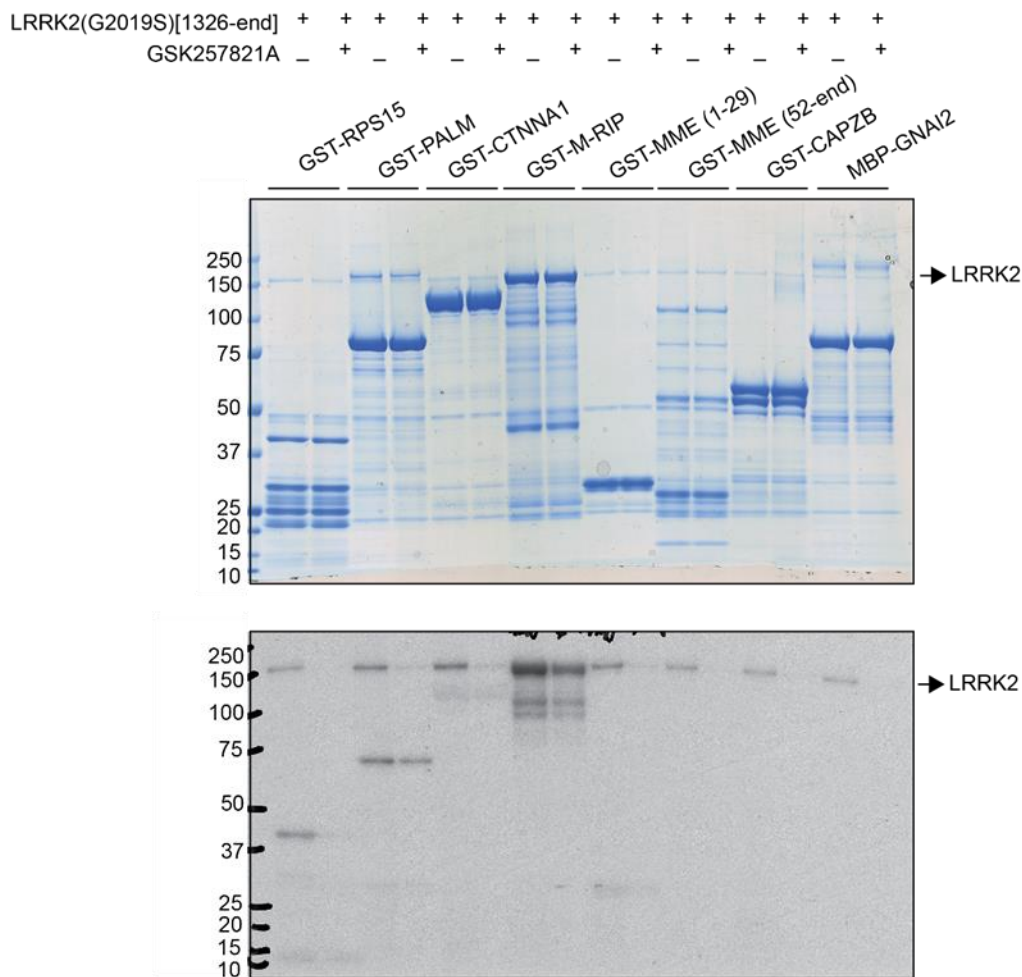


Figure 5.15: *In vitro* phosphorylation screen by LRRK2. GST-bacterially purified indicated proteins were subjected to an *in vitro* kinase assay by HEK293-purified LRRK2 [G2019S] in the presence or absence of 1 μ M LRRK2 kinase inhibitor. Proteins were then resolved in SDS gel and developed by autoradiography.

From this data is clear that RPS15 is phosphorylated by LRRK2 and inhibition of LRRK2 kinase activity blocks this phosphorylation. PALM and MRIP seem to be phosphorylated by LRRK2 but this phosphorylation is not abolished by the LRRK2 inhibitor indicating that it is not specific. Other proteins were not shown to be significantly phosphorylated by LRRK2.

5.2.4. LRRK2 might not be a threonine specific kinase

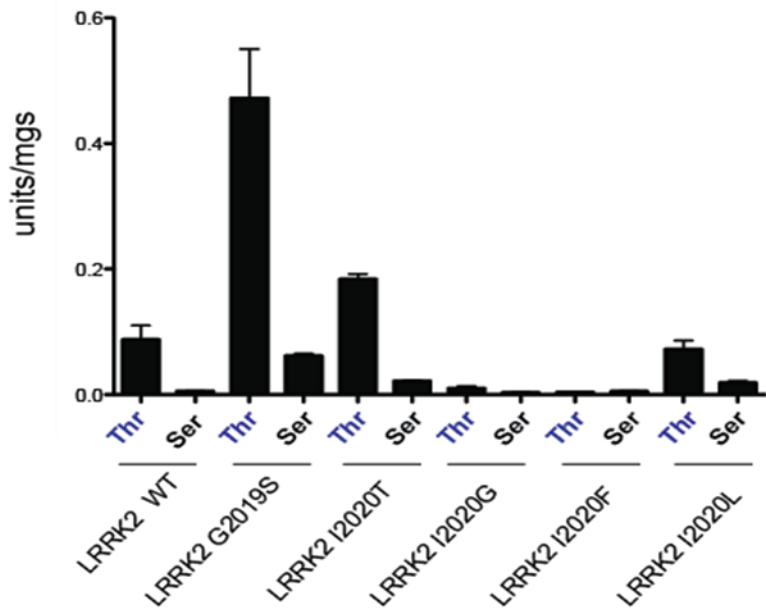
As mentioned before, previous work in our lab has shown that moesin, a member of the ERM (ezrin/radixin/moesin) is efficiently phosphorylated by LRRK2 *in vitro* at

T558, a previously identified *in vivo* phosphorylation site that regulates the ability of moesin to bind actin (Jaleel et al., 2007). In addition, it was shown, that LRRK2 phosphorylates the other ERM proteins, ezrin and radixin, that are related to moesin at the residue equivalent to T558 as well as peptide encompassing T558. This peptide was named LRRKtide: RLGRDKYKTLRQIRQ (Nichols et al., 2009b). Furthermore, a scanning library approach was used to improve the optimal phosphorylation motif of LRRK2. It was found that the optimal LRRK2 phosphorylation motif between -5 and +4 positions is WWRFYTLRRA, which was substituted into the moesin sequence from which the LRRKtide was derived. The resulting sequence was called Nictide: RLGWWRFYTLRRARQGNTKQR. Nictide was shown to be phosphorylated to a much greater extent by LRRK2 [G2019S] (1326-end) compared to LRRKtide or moesin (Nichols et al., 2009b). Moreover, it was reported that mutation of Thr in Nictide peptide to Ser abolished phosphorylation of LRRK2 suggesting that LRRK2 has a marked preference for phosphorylating threonines instead of serines (Nichols et al., 2009a). To date, most identified LRRK2 phosphorylation sites are threonines, including RPS15 T136.

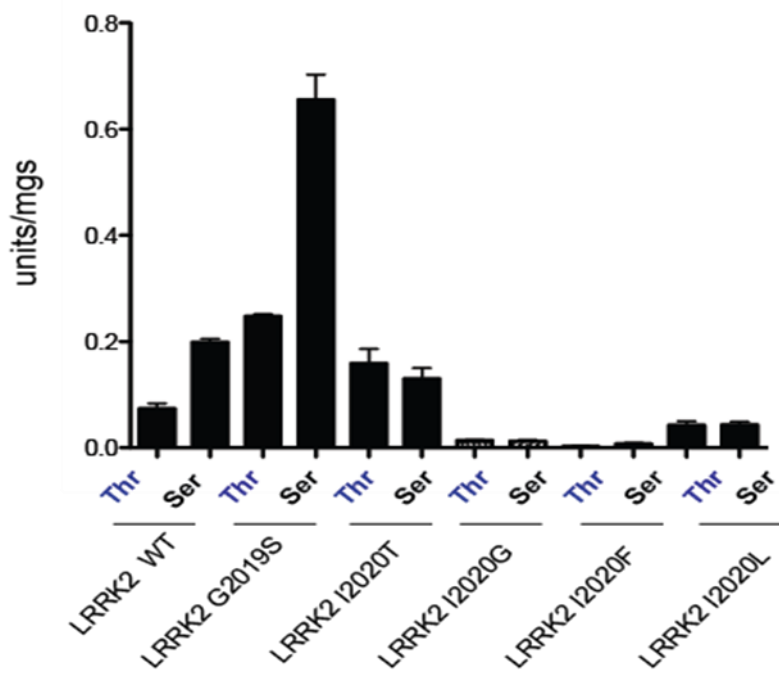
Recently, Ben Turk' laboratory from the University of Yale discovered that the residue located at position + 1 from the DFG motif plays a critical role in controlling whether protein kinases phosphorylate Ser or Thr residues (C. Chen et al., 2014). His work suggests that protein kinases with an Ile residue at this position makes protein kinases phosphorylate Thr residues rather than Ser residues. This is very interesting because LRRK2 has a Ile2020 at this position that is also mutated to Thr in patients with Parkinson's disease. Therefore, I wanted to explore how LRRK2 mutations of I2020T and G2019S impact on Thr/Ser phosphorylation substrate specificity of LRRK2

To test this hypothesis, recombinant GST fused LRRK2 (1326-end) proteins comprising the following mutations LRRK2 [G2019S], LRRK2 [I2020T], LRRK2 [I2020L], LRRK2 [I2020F], LRRK2 [I2020G] and the wild type were HEK293-purified. Nictide and LRRKtide peptides, and moesin comprising T or S residue at the phosphorylation site were subjected to phosphorylation by these recombinant proteins (Figure 5.17).

C Nictide 500 μ M (Thr vs Ser)



D LRRKtide 500 μ M (Thr vs Ser)



E

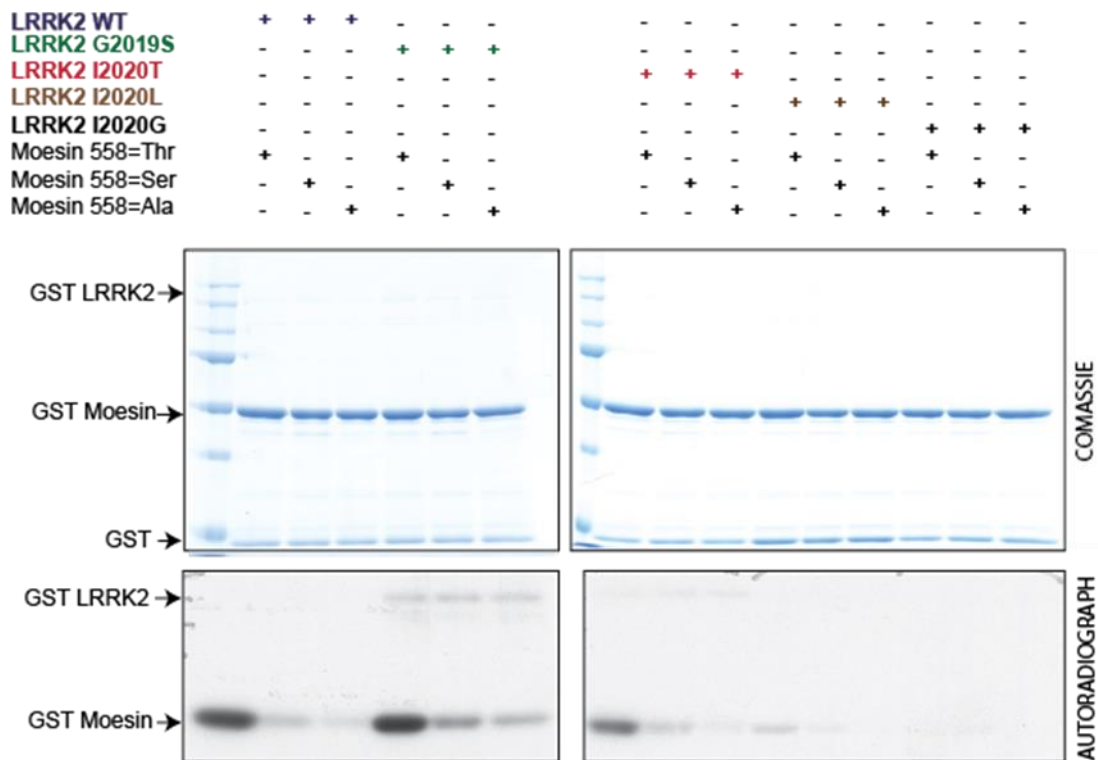


Figure 5.16: Determination of the preferred T/S phosphorylation site for LRRK2 (A) The wild type and indicated mutations of GST-LRRK2-(1326-end) were HEK293-purified and analysed by SDS/PAGE followed by Colloidal Blue staining. **(B)** Amino acid composition of implemented peptides was summarized. **(C)** The same amounts of each form of LRRK2 were assayed against 500 μ M Nictide for 20 mins. Each measurement was taken in triplicate, and the results are the means \pm S.E.M. for peptide phosphorylation relative to wild-type enzyme for each peptide. Similar results were obtained with two independent enzyme preparations. **(D)** The same amounts of each form of LRRK2 were assayed against 500 μ M LRRKtide for 20 mins. Each measurement was taken in triplicate, and the results are the means \pm S.E.M. for peptide phosphorylation relative to wild-type enzyme for each peptide. Similar results were obtained with two independent enzyme preparations. **(E)** GST fused moesin proteins comprising indicated mutations were subjected to phosphorylation by the same amount of indicated form of LRRK2. Reactions were stopped by the addition of sample buffer, and products were subjected to SDS/PAGE. Gels were analysed by staining with Colloidal Blue, and phosphorylation was monitored by autoradiography (32 P).

My results confirmed that Nictide is efficiently phosphorylated by wild type LRRK2. Consistent with previous work G2019S mutation stimulates LRRK2 activity to 4 folds whereas I2020T mutation only slightly increases LRRK2 activity. In accordance with

reported data, mutation of phosphorylated threonine residue in Nictide to serine dramatically decreases LRRK2 phosphorylation. However, LRRK2 [G2019S] does seem to tolerate serine residues in Nictide much better than the wild type. Surprisingly, LRRKtide peptide sequence comprising a serine, as LRRK2 phosphorylation site is much better tolerated by wild type LRRK2 and, G2019S and I2020T mutants. Mutation of threonine in LRRKtide peptide to serine seems to increase LRRK2 phosphorylation. Therefore, my data indicates that LRRK2 might not be a threonine specific kinase. The most important thing that this analysis show is that LRRK2 G2019S mutant might be able to phosphorylate Ser residues much better than the wild type. It was reported that indeed LRRK2 G2019S mutant autophosphorylates at S1292 with much greater extent than the wild type (Sheng et al., 2012). Moreover, in our lab RAB12 was shown to be phosphorylated by LRRK2 in cells at S106 (unpublished work). It would be interesting to compare its phosphorylation by LRRK2 WT and LRRK2 G2019S in more detail.

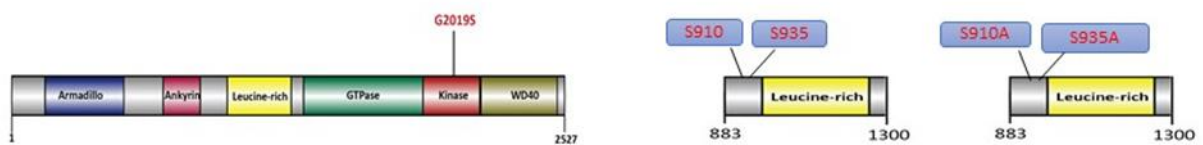
In addition, my results do not provide much evidence to support Ben Turk's model. Mutation of Ile 2020 to Thr (I2020T) or Leu (I2020L) has little impact on Ser/Thr specificity whereas I2020G and I2020F mutations resulted to be catalytically inactive. Maybe for some kinases this residue is important for Ser/Thr specificity but my data suggests that this is not the case for LRRK2.

5.2.5 MAP4 kinases phosphorylate LRRK2 S910 and S935 *in vitro* but not *in vivo*

Previously in our laboratory, Paul Davies demonstrated that LRRK2 is phosphorylated by MAP4 kinase *in vitro*. However, there was no evidence for this to be true in cell. To test whether LRRK2 is phosphorylated by MAP4 kinases in cells I first confirmed that these sites were phosphorylated by MAP4 kinase *in vitro*. For this

purpose I used purified GST-tagged MAP4K3 recombinant protein available in our lab to phosphorylate commercially purified recombinant GST-tagged LRRK2 full length protein as well as truncate LRRK2 (880-1300) WT and (880-1300) [S910A+S935A] mutant in the presence of Mg^{2+} and ATP at 30 mins at 30°C. Reactions were stopped by 4xloading buffer, resolved on a SDS gel and subjected to immunoblot analysis (Figure 5.18).

A



B

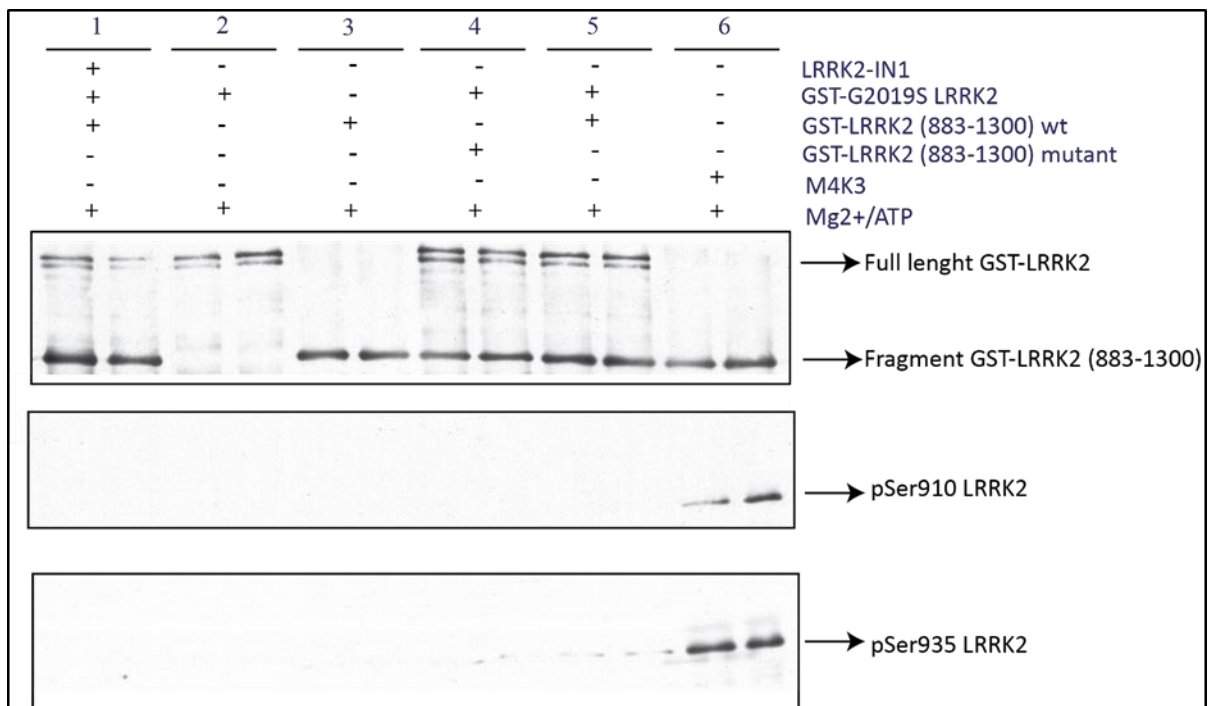


Figure 5.17: MAP4K3 phosphorylates LRRK2 in vitro at S910 and S935. (A) Schematic representation of LRRK2 protein fragments employed in this assay. (B) Recombinant GST MAP4K3 kinase was incubated with recombinant G2019S LRRK2 (Invitrogen) full length protein as well as its fragments LRRK2 (883-1300) WT and mutant (S910A and S935A) in the presence of Mg^{2+} and ATP at 30°C for 30 mins at 1000 rpm. Reactions were stopped by the sample loading buffer and resolved on a SDS gel, which has been subjected to immunoblot analysis with the indicated antibodies.

Interestingly, Guan, Kun-Liang laboratory reported that they selectively knocked out all isoforms of MAP4 kinases (1-9) in HEK293 cells (Meng et al., 2015). Guan's lab kindly shared these HEK293 MAP4 kinase null cells with us so that we could test whether deletion of MAP4 kinases from cells impairs LRRK2 S910 and S935 phosphorylation. To test this, I have immunoprecipitated endogenous LRRK2 from HEK 293 or HEK293 MAP4 null cells treated with DMSO or 1 μ M of GSK2578215A inhibitor and assessed LRRK2 S935 phosphorylation in these conditions (Figure 5.19).

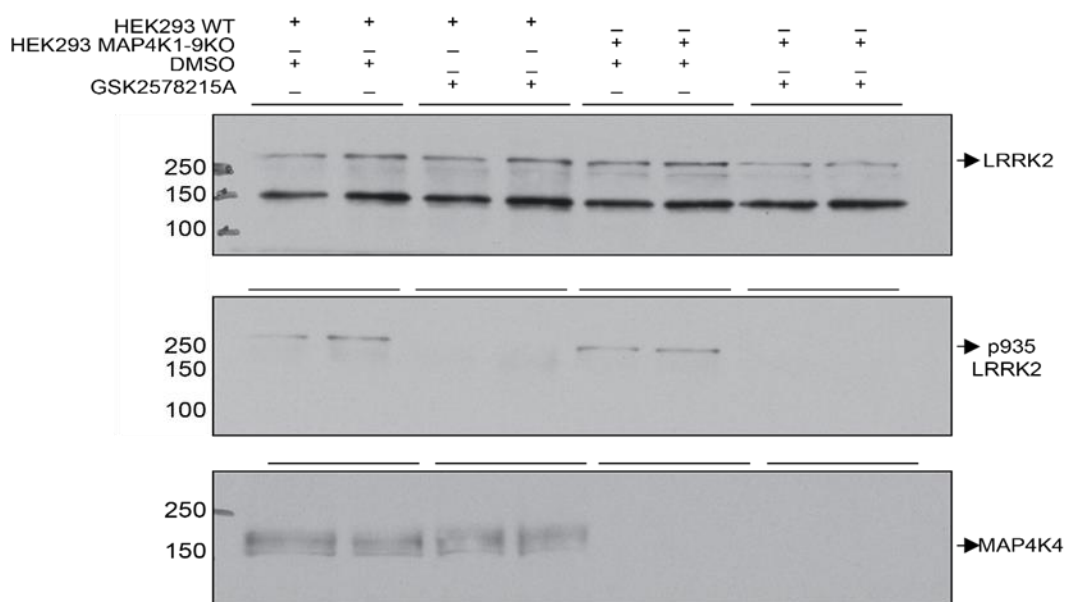


Figure 5.18: LRRK2 S935 phosphorylation is not affected by deletion of MAP4K1-9 isoforms. HEK293 MAP4K1-9 knock-out cells as well as HEK293 control cells were treated with LRRK2 specific inhibitor or DMSO. Cell lysates were then subjected to immunoprecipitation with monoclonal LRRK2 antibody and subjected to phospho S935 and total LRRK2 antibodies. Also cell lysates were subjected to immunoblot analysis with MAP4K4 antibody.

To confirm MAP4 kinase isoform deletion, I used MAP4K4 antibody, which specifically recognized MAP4K4 protein in HEK293 WT cells but not in HEK293 MAP4K 1-9 null cells. Treatment of HEK293 WT cells with LRRK2 specific kinase

inhibitor as expected resulted in dephosphorylation of S935. Moreover, S935 phosphorylation in HEK293 WT cells is the same as in HEK293 MAP4 (1-9) null cells, suggesting that deletion of MAP4 kinases did not have any effect on LRRK2 phosphorylation under basal conditions.

5.3 Summary

To summarise, RPS15, a previously reported LRRK2 substrate, is efficiently phosphorylated by LRRK2 *in vitro* at T136 and mutation of this site to alanine significantly abolishes LRRK2 phosphorylation. Also, addition of LRRK2 specific inhibitor blocks RPS15 phosphorylation by LRRK2. However, in overexpressed cells, inhibition of LRRK2 kinase activity does not lead to any obvious changes in RPS15 phosphorylation at T136. This could be explained by incorrect RPS15 folding in cells due to its over-expression. Alternatively, it could also be that other kinases phosphorylate this site in cells and that LRRK2 is not a rate limiting kinase for this protein. However, to date there is not known, which kinase could phosphorylate RPS15 at this site. The attempt to assess phosphorylation of T136 in cells was unsuccessful as generated phospho-specific antibodies for this site were proven to be not sufficiently selective and therefore, could not be used.

In order to identify novel LRRK2 interactors, I used a comparative mass spectrometry analysis derived from LRRK2 immunoprecipitates of LRRK2 WT, MEF LRRK32 [S910A+S935A] and LRRK2 KO MEFs. My data revealed a great number of proteins coming down with the wild type LRRK2. Interestingly, a significantly reduced number of proteins were shown to come down with knock-in LRRK2. Reported proteins should be validated as a number of factors could affect the results. I have tested at least ten different proteins from the mass spectrometry list I generated including CTNNA1, TSB1, MRIP, PALM, GNAI, VDAC1, SNAP23, NRAS,

NEP, RAB11, CRAF and MRCK but my data did not provide strong evidence that any of these proteins bind LRRK2 specifically. PALM was the only protein that looked promising initially as it was binding strongly to LRRK2 *in vitro* but further research revealed that this binding was most likely to be non-specific as it seems to bind other FLAG-tagged proteins similarly to LRRK2. In spite of the fact that PALM and PALMD are phosphorylated by LRRK2 *in vitro*, inhibition of LRRK2 kinase activity did not block its phosphorylation, indicating that this phosphorylation was likely caused by another kinase that associated with LRRK2 from HEK293 cells.

In my opinion, one of the major limitations of this mass spectrometry experiment is that littermate MEFs used were spontaneously immortalized in parallel and this could have led to accumulation of distinct mutation between these lines. These diverse mutations, which took places during immortalization process could have altered differently each littermate cell line and as a result influence my data. In order, to obtain more homogeneous cells, one could use primary non-immortalized cells or immunoprecipitate LRRK2 directly from mouse tissues of LRRK2 wild type, knock-in or knock-out cells. Also, considering the evidence that penetrant mutations in LRRK2 such as R1441G massively increase the efficiency of LRRK2 mediated phosphorylation of Rabs, it would be important to validate future MS hits using these mutants. Mass spectrometry experiments could also be conducted using endogenous knock in models of these mutations.

In addition, my LRRK2 substrate specificity data provides no evidence to support Ben Turk's model. This is because mutation of Ile 2020 to T (I2020T) or L (I2020L) has little impact on Ser/Thr specificity. Maybe for some kinases this residue is important for Ser/Thr specificity but my data indicates that this is not the case for LRRK2. Furthermore, mutation of threonine in LRRKtide peptide to serine seems to

increase LRRK2 phosphorylation. Therefore, my data indicates that LRRK2 might not be a threonine specific kinase, as it was reported previously, because it also efficiently phosphorylates serines.

Finally, it has been proposed that MAP4 kinases could phosphorylate LRRK2 at S910 and S935 but to date there was no evidence to support this hypothesis in cells. It was not until Guan's lab managed to produce MAP4 (1-9) null cells I could test that deletion of MAP4 kinases from HEK293 cells had no effect on LRRK2 S935 phosphorylation.

BIBLIOGRAPHY

- Abou-Sleiman, P. M., Healy, D. G., Quinn, N., Lees, A. J., & Wood, N. W. (2003). The role of pathogenic DJ-1 mutations in Parkinson's disease. *Ann Neurol*, *54*(3), 283-286. doi:10.1002/ana.10675
- Alessi, D., MacDougall, L. K., Sola, M. M., Ikebe, M., & Cohen, P. (1992). The control of protein phosphatase-1 by targetting subunits. The major myosin phosphatase in avian smooth muscle is a novel form of protein phosphatase-1. *Eur J Biochem*, *210*(3), 1023-1035.
- Bailey, R. M., Covy, J. P., Melrose, H. L., Rousseau, L., Watkinson, R., Knight, J., . . . Lewis, J. (2013). LRRK2 phosphorylates novel tau epitopes and promotes tauopathy. *Acta Neuropathol*, *126*(6), 809-827. doi:10.1007/s00401-013-1188-4
- Baptista, M. A., Dave, K. D., Frasier, M. A., Sherer, T. B., Greeley, M., Beck, M. J., . . . Fiske, B. K. (2013). Loss of leucine-rich repeat kinase 2 (LRRK2) in rats leads to progressive abnormal phenotypes in peripheral organs. *PLoS One*, *8*(11), e80705. doi:10.1371/journal.pone.0080705
- Belluzzi, E., Gonnelli, A., Cirnaru, M. D., Marte, A., Plotegher, N., Russo, I., . . . Greggio, E. (2016). LRRK2 phosphorylates pre-synaptic N-ethylmaleimide sensitive fusion (NSF) protein enhancing its ATPase activity and SNARE complex disassembling rate. *Mol Neurodegener*, *11*, 1. doi:10.1186/s13024-015-0066-z
- Berry, C., La Vecchia, C., & Nicotera, P. (2010). Paraquat and Parkinson's disease. *Cell Death Differ*, *17*(7), 1115-1125. doi:10.1038/cdd.2009.217
- Boudeau, J., Miranda-Saavedra, D., Barton, G. J., & Alessi, D. R. (2006). Emerging roles of pseudokinases. *Trends Cell Biol*, *16*(9), 443-452. doi:10.1016/j.tcb.2006.07.003
- Brooks, S. P., & Dunnett, S. B. (2009). Tests to assess motor phenotype in mice: a user's guide. *Nat Rev Neurosci*, *10*(7), 519-529. doi:10.1038/nrn2652
- Broustas, C. G., Grammatikakis, N., Eto, M., Dent, P., Brautigan, D. L., & Kasid, U. (2002). Phosphorylation of the myosin-binding subunit of myosin phosphatase by Raf-1 and inhibition of phosphatase activity. *J Biol Chem*, *277*(4), 3053-3059. doi:10.1074/jbc.M106343200
- Burnett, G., & Kennedy, E. P. (1954). The enzymatic phosphorylation of proteins. *J Biol Chem*, *211*(2), 969-980.
- Cardona, F., Sanchez-Mut, J. V., Dopazo, H., & Perez-Tur, J. (2011). Phylogenetic and in silico structural analysis of the Parkinson disease-related kinase PINK1. *Hum Mutat*, *32*(4), 369-378. doi:10.1002/humu.21444
- Chartier, M., Chenard, T., Barker, J., & Najmanovich, R. (2013). Kinome Render: a stand-alone and web-accessible tool to annotate the human protein kinome tree. *PeerJ*, *1*, e126. doi:10.7717/peerj.126
- Checkoway, H., Powers, K., Smith-Weller, T., Franklin, G. M., Longstreth, W. T., Jr., & Swanson, P. D. (2002). Parkinson's disease risks associated with cigarette smoking, alcohol consumption, and caffeine intake. *Am J Epidemiol*, *155*(8), 732-738.
- Chen, C., Ha, B. H., Thevenin, A. F., Lou, H. J., Zhang, R., Yip, K. Y., . . . Turk, B. E. (2014). Identification of a major determinant for serine-threonine kinase phosphoacceptor specificity. *Mol Cell*, *53*(1), 140-147. doi:10.1016/j.molcel.2013.11.013
- Chen, M. K., Kuwabara, H., Zhou, Y., Adams, R. J., Brasic, J. R., McGlothan, J. L., . . . Guilarte, T. R. (2008). VMAT2 and dopamine neuron loss in a primate model of Parkinson's disease. *J Neurochem*, *105*(1), 78-90. doi:10.1111/j.1471-4159.2007.05108.x
- Chen, Y. P., Song, W., Huang, R., Chen, K., Zhao, B., Li, J., . . . Shang, H. F. (2013). GAK rs1564282 and DGKQ rs11248060 increase the risk for Parkinson's disease in a Chinese population. *J Clin Neurosci*, *20*(6), 880-883. doi:10.1016/j.jocn.2012.07.011

- Cheng, X., Ma, Y., Moore, M., Hemmings, B. A., & Taylor, S. S. (1998). Phosphorylation and activation of cAMP-dependent protein kinase by phosphoinositide-dependent protein kinase. *Proc Natl Acad Sci U S A*, *95*(17), 9849-9854.
- Cohen, P. (2000). The regulation of protein function by multisite phosphorylation--a 25 year update. *Trends Biochem Sci*, *25*(12), 596-601.
- Conway, K. A., Harper, J. D., & Lansbury, P. T. (1998). Accelerated in vitro fibril formation by a mutant alpha-synuclein linked to early-onset Parkinson disease. *Nat Med*, *4*(11), 1318-1320. doi:10.1038/3311
- Conway, K. A., Lee, S. J., Rochet, J. C., Ding, T. T., Williamson, R. E., & Lansbury, P. T., Jr. (2000). Acceleration of oligomerization, not fibrillization, is a shared property of both alpha-synuclein mutations linked to early-onset Parkinson's disease: implications for pathogenesis and therapy. *Proc Natl Acad Sci U S A*, *97*(2), 571-576.
- Dauer, W., & Przedborski, S. Parkinson's Disease. *Neuron*, *39*(6), 889-909. doi:10.1016/S0896-6273(03)00568-3
- Deng, X., Dzamko, N., Prescott, A., Davies, P., Liu, Q., Yang, Q., . . . Gray, N. S. (2011). Characterization of a selective inhibitor of the Parkinson's disease kinase LRRK2. *Nat Chem Biol*, *7*(4), 203-205. doi:10.1038/nchembio.538
- Di Fonzo, A., Dekker, M. C., Montagna, P., Baruzzi, A., Yonova, E. H., Correia Guedes, L., . . . Bonifati, V. (2009). FBXO7 mutations cause autosomal recessive, early-onset parkinsonian-pyramidal syndrome. *Neurology*, *72*(3), 240-245. doi:10.1212/01.wnl.0000338144.10967.2b
- Doggett, E. A., Zhao, J., Mork, C. N., Hu, D., & Nichols, R. J. (2012). Phosphorylation of LRRK2 serines 955 and 973 is disrupted by Parkinson's disease mutations and LRRK2 pharmacological inhibition. *J Neurochem*, *120*(1), 37-45. doi:10.1111/j.1471-4159.2011.07537.x
- Dzamko, N., Deak, M., Hentati, F., Reith, A. D., Prescott, A. R., Alessi, D. R., & Nichols, R. J. (2010). Inhibition of LRRK2 kinase activity leads to dephosphorylation of Ser(910)/Ser(935), disruption of 14-3-3 binding and altered cytoplasmic localization. *Biochem J*, *430*(3), 405-413. doi:10.1042/bj20100784
- Dzamko, N., Inesta-Vaquera, F., Zhang, J., Xie, C., Cai, H., Arthur, S., . . . Alessi, D. R. (2012). The IkappaB kinase family phosphorylates the Parkinson's disease kinase LRRK2 at Ser935 and Ser910 during Toll-like receptor signaling. *PLoS One*, *7*(6), e39132. doi:10.1371/journal.pone.0039132
- Exner, N., Lutz, A. K., Haass, C., & Winklhofer, K. F. (2012). Mitochondrial dysfunction in Parkinson's disease: molecular mechanisms and pathophysiological consequences. *Embo j*, *31*(14), 3038-3062. doi:10.1038/emboj.2012.170
- Farrer, M. J., Haugarvoll, K., Ross, O. A., Stone, J. T., Milkovic, N. M., Cobb, S. A., . . . Toft, M. (2006). Genomewide association, Parkinson disease, and PARK10. *Am J Hum Genet*, *78*(6), 1084-1088; author reply 1092-1084. doi:10.1086/504728
- Fell, M. J., Mirescu, C., Basu, K., Cheewatrakoolpong, B., DeMong, D. E., Ellis, J. M., . . . Morrow, J. A. (2015). MLI-2, a Potent, Selective, and Centrally Active Compound for Exploring the Therapeutic Potential and Safety of LRRK2 Kinase Inhibition. *J Pharmacol Exp Ther*, *355*(3), 397-409. doi:10.1124/jpet.115.227587
- Fischer, E. H., Graves, D. J., Crittenden, E. R., & Krebs, E. G. (1959). Structure of the site phosphorylated in the phosphorylase b to a reaction. *J Biol Chem*, *234*(7), 1698-1704.
- Fischer, E. H., & Krebs, E. G. (1955). Conversion of phosphorylase b to phosphorylase a in muscle extracts. *J Biol Chem*, *216*(1), 121-132.
- Frodin, M., Antal, T. L., Dummler, B. A., Jensen, C. J., Deak, M., Gammeltoft, S., & Biondi, R. M. (2002). A phosphoserine/threonine-binding pocket in AGC kinases and PDK1 mediates activation by hydrophobic motif phosphorylation. *Embo j*, *21*(20), 5396-5407.
- Fuji, R. N., Flagella, M., Baca, M., Baptista, M. A., Brodbeck, J., Chan, B. K., . . . Watts, R. J. (2015). Effect of selective LRRK2 kinase inhibition on nonhuman primate lung. *Sci Transl Med*, *7*(273), 273ra215. doi:10.1126/scitranslmed.aaa3634

- Funayama, M., Hasegawa, K., Kowa, H., Saito, M., Tsuji, S., & Obata, F. (2002). A new locus for Parkinson's disease (PARK8) maps to chromosome 12p11.2-q13.1. *Ann Neurol*, *51*(3), 296-301.
- Funayama, M., Hasegawa, K., Ohta, E., Kawashima, N., Komiyama, M., Kowa, H., . . . Obata, F. (2005). An LRRK2 mutation as a cause for the parkinsonism in the original PARK8 family. *Ann Neurol*, *57*(6), 918-921. doi:10.1002/ana.20484
- Funayama, M., Ohe, K., Amo, T., Furuya, N., Yamaguchi, J., Saiki, S., . . . Hattori, N. (2015). CHCHD2 mutations in autosomal dominant late-onset Parkinson's disease: a genome-wide linkage and sequencing study. *Lancet Neurol*, *14*(3), 274-282. doi:10.1016/S1474-4422(14)70266-2
- Gasser, T., Muller-Myhsok, B., Wszolek, Z. K., Oehlmann, R., Calne, D. B., Bonifati, V., . . . Horstmann, R. D. (1998). A susceptibility locus for Parkinson's disease maps to chromosome 2p13. *Nat Genet*, *18*(3), 262-265. doi:10.1038/ng0398-262
- Gillies, G. E., Pienaar, I. S., Vohra, S., & Qamhawi, Z. (2014). Sex differences in Parkinson's disease. *Front Neuroendocrinol*, *35*(3), 370-384. doi:10.1016/j.yfrne.2014.02.002
- Gloeckner, C. J., Schumacher, A., Boldt, K., & Ueffing, M. (2009). The Parkinson disease-associated protein kinase LRRK2 exhibits MAPKKK activity and phosphorylates MKK3/6 and MKK4/7, in vitro. *J Neurochem*, *109*(4), 959-968. doi:10.1111/j.1471-4159.2009.06024.x
- Goldenberg, M. M. (2008). Medical Management of Parkinson's Disease. *Pharmacy and Therapeutics*, *33*(10), 590-606.
- Greene, A. W., Grenier, K., Aguilera, M. A., Muise, S., Farazifard, R., Haque, M. E., . . . Fon, E. A. (2012). Mitochondrial processing peptidase regulates PINK1 processing, import and Parkin recruitment. *EMBO Rep*, *13*(4), 378-385. doi:10.1038/embor.2012.14
- Greenfield, J. G., & Bosanquet, F. D. (1953). The brain-stem lesions in Parkinsonism. *J Neurol Neurosurg Psychiatry*, *16*(4), 213-226.
- Greggio, E., Zambrano, I., Kaganovich, A., Beilina, A., Taymans, J. M., Daniels, V., . . . Cookson, M. R. (2008). The Parkinson disease-associated leucine-rich repeat kinase 2 (LRRK2) is a dimer that undergoes intramolecular autophosphorylation. *J Biol Chem*, *283*(24), 16906-16914. doi:10.1074/jbc.M708718200
- Guo, L., Gandhi, P. N., Wang, W., Petersen, R. B., Wilson-Delfosse, A. L., & Chen, S. G. (2007). The Parkinson's disease-associated protein, leucine-rich repeat kinase 2 (LRRK2), is an authentic GTPase that stimulates kinase activity. *Exp Cell Res*, *313*(16), 3658-3670. doi:10.1016/j.yexcr.2007.07.007
- Guo, X. Y., Chen, Y. P., Song, W., Zhao, B., Cao, B., Wei, Q. Q., . . . Shang, H. F. (2014). An association analysis of the rs1572931 polymorphism of the RAB7L1 gene in Parkinson's disease, amyotrophic lateral sclerosis and multiple system atrophy in China. *Eur J Neurol*, *21*(10), 1337-1343. doi:10.1111/ene.12490
- Hagen, T., & Vidal-Puig, A. (2002). Characterisation of the phosphorylation of beta-catenin at the GSK-3 priming site Ser45. *Biochem Biophys Res Commun*, *294*(2), 324-328. doi:10.1016/s0006-291x(02)00485-0
- Hampe, C., Ardila-Osorio, H., Fournier, M., Brice, A., & Corti, O. (2006). Biochemical analysis of Parkinson's disease-causing variants of Parkin, an E3 ubiquitin-protein ligase with monoubiquitylation capacity. *Hum Mol Genet*, *15*(13), 2059-2075. doi:10.1093/hmg/ddl131
- Hamza, T. H., Zabetian, C. P., Tenesa, A., Laederach, A., Montimurro, J., Yearout, D., . . . Payami, H. (2010). Common genetic variation in the HLA region is associated with late-onset sporadic Parkinson's disease. *Nat Genet*, *42*(9), 781-785. doi:10.1038/ng.642
- Hanks, S. K., & Hunter, T. (1995). Protein kinases 6. The eukaryotic protein kinase superfamily: kinase (catalytic) domain structure and classification. *FASEB J*, *9*(8), 576-596.
- Hardy, J., Cai, H., Cookson, M. R., Gwinn-Hardy, K., & Singleton, A. (2006). Genetics of Parkinson's disease and parkinsonism. *Ann Neurol*, *60*(4), 389-398. doi:10.1002/ana.21022

- Hedrich, K., Eskelson, C., Wilmot, B., Marder, K., Harris, J., Garrels, J., . . . Kramer, P. (2004). Distribution, type, and origin of Parkin mutations: review and case studies. *Mov Disord*, *19*(10), 1146-1157. doi:10.1002/mds.20234
- Herzig, M. C., Kolly, C., Persohn, E., Theil, D., Schweizer, T., Hafner, T., . . . Shimshek, D. R. (2011). LRRK2 protein levels are determined by kinase function and are crucial for kidney and lung homeostasis in mice. *Human Molecular Genetics*, *20*(21), 4209-4223. doi:10.1093/hmg/ddr348
- Hinkle, K. M., Yue, M., Behrouz, B., Dachsel, J. C., Lincoln, S. J., Bowles, E. E., . . . Melrose, H. L. (2012). LRRK2 knockout mice have an intact dopaminergic system but display alterations in exploratory and motor co-ordination behaviors. *Mol Neurodegener*, *7*, 25. doi:10.1186/1750-1326-7-25
- Ho, D. H., Kim, H., Kim, J., Sim, H., Ahn, H., Kim, J., . . . Seol, W. (2015). Leucine-Rich Repeat Kinase 2 (LRRK2) phosphorylates p53 and induces p21(WAF1/CIP1) expression. *Mol Brain*, *8*, 54. doi:10.1186/s13041-015-0145-7
- Holt, L. J., Tuch, B. B., Villen, J., Johnson, A. D., Gygi, S. P., & Morgan, D. O. (2009). Global analysis of Cdk1 substrate phosphorylation sites provides insights into evolution. *Science*, *325*(5948), 1682-1686. doi:10.1126/science.1172867
- Hultqvist, G., Ocampo Daza, D., Larhammar, D., & Kilimann, M. W. (2012). Evolution of the vertebrate paralemmin gene family: ancient origin of gene duplicates suggests distinct functions. *PLoS One*, *7*(7), e41850. doi:10.1371/journal.pone.0041850
- Hutagalung, A. H., & Novick, P. J. (2011). Role of Rab GTPases in membrane traffic and cell physiology. *Physiol Rev*, *91*(1), 119-149. doi:10.1152/physrev.00059.2009
- Imai, Y., Gehrke, S., Wang, H. Q., Takahashi, R., Hasegawa, K., Oota, E., & Lu, B. (2008). Phosphorylation of 4E-BP by LRRK2 affects the maintenance of dopaminergic neurons in *Drosophila*. *Embo j*, *27*(18), 2432-2443. doi:10.1038/emboj.2008.163
- Ito, G., Fujimoto, T., Kamikawaji, S., Kuwahara, T., & Iwatsubo, T. (2014). Lack of Correlation between the Kinase Activity of LRRK2 Harboring Kinase-Modifying Mutations and Its Phosphorylation at Ser910, 935, and Ser955. *PLoS One*, *9*(5), e97988. doi:10.1371/journal.pone.0097988
- Ito, G., Katsemonova, K., Tonelli, F., Lis, P., Baptista, M., Shpiro, N., . . . Alessi, D. R. (2016). Phos-tag analysis of Rab10 phosphorylation by LRRK2: a powerful assay for assessing kinase function and inhibitors. *Biochem J*. doi:10.1042/bcj20160557
- Ito, M., Nakano, T., Erdodi, F., & Hartshorne, D. J. (2004). Myosin phosphatase: structure, regulation and function. *Mol Cell Biochem*, *259*(1-2), 197-209.
- Jaleel, M., Nichols, R. J., Deak, M., Campbell, D. G., Gillardon, F., Knebel, A., & Alessi, D. R. (2007). LRRK2 phosphorylates moesin at threonine-558: characterization of how Parkinson's disease mutants affect kinase activity. *Biochem J*, *405*(2), 307-317. doi:10.1042/BJ20070209
- Kachergus, J., Mata, I. F., Hulihan, M., Taylor, J. P., Lincoln, S., Aasly, J., . . . Toft, M. (2005). Identification of a novel LRRK2 mutation linked to autosomal dominant parkinsonism: evidence of a common founder across European populations. *Am J Hum Genet*, *76*(4), 672-680. doi:10.1086/429256
- Kalinderi, K., Bostantjopoulou, S., & Fidani, L. (2016). The genetic background of Parkinson's disease: current progress and future prospects. *Acta Neurol Scand*. doi:10.1111/ane.12563
- Kang, R., Wan, J., Arstikaitis, P., Takahashi, H., Huang, K., Bailey, A. O., . . . El-Husseini, A. (2008). Neural palmitoyl-proteomics reveals dynamic synaptic palmitoylation. *Nature*, *456*(7224), 904-909. doi:10.1038/nature07605
- Kazlauskaitė, A., Kelly, V., Johnson, C., Baillie, C., Hastie, C. J., Peggie, M., . . . Muqit, M. M. (2014). Phosphorylation of Parkin at Serine65 is essential for activation: elaboration of a Miro1 substrate-based assay of Parkin E3 ligase activity. *Open Biol*, *4*, 130213. doi:10.1098/rsob.130213
- Kazlauskaitė, A., Martinez-Torres, R. J., Wilkie, S., Kumar, A., Peltier, J., Gonzalez, A., . . . Muqit, M. M. (2015). Binding to serine 65-phosphorylated ubiquitin primes Parkin for optimal PINK1-

- dependent phosphorylation and activation. *EMBO Rep*, 16(8), 939-954. doi:10.15252/embr.201540352
- Kazlauskaite, A., & Muqit, M. M. (2015). PINK1 and Parkin - mitochondrial interplay between phosphorylation and ubiquitylation in Parkinson's disease. *Febs j*, 282(2), 215-223. doi:10.1111/febs.13127
- Kimura, K., Ito, M., Amano, M., Chihara, K., Fukata, Y., Nakafuku, M., . . . Kaibuchi, K. (1996). Regulation of myosin phosphatase by Rho and Rho-associated kinase (Rho-kinase). *Science*, 273(5272), 245-248.
- Kinoshita, E., Kinoshita-Kikuta, E., Takiyama, K., & Koike, T. (2006). Phosphate-binding tag, a new tool to visualize phosphorylated proteins. *Mol Cell Proteomics*, 5(4), 749-757. doi:10.1074/mcp.T500024-MCP200
- Kinoshita, E., Takahashi, M., Takeda, H., Shiro, M., & Koike, T. (2004). Recognition of phosphate monoester dianion by an alkoxide-bridged dinuclear zinc(II) complex. *Dalton Trans*(8), 1189-1193. doi:10.1039/b400269e
- Kinoshita, E., Yamada, A., Takeda, H., Kinoshita-Kikuta, E., & Koike, T. (2005). Novel immobilized zinc(II) affinity chromatography for phosphopeptides and phosphorylated proteins. *J Sep Sci*, 28(2), 155-162. doi:10.1002/jssc.200401833
- Klein, C., & Westenberger, A. (2012). Genetics of Parkinson's disease. *Cold Spring Harb Perspect Med*, 2(1), a008888. doi:10.1101/cshperspect.a008888
- Knighton, D. R., Zheng, J. H., Ten Eyck, L. F., Ashford, V. A., Xuong, N. H., Taylor, S. S., & Sowadski, J. M. (1991). Crystal structure of the catalytic subunit of cyclic adenosine monophosphate-dependent protein kinase. *Science*, 253(5018), 407-414.
- Kondapalli, C., Kazlauskaite, A., Zhang, N., Woodroof, H. I., Campbell, D. G., Gourlay, R., . . . Muqit, M. M. (2012). PINK1 is activated by mitochondrial membrane potential depolarization and stimulates Parkin E3 ligase activity by phosphorylating Serine 65. *Open Biol*, 2(5), 120080. doi:10.1098/rsob.120080
- Krebs, E. G., & Fischer, E. H. (1956). The phosphorylase b to a converting enzyme of rabbit skeletal muscle. *Biochim Biophys Acta*, 20(1), 150-157.
- Kutzleb, C., Sanders, G., Yamamoto, R., Wang, X., Lichte, B., Petrasch-Parwez, E., & Kilimann, M. W. (1998). Paralemmin, a prenyl-palmitoyl-anchored phosphoprotein abundant in neurons and implicated in plasma membrane dynamics and cell process formation. *J Cell Biol*, 143(3), 795-813.
- Kuwahara, T., Inoue, K., D'Agati, V. D., Fujimoto, T., Eguchi, T., Saha, S., . . . Abeliovich, A. (2016). LRRK2 and RAB7L1 coordinately regulate axonal morphology and lysosome integrity in diverse cellular contexts. *Sci Rep*, 6, 29945. doi:10.1038/srep29945
- Lai, Y. C., Kondapalli, C., Lehneck, R., Procter, J. B., Dill, B. D., Woodroof, H. I., . . . Muqit, M. M. (2015). Phosphoproteomic screening identifies Rab GTPases as novel downstream targets of PINK1. *Embo j*, 34(22), 2840-2861. doi:10.15252/embj.201591593
- Lautier, C., Goldwurm, S., Durr, A., Giovannone, B., Tsiaras, W. G., Pezzoli, G., . . . Smith, R. J. (2008). Mutations in the GIGYF2 (TNRC15) gene at the PARK11 locus in familial Parkinson disease. *Am J Hum Genet*, 82(4), 822-833. doi:10.1016/j.ajhg.2008.01.015
- Lazarou, M., Jin, S. M., Kane, L. A., & Youle, R. J. (2012). Role of PINK1 binding to the TOM complex and alternate intracellular membranes in recruitment and activation of the E3 ligase Parkin. *Dev Cell*, 22(2), 320-333. doi:10.1016/j.devcel.2011.12.014
- Lesage, S., Bras, J., Cormier-Dequaire, F., Condroyer, C., Nicolas, A., Darwent, L., . . . the International Parkinson's Disease Genomics, C. (2015). Loss-of-function mutations in RAB39B are associated with typical early-onset Parkinson disease. *Neurol Genet*, 1(1), e9. doi:10.1212/NXG.0000000000000009
- Lesage, S., Drouet, V., Majounie, E., Deramecourt, V., Jacoupy, M., Nicolas, A., . . . International Parkinson's Disease Genomics, C. (2016). Loss of VPS13C Function in Autosomal-Recessive

- Parkinsonism Causes Mitochondrial Dysfunction and Increases PINK1/Parkin-Dependent Mitophagy. *Am J Hum Genet*, 98(3), 500-513. doi:10.1016/j.ajhg.2016.01.014
- Li, J. Q., Tan, L., & Yu, J. T. (2014). The role of the LRRK2 gene in Parkinsonism. *Mol Neurodegener*, 9, 47. doi:10.1186/1750-1326-9-47
- Li, Y., Liu, W., Oo, T. F., Wang, L., Tang, Y., Jackson-Lewis, V., . . . Li, C. (2009). Mutant LRRK2(R1441G) BAC transgenic mice recapitulate cardinal features of Parkinson's disease. *Nat Neurosci*, 12(7), 826-828. doi:10.1038/nn.2349
- Lin, W., & Kang, U. J. (2008). Characterization of PINK1 processing, stability, and subcellular localization. *J Neurochem*, 106(1), 464-474. doi:10.1111/j.1471-4159.2008.05398.x
- Liu, Y., Fallon, L., Lashuel, H. A., Liu, Z., & Lansbury, P. T., Jr. (2002). The UCH-L1 gene encodes two opposing enzymatic activities that affect alpha-synuclein degradation and Parkinson's disease susceptibility. *Cell*, 111(2), 209-218.
- Liu, Z., Mobley, J. A., DeLucas, L. J., Kahn, R. A., & West, A. B. (2016). LRRK2 autophosphorylation enhances its GTPase activity. *FASEB J*, 30(1), 336-347. doi:10.1096/fj.15-277095
- Lochte, T., Bruggemann, N., Vollstedt, E. J., Krause, P., Domingo, A., Rosales, R., . . . Lohmann, K. (2016). RAB39B mutations are a rare finding in Parkinson disease patients. *Parkinsonism Relat Disord*, 23, 116-117. doi:10.1016/j.parkreldis.2015.12.014
- Lucking, C. B., Durr, A., Bonifati, V., Vaughan, J., De Michele, G., Gasser, T., . . . European Consortium on Genetic Susceptibility in Parkinson's, D. (2000). Association between early-onset Parkinson's disease and mutations in the parkin gene. *N Engl J Med*, 342(21), 1560-1567. doi:10.1056/NEJM200005253422103
- MacDonald, J. A., Eto, M., Borman, M. A., Brautigan, D. L., & Haystead, T. A. (2001). Dual Ser and Thr phosphorylation of CPI-17, an inhibitor of myosin phosphatase, by MYPT-associated kinase. *FEBS Lett*, 493(2-3), 91-94.
- Mackintosh, C. (2004). Dynamic interactions between 14-3-3 proteins and phosphoproteins regulate diverse cellular processes. *Biochem J*, 381(Pt 2), 329-342. doi:10.1042/bj20031332
- MacKintosh, C., Beattie, K. A., Klumpp, S., Cohen, P., & Codd, G. A. (1990). Cyanobacterial microcystin-LR is a potent and specific inhibitor of protein phosphatases 1 and 2A from both mammals and higher plants. *FEBS Lett*, 264(2), 187-192.
- MacLeod, D. A., Rhinn, H., Kuwahara, T., Zolin, A., Di Paolo, G., McCabe, B. D., . . . Abeliovich, A. (2013). RAB7L1 interacts with LRRK2 to modify intraneuronal protein sorting and Parkinson's disease risk. *Neuron*, 77(3), 425-439. doi:10.1016/j.neuron.2012.11.033
- Manning, G. (2005). Genomic overview of protein kinases. *WormBook*, 1-19. doi:10.1895/wormbook.1.60.1
- Manning, G., Whyte, D. B., Martinez, R., Hunter, T., & Sudarsanam, S. (2002). The protein kinase complement of the human genome. *Science*, 298(5600), 1912-1934. doi:10.1126/science.1075762
- Marraffini, L. A., & Sontheimer, E. J. (2010). CRISPR interference: RNA-directed adaptive immunity in bacteria and archaea. *Nature reviews. Genetics*, 11(3), 181-190. doi:10.1038/nrg2749
- Martin, I., Kim, J. W., Lee, B. D., Kang, H. C., Xu, J. C., Jia, H., . . . Dawson, V. L. (2014). Ribosomal protein s15 phosphorylation mediates LRRK2 neurodegeneration in Parkinson's disease. *Cell*, 157(2), 472-485. doi:10.1016/j.cell.2014.01.064
- Mata, I. F., Wedemeyer, W. J., Farrer, M. J., Taylor, J. P., & Gallo, K. A. (2006). LRRK2 in Parkinson's disease: protein domains and functional insights. *Trends Neurosci*, 29(5), 286-293. doi:10.1016/j.tins.2006.03.006
- Matikainen-Ankney, B. A., Kezunovic, N., Mesias, R. E., Tian, Y., Williams, F. M., Huntley, G. W., & Benson, D. L. (2016). Altered Development of Synapse Structure and Function in Striatum Caused by Parkinson's Disease-Linked LRRK2-G2019S Mutation. *J Neurosci*, 36(27), 7128-7141. doi:10.1523/JNEUROSCI.3314-15.2016
- Meixner, A., Boldt, K., Van Troys, M., Askenazi, M., Gloeckner, C. J., Bauer, M., . . . Ueffing, M. (2011). A QUICK screen for Lrrk2 interaction partners--leucine-rich repeat kinase 2 is involved in

- actin cytoskeleton dynamics. *Mol Cell Proteomics*, 10(1), M110 001172. doi:10.1074/mcp.M110.001172
- Meng, Z., Moroishi, T., Mottier-Pavie, V., Plouffe, S. W., Hansen, C. G., Hong, A. W., . . . Guan, K. L. (2015). MAP4K family kinases act in parallel to MST1/2 to activate LATS1/2 in the Hippo pathway. *Nat Commun*, 6, 8357. doi:10.1038/ncomms9357
- Moore, D. J. (2006). Parkin: a multifaceted ubiquitin ligase. *Biochem Soc Trans*, 34(Pt 5), 749-753. doi:10.1042/bst0340749
- Mosavi, L. K., Cammett, T. J., Desrosiers, D. C., & Peng, Z.-y. (2004). The ankyrin repeat as molecular architecture for protein recognition. *Protein Science : A Publication of the Protein Society*, 13(6), 1435-1448. doi:10.1110/ps.03554604
- Muda, K., Bertinetti, D., Gesellchen, F., Hermann, J. S., von Zweyendorf, F., Geerloff, A., . . . Herberg, F. W. (2014). Parkinson-related LRRK2 mutation R1441C/G/H impairs PKA phosphorylation of LRRK2 and disrupts its interaction with 14-3-3. *Proc Natl Acad Sci U S A*, 111(1), E34-43. doi:10.1073/pnas.1312701111
- Muranyi, A., MacDonald, J. A., Deng, J. T., Wilson, D. P., Haystead, T. A., Walsh, M. P., . . . Hartshorne, D. J. (2002). Phosphorylation of the myosin phosphatase target subunit by integrin-linked kinase. *Biochem J*, 366(Pt 1), 211-216. doi:10.1042/BJ20020401
- Muranyi, A., Zhang, R., Liu, F., Hirano, K., Ito, M., Epstein, H. F., & Hartshorne, D. J. (2001). Myotonic dystrophy protein kinase phosphorylates the myosin phosphatase targeting subunit and inhibits myosin phosphatase activity. *FEBS Lett*, 493(2-3), 80-84.
- Nichols, R. J., Dzamko, N., Huttli, J. E., Cantley, L. C., Deak, M., Moran, J., . . . Alessi, D. R. (2009a). Substrate specificity and inhibitors of LRRK2, a protein kinase mutated in Parkinson's disease. *The Biochemical journal*, 424(1), 47-60. doi:10.1042/BJ20091035
- Nichols, R. J., Dzamko, N., Huttli, J. E., Cantley, L. C., Deak, M., Moran, J., . . . Alessi, D. R. (2009b). Substrate specificity and inhibitors of LRRK2, a protein kinase mutated in Parkinson's disease. *Biochem J*, 424(1), 47-60. doi:10.1042/BJ20091035
- Nichols, R. J., Dzamko, N., Morrice, N. A., Campbell, D. G., Deak, M., Ordureau, A., . . . Alessi, D. R. (2010). 14-3-3 binding to LRRK2 is disrupted by multiple Parkinson's disease-associated mutations and regulates cytoplasmic localization. *Biochem J*, 430(3), 393-404. doi:10.1042/BJ20100483
- Ohta, E., Kawakami, F., Kubo, M., & Obata, F. (2011). LRRK2 directly phosphorylates Akt1 as a possible physiological substrate: impairment of the kinase activity by Parkinson's disease-associated mutations. *FEBS Lett*, 585(14), 2165-2170. doi:10.1016/j.febslet.2011.05.044
- Okamoto, R., Ito, M., Suzuki, N., Kongo, M., Moriki, N., Saito, H., . . . Nakano, T. (2005). The targeted disruption of the MYPT1 gene results in embryonic lethality. *Transgenic Res*, 14(3), 337-340.
- Ozelius, L. J., Senthil, G., Saunders-Pullman, R., Ohmann, E., Deligtisch, A., Tagliati, M., . . . Bressman, S. B. (2006). LRRK2 G2019S as a cause of Parkinson's disease in Ashkenazi Jews. *N Engl J Med*, 354(4), 424-425. doi:10.1056/NEJMc055509
- Paisan-Ruiz, C., Jain, S., Evans, E. W., Gilks, W. P., Simon, J., van der Brug, M., . . . Singleton, A. B. (2004). Cloning of the gene containing mutations that cause PARK8-linked Parkinson's disease. *Neuron*, 44(4), 595-600. doi:10.1016/j.neuron.2004.10.023
- Pankratz, N., & Foroud, T. (2007). Genetics of Parkinson disease. *Genet Med*, 9(12), 801-811. doi:10.1097/GIM.0b013e31815bf97c
- Parisiadou, L., Xie, C., Cho, H. J., Lin, X., Gu, X. L., Long, C. X., . . . Cai, H. (2009). Phosphorylation of ezrin/radixin/moesin proteins by LRRK2 promotes the rearrangement of actin cytoskeleton in neuronal morphogenesis. *J Neurosci*, 29(44), 13971-13980. doi:10.1523/JNEUROSCI.3799-09.2009
- Parkinson, J. (2002). An essay on the shaking palsy. 1817. *J Neuropsychiatry Clin Neurosci*, 14(2), 223-236; discussion 222. doi:10.1176/jnp.14.2.223

- Polymeropoulos, M. H., Lavedan, C., Leroy, E., Ide, S. E., Dehejia, A., Dutra, A., . . . Nussbaum, R. L. (1997). Mutation in the alpha-synuclein gene identified in families with Parkinson's disease. *Science*, *276*(5321), 2045-2047.
- Puschmann, A., Englund, E., Ross, O. A., Vilarino-Guell, C., Lincoln, S. J., Kachergus, J. M., . . . Nilsson, C. (2012). First neuropathological description of a patient with Parkinson's disease and LRRK2 p.N1437H mutation. *Parkinsonism Relat Disord*, *18*(4), 332-338. doi:10.1016/j.parkreldis.2011.11.019
- Quadri, M., Fang, M., Picillo, M., Olgiati, S., Breedveld, G. J., Graafland, J., . . . Bonifati, V. (2013). Mutation in the SYNJ1 gene associated with autosomal recessive, early-onset Parkinsonism. *Hum Mutat*, *34*(9), 1208-1215. doi:10.1002/humu.22373
- Ramirez, A., Heimbach, A., Grundemann, J., Stiller, B., Hampshire, D., Cid, L. P., . . . Kubisch, C. (2006). Hereditary parkinsonism with dementia is caused by mutations in ATP13A2, encoding a lysosomal type 5 P-type ATPase. *Nat Genet*, *38*(10), 1184-1191. doi:10.1038/ng1884
- Reith, A. D., Bamborough, P., Jandu, K., Andreotti, D., Mensah, L., Dossang, P., . . . Gray, N. S. (2012). GSK2578215A; a potent and highly selective 2-arylmethoxy-5-substituent-N-arylbenzamide LRRK2 kinase inhibitor. *Bioorg Med Chem Lett*, *22*(17), 5625-5629. doi:10.1016/j.bmcl.2012.06.104
- Reyniers, L., Del Giudice, M. G., Civiero, L., Belluzzi, E., Lobbestael, E., Beilina, A., . . . Taymans, J. M. (2014). Differential protein-protein interactions of LRRK1 and LRRK2 indicate roles in distinct cellular signaling pathways. *J Neurochem*, *131*(2), 239-250. doi:10.1111/jnc.12798
- Riederer, P., & Wuketich, S. (1976). Time course of nigrostriatal degeneration in parkinson's disease. A detailed study of influential factors in human brain amine analysis. *J Neural Transm*, *38*(3-4), 277-301.
- Riley, B. E., Loughheed, J. C., Callaway, K., Velasquez, M., Brecht, E., Nguyen, L., . . . Johnston, J. A. (2013). Structure and function of Parkin E3 ubiquitin ligase reveals aspects of RING and HECT ligases. *Nat Commun*, *4*, 1982. doi:10.1038/ncomms2982
- Robison, G. A., & Sutherland, E. W. (1971). Cyclic AMP and the function of eukaryotic cells: an introduction. *Ann N Y Acad Sci*, *185*, 5-9.
- Rojas-Fernandez, A., Herhaus, L., Macartney, T., Lachaud, C., Hay, R. T., & Sapkota, G. P. (2015). Rapid generation of endogenously driven transcriptional reporters in cells through CRISPR/Cas9. *Scientific Reports*, *5*, 9811. doi:10.1038/srep09811
- <http://www.nature.com/articles/srep09811#supplementary-information>
- Ross, O. A., Braithwaite, A. T., Skipper, L. M., Kachergus, J., Hulihan, M. M., Middleton, F. A., . . . Farrer, M. J. (2008). Genomic investigation of α -Synuclein multiplication and parkinsonism. *Annals of neurology*, *63*(6), 10.1002/ana.21380. doi:10.1002/ana.21380
- Rubin, G. M., Yandell, M. D., Wortman, J. R., Gabor Miklos, G. L., Nelson, C. R., Hariharan, I. K., . . . Lewis, S. (2000). Comparative genomics of the eukaryotes. *Science*, *287*(5461), 2204-2215.
- Sanjana, N. E., Cong, L., Zhou, Y., Cunniff, M. M., Feng, G., & Zhang, F. (2012). A transcription activator-like effector toolbox for genome engineering. *Nat Protoc*, *7*(1), 171-192. doi:10.1038/nprot.2011.431
- Satake, W., Nakabayashi, Y., Mizuta, I., Hirota, Y., Ito, C., Kubo, M., . . . Toda, T. (2009). Genome-wide association study identifies common variants at four loci as genetic risk factors for Parkinson's disease. *Nat Genet*, *41*(12), 1303-1307. doi:10.1038/ng.485
- Schulte, E. C., Ellwanger, D. C., Dihanich, S., Manzoni, C., Stangl, K., Schormair, B., . . . Winkelmann, J. (2014). Rare variants in LRRK1 and Parkinson's disease. *Neurogenetics*, *15*(1), 49-57. doi:10.1007/s10048-013-0383-8
- Scotto-Lavino, E., Garcia-Diaz, M., Du, G., & Frohman, M. A. (2010). Basis for the isoform-specific interaction of myosin phosphatase subunits protein phosphatase 1c beta and myosin phosphatase targeting subunit 1. *J Biol Chem*, *285*(9), 6419-6424. doi:10.1074/jbc.M109.074773

- Shen, J. (2004). Protein kinases linked to the pathogenesis of Parkinson's disease. *Neuron*, 44(4), 575-577. doi:10.1016/j.neuron.2004.11.008
- Sheng, Z., Zhang, S., Bustos, D., Kleinheinz, T., Le Pichon, C. E., Dominguez, S. L., . . . Zhu, H. (2012). Ser1292 autophosphorylation is an indicator of LRRK2 kinase activity and contributes to the cellular effects of PD mutations. *Sci Transl Med*, 4(164), 164ra161. doi:10.1126/scitranslmed.3004485
- Spanaki, C., Latsoudis, H., & Plaitakis, A. (2006). LRRK2 mutations on Crete: R1441H associated with PD evolving to PSP. *Neurology*, 67(8), 1518-1519. doi:10.1212/01.wnl.0000239829.33936.73
- Spillantini, M. G., Schmidt, M. L., Lee, V. M., Trojanowski, J. Q., Jakes, R., & Goedert, M. (1997). Alpha-synuclein in Lewy bodies. *Nature*, 388(6645), 839-840. doi:10.1038/42166
- Stefanis, L. (2012). alpha-Synuclein in Parkinson's disease. *Cold Spring Harb Perspect Med*, 2(2), a009399. doi:10.1101/cshperspect.a009399
- Steger, M., Tonelli, F., Ito, G., Davies, P., Trost, M., Vetter, M., . . . Mann, M. (2016). Phosphoproteomics reveals that Parkinson's disease kinase LRRK2 regulates a subset of Rab GTPases. *Elife*, 5. doi:10.7554/eLife.12813
- Stenmark, H., & Olkkonen, V. M. (2001). The Rab GTPase family. *Genome Biology*, 2(5), reviews3007.3001-reviews3007.3007.
- Strauss, K. M., Martins, L. M., Plun-Favreau, H., Marx, F. P., Kautzmann, S., Berg, D., . . . Kruger, R. (2005). Loss of function mutations in the gene encoding Omi/HtrA2 in Parkinson's disease. *Hum Mol Genet*, 14(15), 2099-2111. doi:10.1093/hmg/ddi215
- Tagliaferro, P., Kareva, T., Oo, T. F., Yarygina, O., Kholodilov, N., & Burke, R. E. (2015). An early axonopathy in a hLRRK2(R1441G) transgenic model of Parkinson disease. *Neurobiol Dis*, 82, 359-371. doi:10.1016/j.nbd.2015.07.009
- Takizawa, N., Koga, Y., & Ikebe, M. (2002). Phosphorylation of CPI17 and myosin binding subunit of type 1 protein phosphatase by p21-activated kinase. *Biochem Biophys Res Commun*, 297(4), 773-778.
- Taymans, J. M. (2012). The GTPase function of LRRK2. *Biochem Soc Trans*, 40(5), 1063-1069. doi:10.1042/BST20120133
- Terrak, M., Kerff, F., Langsetmo, K., Tao, T., & Dominguez, R. (2004). Structural basis of protein phosphatase 1 regulation. *Nature*, 429(6993), 780-784. doi:10.1038/nature02582
- Tong, Y., Giaime, E., Yamaguchi, H., Ichimura, T., Liu, Y., Si, H., . . . Shen, J. (2012). Loss of leucine-rich repeat kinase 2 causes age-dependent bi-phasic alterations of the autophagy pathway. *Mol Neurodegener*, 7, 2. doi:10.1186/1750-1326-7-2
- Trempe, J. F., Sauve, V., Grenier, K., Seirafi, M., Tang, M. Y., Menade, M., . . . Gehring, K. (2013). Structure of parkin reveals mechanisms for ubiquitin ligase activation. *Science*, 340(6139), 1451-1455. doi:10.1126/science.1237908
- Tsika, E., & Moore, D. J. (2013). Contribution of GTPase activity to LRRK2-associated Parkinson disease. *Small GTPases*, 4(3), 164-170. doi:10.4161/sgtp.25130
- Tucci, A., Nalls, M. A., Houlden, H., Revesz, T., Singleton, A. B., Wood, N. W., . . . Paisan-Ruiz, C. (2010). Genetic variability at the PARK16 locus. *Eur J Hum Genet*, 18(12), 1356-1359. doi:10.1038/ejhg.2010.125
- Ubersax, J. A., & Ferrell, J. E., Jr. (2007). Mechanisms of specificity in protein phosphorylation. *Nat Rev Mol Cell Biol*, 8(7), 530-541. doi:10.1038/nrm2203
- Valente, E. M., Abou-Sleiman, P. M., Caputo, V., Muqit, M. M., Harvey, K., Gispert, S., . . . Wood, N. W. (2004). Hereditary early-onset Parkinson's disease caused by mutations in PINK1. *Science*, 304(5674), 1158-1160. doi:10.1126/science.1096284
- Vilarino-Guell, C., Wider, C., Ross, O. A., Dachsel, J. C., Kachergus, J. M., Lincoln, S. J., . . . Farrer, M. J. (2011). VPS35 mutations in Parkinson disease. *Am J Hum Genet*, 89(1), 162-167. doi:10.1016/j.ajhg.2011.06.001

- Wenzel, D. M., Lissounov, A., Brzovic, P. S., & Klevit, R. E. (2011). UBC7 reactivity profile reveals parkin and HHARI to be RING/HECT hybrids. *Nature*, *474*(7349), 105-108. doi:10.1038/nature09966
- Williams-Gray, C. H., Goris, A., Foltynie, T., Brown, J., Maranian, M., Walton, A., . . . Barker, R. A. (2006). Prevalence of the LRRK2 G2019S mutation in a UK community based idiopathic Parkinson's disease cohort. *Journal of Neurology, Neurosurgery, and Psychiatry*, *77*(5), 665-667. doi:10.1136/jnnp.2005.085019
- Wise-Scira, O., Aloglu, A. K., Dunn, A., Sakallioğlu, I. T., & Coskuner, O. (2013). Structures and Free Energy Landscapes of the Wild-Type and A30P Mutant-Type α -Synuclein Proteins with Dynamics. *ACS Chemical Neuroscience*, *4*(3), 486-497. doi:10.1021/cn300198q
- Yamashiro, S., Yamakita, Y., Totsukawa, G., Goto, H., Kaibuchi, K., Ito, M., . . . Matsumura, F. (2008). MYOSIN PHOSPHATASE TARGETING SUBUNIT1 REGULATES MITOSIS BY ANTAGONIZING POLO-LIKE KINASE1. *Dev Cell*, *14*(5), 787-797. doi:10.1016/j.devcel.2008.02.013
- Yoshino, H., Tomiyama, H., Tachibana, N., Ogaki, K., Li, Y., Funayama, M., . . . Hattori, N. (2010). Phenotypic spectrum of patients with PLA2G6 mutation and PARK14-linked parkinsonism. *Neurology*, *75*(15), 1356-1361. doi:10.1212/WNL.0b013e3181f73649
- Yun, H. J., Kim, H., Ga, I., Oh, H., Ho, D. H., Kim, J., . . . Seol, W. (2015). An early endosome regulator, Rab5b, is an LRRK2 kinase substrate. *J Biochem*, *157*(6), 485-495. doi:10.1093/jb/mvv005
- Yun, H. J., Park, J., Ho, D. H., Kim, H., Kim, C. H., Oh, H., . . . Seol, W. (2013). LRRK2 phosphorylates Snapin and inhibits interaction of Snapin with SNAP-25. *Exp Mol Med*, *45*, e36. doi:10.1038/emm.2013.68
- Zecca, L., Tampellini, D., Gerlach, M., Riederer, P., Fariello, R. G., & Sulzer, D. (2001). Substantia nigra neuromelanin: structure, synthesis, and molecular behaviour. *Mol Pathol*, *54*(6), 414-418.
- Zhang, Y., Gao, J., Chung, K. K., Huang, H., Dawson, V. L., & Dawson, T. M. (2000). Parkin functions as an E2-dependent ubiquitin- protein ligase and promotes the degradation of the synaptic vesicle-associated protein, CDCrel-1. *Proc Natl Acad Sci U S A*, *97*(24), 13354-13359. doi:10.1073/pnas.240347797
- Zheng, X., & Hunter, T. (2013). Parkin mitochondrial translocation is achieved through a novel catalytic activity coupled mechanism. *Cell Res*, *23*(7), 886-897. doi:10.1038/cr.2013.66
- Zimprich, A., Biskup, S., Leitner, P., Lichtner, P., Farrer, M., Lincoln, S., . . . Gasser, T. (2004). Mutations in LRRK2 cause autosomal-dominant parkinsonism with pleomorphic pathology. *Neuron*, *44*(4), 601-607. doi:10.1016/j.neuron.2004.11.005